CHARACTERIZATION OF ELECTRODEPOSITED Zn-Ni ALLOY COATINGS AS A REPLACEMENT FOR ELECTRODEPOSITED Zn AND Cd COATINGS

by

Sriraman Kankoduthavanitham Rajagopalan

Department of Mining & Materials Engineering
McGill University, Montreal, Quebec, Canada
August 2012

A thesis submitted to Faculty of Graduate studies, McGill University, in partial fulfillment of the requirements of the degree of Doctor of Philosophy

Abstract

Sacrificial metallic coatings, such as those based on Zn and Cd are used to protect steel components against corrosion. Growing environmental and health concerns have limited the use of Cd in any form since Cd plating bath is cyanide based and Cd compounds are carcinogenic. This thesis investigates Zn-Ni as a potential replacement for Cd and Cd based alloy coatings used in aerospace industries and Zn in automotive industries with respect to their tribological, corrosion and tribocorrosion resistance and hydrogen embrittlement susceptibility.

In situ tribometry and additional *ex situ* analyses revealed that Zn-Ni coatings had superior resistance to adhesive wear compared to cadmium coatings. The microhardness of Zn-Ni coatings was higher than Zn and Cd coatings. Hardness on the wear track of Zn-Ni coatings showed the formation of strain hardened tribo layer.

Zn-Ni coatings had higher polarization resistance after wear testing as compared to zinc and cadmium coatings. The mass loss due to wear enhanced corrosion was less with Zn-Ni than with Zn and Cd coatings. Zn-Ni coatings are a suitable replacement to Cd coatings when the surfaces are subjected to simultaneous wear and corrosion.

Zn-Ni coatings had higher polarization resistance after the 24 hour immersion tests compared to zinc and cadmium coatings. Zn-Ni coatings offer better sacrificial corrosion protection because of low corrosion rates, and are a suitable replacement for Cd coatings. The Passivated Zn-Ni coatings showed lower corrosion resistance when heat treated due to localized damage of passive films while there was no effect of heat treatment on corrosion resistance of as plated Zn-Ni coatings.

During the electrodeposition of metals, hydrogen is evolved due to electrolysis. The evolved hydrogen may diffuse outward and become trapped in the substrate/coating interface or migrate inward into the steel lattice causing delayed embrittlement when the component is subjected to stress. This study reports two principal variables for Zn, Zn-Ni, and Cd coatings: (i) quantity of hydrogen absorbed by the coating and substrate, by vacuum thermal desorption (ii) permeability of the coating material to hydrogen, by electrochemical permeation. The findings were analyzed in correlation with microstructural characteristics of both the coating material and the coating/substrate interface. With Zn-Ni, both coating process and coating material combined to significantly reduce the risk of internal hydrogen embrittlement by: (i) introducing the least amount hydrogen during the electrodeposition process, and (ii) by the ease with which hydrogen can be extracted by baking due to the presence of cracks in the coating.

Keywords: Zn-Ni, Cd, Cd-Ti, Zn, EIS, insitu tribology, tribocorrosion, hydrogen permeation, TDS

Résumé

Les revêtements métalliques sacrificiels à base de zinc et cadmium sont utilisés pour protéger les composants en acier contre la corrosion. Les préoccupations environnementales et de la santé ont limité l'utilisation du cadmium car les bains de d'électrodéposition au Cd sont normalement à base de cyanure et en plus le Cd est cancérigène. Cette thèse examine le revêtement Zn-Ni pour remplacer le Cd et les revêtements à base de Cd pour utilisation dans l'industrie aérospatiale, ainsi que pour remplacer le Zn dans l'industrie automobile. Les caractéristiques étudiées sont les propriétés tribologique, la résistance à la corrosion et la tribocorrosion, ainsi que la susceptibilité à la fragilisation par l'hydrogène.

La tribométrie *in situ* a révélé que les revêtements Zn-Ni on une résistance supérieure à l'usure adhésive par rapport aux revêtements cadmium. La micro-dureté des revêtements Zn-Ni était plus élevé que les celle des revêtements Zn et Cd. La dureté de la piste d'usure des revêtements Zn-Ni témoigne la formation d'une tribo-couche écrouie.

Les revêtements Zn-Ni ont une plus grande résistance à polarisation après l'essai d'usure comparés aux revêtements Zn et Cd. La perte de masse due à l'usure améliorée à la corrosion était moins que pour les revêtements Zn et Cd. Les revêtements Zn-Ni sont un substitut approprié pour les revêtements Cd lorsque les surfaces sont soumises à l'usure et la corrosion simultanée.

L'effet du traitement thermique et de la passivation au chrome trivalent sur la corrosion des revêtements Zn-Ni est également décrit. Les revêtements Zn-Ni démontrent une plus grande résistance à la polarisation lors des essais d'immersion comparés aux revêtements Cd. Les revêtements Zn-Ni offrent une meilleure protection à la corrosion sacrificielle en raison des faibles taux de corrosion, et sont de ce point de vue un substitut approprié de revêtements Cd.

Au cours de l'électrodéposition de métaux, l'hydrogène se dégage par électrolyse. L'hydrogène peut soit diffuser vers l'extérieur et se piéger à l'interface entre le substrat en acier et le revêtement, soit migrer vers l'intérieur dans l'acier provoquant une fragilisation retardée lorsque le composant est soumis à une contrainte. Cette étude rapporte deux variables principales pour le Zn, Zn-Ni, et les revêtements Cd: (i) la quantité d'hydrogène absorbé par le revêtement et le substrat, mesurée par désorption thermique sous vide, et (ii) la perméabilité du matériau de revêtement à l'hydrogène, mesurée par perméation électrochimique. Les résultats sont analysés en corrélant les caractéristiques de la microstructure du matériau de revêtement et de l'interface entre le revêtement et le substrat en acier. Pour le Zn-Ni, le procès de revêtement ainsi que le matériau de revêtement, ensemble diminuent le risque de fragilisation par l'hydrogène en: (i) introduisant une quantité minimum d’hydrogène lors du processus d'électrodéposition, et (ii) par la facilité avec laquelle l'hydrogène peut être extrait par traitement thermique grâce à la présence de fissures dans le revêtement.

Mots-clés: Zn-Ni, Cd, Cd-Ti, Zn, tribologie in situ, tribocorrosion, perméation de l'hydrogène.

Contribution of Co-Authors

The dissertation presented here is in manuscript format, with each chapter based on a published journal article or manuscript to be submitted as a journal article. The full bibliographic citations of the papers presented in this dissertation are as follows:

Chapter 3

K. R. Sriraman, H. W. Strauss, S. Brahimi, R. R. Chromik, J. A. Szpunar, J. H. Osborne and S. Yue, Tribological behavior of electrodeposited Zn, Zn–Ni, Cd and Cd–Ti coatings on low carbon steel substrates, Tribology international 56 (2012), 107-120.

In this article I, Sriraman K Rajagopalan, as the first author did the experiments and wrote the manuscript. H. W. Strauss was my fellow graduate student who helped me in conducting experiments with in-situ tribology. S. Brahimi gave an analysis of the work from an industrial perspective. Prof. Chromik was the expert tribologist who provided technical support and supervision in this particular project and helped me a great deal with his suggestions and ideas to write this manuscript. Prof. Stephen Yue was the group leader and my thesis advisor. Prof. Jerzy Szpunar was my co-advisor. Dr. Joseph Osborne was the industrial sponsor from Boeing Research & Technology, Seattle USA, who provided aerospace perspective, as well as specimens. All the Co-Authors provided valuable suggestions and comments and reviewed the manuscript before submission.

Chapter 4

K. R. Sriraman, S. Brahimi, J. A. Szpunar, J. H. Osborne & S. Yue, Tribocorrosion behavior of electrodeposited Zn, Zn-Ni, Cd and Cd-Ti coatings on low carbon steel substrates, Article to be submitted to the journal Surface & Coatings Technology, Elsevier Publications.

Chapter 5

K. R. Sriraman, S. Brahimi, J. A. Szpunar, J. H. Osborne & S. Yue, Corrosion behavior of electrodeposited Zn, Zn-Ni, Cd and Cd-Ti coatings on low carbon steel substrates, Article to be submitted to the journal of Coatings Research & Technology, Springer publications, New York.

The two articles in chapter four and five, as the first author myself, Sriraman K. Rajagopalan, conducted all the experiments analyzed the results and wrote the research article. S. Brahimi gave an analysis of the work from an industrial perspective. Prof. Stephen Yue was the group leader and my thesis advisor. Prof. Jerzy Szpunar was my co-advisor. Dr. Joseph Osborne was the industrial sponsor from Boeing Research & Technology, Seattle USA, who provided aerospace perspective, as well as specimens. All the co-authors provided valuable suggestions comments and reviewed the manuscript before submission.

Chapter 6

K. R. Sriraman, S. Brahimi, J. A. Szpunar & S. Yue, Hydrogen embrittlement of Zn, Zn-Ni and Cd coated high strength steel. Article to be submitted to the journal of Material Science & Engineering A, Elsevier publications.

In this article as the first author myself, Sriraman K. Rajagopalan conducted the experiments analyzed the results and wrote this manuscript. S. Brahimi gave an analysis of the work from an industrial perspective. Prof. Stephen Yue was the group leader and my thesis advisor. Prof. Jerzy Szpunar was my co-advisor. All the co-authors provided valuable suggestions comments and reviewed the manuscript before submission.

Acknowledgements

Completion of the PhD program has been the most challenging task so far in my life. I would like to individually acknowledge everyone who helped me sail this journey, but due to lack of space I have mentioned most important personnel at McGill University who had helped me in completing my research.

First and foremost I would like to express my heartfelt gratitude to my thesis supervisor Prof. Stephen Yue for his invaluable guidance, encouragement and support during the course of this research program. I am indebted to him for his knowledge sharing in research approach, and the liberty he gave me in pursuing my research.

I am grateful to Prof. Jerzy Szpunar for his guidance and supervision. I would like to express my gratitude to him for allowing me to utilize his research facilities, which helped me in gaining expertise in various experimental techniques.

I express my gratitude to Mr. Salim Brahimi, my research program manager for his guidance, moral support, mentoring and providing industrial insight to the research program.

A special thanks to Prof. Richard Chromik for his contributions and suggestions in experimental techniques during the course of this research.

I wish to extend my warmest regards to my friends Dr. Kiran Kumar, Dr. Raghavendran, Dr. Guru Venkat, Manas Paliwal, and Venkat Veer for their unconditional support. Their wits and jests made life at McGill memorable. I also extend my gratitude to my colleagues Dr. Majid Hoseini, Dr. Muhammad Arafin and Holger Strauss for their help in conducting experiments and scientific discussions.

I also wish to acknowledge my industrial sponsors, Boeing Research & Technology, for their technical and financial support, and Natural Sciences and Engineering Research Council of Canada (NSERC) for financial support.

Last but not the least I am indebted to my parents and brother for their unconditional love and support during the course of this research. I have no words to describe the affection; support and patience showered by my wife Ramya, bearing with all my idiosyncrasies during the torrid times and bestowing me the best gift of my life our son Atul.

Table of Contents

List of Figures

List of Tables

Chapter 1 Introduction

1.1 General background

Sacrificial metallic coatings, such as those based on Zn and Cd are used to protect steel components against corrosion. Zinc is used in automotive applications, but Cd coatings are at present used in defense and aerospace industries owing to its superior sacrificial protection capabilities. Growing environmental and health concerns led to the formation of stringent regulations, which has limited the use of Cd in any form, since Cd plating bath is cyanide based and Cd compounds are carcinogenic. These limitations have led to the development of environmental friendly Zn based alloy coatings namely Zn-Ni, Zn-Fe, Zn-Co, Zn-Al [1] and Zn-Fe-Co [2, 3]. Of all these coatings Zn-Ni alloys have been found to be the most attractive one to replace Cd because of its superior corrosion resistance [4-8], hardness [9-11] thermal stability [9, 12] and wear resistance [13].

In the aerospace industry Cd is currently used in electrical connectors, landing gear structures and in fasteners to impart superior corrosion resistance. In the particular case of fasteners, the coating should possess sufficient wear resistance to withstand the torque and should have enough galling resistance during the tightening process. Even though extensive investigations have been carried out on the Zn-Ni alloys with respect to hardness and sliding wear resistance, in depth analyses of contact conditions, wear debris formation, transfer film formation and third body contributions in friction and wear of metallic coatings have not been thoroughly performed. Both Zn–Ni- and Cd-based coatings have been investigated in the past [13-15] using conventional pin on disc or sliding cylinder experiments, with any insight on the wear mechanisms inferred from *ex situ* techniques. Hence there is a need for *in situ* tribometry technique developed to probe the interface between the contact surfaces, to study the interface chemistry and role of third bodies in friction and wear behavior of coatings.

Corrosion resistances of Zn-Ni and Cd coatings have been well documented in the literature [4-8]. Both the coatings protect the steel anodically by sacrificial corrosion protection. Even though both the coatings have been studied by various techniques for corrosion resistance determination such as polarization curves, salt spray testing, electrochemical impedance spectroscopy (EIS) etc., the available literature on the performance of Zn-Ni and Cd coatings on similar coating thicknesses and testing parameters is limited. Surface engineering of a coating is not limited to basic parameters like micro hardness, wear resistance and corrosion resistance of a coating. In practical applications, for example coatings in aerospace landing gear, coatings are subjected to simultaneous action of wear and corrosion. Thus there is a necessity to evaluate these coatings for tribocorrosion performance.

Both Zn-Ni and Cd coatings are applied on the steel components by electrodeposition process. Apart from the corrosion and wear resistance of the coating, the coating process should not make the substrate material susceptible to hydrogen embrittlement. The hydrogen uptake during the plating processes by Zn-Ni and Cd coatings has been investigated [3] in the past, but the actual permeability of the coating to co-evolved hydrogen is still not quantified. Also the amount of hydrogen generated by the coating process has not been well documented. Defects such as pores, discontinuities and microcracks present in the coatings owing to the plating processes may facilitate the escape of co evolved hydrogen. These defects may also affect the effective hydrogen permeability of the coated steel. These are important factors to be understood to characterize a coating for its complete performance.

1.2 Objectives

The current research provides insight on how Zn-Ni coating can act as a replacement for Cd coatings by understanding of friction and wear resistance, corrosion and tribocorrosion resistance, and hydrogen embrittlement susceptibility of the plating process. The objectives of this research is listed below

1. To utilize *in situ* tribology technique, *to* evaluate the wear resistance of Zn-Ni, Zn, and Cd coatings. To understand friction and wear mechanism of the coatings and to provide insight on the contact conditions, transfer film and wear debris formation and the contribution of third bodies in metallic friction and wear
2. To understand the tribocorrosion resistance of Zn-Ni, Zn and Cd coatings in 3.5 % NaCl solution. Evaluation of wear enhanced corrosion of the coatings in impressed anodic potentials. Understanding the nature of wear enhanced corrosion by electrochemical impedance spectroscopy (EIS).
3. Evaluation of corrosion resistance of Zn-Ni, Zn and Cd coatings under identical testing conditions and similar coatings thicknesses. Determination of long term corrosion resistance by potentiodynamic polarization and EIS. Correlation of the corrosion resistance of the coatings with the microstructure. Effect of heat treatment of Zn-Ni coatings on the corrosion resistance.

4. To understand how much the plating process makes the substrate steel susceptible to hydrogen embrittlement by understanding the hydrogen permeability of the coatings, amount of hydrogen generated during the plating process and the role of defects and microcracks developed in the coating by the plating process on the hydrogen permeability of the coating.
5. To develop clear understanding of experimental results and various behavioral mechanisms of Zn-Ni coatings to determine its suitability as a replacement for Cd in industrial applications and also optimization of Zn-Ni coating performance.

1.3 Dissertation format

The research performed in this dissertation has been published or communicated as a research article in peer-reviewed scientific journals.

Chapter 1: covers the basic information about Zn-Ni and Cd coatings, their properties and applications in aerospace industries. As each individual chapter contains an introduction section this chapter was intentionally kept short

Chapter 2: gives extensive review of current available literature. The intention of literature review is to provide information on the coating characteristics, microstructure, mechanical properties, thermal stability, wear and corrosion resistance and hydrogen embrittlement studies. The literature review is followed by four chapters containing the journal articles (one published and three to be submitted).

Chapter 3: contains an article published in the Journal of *Tribology international,* titled "Tribological studies of electrodeposited Zn, Zn-Ni, Cd and Cd-Ti coatings on low carbon steel substrates". This paper analyzes the tribology of Zn, Zn-Ni and Cd coatings. The role of third bodies and transfer film was understood in friction and wear behavior of these coatings.

Chapter 4: contains an article to be submitted to the Journal of *Surface & Coatings Technology,* entitled "Tribocorrosion behavior of electrodeposited Zn, Zn-Ni, Cd and Cd-Ti coatings on low carbon steel substrates. This paper investigates the synergy of wear and corrosion of the coatings. The paper also investigates wear enhanced corrosion of the coatings under anodic impressed potentials. The corrosion resistance of the coatings during wear was determined by EIS technique.

Chapter 5: contains an article to be submitted to the Journal of *Coatings Research & Technology,* entitled "Corrosion behavior of Zn, Zn-Ni, Cd and Cd-Ti electrodeposited on low carbon steel substrates". In this chapter the corrosion resistances of the coatings were determined by potentiodynamic polarization method and the EIS. The corrosion resistances of the coatings were correlated to the coating microstructure. The effects of passivation and heat treatment on corrosion resistances of Zn-Ni coatings were investigated.

Chapter 6: contains an article to be submitted to the Journal of *Material Science & Engineering A,* entitled "Hydrogen embrittlement of Zn, Zn-Ni and Cd coated high strength steel". The chapter describes the hydrogen embrittlement susceptibility of the coating process to the steel substrate by determining the amount of hydrogen generated during the coating process. The hydrogen permeability of the coatings was determined. The effect of coating defects on permeability of hydrogen was also investigated.

Chapters 7 & 8: contain the conclusions of this work and the contribution to original knowledge respectively.

References

[1] Winand R. Electrodeposition of Zinc and Zinc Alloys. Modern Electroplating: John Wiley & Sons, Inc.; 2010. p. 285-307.

[2] Hillier EMK, Robinson MJ. Hydrogen embrittlement of high strength steel electroplated with zinc-cobalt alloys. Corrosion Science. 2004;46:715-27.

[3] Hillier EMK, Robinson MJ. Permeation measurements to study hydrogen uptake by steel electroplated with zinc-cobalt alloys. Corrosion Science. 2006;48:1019-35.

[4] Alfantazi AM, Erb U. Corrosion properties of pulse-plated zinc-nickel alloy coatings. Corrosion. 1996;52:880-8.

[5] Barceló G, Sarret M, Müller C, Pregonas J. Corrosion resistance and mechanical properties of zinc electrocoatings. Electrochimica Acta. 1998;43:13-20.

[6] Park H, Szpunar JA. The role of texture and morphology in optimizing the corrosion resistance of zinc-based electrogalvanized coatings. Corrosion Science. 1998;40:525-45.

[7] Wilcox GD, Gabe DR. Electrodeposited Zinc Alloy Coatings. Corrosion Science. 1993;35:1251-8.

[8] Lambert MR, Hart RG, Townsend HE. Corrosion mechanism of Zn-Ni alloy electrodeposited coatings. Proceedings - Society of Automotive Engineers. Dearborn, MI, USA: SAE; 1983. p. 81-7.

[9] Alfantazi AM, Erb U. Microhardness and thermal stability of pulse-plated Zn-Ni alloy coatings. Mat Sci Eng a-Struct. 1996;212:123-9.

[10] Brooks I, Erb U. Hardness of electrodeposited microcrystalline and nanocrystalline gamma-phase Zn-Ni alloys. Scripta Mater. 2001;44:853-8.

[11] Bruet-Hotellaz, Bonino JP, Rousset A, Marolleau, Chauveau E. Structure of zinc-nickel alloyelectrodeposits. Journal of Materials Science. 1999;34:881-6.

[12] Bories C, Bonino JP, Rousset A. Structure and thermal stability of zinc-nickel electrodeposits. J Appl Electrochem. 1999;29:1045-51.

[13] Panagopoulos CN, Georgarakis KG, Agathocleous PE. Sliding wear behaviour of Zinc-Nickel alloy electrodeposits. Tribol Int. 2003;36:619-23.

[14] Jahanmir S, Abrahamson EP, Suh NP. Sliding Wear-Resistance of Metallic Coated Surfaces. Wear. 1976;40:75-84.

[15] Jahanmir S, Suh NP, Abrahamson Ii EP. The delamination theory of wear and the wear of a composite surface. Wear. 1975;32:33-49.

2.0 Literature Review

The literature review is split into different sections namely 1) Zn-Ni alloy plating process: this section discusses about the various plating procedures followed in the literature 2) microstructure, phase, composition of Zn-Ni alloy electrodeposits 3) hardness and thermal stability of Zn-Ni alloy electrodeposits 4) Corrosion behavior of Zn-Ni electrodeposits 5) Tribocorrosion resistance: basic methodology and various approaches utilized to understand tribocorrosion evaluation of materials 6) *In-situ* tribology: an overview of *in situ* tribology approach and how this method has been successfully utilized to understand tribology of coatings 7) Hydrogen permeability in Zn-Ni and Cd electrodeposits 8) Vacuum thermal desorption of hydrogen: how thermal desorption spectrometry approach is utilized to quantify hydrogen embrittlement susceptibility of material or the plating process. All the alloy compositions in this section are reported in wt. % unless stated otherwise.

2.1 Zn-Ni Plating Process

For decades Zn has been used to protect steel by sacrificial corrosion. Due to the modern industrial demands for a better corrosion resistant product, with longer life, and stringent environmental regulations led to the development of Zn based alloys. Just like pure Zn, Zn-Ni alloy can be electroplated on to the steel substrate from both acid based and alkaline plating solutions. A standard industrial practice to electroplate components is Rack and Barrel plating [1].

Barrel plating is a process where components are put in a bulk in a large rotating barrel with the plating solution contained inside and the lining of the barrel acts as the anode. Barrel plating procedures are performed for smaller components. Rack plating is usually performed for components with larger length and diameters. Components are placed on individual racks /fixtures with individual connections and then electroplated. Midway through the electroplating cycle the racks are repositioned so that build up of layer on one direction can be avoided. Typical Zn-Ni plating conditions for both acidic and alkaline plating baths are shown in Table 2.1 below[2].

Table 2.1 Acid and Alkaline Zn-Ni plating bath compositions [2]

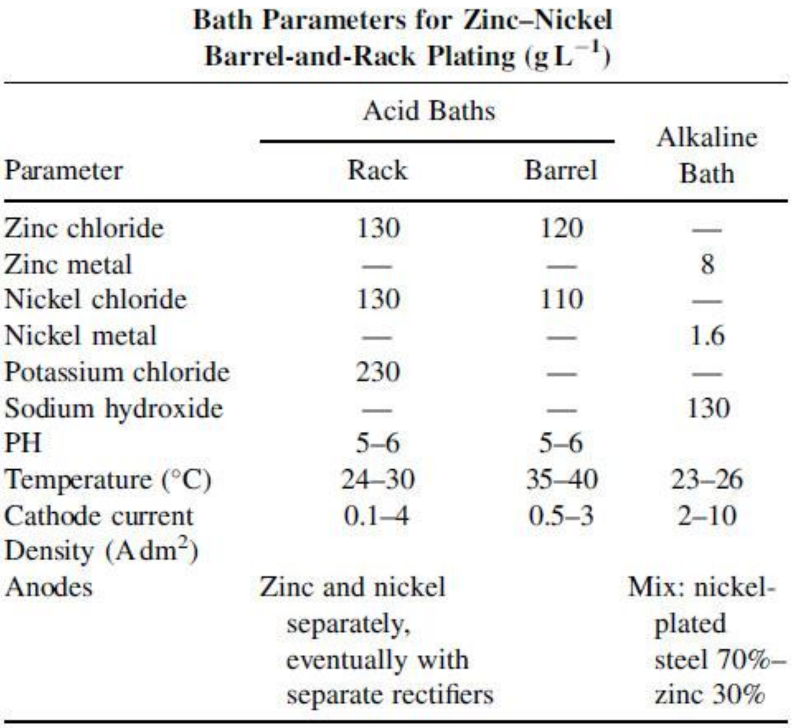

Bath Parameters for Zinc–Nickel Barrel-and-Rack Plating (g L^{-1})

Parameter	Acid Baths		Alkaline Bath
	Rack	Barrel	
Zinc chloride	130	120	—
Zinc metal	—	—	8
Nickel chloride	130	110	—
Nickel metal	—	—	1.6
Potassium chloride	230	—	—
Sodium hydroxide	—	—	130
PH	5–6	5–6	
Temperature (°C)	24–30	35–40	23–26
Cathode current Density (A dm^2)	0.1–4	0.5–3	2–10
Anodes	Zinc and nickel separately, eventually with separate rectifiers		Mix: nickel-plated steel 70%–zinc 30%

Even though both acid and alkaline plating baths are available, the alkaline plating baths are preferred in various industrial applications. The reason behind this preference is the uniform thickness distribution obtained from the alkaline plating procedures and also the resultant microstructure. The uniform columnar microstructures of the platelets that are obtained from an alkaline plating bath are preferred to the lamellar microstructure obtained from the acid bath if the component has to be formed after electroplating [2].

2.2 Microstructure, Phase and Composition of Zn-Ni electrodeposits

The structure of Zn-Ni electrodeposits differ from the conventional hexagonal close packed structure (HCP) of Zn. Several investigations that have been carried out have revealed that there is a phase transformation in Zn-Ni alloys with respect to composition [3-6]. It was reported by Bruet et al. [5] and Bories et al. [4] that the phases obtained from electrodeposition in Zn-Ni alloys are different from the equilibrium phase diagram. The corresponding interpretation is given in Figs. 2.1 a and b.

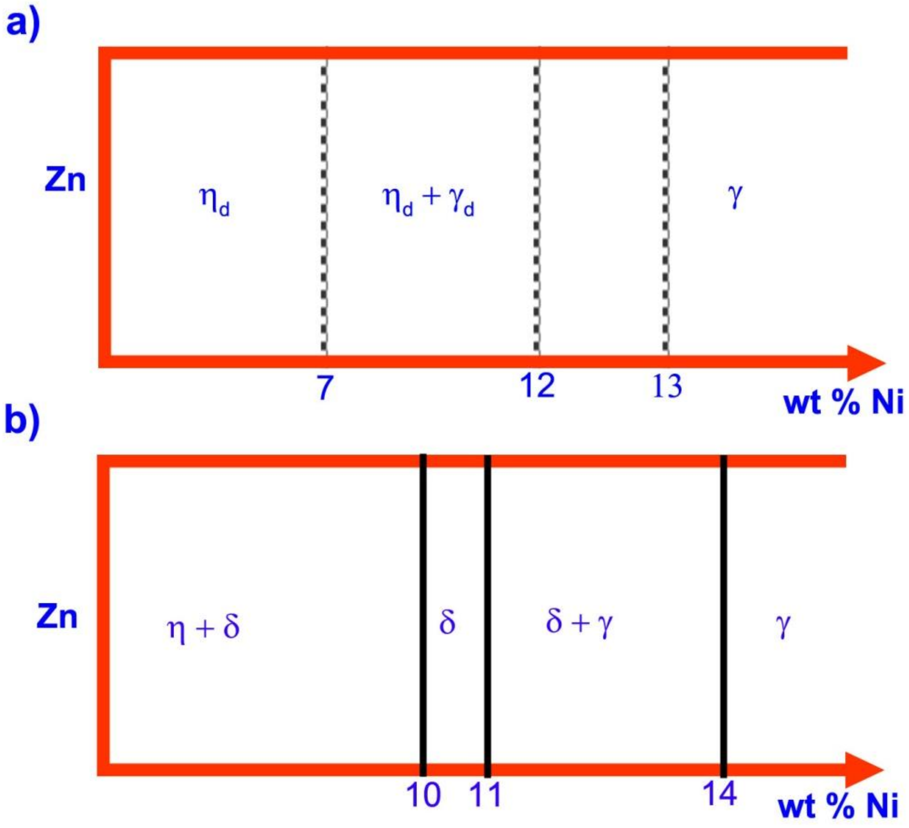

Fig. 2.1 Phases obtained in Zn-Ni alloys by (a) electrodeposition process [4, 5] and (b) from equilibrium phase diagram (details see paragraph 1 page 11 and 12) [5]

During electrodeposition of Zn-Ni, the crystal structure remains as HCP from 0-7% Ni. The addition of Ni in the Zn matrix modifies the Zn lattice by decreasing the 'c' axis rapidly and increasing the 'a' axis slowly. As seen in Fig. 2.1 (a), on the Zinc rich side a solid solution (η_d phase) is formed where the maximum solubility of Ni is 7.4. When the composition of the alloy reaches 7.4% Ni, a cubic, non-stoichiometric, intermetallic phase, γ_d is formed. In this two phase region further addition of Ni in Zn matrix increases the volume fraction of the γ_d phase which has maximum solubility of Ni at 12.5%. From Ni

12 to 13%, the γ_d and γ phases co-exist. When the Ni content is increased beyond 13 % the lattice parameter decreases to the value corresponding to the equilibrium phase diagram, which is designated as γ. The incorporation of Ni in Zn matrix also resulted in the change of surface morphology of the coatings [4-6]. The pure Zn morphology resulted in an agglomeration of random hexagonal platelets with larger grain morphology. Alloying pure Zn with 2.8 % Ni causes the substitution of Zn atoms with Ni which results in smaller grain size with isotropic shapes in the coating microstructure. As the Ni content in the deposit increased, to 7.4 %, the shape of the grains changed to hexagonal, owing to change in orientation in pyramidal planes. Further increase in Ni content to 13 % resulted in fine grain structure and an even distribution of platelets with reduced surface roughness and more surface coverage.

2.3 Microhardness and Thermal Stability of electrodeposited Zn-Ni alloys

The compositional variation in microhardness of Zn-Ni alloys has been investigated by various researchers [3, 6-8]. Zn-Ni alloys are harder than pure Zn. As noted above, the Zn-Ni phases obtained through electrodeposition were different from the ones predicted by thermodynamic equilibrium. The compositions obtained through electrodeposition were also non stoichiometric in nature. The microhardness of the coatings varied with the addition of Ni. The hardness varied from 80- 120 VHN for Zn-Ni up to 4 % Ni [6-8]. The hardness increased to 180 VHN for 8-9% Ni, and 375 -450 VHN for Zn-15% Ni. When the Ni content in the deposit was increased to more than 20%, the hardness values stabilized at 500 -525 VHN [7]. Various reasons were proposed for the increase in hardness for the Zn-Ni alloys. Alfantazi and Erb [7], suggested that the increase in hardness could be due to solid solution strengthening (in the η region) owing to the Ni addition and also due to Hall-Petch strengthening (in the γ region) owing to the grain size refinement. Brooks and Erb [8] suggested that the major reason for increase in hardness beyond 9% Ni was not due to grain size refinement alone. Since the γ phase in Zn-Ni alloys has a solubility between 10-15 % Ni, the reason for increase in the hardness in single phase alloys was due to the formation of nonstochiometric γ phase over wide range of composition.

Thermal stability of Zn-Ni alloys were investigated by Bories et al. [4], Bruet et al. [5] and Alfantazi et al. [7]. Bories and Bruet et al. investigated the thermal stability of the alloys ranging from 2.5 % Ni till 13 wt % Ni. The alloys were heat treated at 200 and 300 °C. For the alloys containing less than 6.5 % Ni, no change was reported in the phase formation. Alloys containing the distorted η_d and γ_d transformed to more stable δ and γ phase. For single phase alloys which had γ phase in the composition range of 12 – 13 % Ni no structural or phase changes were reported, indicating the stability of the γ phase at compositions beyond 13 % Ni. Alfantazi and Erb [7] also confirmed the results reported by Bories and Bruet et al. They reported that the microcrystalline Zn - 14 % Ni γ phase alloy was stable for 24 hrs at 200 °C. Extensive grain coarsening was observed for nanocrystalline Zn-55% Ni alloy within minutes when exposed to electron beam irradiation in a TEM.

2.4 Corrosion behavior of Zn-Ni alloy coatings

Corrosion behavior of Zn-Ni alloys was investigated by different types of techniques, namely the polarization method, measurement of OCP, long term immersion technique and the electrochemical impedance spectroscopy. Tian et al. [9] and Gavrila et al. [9] compared the corrosion resistance of Zn-Ni alloys with Cd and Cd-Ti coatings. Tian et al. compared the corrosion reisistance of Zn-Ni coatings prepared from the acid chloride bath with Ni contents varying from 6 – 15 %. Salt spray chamber testing and measurement of open circuit potentials were utilized to estimate corrosion resistance. It was concluded that Zn-12% Ni coating provided excellent corrosion resistance compared to Cd, Cd-Ti and Zn coatings in salt spray testing. Apart from the presence of stable γ phase, the reason attributed to the higher corrosion resistance was the presence of a Ni enriched surface layer, which stabilized the Zn(OH) as the corrosion product, as opposed to the ZnO as the corrosion product, which prevented further corrosion of underlying coating layer.

Gavrila et al. compared both acidic and alkaline Zn-Ni to Cd and Zn coatings by polarization techniques and OCP measurements. It was concluded that the corrosion protection offered by the Zn-Ni alloys depends on the Ni content and the microstructure. Long term immersion tests proved to be severe on the coatings, leading to formation of localized cracking on the surface. It was observed that localized corrosion with appearance of surface cracking is the predominant mechanism of corrosion in Zn-Ni alloys while Cd coatings showed more uniform corrosion. Additional protection layers such as application of black chromate passive films, with or without heat treatment [10, 11] and crystalline phosphate films [12] were observed to be improve the corrosion resistance of Zn-Ni coatings two to three times than the original coating alone.

Zn-Ni coatings obtained from acid and alkaline plating baths, with Ni content ranging from 7 -12 % , from both rack and barrel plating procedures were also studied [13]. It was reported that corrosion resistance of the Zn-Ni coatings was higher than Zn coating when tested in salt spray chamber and in immersion tests in neutral solutions. Zn-Ni coatings showed poor performance in aerated acidic solution due to lower over voltage for hydrogen reduction present on the Ni enriched surface. Also the corrosion resistances of the coatings were correlated to structural homogeneity of the coating; extensive localized cracking resulted in poor corrosion resistance.

Zn-Ni containing 14-20% Ni (γ phase), was studied by Alfantazi and Erb [14] and Sitari et al. [15]. Alfantazi and Erb reported that the chemical composition, grain size and phase formation was mainly responsible for the corrosion resistance of Zn-Ni coatings. Among different compositions of Ni in Zn the γ Zn-Ni with Zn 14-20% Ni possessed superior corrosion resistance in salt spray chamber testing compared to those of pure Zn and galvanealed coatings. Siitari et al. found that in Zn-Ni alloys with more than 8% Ni, localized corrosion occurred during salt spray chamber testing. Zn-13 % Ni coating possessed maximum resistance to red rust owing to the presence of a thin and closely spaced distributed crack network. Distributed crack networks were reported to be responsible in spreading the anodic reactions throughout the coating layer, thereby preventing localized corrosion and increasing the life of the coating. Large microcracks were observed for coatings with Ni contents as high as 20%. The reason could be attributed to the presence of higher tensile residual stresses due to the plating process. It was suggested that optimal plating conditions and crack network distribution could lead to higher corrosion performance.

The crack network distribution was also investigated by Miranda [16] by electrochemical impedance spectroscopy (EIS). Long term immersion tests as long as three years were carried out for Zn and Zn-Ni (14 % Ni) alloys and then the corrosion resistance was tested by EIS. It was concluded that Zn-Ni alloys had higher corrosion resistance than the Zn coating and the corrosion mechanisms for both the coatings were completely different. It was reported that the Ni enrichment and barrier layer formation by corrosion products had limited effect on corrosion resistance. The main mechanism for corrosion resistance in Zn-Ni coatings was formation of distributed crack network during the corrosion of the coating increased the protective capability of the coating.

2.5 Tribocorrosion evaluation of materials

Tribocorrosion studies are undertaken for designing new surfaces in future equipments and processes by minimizing operating costs. Tribocorrosion research is undertaken to address surface degradation when the surfaces are subjected to simultaneous action of wear and chemical / electrochemical processes [17]. Marine applications where tribocorrosion is significant include fluid handling equipments. Automotive applications include valves, cylinder linings, bearings, and brake linings. Tribocorrosion in cylinder linings in diesel engines lead to particle generation and increased pollution [18]. Food processing industries encounter tribocorrosion issues in mixers, extruders pipes etc. In biomedical applications, implants which are subjected to tribocorrosion damage leads to debris generation, inflammation of tissues and final rejection of the implant [19] [20].

Different types of tribocorrosion tests that are followed are [18-21]

1. Galvanic Cells
2. Measurement of open circuit potentials (OCP)
3. Potentiostatic techniques
4. Potentiodynamic studies
5. Electrochemical impedance spectroscopy before and after wear.

In galvanic cell method the galvanic current during wear is monitored by the ammeter. A reference sample is galvanically coupled to the sample which is wearing. Both of same material and the circuit is completed with an ammeter to measure the current. It is a semi quantitative method and helps in comparing the galvanic couples. Absolute determination of corrosion volume is not possible by this method.

The measurement of open circuit potential during sliding or wear is a very simple technique which helps in monitoring the surface states of the sliding material but this technique cannot define the kinetics of corrosion reaction. During rubbing or sliding the measured corrosion potential reflects the galvanic coupling of two distinct surface states of the metal i.e. the unworn area and worn area exposed to the solution by abrasion of the passive film. Ponthaiux et al. [21]

found that the corrosion potential of active metals is not significantly affected by rubbing since the worn and unworn areas exhibit similar surface states.

Parameters affecting the open circuit potentials are

1. Intrinsic corrosion potential of the worn and unworn areas
2. Ratio between the area of worn and unworn areas
3. The relative position of worn and unworn areas
4. Kinetics involved in the corrosion reactions

In the potentiostatic method an over potential (anodic or cathodic) is applied to the working electrode which is the material of interest in the sliding condition in a three electrode electrochemical cell. The resultant current flowing in the circuit is measured by the potentiostat. Anodic overpotential is commonly impressed in the sliding material to determine the corrosion current during wear. Interestingly the current flowing through the material during wear is through the wear track area which is predominantly smaller compared to the unworn area. The measured current is the sum of both cathodic and anodic current but at anodic overpotentials the cathodic current is negligible, hence the measured current is the anodic current which translates to the corrosion current.

$$m = \frac{I * M * t}{n * F}$$

m = mass of the metal oxidized in time t, M = molar mass of the sliding material
t = sliding time n= oxidation valence F= faradays constant

Mass loss due to wear enhanced corrosion is determined by integrating current transient plot determined during sliding, assuming that the current is completely anodic and it flows through the active wear track area. The disadvantage of this method is to determine the exact oxidation state of the metal during corrosion. For pure metals with known oxidation state the method is very good but for alloys with unknown oxidation states it becomes difficult the determine the mass of metal corroded due to wear enhanced corrosion. Besides measuring wear enhanced corrosion it helps in simulating various corrosion conditions like presence of oxidizing agents in corroding media. By applying anodic overpotential the wear tests are done to simulate the actual material / component wear in aggressive solutions containing oxidizing agents.

In potentiodynamic studies, a constant potential sweep using function generator in a potentiostat, is applied to the material during wear test. This method monitors the effect of sliding on the electrochemical reactions at different potentials. The major limitation of this technique is that the effect of potential sweep on electrochemical reactions is proportional to the ratio of worn and unworn areas. If the ratio was found to be low then the effect of potential sweep was found to be negligible. Time dependent wear transition mechanisms interfered with the potential sweep rendering this method rather useless.

As compared to the other techniques which are DC (direct current) based electrochemical impedance spectroscopy (EIS) approach is where the material behavior is examined by impressing an AC (alternating current) potential on the working electrode which is the specimen of interest and then studying the current through the cell. The resistance offered by the material to this AC current flow is called the impedance. This impedance has both the real and imaginary systems and it is translated to Nyquist and Bode plots which are used in conjunction with equivalent electrical circuits to derive charge transfer or the polarization resistance, and the double layer capacitance offered by the material

[22, 23]. With the help of EIS it is possible to determine the intermediate species which are absorbed during the tribocorrosion process and it can be used as a tool to determine the reaction mechanisms and kinetics before and after the wear tests [21].

Various tribocorrosion methods were used by different researchers to investigate variety of metals and coatings in different environments. M. Azzi et al. [24] studied tribocorrosion behavior in DLC (Diamond like carbon) coated 316 stainless steel, with an intermediate nitride layer as a bond coat and a modified SiN*x*:H layer, in a simulated body fluid environment. This coating combination was suggested as a potential candidate for biomedical implants. With the help of open circuit potential measurements and EIS before and after wear, they were able to determine that SiN coated stainless steel processed better tribocorrosion resistance in simulated body fluid environment due to its higher infiltration resistance and also prevented the interface detachment during sliding.

M. Azzi et al. [25] also investigated the tribocorrosion behavior of magnetron sputtered CrSiN coating on 301 stainless steel in 1% NaCl solution. The CrN based hard have capabilities to be used in aerospace and automotive applications. In this study the effect of pre deposition nitriding of the steel surface on the tribocorrosion behavior of the coatings were evaluated by tribocorrosion tests at OCP and impressed anodic and cathodic potentials. It was demonstrated from the experiments that electrochemical reactions at the interface during the wear tests was responsible for coating layer detachment during the tests. It was also concluded that the coating layer detachment was avoided at cathodic potentials when the reactions were suppressed. Nitriding of the steel before coating deposition was observed to be detrimental to tribocorrosion behavior as nitriding process created peculiar surface morphologies on the steel surface which facilitated the liquid infiltration.

A combination of different coating substrate subsystems like SiC and SiN hard coatings on stainless steels [26, 27], electrodeposited Ni based composite coatings on steel substrates [28, 29], passive oxide films on stainless steels [30] plasma nitrided Ni-Cr alloys [31] were performed by researchers. The coatings and substrate systems mentioned above are coatings which have electrode potentials nobler than the steel substrates which it protects. The bare materials investigated were stainless steels that develop a passive film which give cathodic protection to the substrate. The wear behavior of Zn-Ni coatings have been evaluated under dry sliding conditions [32] and corrosion behavior of the coating has been evaluated by various investigators mentioned in above sections. So far the synergy of wear and corrosion in sacrificial type coatings like Zn-Ni and Cd has never been undertaken.

2.6 *In situ* Tribology: Methods and evaluation of materials

When two solids are in sliding contact with each other transfer of material, debris and interfacial films are generated. These films are generated at the interface and are responsible for friction and wear characteristics of the sliding contacts. These interfacial films cannot be observed by conventional tribometry [33]. With the advent engineering applications in outer space and marine environments, development of solid lubricant coatings, chameleon coatings [34] were developed. These coatings are adaptive to different kinds of surface engineering requirements providing higher hardness, superior mechanical properties in contact conditions with lower friction coefficients and inherent solid lubrication behaviors. Characterization of their tribological behavior requires an approach which is adaptive with characterization techniques coupled with the conventional tribometry.

If microscopic analysis for observing the contact conditions and spectrometry for chemical analysis have to be performed *in situ* during the wear then the counter surface should be responsive to these techniques, i.e. the counter surface should be transparent [33, 35]. A typical example of *in situ* tribometer is shown in Fig. 2.2, where a transparent counter surface enables probing the interface with the help of a microscope generating the images and characterizing the contact conditions and interfacial film stability. Depending on the analysis requirements and the contact scales a tribometer can be custom made to perform microscopic, spectroscopic, thermo electric and interferometric analysis [33, 35]. A brief overview of various probing techniques available currently which are coupled *in situ* with a reciprocating tribometer, is listed in Fig. 2.3.

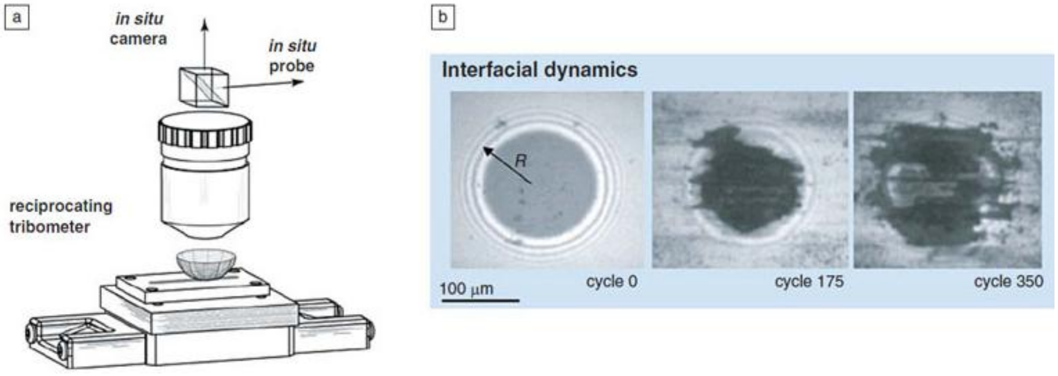

Fig. 2.2 (a) illustration of test configuration of insitu video microscopy through a transparent hemisphere (b) examples of interfacial films depicting various stages of film formation initial point contact with Newton rings, interfacial film formation followed by thinning and shearing of transfer films in real time [33]

Scharf and Singer [36] studied the role of third body contribution and transfer film formation in friction and wear behavior of diamond like carbon coatings (DLC) against sapphire and steel hemispheres with the help of a custom built *in situ* tribometer. The lowest friction coefficient was observed when an adherent transfer film was formed at the interface. The friction coefficient instability and eventually higher friction was observed when the transfer films were detached from the contact phase. The effect of environment on the friction and wear behavior of the DLC coatings like the humidity was also investigated by *in situ* approach. *In situ* Raman spectroscopy was performed by same investigators [37] to observe the transfer film formation, thickening and changes in the interface for DLC coatings.

Chromik et al. [38] studied the friction and wear behavior, interfacial sliding, transfer film plowing, localized deformation and transfer film shearing in a nanocomposite coating comprised of Yitria stabilized Zirconia (YSZ), Au, C and MoS_2 using an *in situ* tribology approach. Velocity accommodation modes and transfer film formation were identified and correlated with the environment (dry and humid conditions) and also the composition and mechanical properties of the coatings.

Dvorak et al. [39] studied the friction and wear behavior of boric acid and boron carbide coatings with *in situ* tribometry approach with a transparent hemisphere as a sliding counterface. The correlation between the transfer film formation, amount of solid lubricants generated and third body formation during friction and wear was established with the help of *in situ* tribometry and *in situ* Raman spectroscopy.

Strauss et al. [40] studied the friction and wear behavior of Ti-Si-C-N nanocomposite coatings using *in situ* tribometry approach with a transparent sapphire hemisphere as a counterface. The buried interface was examined with *in situ* video microscope and the transfer film formation and velocity accumulation modes were identified. It was reported from *in situ* tribometry approach, that the wear resistance of the coatings which formed stable transfer films were higher than the coatings which do not form stable transfer films regardless of their inherent mechanical properties.

All the investigations mentioned above were undertaken for coatings such as solid lubricant coatings, nanocomposite coatings, and diamond like carbon coatings which are optically responsive. So far metallic materials have never been studied by this approach since it was presumed that metallic materials would provide an opaque interface which would be difficult to examine by *in situ* methods. While many textbooks present a well established theory on metallic friction and wear (*e.g.*[41] and [42]), no one as yet has conducted an investigation of metals by *in situ* tribometry. In the early eighties, Blau [43] recommended the application of *in situ* methods to better understand and validate theories surrounding metallic friction and wear. Thus there is a necessity to utilize the *in situ* tribometry approach along with the available *ex situ* analysis to understand metallic friction and wear behavior.

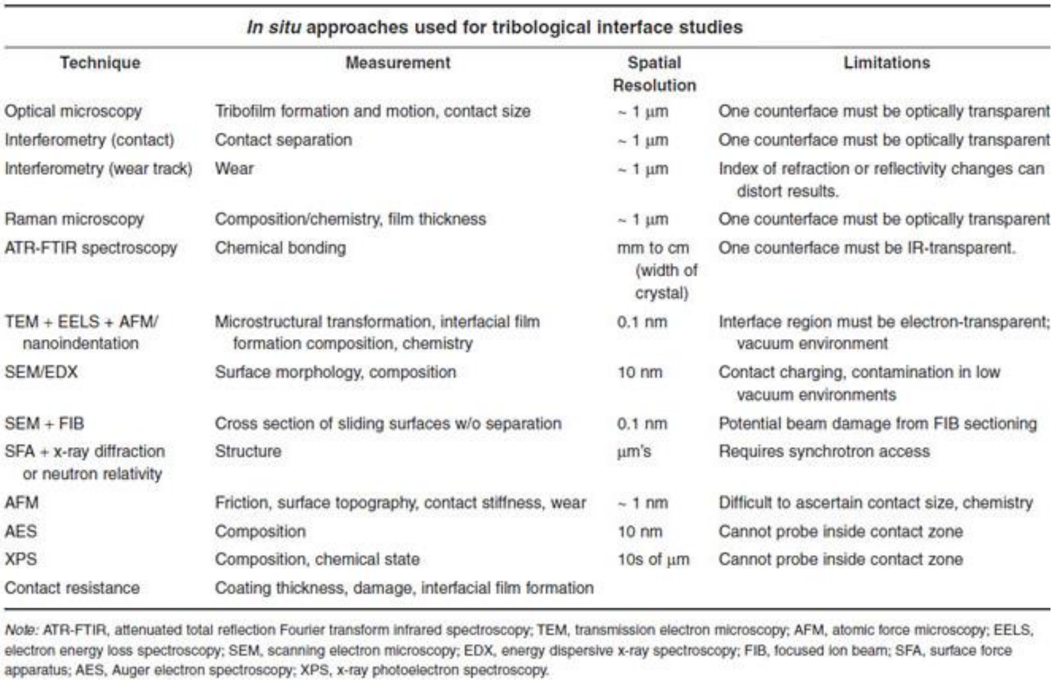

In situ **approaches used for tribological interface studies**

Technique	Measurement	Spatial Resolution	Limitations
Optical microscopy	Tribofilm formation and motion, contact size	~ 1 µm	One counterface must be optically transparent
Interferometry (contact)	Contact separation	~ 1 µm	One counterface must be optically transparent
Interferometry (wear track)	Wear	~ 1 µm	Index of refraction or reflectivity changes can distort results.
Raman microscopy	Composition/chemistry, film thickness	~ 1 µm	One counterface must be optically transparent
ATR-FTIR spectroscopy	Chemical bonding	mm to cm (width of crystal)	One counterface must be IR-transparent.
TEM + EELS + AFM/ nanoindentation	Microstructural transformation, interfacial film formation composition, chemistry	0.1 nm	Interface region must be electron-transparent; vacuum environment
SEM/EDX	Surface morphology, composition	10 nm	Contact charging, contamination in low vacuum environments
SEM + FIB	Cross section of sliding surfaces w/o separation	0.1 nm	Potential beam damage from FIB sectioning
SFA + x-ray diffraction or neutron relativity	Structure	µm's	Requires synchrotron access
AFM	Friction, surface topography, contact stiffness, wear	~ 1 nm	Difficult to ascertain contact size, chemistry
AES	Composition	10 nm	Cannot probe inside contact zone
XPS	Composition, chemical state	10s of µm	Cannot probe inside contact zone
Contact resistance	Coating thickness, damage, interfacial film formation		

Note: ATR-FTIR, attenuated total reflection Fourier transform infrared spectroscopy; TEM, transmission electron microscopy; AFM, atomic force microscopy; EELS, electron energy loss spectroscopy; SEM, scanning electron microscopy; EDX, energy dispersive x-ray spectroscopy; FIB, focused ion beam; SFA, surface force apparatus; AES, Auger electron spectroscopy; XPS, x-ray photoelectron spectroscopy.

Fig. 2.3 Various instrumentations and techniques available to probe the interface *in situ* during a wear test [35]

2.7 Hydrogen Permeability of Zn and Cd coatings

Hydrogen permeation experiments help to determine the resistance offered by the coating to hydrogen permeation. Zheng et al. studied the effect of hydrogen ingress in SAE 4340 steel and Inconel alloy under the presence and absence of zinc ions[44]. From their observation in the permeation flux, hydrogen ingress in SAE 4340 steel was reduced by 51 % and in Inconel alloy by 40 % compared to bare substrates. Similar results[45, 46] were reported by few other researchers who propose that electrodeposited zinc acts as a barrier to hydrogen diffusion. The barrier behavior of a coating is very important in certain aspect. If considerable amount of hydrogen is generated during the initial deposition of the coating and gets trapped in between the coating and the substrate layer, this may lead to hydrogen ingress into the steel and thereby causing embrittlement. Thus the coating's permeability should be optimized to minimize hydrogen embrittlement.

There are many factors which can contribute to the permeability of the coatings, including the microstructure, defect density, phase composition etc. Texture or preferred orientation of the grains in the microstructure of a material plays an important role in hydrogen diffusion. The diffusion of hydrogen in metal membrane depends on the type of microstructure. The effect of texture on hydrogen permeation in nickel electrodeposits was investigated in detail by Cao [47]. Nickel electrodeposits having two different fiber texture components of (100) and (110) exhibited different diffusion coefficients for hydrogen diffusion. Further annealing of the electrodeposits changed the texture as well as the hydrogen diffusion coefficient. Diffusion coefficients of (001) and (110) textured polycrystalline nickel membranes were higher than the single crystal membranes. In both the cases the diffusion coefficient of (001) textured nickel membrane produced by electrodeposition exhibited higher hydrogen diffusion coefficient than the (110) textured membrane.

The crystallographic orientation of zinc electrodeposits depends on numerous factors. The texture of zinc electrodeposits depend on plating conditions, current density, pH of the plating bath, substrate grain orientation, nature of surface finish of the substrate and nucleation and grain growth mechanism [48-51]. Higher current density and pH resulted in lower volume fraction of (002) planes with more of higher order prism or pyramidal plane orientation in HCP zinc. Substrate surface finish also plays an important role in preferred orientation of zinc. Finer surface finishes resulted in larger volume fraction of (002) planes than coarse surface finishes. In most of zinc based coatings and alloys the larger volume fraction of basal planes is preferred owing to better surface coverage resulting in superior corrosion resistance. But the role of preferred orientation in the microstructure of zinc has not been investigated and could also play a role in hydrogen permeation.

Zn-14% Ni coatings on high strength steel are of interest because of its very low hydrogen embrittlement index, as compared to the pure electrodeposited zinc. This coating provides excellent corrosion resistance, comparable to pure electrodeposited cadmium. But the microstructure of these coatings provides a challenge as this coating is susceptible to hydrogen re-embrittlement i.e. the hydrogen embrittlement caused during corrosion of this coating during service. The hydrogen re-embrittlement was quantified using slow strain mechanical tests. This re-embrittlement was found to occur due to inter-granular cracks and through thickness pores. The inter-granular cracks and through thickness pores formed in the coating due to the residual stresses may lead to possible sites for hydrogen diffusion [52].

It is understood that pure zinc nickel coatings, without any presence of defects, provide excellent hydrogen barrier properties. Coleman et al [45] investigated the hydrogen permeation inhibition effect of electrodeposited zinc nickel, electrodeposited zinc and nickel membranes. The permeation resistance of zinc nickel alloy was 80 % more than bare iron membrane. It was also proposed that increasing the membrane thickness by increasing the plating time further improved the permeation resistance up to 95 %. Though the mechanical property tests give an idea of the embrittlement index, quantitative information can be obtained by permeability tests of the coatings with and without the presence of defects, which in turn provide further insight on understanding the effect of defects on hydrogen permeability and the barrier properties of the coatings [52].

Alloying pure zinc with either Ni or Co reduced the embrittling characteristic of the coating. Zinc with 10 % Ni or zinc with 1 % Co promoted lower embrittlement than the pure zinc plating because of the formation of a pure nickel or cobalt rich layer on the initial stages of deposition. Pure nickel has low hydrogen diffusivities as compared to the zinc and thus may lead to lower hydrogen embrittling characteristic during the plating process [53].

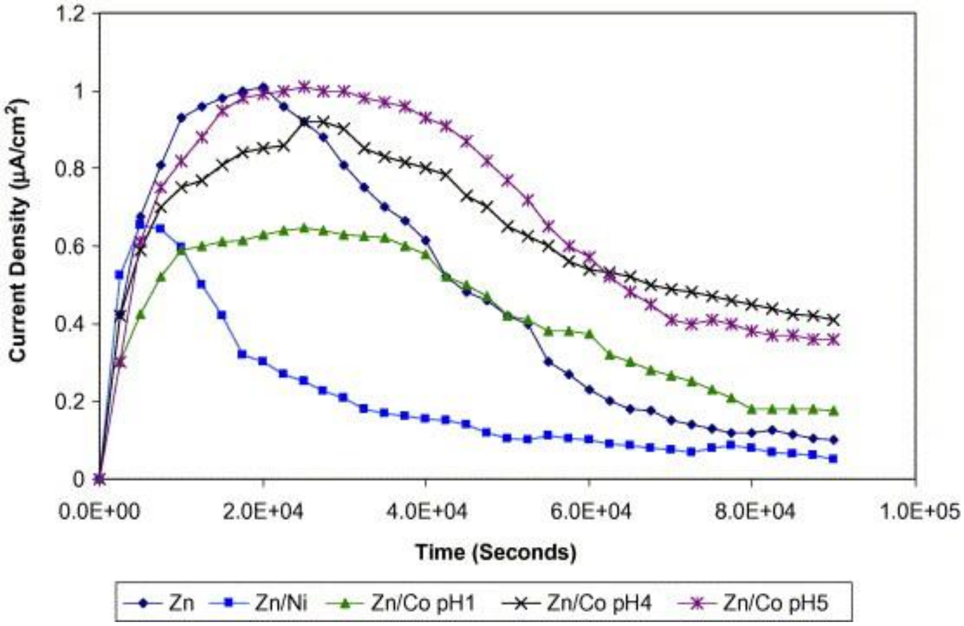

Fig. 2.4 Hydrogen uptake comparison between Zn, Zn-Ni and Zn-Co coatings [54]

In fact an attempt has been made to measure the hydrogen uptake during different plating processes as shown in Fig. 2.1 (Zn, Zn-Ni and Zn-Co) [54]. The investigators reported minimum hydrogen uptake by Zn-Ni plating process by measuring the permeated hydrogen during the plating process, on the exit side of the Devanathan twin cell. This method, even though gives the amount of hydrogen, generated by the plating process, which is responsible for the failure, does not account for the true barrier behavior of the coating [54].

Alloying zinc with nickel or cobalt changes the microstructure of the deposit. The microstructure of zinc nickel deposit changed with the incorporation of nickel into zinc matrix. Below 2.8% nickel the microstructure comprises of randomly oriented platelets [5]. Zinc nickel deposit with Ni 7 %

consists of hexagonal shaped grains with the grains growing in the vertical direction. This morphology appears to be associated with the pyramidal crystallographic planes. Zinc nickel deposit with still higher nickel contents had finer platelet size with higher degree of roughness[5]. X ray diffraction analysis of Zinc (10-14 %) Ni alloy coatings showed the presence of γ phase instead of mixture of δ and γ phase according to the equilibrium Zn-Ni phase diagram. Predominantly zinc nickel alloys exhibit (330), (600) and (442) reflections which are characteristic of γ phase and the composition ranging between 11 to 14 % Ni [3, 5, 6]. In electrodeposited zinc-nickel, effect of gamma phase, defect density [52] and post bake treatment, nickel rich monolayer [55] etc. have been found to be the causes for lower hydrogen embrittlement susceptibility.

So far the hydrogen embrittlement characteristics of these coated steels have been predominantly quantified only using mechanical property tests. Further insight should be provided by evaluating the permeability of the coatings with varying chemical composition and thereby varying the phase distribution. This could prove an important role in understanding hydrogen permeability due to the formation of intermetallic phases.

The Zn-Ni alloys are prone to have microcracks originating from the surface due to residual stresses [56]. These crack networks may spread across evenly during corrosion of the coatings [15, 57]. Most of the plated components are given a post bake heat treatment to overcome hydrogen embrittlement. To be more specific the aerospace industry recommends components which are electroplated to have to undergo a post plating heat treatment at 200 °C [58]. Since the coefficient of expansion of the substrate steel and the coating are different, the coating may undergo a non uniform expansion and result in extensive cracking. So far no available literature correlates the effects of microstructural defects such as the cracks and discontinuities in the coatings on hydrogen permeability of coated steel.

2.8 Vacuum Thermal desorption of hydrogen

Thermal desorption spectroscopy is another versatile method to quantify hydrogen in metals. The theory is based on the fact that, hydrogen in metal lattice, trapped in various trap sites like dislocations, grain boundaries, diffuses upon heating. As the metal is heated, atoms gain kinetic energy to the point where hydrogen atoms can the jump from trap sites to the normal lattice interstitial sites. The atoms in normal lattice sites and the ones evolved from the trap sites recombine and saturate the matrix then diffusing to the sample surface and subsequently to the surrounding atmosphere [59]. The diffused hydrogen from the specimen can be detected within a closed system by a pressure gauge, a gas chromatograph, or a mass spectrometer [60-62].

Addach et al[60] used a gas chromatograph to determine hydrogen in zinc and chromium plated steel. The experiment consisted of hot extraction in a tube furnace, coupled with gas chromatography analysis and determination of thermal desorption kinetics of hydrogen occluded in electroplated parts, for both zinc and chrome plated steels. The substrate material was low carbon steel of 0.38% C. After a predetermined time the samples were preheated to an elevated constant temperature. The released hydrogen from the samples is injected by carrier gas into the detector of the gas chromatograph. Based on the retention time between the calibration curve and the hydrogen evolved from the specimen the nature of hydrogen (atomic or molecular) can be determined. The zinc plated samples were progressively heated to different temperatures and hydrogen content was measured in a manner described above. They observed the change in hydrogen desorbed from the zinc coated steel differed with baking temperatures. At various baking temperatures i.e. the post baking for zinc plating, hydrogen evolution characteristics were studied. It was observed that at 130°C the hydrogen evolution was practically none. By raising the extraction temperature the hydrogen evolved changed more rapidly and at 350 °C it came to an end. At 300 °C it took 50 min for the hydrogen to be completely desorbed while at 220° C the hydrogen desorption was not complete even after 150 min.

Nagumo et al. [63] studied the susceptibility of hydrogen embrittlement of martensitic steels by means of thermal desorption analysis. They used the thermal desorption analysis along with the delayed fracture mechanical test to evaluate hydrogen embrittlement. Hydrogen was charged into steel after preloading the specimen and was also simultaneously loaded and charged. The thermal desorption studies were carried out using a gas chromatograph with a predetermined high purity mixture of hydrogen and argon as a calibration standard. From the thermal desorption spectrometry (TDS) it was observed that the maximum desorption occurred at the temperature range of 50 – 200 ºC. It was also observed that the highest desorption peak was observed for the specimen which was charged while loading, followed by the preloaded specimen and finally by the specimen which was not charged with hydrogen. By observing the nature of TDS peaks they studied the nature of temper treatment. They concluded that temper treatment of steels created point defects that acted as hydrogen trap sites, which was evident by maximum desorption at low temperature region.

Edigaryan et al [64] utilized the quadrupole mass spectrometer to analyze the hydrogen content in electroplated chromium and nickel chromium multi layered coatings. The hydrogen content in the coatings was examined by thermal extraction at 400 °C in a vacuum chamber at 10^{-4} Pascal using the mass analyzer and ion source. From their observation they concluded that the direct current electroplating of chromium resulted in lower hydrogen generation than the pulse plated chromium coatings. Moreover they observed lower amounts of hydrogen evolved during multilayered Ni-Cr coatings, compared to pure chromium electrodeposits.

Wang et al. [65] determined hydrogen embrittlement susceptibility of high strength boron steels by slow stain rate tests and determined the amount of hydrogen ingress by using a quadruple mass spectrometer. The steel specimens were charged with hydrogen in aqueous charging medium and then they were tested for mechanical properties with slow strain tests. The fractured specimens were then preserved in liquid nitrogen to prevent the loss of hydrogen. The fractured specimen were then heated to different temperatures to extract hydrogen in vacuum and followed by the analysis using a quadrupole mass spectrometer. With the help of the quantity of diffusible hydrogen measured by TDS they concluded that the fracture strength of the material decreased exponentially with increase in the amount of diffusible hydrogen.

These are some of the examples where, apart from the mechanical property measurements like the slow strain rate tests or the fatigue tests, the amount of diffusible hydrogen determined by the thermal desorption method becomes useful in quantifying the extent of hydrogen induced damage in a coated steel specimen or bare substrate which is charged with hydrogen. The thermal desorption method gives quantitative analysis as to whether a coating process is susceptible to hydrogen damage or a material itself is susceptible to internal hydrogen embrittlement due to the charging environment.

References

[1] Bickford JH, Nassar S. Handbook of bolts and bolted joints. New York: M. Dekker; 1998.

[2] Winand R. Electrodeposition of Zinc and Zinc Alloys. Modern Electroplating: John Wiley & Sons, Inc.; 2010. p. 285-307.

[3] Barceló G, García E, Sarret M, Müller C, Pregonas J. Characterization of zinc–nickel alloys obtained from an industrial chloride bath. Journal of Applied Electrochemistry. 1998;28:1113-20.

[4] Bories C, Bonino JP, Rousset A. Structure and thermal stability of zinc–nickel electrodeposits. Journal of Applied Electrochemistry. 1999;29:1045-51.

[5] Bruet H, Bruet H, Bonino JP, Rousset A, Marolleau, Marolleau, et al. Structure of zinc–nickel alloyelectrodeposits. Journal of Materials Science. 1999;34:881-6.

[6] Felloni L, Fratesi R, Quadrini E, Roventi G. Electrodeposition of zinc-nickel alloys from chloride solution. Journal of Applied Electrochemistry. 1987;17:574-82.

[7] Alfantazi AM, Erb U. Microhardness and thermal stability of pulse-plated Zn-Ni alloy coatings. Mat Sci Eng a-Struct. 1996;212:123-9.

[8] Brooks I, Erb U. Hardness of electrodeposited microcrystalline and nanocrystalline gamma-phase Zn-Ni alloys. Scripta Mater. 2001;44:853-8.

[9] Tian W, Xie FQ, Wu XQ, Yang ZZ. Study on corrosion resistance of electroplating zinc-nickel alloy coatings. Surface and Interface Analysis. 2009;41:251-4.

[10] Muller C, Sarret M, Garcia E. Heat-treatment on black-passivated ZnNi alloys. J Electrochem Soc. 2003;150:C212-C8.

[11] Müller C, Sarret M, García E. Heat treatment effect on the corrosion behaviour of black passivated ZnNi alloys. Corrosion Science. 2005;47:307-21.

[12] Girčienė O, Gudavičiūtė L, Juškėnas R, Ramanauskas R. Corrosion resistance of phosphated Zn–Ni alloy electrodeposits. Surface and Coatings Technology. 2009;203:3072-7.

[13] Fratesi R, Roventi G. Corrosion resistance of Zn-Ni alloy coatings in industrial production. Surface and Coatings Technology. 1996;82:158-64.

[14] Alfantazi AM, Erb U. Corrosion properties of pulse-plated zinc-nickel alloy coatings. Corrosion. 1996;52:880-8.

[15] Siitari DW, Sagiyama M, Hara T. Corrosion of Ni-Zn Electrodeposited Alloy. T Iron Steel I Jpn. 1983;23:959-66.

[16] Fabri Miranda FJ. Corrosion behavior of zinc-nickel alloy electrodeposited coatings. Corrosion. 1999;55:732-42.

[17] Wood RJK. Tribo-corrosion of coatings: a review. Journal of Physics D: Applied Physics. 2007;40:5502.

[18] Landolt D. Electrochemical and materials aspects of tribocorrosion systems. Journal of Physics D: Applied Physics. 2006;39:3121.

[19] Landolt D, Mischler S, Stemp M. Electrochemical methods in tribocorrosion: a critical appraisal. Electrochimica Acta. 2001;46:3913-29.

[20] Mischler S. Triboelectrochemical techniques and interpretation methods in tribocorrosion: A comparative evaluation. Tribology International. 2008;41:573-83.

[21] Ponthiaux P, Wenger F, Drees D, Celis JP. Electrochemical techniques for studying tribocorrosion processes. Wear. 2004;256:459-68.

[22] Mansfeld F, Shih H, Greene H, Tsai CHR. Analysis of Eis Data for Common Corrosion Processes. Am Soc Test Mater. 1993;1188:37-53.

[23] GAMRY. Basics of EIS http://www.gamry.com/assets/Application-Notes/Basics-of-EIS.pdf. 2012.

[24] Azzi M, Paquette M, Szpunar JA, Klemberg-Sapieha JE, Martinu L. Tribocorrosion behaviour of DLC-coated 316L stainless steel. Wear. 2009;267:860-6.

[25] Azzi M, Benkahoul M, Szpunar JA, Klemberg-Sapieha JE, Martinu L. Tribological properties of CrSiN-coated 301 stainless steel under wet and dry conditions. Wear. 2009;267:882-9.

[26] Guruvenket S, Azzi M, Li D, Szpunar JA, Martinu L, Klemberg-Sapieha JE. Structural, mechanical, tribological, and corrosion properties of a-SiC:H coatings prepared by PECVD. Surface and Coatings Technology. 2010;204:3358-65.

[27] Li D, Guruvenket S, Azzi M, Szpunar JA, Klemberg-Sapieha JE, Martinu L. Corrosion and tribo-corrosion behavior of a-SiCx:H, a-SiNx:H and a-SiCxNy:H coatings on SS301 substrate. Surface and Coatings Technology. 2010;204:1616-22.

[28] Benea L, Wenger F, Ponthiaux P, Celis JP. Tribocorrosion behaviour of Ni–SiC nano-structured composite coatings obtained by electrodeposition. Wear. 2009;266:398-405.

[29] Hassani S, Raeissi K, Azzi M, Li D, Golozar MA, Szpunar JA. Improving the corrosion and tribocorrosion resistance of Ni–Co nanocrystalline coatings in NaOH solution. Corrosion Science. 2009;51:2371-9.

[30] Mischler S, Spiegel A, Landolt D. The role of passive oxide films on the degradation of steel in tribocorrosion systems. Wear. 1999;225–229, Part 2:1078-87.

[31] Espallargas N, Mischler S. Dry wear and tribocorrosion mechanisms of pulsed plasma nitrided Ni–Cr alloy. Wear. 2011;270:464-71.

[32] Panagopoulos CN, Georgarakis KG, Agathocleous PE. Sliding wear behaviour of Zinc-Nickel alloy electrodeposits. Tribology International. 2003;36:619-23.

[33] Wahl KJ, Sawyer WG. Observing interfacial sliding processes in solid - Solid contacts. MRS Bulletin. 2008;33:1159-67.

[34] Muratore C, Voevodin AA. Chameleon Coatings: Adaptive Surfaces to Reduce Friction and Wear in Extreme Environments. Annual Review of Materials Research. 2009;39:297-324.

[35] Sawyer WG, Wahl KJ. Accessing inaccessible interfaces: In situ approaches to materials tribology. MRS Bulletin. 2008;33:1145-50.

[36] Scharf TW, Singer IL. Role of Third Bodies in Friction Behavior of Diamond-like Nanocomposite Coatings Studied by In Situ Tribometry. Tribology Transactions. 2002;45:363-71.

[37] Scharf TW, Singer IL. Monitoring Transfer Films and Friction Instabilities with <i>In Situ Raman Tribometry. Tribology Letters. 2003;14:3-8.

[38] Chromik RR, Baker CC, Voevodin AA, Wahl KJ. In situ tribometry of solid lubricant nanocomposite coatings. Wear. 2007;262:1239-52.

[39] Dvorak SD, Wahl KJ, Singer IL. Friction Behavior of Boric Acid and Annealed Boron Carbide Coatings Studied by In Situ Raman Tribometry. Tribology Transactions. 2002;45:354-62.

[40] Strauss HW, Chromik RR, Hassani S, Klemberg-Sapieha JE. In situ tribology of nanocomposite Ti–Si–C–H coatings prepared by PE-CVD. Wear. 2011;272:133-48.

[41] Rabinowicz E. Friction and Wear of Materials. New York: John Wiley; 1964.

[42] Stachowiak G, Batchelor AW. Engineering Tribology. 3 ed: Butterworth Heinemann; 2006.

[43] Blau PJ. Mechanisms for Transitional Friction and Wear Behavior of Sliding Metals. Wear. 1981;72:55-66.

[44] Zheng G, Popov BN, White RE. Surface treatment for mitigation of hydrogen absorption and penetration into AISI 4340 steel and Inconel 718 alloy. Journal of Applied Electrochemistry. 1995;25:212-8.

[45] Coleman DH, Popov BN, White RE. Hydrogen permeation inhibition by thin layer Zn–Ni alloy electrodeposition. Journal of Applied Electrochemistry. 1998;28:889-94.

[46] Kim H, Popov BN, Chen KS. Comparison of corrosion-resistance and hydrogen permeation properties of Zn-Ni, Zn-Ni-Cd and Cd coatings on low-carbon steel. Corrosion Science. 2003;45:1505-21.

[47] Cao Y. Influence of structure of palladium and nickel based membranes on hydrogen permeation [Thesis (Ph.D.)]. Montreal: Mcgill University; 2002.

[48] Raeissi K, Bateni MR, Saatchi A, Golozar MA, Szpunar JA. The effect of [gamma]-fiber texture intensity of carbon steel substrate on zinc hetero-epitaxial growth. Surface and Coatings Technology. 2006;201:3116-22.

[49] Raeissi K, Saatchi A, Golozar MA. Effect of nucleation mode on the morphology and texture of electrodeposited zinc. Journal of Applied Electrochemistry. 2003;33:635-42.

[50] Raeissi K, Saatchi A, Golozar MA, Szpunar JA. Texture and surface morphology in zinc electrodeposits. Journal of Applied Electrochemistry. 2004;34:1249-58.

[51] Raeissi K, Saatchi A, Golozar MA, Szpunar JA. Effect of surface preparation on zinc electrodeposited texture. Surface and Coatings Technology. 2005;197:229-37.

[52] Figueroa D, Robinson MJ. The effects of sacrificial coatings on hydrogen embrittlement and re-embrittlement of ultra high strength steels. Corrosion Science. 2008;50:1066-79.

[53] Hillier EMK, Robinson MJ. Hydrogen embrittlement of high strength steel electroplated with zinc-cobalt alloys. Corrosion Science. 2004;46:715-27.

[54] Hillier EMK, Robinson MJ. Permeation measurements to study hydrogen uptake by steel electroplated with zinc-cobalt alloys. Corrosion Science. 2006;48:1019-35.

[55] El hajjami A, Gigandet MP, De Petris-Wery M, Catonne JC, Duprat JJ, Thiery L, et al. Hydrogen permeation inhibition by zinc–nickel alloy plating on steel XC68. Applied Surface Science. 2008;255:1654-60.

[56] Sasaki T, Hirose Y. Residual stress distribution in electroplated Zn • Ni alloy layer determined by X-ray diffraction. Thin Solid Films. 1994;253:356-61.

[57] Lin C, Lee H, Hsieh S. Microcracking of flash coatings and its effect on the Zn-Ni coating adhesion of electrodeposited sheet steel. Metallurgical and Materials Transactions A. 1999;30:437-48.

[58] ASTM. F1941-00 Standard specification for electrodeposited coatings on threaded fasteners (Unified Inch Screw Threads (UN/UNR)). ASTM International, West Conshohocken, PA, 19428-2959, DOI: 10.1520/F1941-07 www.astm.org2006

[59] Turnbull A, Hutchings RB, Ferriss DH. Modelling of thermal desorption of hydrogen from metals. Materials Science and Engineering A. 1997;238:317-28.

[60] Addach H, Bercot P, Wery M, Rezrazi M. Quantitative determination of hydrogen in solids by gas chromatography. Journal of Chromatography A. 2004;1057:219-23.

[61] Shvachko V. Analysis and investigation of hydrogen in steels by the mass-spectral method. Materials Science. 1998;34:544-58.

[62] Anghel C, Dong Q. A gas phase analysis technique applied to in-situ studies of gas–solid interactions. Journal of Materials Science. 2007;42:3440-53.

[63] Nagumo M, Nakamura M, Takai K. Hydrogen Thermal Desorption Relevant to Delayed-Fracture Susceptibility of High-Strength Steels. Metallurgical and Materials Transactions A. 2001;32:339-47.

[64] Edigaryan AA, Lubnin EN, Lyakhov BF, Molodkina EB, Polukarov YM. Hydrogen Content in Chromium and Multilayer Nickel–Chromium Coatings Deposited by Periodic Current1. Protection of Metals. 2003;39:405-10.

[65] Wang M, Akiyama E, Tsuzaki K. Hydrogen degradation of a boron-bearing steel with 1050 and 1300 MPa strength levels. Scripta Materialia. 2005;52:403-8.

3.0 Tribological behavior of electrodeposited Zn, Zn–Ni, Cd and Cd–Ti coatings on low carbon steel substrates

Preface

In this chapter, the friction and wear behavior of electrodeposited Zn-Ni, Zn, Cd and Cd-Ti coatings investigated by *in situ* tribology technique are analyzed to understand friction and wear mechanisms, contact conditions and third body contributions. The nature of transfer film formation, wear debris generation and contact conditions were observed to be different in Zn-Ni, Zn and Cd coatings. Transfer films were also analyzed by ex situ methods, such as scanning electron microscopy, X-ray diffraction and indentation hardness. The transfer film behavior observed by *in situ* methods was correlated to friction and wear behavior, mechanical properties phase and composition of metallic coatings. This chapter brings in a new dimension of the study of metallic friction and wear through an *in-situ* tribology technique. From these studies, Zn-Ni coating emerges as a suitable candidate to replace Cadmium coatings. The contents of this chapter have been published as a manuscript in the journal *Tribology international* 56 (2012), 107-120.

Abstract

The tribological behavior of electrodeposited Zn–Ni alloy coatings was investigated for its suitability to replace Zn-and Cd-based coatings. An *in situ* tribometry technique with a transparent sapphire hemisphere as a counter face on a pin on flat tribometer was utilized to examine the contribution of third bodies in friction and wear behavior. Wear mechanisms and tribo/transfer film morphology were also studied with the X-ray diffraction and electron microscopy. *In situ* tribometry and additional ex situ analyses revealed that Zn–Ni coatings had superior resistance to adhesive wear compared to cadmium coatings. Microhardness of Zn–Ni coatings was higher than Zn and Cd coatings. Hardness on the wear track of Zn–Ni coatings showed the formation of a strain hardened tribolayer.

Highlights

► Utilization of *in situ* tribometry to understand tribology of metal coatings. ► Transfer film formation, debris and contact conditions in Zn–Ni, Zn and Cd coatings. ► Correlation of TF and coating characteristics to tribology of metal coatings. ► Cd replacement with Zn–Ni by utilizing *in situ* tribometry and *ex situ* analysis.

Keywords: Electrodeposited Zn-Ni, Cd, Zn coatings, *in situ* tribology, transfer film, tribofilm

3.1. Introduction

Electrodeposited cadmium based sacrificial coatings are being used in aerospace industries for anodic protection of high strength steel components. Stringent environmental concerns have restricted the extensive use of cadmium in aerospace industries. Among various coatings developed in the recent past as a replacement to Cd, Zn–Ni alloys are leading candidates that have sufficient corrosion resistance and improved mechanical properties compared to Cd based coatings. Electrodeposited Zn–Ni alloys have also shown properties of interest for automotive and aerospace industries, including their corrosion resistance [1], [2], [3], [4], [5], [6], [7] and [8], hardness [2], [9], [10], [11], [12], [13] and [14] and thermal stability [11] and [13]. The anodic corrosion protection offered by Zn–Ni alloys makes it a suitable candidate to replace cadmium in aerospace industries [4].

High strength steel fasteners used in automotive and aerospace industries are often coated with Zn- or Cd-based coatings for anodic protection [15]. In addition to corrosion protection, it is also important for the coatings to have sufficient wear resistance to withstand the wear and abrasion during handling and torquing of the fasteners. It has been shown in the previous work that Zn–Ni coatings are harder than Zn [2] and [11]. Adequate wear resistance of Zn–Ni has been reported by Panagopoulos et al. [16] using an alumina pin on a Zn–Ni coated mild steel disc. In contrast, Cd, being a soft metal, has been shown to act as a solid lubricant during wear tests under extremely high loading conditions [17], but exhibited limited effectiveness in preventing wear. There have been several investigations on the tribological behavior of thin coating of cadmium over plated steel components to understand its friction and wear behavior under extreme conditions and controlled environments [17], [18] and [19]. While the wear resistance of Zn–Ni and Cd have been evaluated individually in past studies, it is essential to evaluate the tribological behavior of the coatings of similar thickness under the same running conditions.

Both Zn–Ni- and Cd-based coatings have been investigated in the past [16], [17] and [19] using conventional pin on disc or sliding cylinder experiments with any insight on the wear mechanisms inferred from *ex situ* techniques. While many textbooks present a well established theory on metallic friction and wear (*e.g.* [20] and [21]), no one as yet has conducted an investigation of metals by *in situ* tribometry. In the early eighties, Blau recommended the application of *in situ* methods to better understand and validate theories surrounding metallic friction and wear [22]. *In situ* tribometry is a novel technique developed to probe the interface between the contact surfaces to study the interface chemistry and role of third bodies in friction and wear behavior of coatings [23] and [24]. This technique has been successfully utilized in the past to understand the friction and wear characteristics, tribochemistry of transfer/tribo films in boron carbide coatings [23], diamond-like carbon coatings [24] and [25], MoS_2 based solid lubricant coatings [26], nanocrystalline diamond coatings [27], TiC–N [28] and Ti–Si–C–N [29] hard coatings.

The present work focuses on the investigation of tribological behavior of established industrial coating processes of Zn–Ni, Cd, Cd–Ti and Zn, using a pin-on-flat *in situ* tribometer. Wear mechanisms are examined with the help of indentation hardness, *ex situ* examination of wear track morphology, and the phase and composition of tribo/transfer films.

3.2. Experimental methodology

3.2.1. Coating processes

Five coatings on low carbon steel substrates were plated in the fashion described below. All coatings were deposited on 10×16 cm, 0.8 mm thick sheets of low carbon steel (SAE 1006). The nominal composition of the steel correspond to C, 0.04%; Mn, 0.264%; Si, 0.008%; S, 0.013%; P, 0.006%; Ti, Nb, V in traces. After deposition, the coated sheets were then mechanically sheared to 2.5 × 2.5 cm squares for all subsequent testing and analysis.

Boeing LHE Zn–Ni: Low hydrogen embrittling (LHE) Zn–Ni plating process developed by Boeing Research & Technology, USA was used [30]. An alkaline NaOH (135 g/l) and Na_2CO_3 (60 g/l) based plating solution with Zn (9–11 g/l) and Ni (0.8–1.2 g/l) metal concentrations in the ratio of 10–11:1 and additives was used, and plated in an industrial pilot plating tank. The pH of the plating bath was maintained between 12 and 13.5 at 20–25 °C and a plating current density of 48 mA/cm^2 was applied to obtain a coating thickness of 15–20 μm in 1 h. Substrates were aqueous degreased, abrasive grit blasted and activated in HCl before plating. Boeing LHE Zn–Ni will be referred to B-Zn–Ni henceforth in this paper.

Dipsol IZ C17+Zn–Ni: Commercially available Zn–Ni plating solution by Dipsol Inc. was used. An alkaline NaOH (135 g/l) based plating solution with Zn and Ni metal concentrations in the ratio of 10–11:1, with commercial additives was used, and plated in an industrial pilot plating tank. The pH of the plating bath was maintained at 12–13.5 at 25 °C and a plating current density of 28–30 mA/cm^2 was applied to produce a coating thickness of 15–20 μm in one hour. The substrates were grit blasted and acid pickled in HCl before plating. Dipsol IZ C17+ Zn–Ni will be referred to D-Zn–Ni henceforth in this paper.

Zn**:** The plating bath was acid chloride based with $ZnCl_2$ (60 g/l), KCl(250 g/l), H_3BO_3 (25 g/l) and HCl in smaller concentrations to maintain the pH of the bath to 4.5–4.8. The cathode efficiency was 95% and the temperature of the plating was held at 25 °C. Commercial additives were used and electroplating was performed on a laboratory-scale plating setup. A plating current density of 5 mA/cm^2 was used to generate a coating thickness of 15 μm in 2 h. The substrates were polished with 600 # SiC grinding paper and activated in HCl before plating.

LHE Cd**:** Low hydrogen embrittling Cd plating (LHE Cd) was plated in an industrial plating facility using an alkaline cyanide based plating solution with CdO (20–30 g/l), NaCN (90–135 g/l), Na_2CO_3 (0–60 g/l) and NaOH (11–30 g/l). A plating current density of 118–120 mA/cm^2 was used to generate a coating thickness of 15 μm in 5 min. Substrates were solvent degreased, grit blasted and acid pickled before plating. Plating temperature of 15–30 °C was used [31].

Cd–Ti**:** Alkaline cyanide based plating solution with CdO (18–35 g/l), NaCN (74–200 g/l), Na_2CO_3 (0–60 g/l), and NaOH (11–30 g/l) was used, and plated in an industrial pilot plating tank. Ti was added in small concentrations (40–100 ppm) for grain refinement and control of surface morphology. An initial strike was applied at a plating current density of 46–55 mA/cm^2 for 15 s to build-up a flash layer with sufficient adhesion and subsequently a plating current density of 16–32 mA/cm^2 was applied to generate a total coating thickness of 15 μm in 15 min. Substrates were solvent degreased, grit blasted and acid pickled before plating. Plating temperature of 15–30 °C was used [32].

3.2.2. Wear testing

During wear of materials, third bodies are generated between the two contact surfaces. The third bodies are generally classified into categories, namely tribo film, transfer film and wear debris. In terms of a counterface *versus* coating tribosystem, a tribo film (or a tribo layer), is mechanically or chemically modified layer at the coating surface, which may also consist of agglomerated wear debris. [33]. The transfer film is a layer of coating material adhering to the sliding counter face [25]. Wear debris is generally considered as any removed portion of the coating or counterface that is not part of the transfer film or tribo film. An *in situ* study of the transfer film that formed during the wear of passivated coatings was performed using a reciprocating pin on flat tribometer, equipped with a transparent sapphire hemisphere of 1/4″ diameter. By means of a video microscope mounted above the transparent counter face, the transfer film formation and dynamic changes throughout the test can be observed and later analyzed with the recorded video. A more detailed description of the instrument used here is found in [29] and a similar type of instrument is described elsewhere [26] and [27]. The *in situ* tribometry was conducted at a speed of 3 mm/s for 1800 cycles, which correspond to 13.44 m of sliding distance. Using a piezoelectric lateral force sensor, friction forces were recorded at a sampling rate of 2000 Hz. While omitting force recordings from the turn-around points (*ca.* 100 ms or 300 μm on each side), an average friction coefficient for each reciprocating cycle was calculated. The wear experiments were conducted using a stripe test procedure with an initial stripe length of 12 mm reduced by 2 mm successively at 10, 50, 100, 400, and 1000 cycles. Only passivated coatings were investigated for *in situ* studies because passivation is an established industrial process for electrodeposited Zn and Cd based coatings to prolong the life of the coating when the coating undergoes sacrificial corrosion to protect the substrate steel [15]. All the specimens were tested under a same normal load of 4 N, which did not contribute to a substrate effect except for the softer Cd coatings, even though the initial Hertzian contact stresses were different for the different materials: 0.69 GPa for Zn–Ni, 0.66 GPa for Zn and 0.45 GPa for Cd and Cd–Ti.

All industrial electroplated components are given a chromate passivation to prolong the life of the coating, when the coating is undergoing sacrificial corrosion. In order to overcome the risk of hydrogen embrittlement electroplated parts for aerospace applications are given a 24 h post plating baking treatment at 200 °C [15]. To better determine the wear resistances of Zn–Ni coatings, additional wear tests were performed to longer sliding distances. These tests were run for 1800 cycles at a higher sliding speed of 20 mm/s, which correspond to 31.6 m sliding distance compared to 13.44 m in the *in situ* tests. The Zn–Ni samples were tested for wear resistance under four conditions: (i) as-plated, (ii) with chromate passivation, (iii) as plated and baked for 24 h at 200 °C, (iv) with chromate passivation and baked. For endurance testing, *in situ* examination was not required. To minimize the cost impact and to utilize counterface with the same characteristics and composition, the same tribometer with opaque 1/4″ diameter alumina balls as the counterface was used for endurance testing. To determine the progression of wear at different cycle numbers, friction experiments were conducted as stripe tests similar to above but with modified initial sliding stripe lengths, where the initial 12 mm was reduced by 2 mm successively at 400, 800, and 1300 cycles. This procedure resulted in an overall 12 mm long wear scar with 2 mm sections (stripes) worn for 400, 800, and 1300 cycles and one 6 mm section worn for 1800 cycles.

3.2.3. Coating and tribo/transfer film characterization

X-ray diffraction in standard θ–2θ mode was performed on the unworn coating surfaces and wear tracks at different regions without any intentional removal of loose wear debris, using a Bruker Discover D8-2D diffractometer with Co Kα radiation. A DEKTAK contact stylus profilometer was used to determine the wear track profile area, which in turn was used to calculate the wear volume. An average of three profile measurements was taken to determine the wear track profile area. The wear tracks were observed and analyzed using a Philips field emission scanning electron microscope (FE-SEM) at 20 kV accelerating voltage. Compositional analysis of wear tracks was performed using Energy Dispersive Spectrometry (EDS). Microhardness of the Zn–Ni coatings was measured using Vickers hardness tester with 100 g load. For the softer Zn, Cd and Cd–Ti coatings lower loads of 50 g and 25 g were used to minimize the substrate effect. The average value over 10 indents was taken to report the hardness of the coatings. Microhardness testing was additionally carried out within wear tracks for Zn–Ni coatings at reduced load of 50 g.

3.3. Results

3.3.1. Coating characterization

The surface morphology of the unbaked coatings studied is presented in Fig. 3. 1 and the X-ray diffraction results are presented in Fig. 3.3. B–Zn–Ni had uniformly distributed fine platelets less than 1 μm (Fig 3. 1a), while D–Zn–Ni had large platelets with intermittent porosity and platelet size greater than 10 μm (Fig.3. 1b). The X-ray diffraction pattern of the Zn–Ni coatings in Fig.3. 3(a) confirmed the formation of uniform single phase γ Zn–Ni (Ni_2Zn_{11}), which is a typical characteristic of Zn–15% Ni alloy [34]. All the peaks indexed in the diffraction pattern in Fig. 3. 3 (a) for both the Zn–Ni coatings were gamma Zn–Ni except for the peak (7 3 0) which also coincided with the Fe (2 1 1) peak. Both the Zn–Ni coatings had the composition of Zn–15% Ni and very similar phase identification by the X-ray diffraction. However, surface morphologies were quite different (Fig. 3.1(a) and (b)), which was a consequence of differences in plating process conditions namely the bath composition, additives and plating current density.

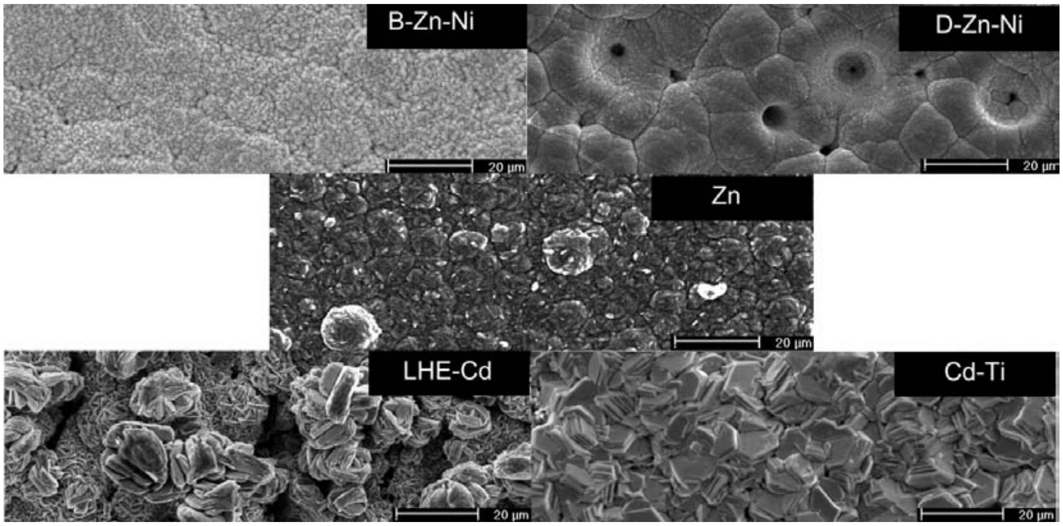

Fig. 3.1. Surface morphology of investigated coatings.

The morphology of Zn coating plated from acid chloride bath in the presence of additives and brighteners were in the form of hemispherical clusters (Fig. 3. 1(c)), which are typical of Zn coatings [35]. The cluster size varied between 5 and 10 μm in size. The XRD of electrodeposited Zn, in Fig. 3.3(b) showed strong (1 0 0) and (1 0 1) reflections for Zn.

Electrodeposited Cd had a spherical hexagonal platelet type morphology (Fig. 3.1(d)) with hexagonal crystals clustering together to form a spherical structure of 10–15 μm in diameter. This type of morphology is a common characteristic of cadmium deposits [36] and [37]. The XRD of Cd and Cd–Ti deposits shown in Fig. 3.3(b) exhibited strong (1 0 1) and (1 0 2) prism plane reflections for Cd. The electrodeposited Cd–Ti coatings were different in morphology compared to the Cd coatings as shown in Fig. 3.1(e). Instead of spheroidal agglomeration of hexagonal crystals, stacking of individual platelets was observed. The Ti addition in the plating solution also resulted in the formation of Cd–Ti solid solution which resulted in this change in morphology.

The cross-sectional SEM of the Zn–Ni coatings is shown in Fig. 3.2. Both the Zn–Ni coatings consisted of through-thickness microcracks which are a typical of intermetallic gamma Zn–Ni. The Zn coating consisted of more uniform cross section devoid of microcracks. The cross-section of LHE Cd coating shown in Fig. 3.2 comprise columns made up of spheres with intermittent discontinuities. From the coating nomenclature, it could be understood that this type of intermittent discontinuities was intentionally provided in the coating owing to the plating conditions to facilitate the escape of co-evolved hydrogen. The cross section of Cd–Ti (Fig. 3.2) was also different from LHE Cd. The platelets were more densely packed without discontinuities. It is believed that the addition of Ti in the plating solution resulted in the formation of a Cd–Ti solid solution causing this change in morphology.

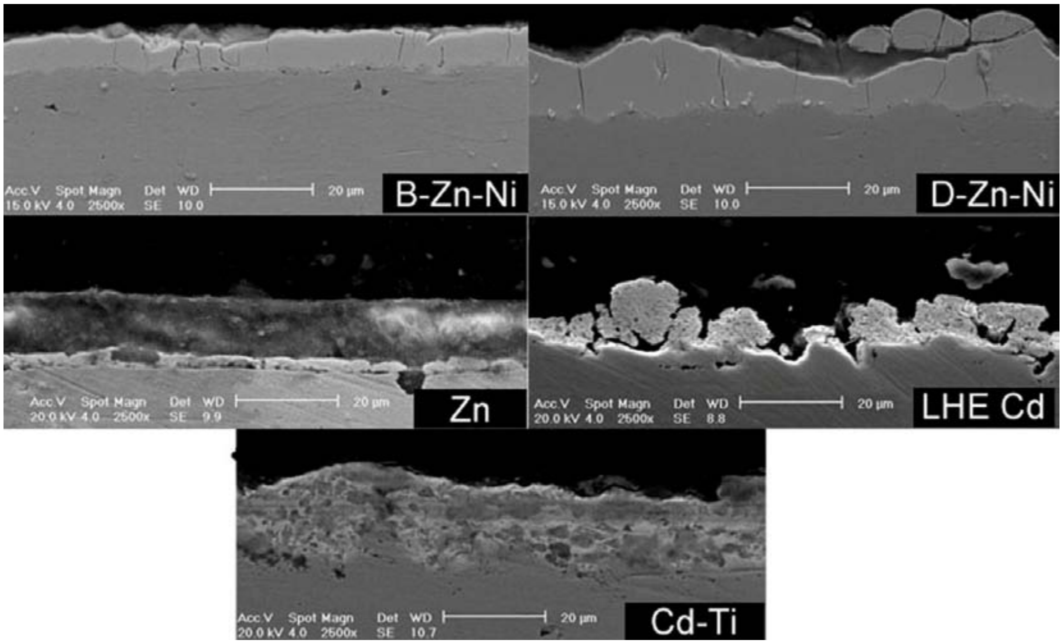

Fig. 3.2. SEM cross-sectional morphologies of the investigated coatings.

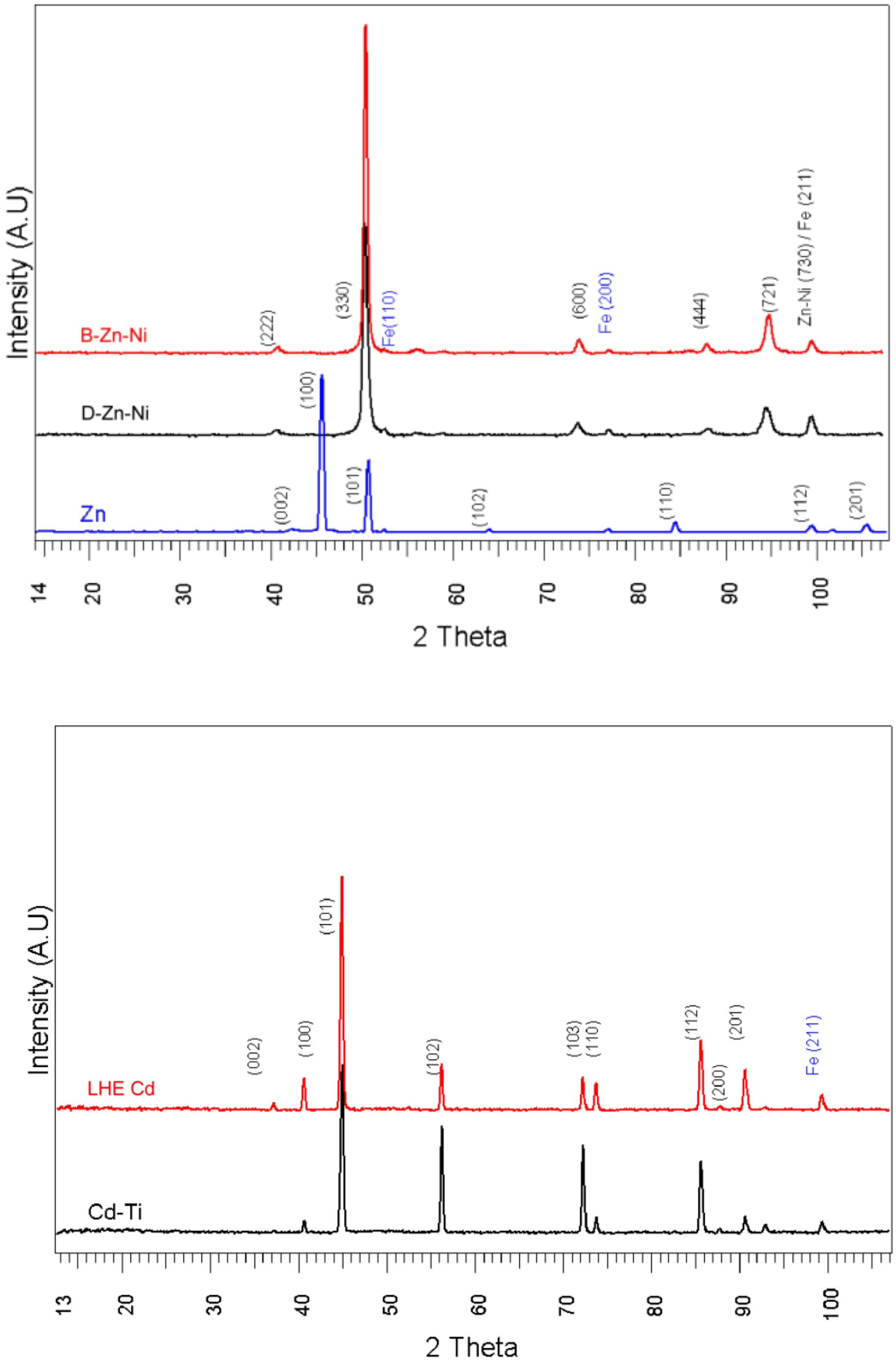

Fig. 3 3. XRD of investigated coatings.

Microhardness values of as-deposited coatings are given in Fig. 3.4. Zn–Ni coatings possess higher hardness compared to Zn, Cd and Cd–Ti coatings. The reason behind higher hardness is attributed to the intermetallic phase γ Zn–Ni (Ni_2Zn_{11}) [11] and [13]. After baking, the hardness of the Zn–Ni coatings slightly increased while no significant changes in hardness were observed for other coatings. According to Alfantazi and Erb [10], the reason could be due to the formation of a more stable intermetallic γ phase, although no phase or structural changes in the coating were observed here due to baking treatment in Zn–Ni alloy. The difference in hardness between the two types of Zn–Ni could be explained by the fact that the intermetallic γ Zn–Ni had non-stoichiometric composition. The γ Zn–Ni can exist in varying compositions (10–14% of Ni) [14]. Hence the difference in the properties could be attributed to these small differences [38]. A student '*T*' test was conducted and proved that the microhardness of the Zn–Ni coatings were statistically independent from each other.

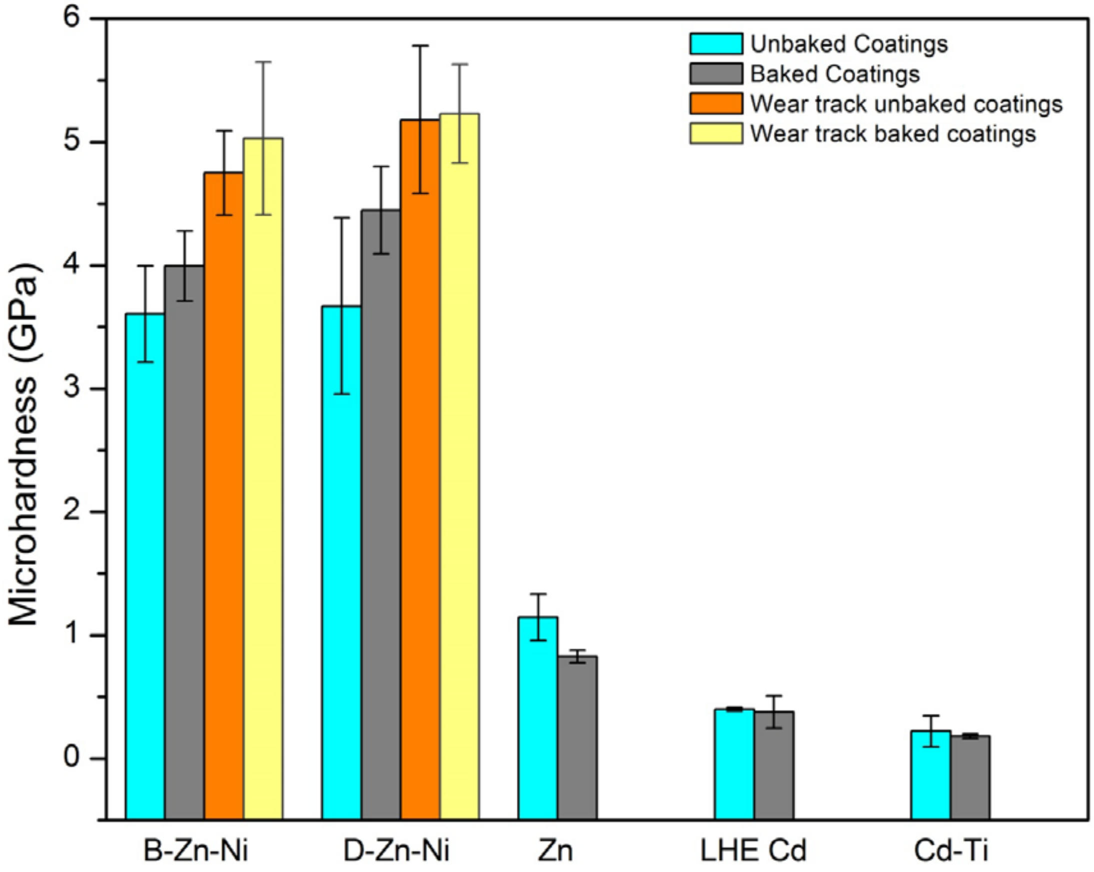

Fig. 3.4. Microhardness distribution of the investigated coatings.

3.3.2. Friction and *in situ* micrographs

The *in situ* micrographs obtained from the test video are shown for B-Zn–Ni in Fig. 3.5(a). During initial stages of wear, the initially rough coating became smooth by plowing of asperities (seen as bright spots for cycles 0 and 5). At the same time, the worn Zn–Ni adhered to the counterface, as can be seen by the rough patch appearing in the center of the micrographs for cycles 0 and 5. The size of this initial contact diameter was roughly 150–220 μm. However, as can be seen in comparing cycles 5 and 12, the adherence of the metal transfer film to the sapphire was not consistently maintained. As wear progressed, transferred material was lost and regained in various regions. In progressing toward cycle 350, the contact area grew wider, the wear track became deep enough to appear continuous and some shearing and mechanical deformation of loose wear debris was observed. At around cycle 500, the central region of transfer film was mostly removed, resulting in an occasional direct contact of sapphire on the coating surface. In progressing from cycle 500 to 600, the direct contact of sapphire on the coating became gradually more visible due to the complete removal of the transfer film within the contact regions (*i.e.* loss of transfer film stability). This led to a more compliant contact. This occurrence was accompanied by an overall increase in contact area due to lateral widening of the wear track. It is also possible that the transferred material left within the outer perimeter of the contact supported some fraction of the load. As can be seen for cycles 1000, 1400 and 1799, the optical interference fringes commonly observed for ball-on-flat contact only appear intermittently. This could be due to the roughness of the wear track, the transferred material supporting some load or a combination of both.

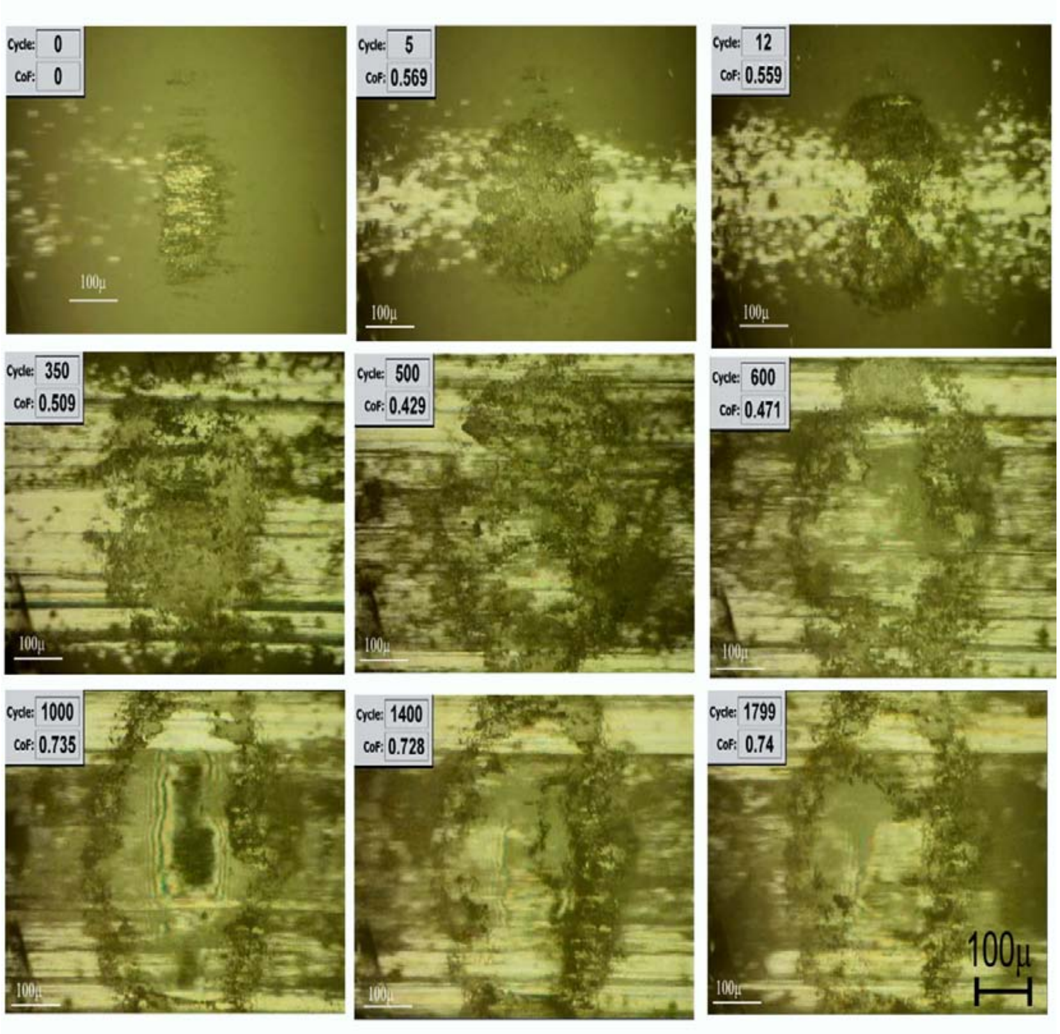
Cycle: 0
CoF: 0
100μ
Cycle: 5
CoF: 0.569
100μ
Cycle: 12
CoF: 0.559
100μ
Cycle: 350
CoF: 0.509
100μ
Cycle: 500
CoF: 0.429
100μ
Cycle: 600
CoF: 0.471
100μ
Cycle: 1000
CoF: 0.735
100μ
Cycle: 1400
CoF: 0.728
100μ
Cycle: 1799
CoF: 0.74
100μ
100μ

(a)

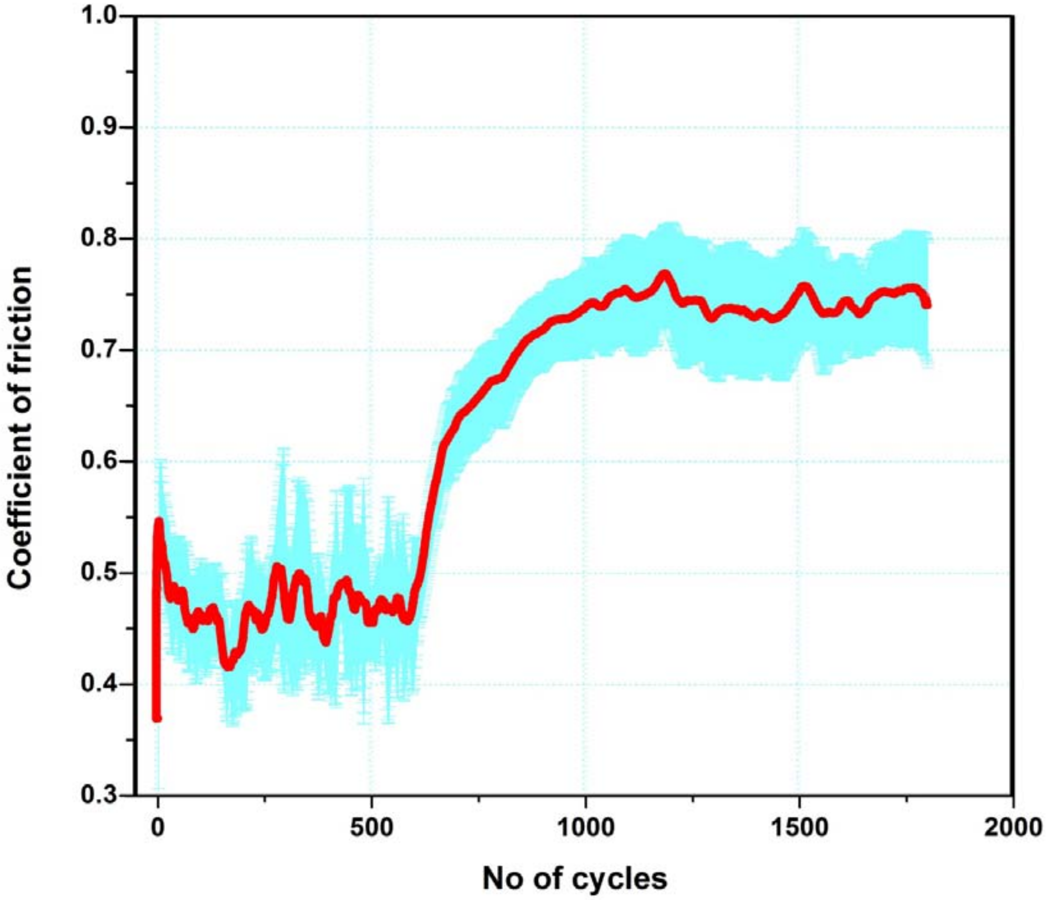

(b)

Fig. 3.5 (a) *In situ* micrographs for B-Zn–Ni and (b) friction coefficient *versus* No. of cycles for B-Zn–Ni.

Friction data for B-Zn–Ni during *in situ* tests is shown in Fig. 3.5(b). As shown in the *in situ* images, the transfer film build-up was very rapid, where surface smoothing and transfer film formation resulted in increased contact area between metallic transfer film and the coating. This metal on metal contact exhibited friction in the range of 0.45–0.5 and was fluctuating. It was also the case that the standard deviation for the friction coefficient, associated with variation in friction across the wear track, was generally high (*i.e.* 0.1). This variation in the friction across the track and from cycle-to-cycle was likely associated with the evolution of the transfer film, with material being removed and replenished in places. The fluctuations in the average friction ceased around cycle 600 and there was a stable rise in the friction coefficient from 0.5 to 0.7 until cycle 1000. This friction rise was associated with contact between sapphire and both third body debris and the hardened coating layer beneath. Beyond 1000 cycles the friction coefficient stabilized to a constant value of 0.7. During this last stage, the average friction coefficient was more stable, despite the contact appearing as intermittent between counter-face and coating.

In situ micrographs are shown for D-Zn–Ni in Fig. 3.6 (a). The initial contact diameter was roughly 150 μm, similar to B-Zn–Ni. In the early cycle, bright spots again show the presence of ploughed asperities. The transfer film formation started more slowly than B-Zn–Ni, becoming visible around the cycle 3 and becoming continuous around cycle 12. Between cycles 12 and 25 the transfer film widened along the sliding direction, but then from cycles 25 to 45 became unstable as transfer film detachment and replenishment was observed. From cycle 45 until cycle 160, the transfer was slowly removed until sapphire on coating contact became predominant. Similar to B-Zn–Ni, the D-Zn–Ni exhibited mostly sapphire *versus* coating contact at higher cycles (see images for 250, 500, 1600 cycles), with some evidence of metal transfer film at the edges of the contact supporting some load.

During the *in situ* tests, the friction characteristics of D-Zn–Ni were found to be similar to B-Zn–Ni, other than a few cycles where there was a COF of 0.15 (Fig. 3.6(b)). Delayed transfer film build-up that was only complete around cycle 25 as opposed to cycle 2 in B-Zn–Ni showed that the initial contact of sapphire on rough coating had lower friction than transfer film *versus* wear track. For both Zn–Ni coatings, the surface smoothing during initial cycles resulted in an increase in contact area and metal-to-metal contact and consequentially higher friction. For D-Zn–Ni, friction becomes higher and starts fluctuating, which also resulted in larger deviation and changes in contact conditions. From cycle 250 onwards, after the transfer film was lost, contact of sapphire with the hardened coating was predominant, and resulted in an increase in friction coefficient.

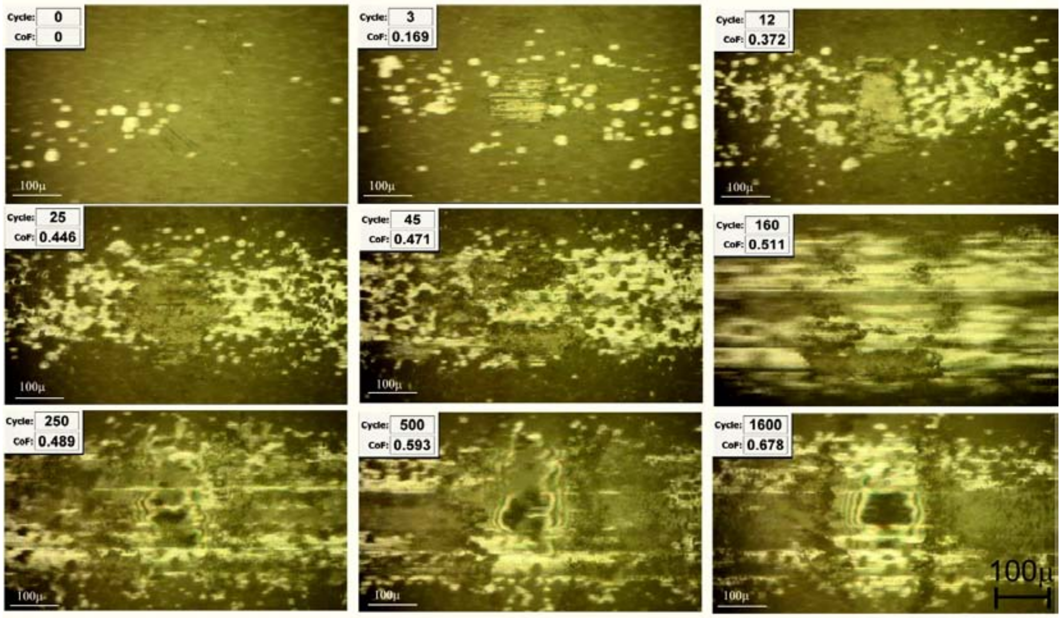

(a)

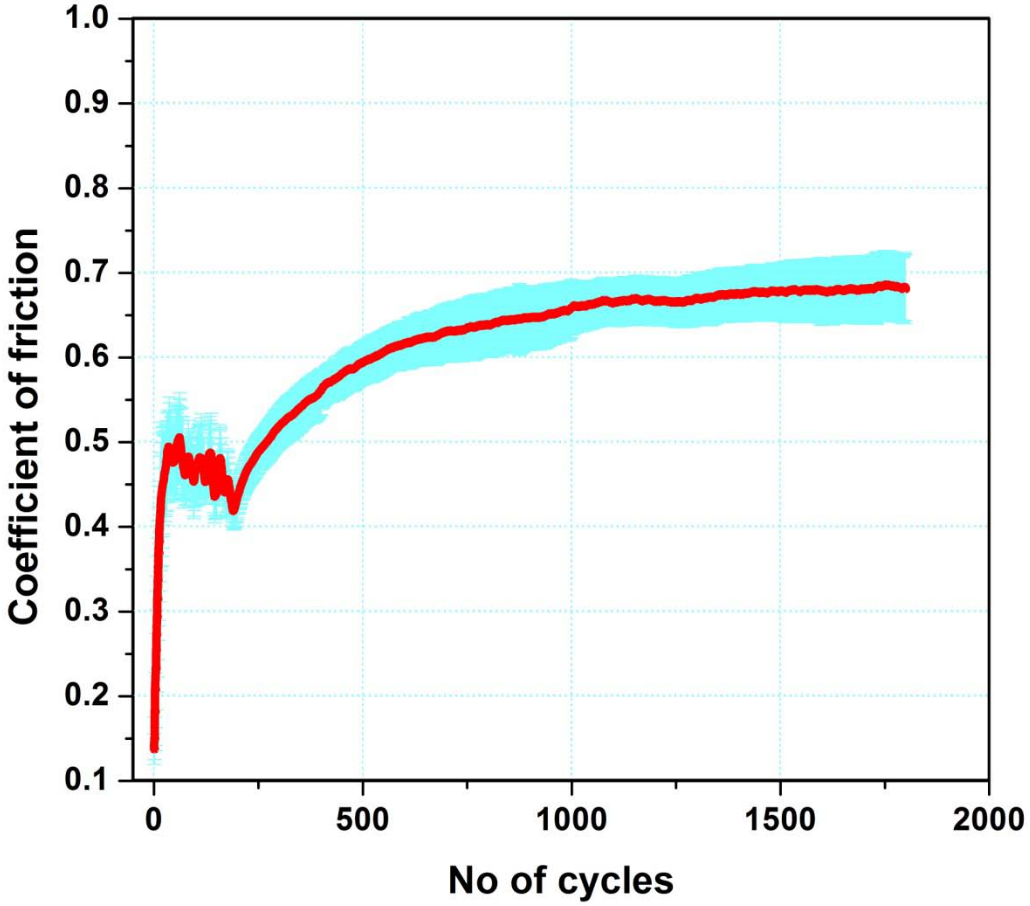

(b)

Fig. 3. 6 (a) *In situ* micrographs for D-Zn–Ni and (b) friction coefficient *versus* No. of cycles for D-Zn–Ni.

Fig. 3.7 (a) shows the *in situ* micrographs for electrodeposited Zn. These micrographs were obtained at a lower magnification and different lighting compared to tests previously discussed. Within the first cycle, rapid formation of transfer film occurred as can be seen by the bright patch in the center of the images for cycle 0. The transfer film build-up continues (see cycles 2 and 30) until the coverage becomes roughly 200 μm across. As wear of the coating progresses, the wear track widens and the outer regions show limited evidence of transferred material, while the central patch remains largely unchanged (see cycle 160). However, from this point onwards (see images for cycles 180 and 200) the transfer film starts being removed until a nearly complete loss of transfer film. The bright patch in the center is now a reflection from the wear track, not a transfer film. Although not as clear for the tests on Zn–Ni coatings, the images for cycles 450, 1000 and 1799 show contact of sapphire with the coating, with intermittent appearance of optical interference fringes.

Friction coefficient *versus* cycle number is shown in Fig. 3.7(b) for the Zn coating. There is a very brief period at the beginning of the test where the friction coefficient is roughly 0.7, corresponding to a time when there was no transfer film and the sapphire was in contact with asperities on the coating surface. Different from the Zn–Ni coatings, this coating exhibited the highest friction (~0.8–0.85) when transfer-film-on-coating was the predominant type of contact. At about cycle 200, the friction drops to about 0.5 which was associated with sapphire-on-coating contact. From this point onwards, the friction gradually rises as the coating wears away and the contact becomes sapphire on steel substrate with some wear debris remaining in between. From separate runs, the friction coefficient of sapphire–steel contact was found to be 0.5–0.55. During the late phases in the experiment, friction only increased slightly to ~0.6, perhaps because the minimal Zn wear debris in the contact provided some solid lubrication.

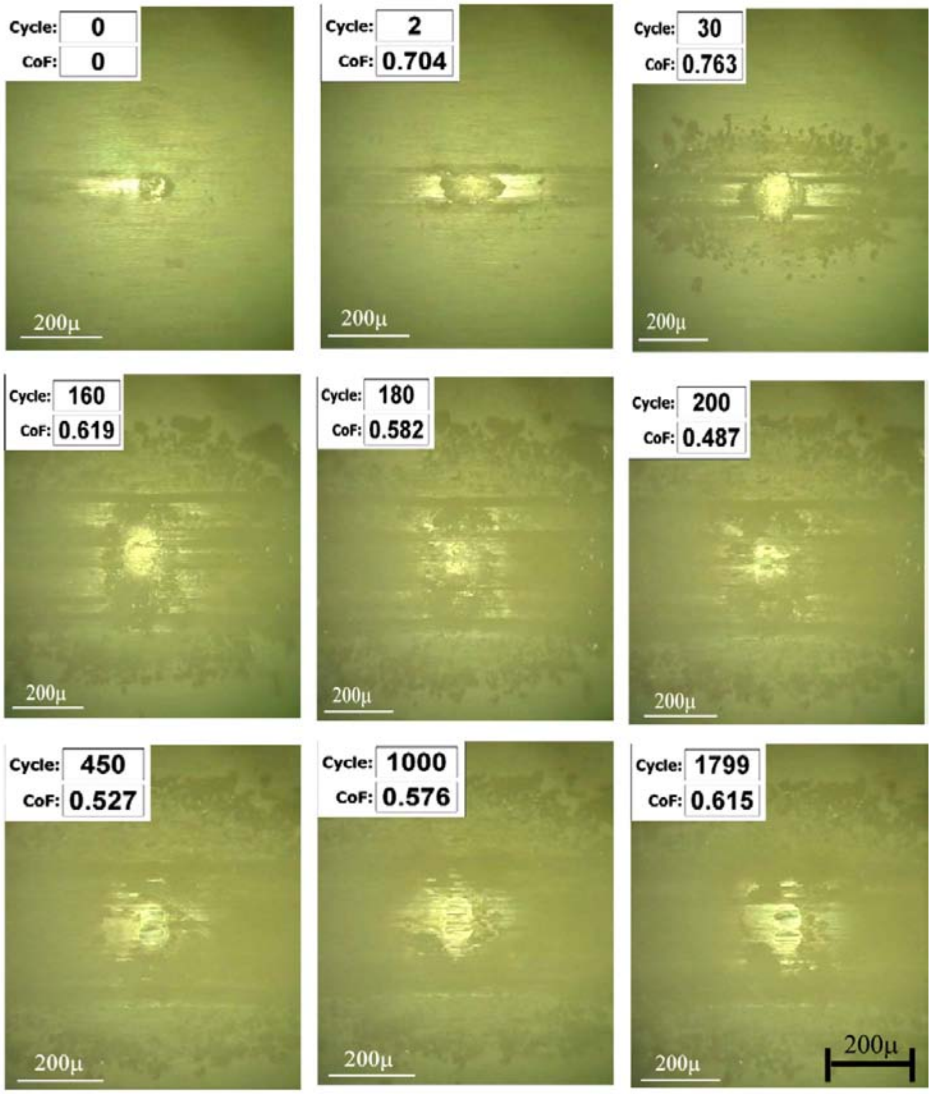
Cycle: 0
CoF: 0
200μ
Cycle: 2
CoF: 0.704
200μ
Cycle: 30
CoF: 0.763
200μ
Cycle: 160
CoF: 0.619
200μ
Cycle: 180
CoF: 0.582
200μ
Cycle: 200
CoF: 0.487
200μ
Cycle: 450
CoF: 0.527
200μ
Cycle: 1000
CoF: 0.576
200μ
Cycle: 1799
CoF: 0.615
200μ
200μ

(a)

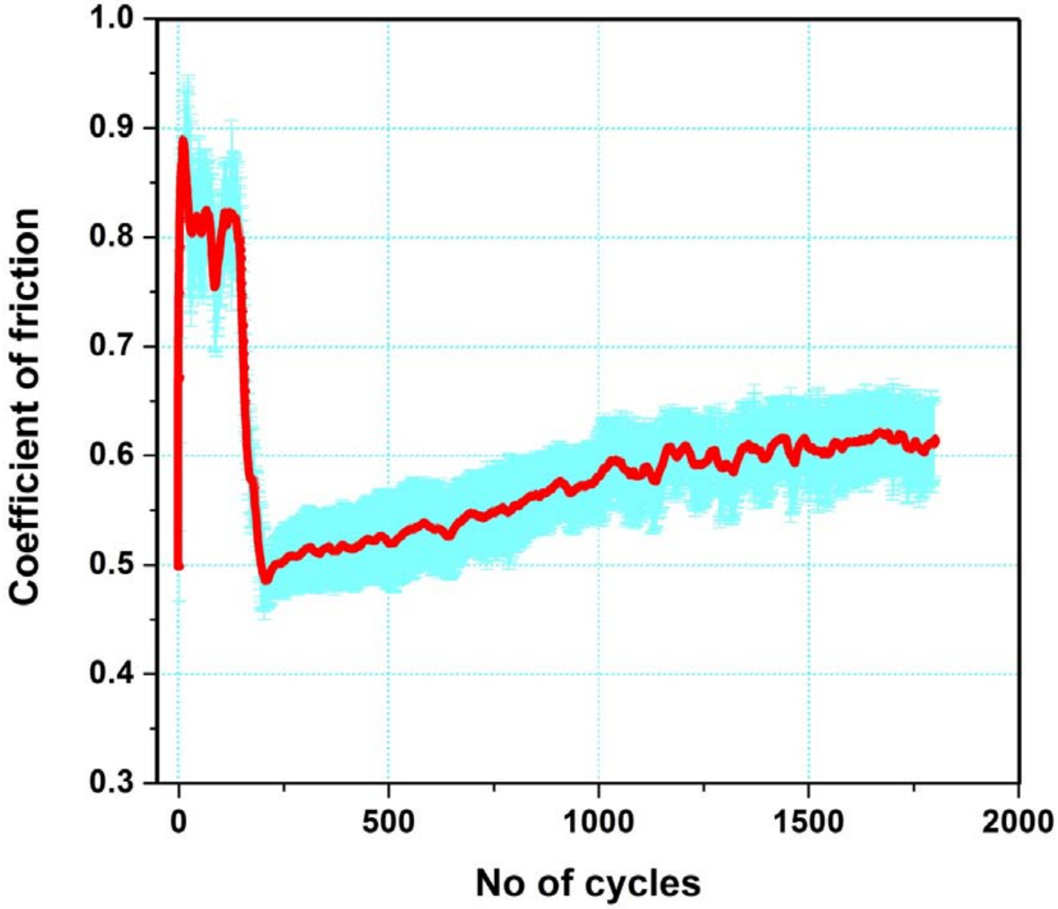

(b)

Fig. 3.7. (a) *In situ* micrographs for Zn and (b) friction coefficient *versus* No. of cycles for Zn

Fig. 3.8(a) shows *in situ* micrographs for the LHE Cd coating. A very wide initial contact diameter of 400 μm was observed immediately upon sliding (see cycle 0). During the initial cycles, extensive transfer film formation was observed, which was thick and wide enough to completely obscure the wear track (see cycles 0 and 3). Partial loss of transfer film was observed in cycle 4, where the wear track is visible on the left-hand side. However, the transfer film was replenished by cycle 14, where the wear track was again completely obscured from view. From cycles 4 to 14, transfer film recirculation occurred, where some amount of transfer film was lost from the contact region and consequently re-accumulated again. From cycles 14 to 30 transfer film growth occurred with widening of the contact area. This was followed by transfer film detachment (see cycle 70). By cycle 200, the center of contact became visible as the transfer film was worn away and only compacted portions remained adhered (see dark patches). By cycle 500, these remaining bits of transfer film had been removed and sapphire on coating contact became apparent with intermittent appearances of the light interference patterns associated with ball on flat contact. From this point onwards, the contact area grew due mostly to coating wear. From cycle 1000 till the end of the test at 1800 cycles, mixed mode contact was observed (see images for cycles 500, 1000, and 1799). The load was primarily carried by the central sapphire on steel region while minor portion of the load was carried by transfer film on the edges of the contact area.

Friction coefficient *versus* cycle number for the LHE Cd coating is shown in Fig. 3.8(b). The friction coefficient starts off at 0.7 and declined to 0.4, remaining at this level but fluctuating until about cycle 500. During this time the primary type of contact was metallic transfer film *versus* the wear track. The reduction in friction occurring between cycles 1 and 250 could be related to work hardening of the transfer film and the cadmium coated surface. The variability in friction from cycles 200 to 500 appears to be related to loss and replenishment of transfer film. The following increase in friction to a level of about 0.55 was related to the formation of primarily sapphire *versus* coating contact that grew progressively for the remainder of the test. During the temporary friction drop from 0.6 to ~0.4 between cycles 1150 and 1200 (see Fig. 3.8(b)), *in situ* micrographs showed sporadic signs of a sapphire-on-coating contact. No other changes could be observed in the video. The explanation is that from outside the field of vision or underneath obstructed parts of the sapphire slider, a new load-carrying contact was created temporarily. The accompanying low friction coefficient of ~0.4 suggests that this contact comprised transfer-film-on-coating.

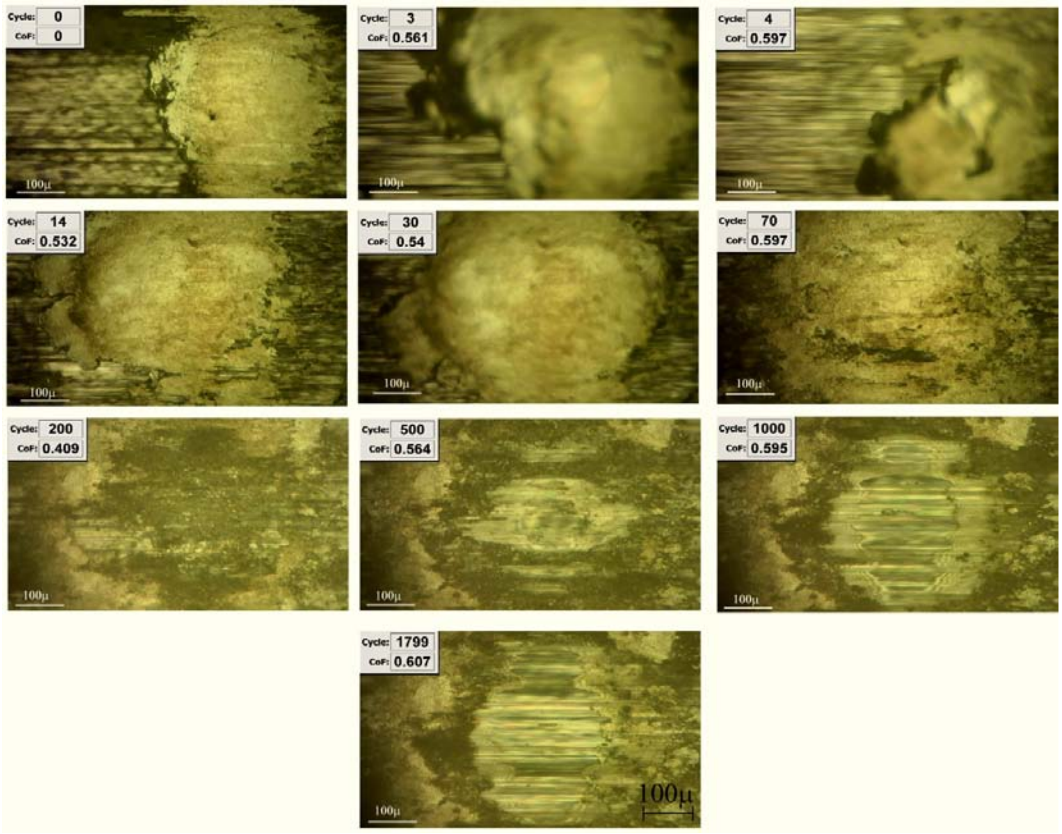

(a)

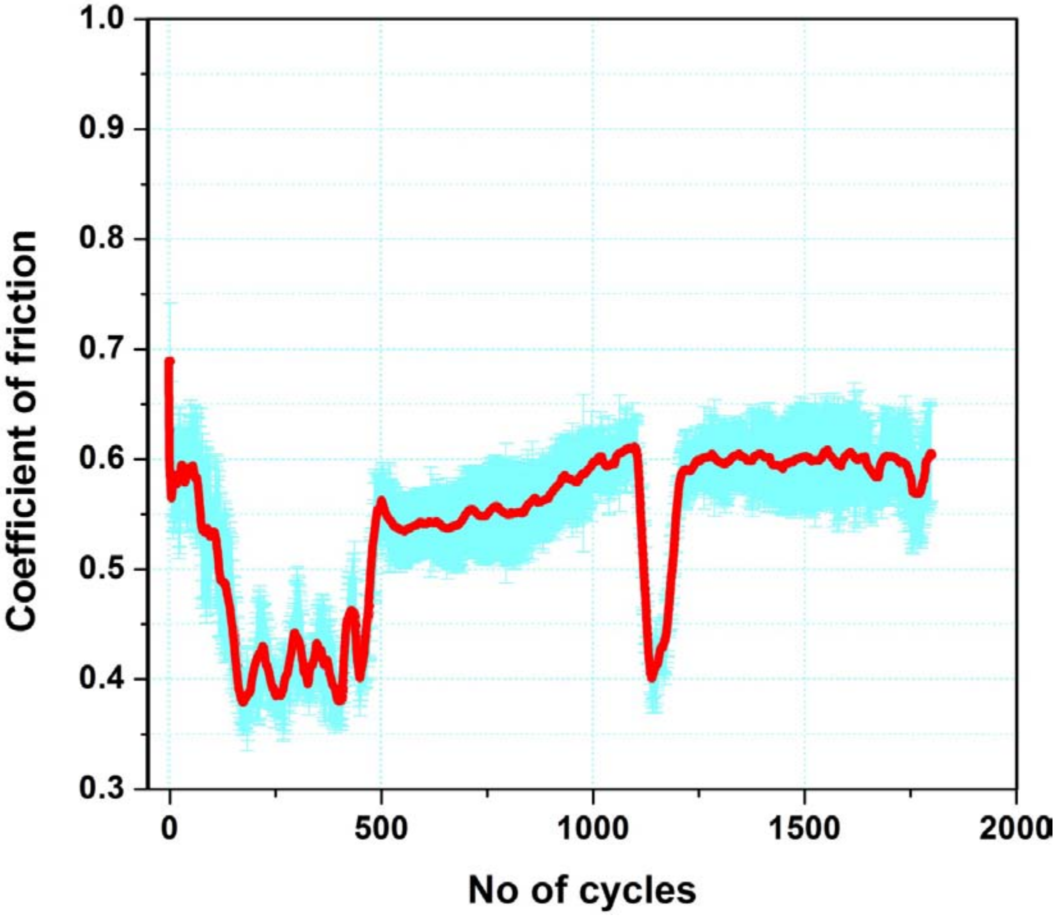

(b)

Fig. 3.8 (a) *In situ* micrographs for LHE Cd and (b) friction coefficient *versus* No. of cycles for LHE Cd

In situ video micrographs of Cd–Ti are shown in Fig. 3.9 (a). The wear characteristics were quite similar to that of Cd with an initial contact area of 150 μm width, observed within the first cycle. Rapid transfer film accumulation was observed again. During cycles 5–30 progressive accumulation of transfer film with partial loss and regain occurred. At cycles 40–60 the wear track width increased from 150 μm to 470 μm. At cycle 180, formation of a hole in the center of the transfer film was observed, followed by gradual widening of the hole during cycles 300 to 900. Around cycle 250, sapphire on coating contact became initially apparent. From cycles 1000 to 1800, a more compliant contact observed along with a reduction in transfer film contact diameter. A complete failure of transfer film was never observed throughout the test. After cycle 200, the contact was shared by both sapphire-on-steel in the center and the transfer-film-on-coating at the edges. However, the coating failed at 250 cycles and was consequently replaced by a tribolayer of wear debris on steel substrate. This observation was confirmed by *ex situ* SEM analysis which will be discussed in detail later.

The friction characteristic of Cd–Ti is shown in Fig. 3.9(b). The friction behavior of the coating was found to be increasing with accumulation of transfer film. The drop in friction coefficient at cycle 250 was due to the partial loss of transfer film. Increase in friction coefficient after 250 cycles till the end of wear test was due to mixed mode contact between the transfer film/wear debris and the steel substrate. The deviation in friction coefficient Fig. 3.8(b) was found to be increasing gradually from cycle 1 to 1000 cycles. Beyond 1000 cycles when sapphire on substrate steel happened to be predominant the friction coefficient as well as the deviation stabilized.

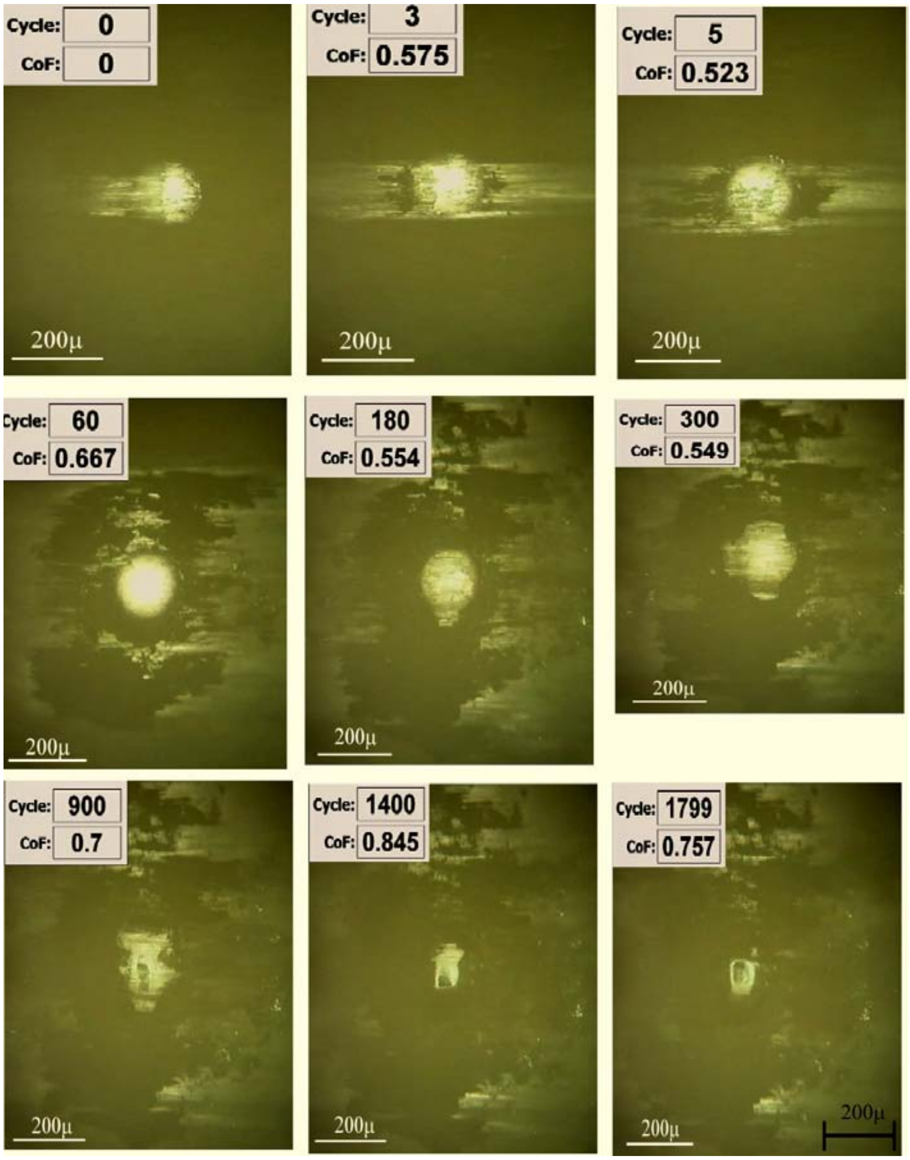
Cycle: 0
CoF: 0
200μ
Cycle: 3
CoF: 0.575
200μ
Cycle: 5
CoF: 0.523
200μ
Cycle: 60
CoF: 0.667
200μ
Cycle: 180
CoF: 0.554
200μ
Cycle: 300
CoF: 0.549
200μ
Cycle: 900
CoF: 0.7
200μ
Cycle: 1400
CoF: 0.845
200μ
Cycle: 1799
CoF: 0.757
200μ
200μ

(a)

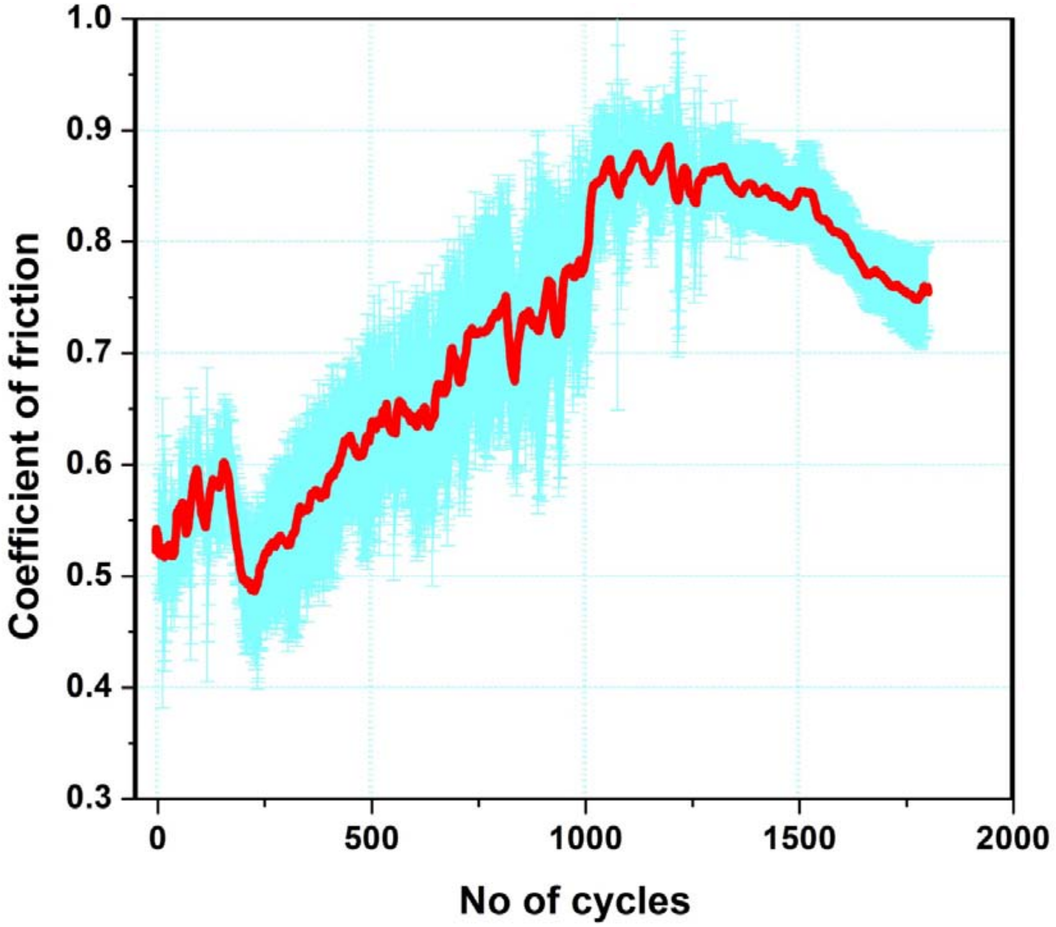

(b)

Fig. 3.9 (a) *In situ* micrographs for Cd–Ti and (b) friction coefficient *versus* No. of cycles for Cd–Ti

3.3.3. Wear results from *in situ* tests

The *in situ* wear data confirmed the trends observed from the friction and tribo images. A change in wear characteristic was observed with the transfer film stability. From Fig. 3.10(a) the wear rates for both the Zn–Ni coatings were higher due to the coating being worn until a stable transfer film was formed (till 100 cycles). The reduction in wear rate was accompanied by the shear of transfer film (600 cycles for B-Zn–Ni and 250 cycles for D-Zn–Ni) and from then on the wear rate was reduced when the sapphire on work hardened coating contact became predominant. The only difference between the B-Zn–Ni and D-Zn–Ni is the onset of transfer film separation/failure leading to formation of strain hardened coating. Fig. 3.10(b) shows the wear rates *versus* cycle for Zn, LHE Cd and Cd–Ti coating. They were much higher compared to Zn–Ni during the initial cycles <50, which was due to rapid transfer film formation and wear of the coating. At higher cycles (>200), the wear rate was reduced after the coating failure in Zn, which resulted in predominant sapphire on steel contact. Wear rates of LHE Cd and Cd–Ti were similar to Zn with initial higher wear rate due to rapid transfer film formation followed by drastic reduction in wear rate when contact condition changed after 250 cycles, i.e. when the coating failed leading to appearance of sapphire on steel contact (see *ex situ* wear track micrographs in Fig. 3.13, Fig. 3.14 and Fig. 3.15). The reduction in wear rates in Zn–Ni coatings was due to formation of a strain hardened layer, which will be discussed in further sections. The reduction in wear rates after the transfer film failure in Zn was due to complete coating failure and in Cd/Cd–Ti coating it was due to partial loss of the transfer film.

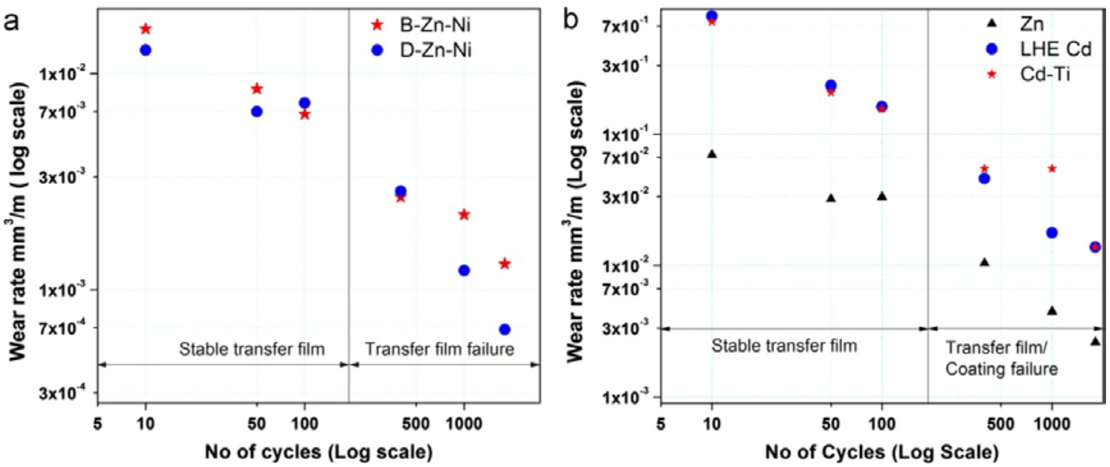

Fig. 3.10 Wear rates before and after transfer film failure of (a) Zn–Ni and (b) Zn, LHE Cd, Cd–Ti coatings

3.3.4. Hardness measurements of tribo film

Hardness of the tribo film for Zn–Ni coatings (Fig. 3.4) showed considerable increase in hardness compared to the unworn coating due to strain hardening [16]. Hardness values of the tribo film could not be obtained for Zn coatings due to the absence of a consistent tribo film and also due to the removal of wear debris from the wear track during the wear tests. For Cd and Cd–Ti coatings the thickness of the tribo film was too thin for hardness measurement as sufficient spall of tribofilm was observed even for a lowest indent load of 10 gf. From the microhardness measurements on the wear track after 400 cycles it can be inferred that a strain hardened tribo film is formed on the Zn–Ni wear track which reduces further material removal and, as a consequence, the Zn–Ni coating lasted the entire duration of the wear test.

3.3.5. Ex situ SEM analysis of tribo/transfer film

Scanning electron microscopy performed on Zn–Ni wear tracks is shown in Fig. 3.11 and Fig. 3.12. From the *in situ* video micrographs it was shown that the nature of wear was quite similar for both the Zn–Ni coatings except for the stability of the transfer film during the wear process. The *ex situ* SEM micrographs of the wear tracks reflected similar observations. The different stages of wear were, initial smoothening of the coating surface with intermittent material removal (Figs. 3.11(a) and 12(a)) followed by loose wear debris accumulation (Figs. 3.11(b) and 12(b)). Subsequently, the loose wear debris and torn patches were entrapped in between the sapphire, transfer film and the underlying coating, forming a cracked abraded surface (Figs. 3.11(c) and 12(c)). This then further transformed to a hardened tribolayer with transverse cracks appearing toward the end of the wear test (Figs. 3.11(d, e) and 12(d, e)). The difference in the onset of change of wear track morphology corresponded to the point where the transfer film lost stability. Also, it may be inferred that the morphology changes and the strain hardening of the coating occurred earlier for D-Zn–Ni at cycle 100 than at 400 cycles observed for B-Zn–Ni.

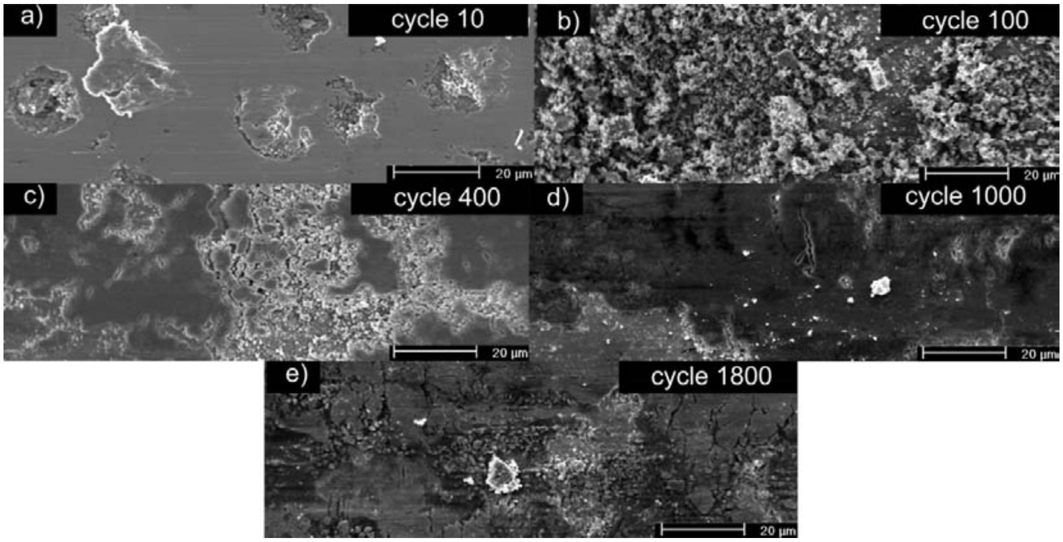

Fig. 3.11 Wear track morphologies of B-Zn–Ni

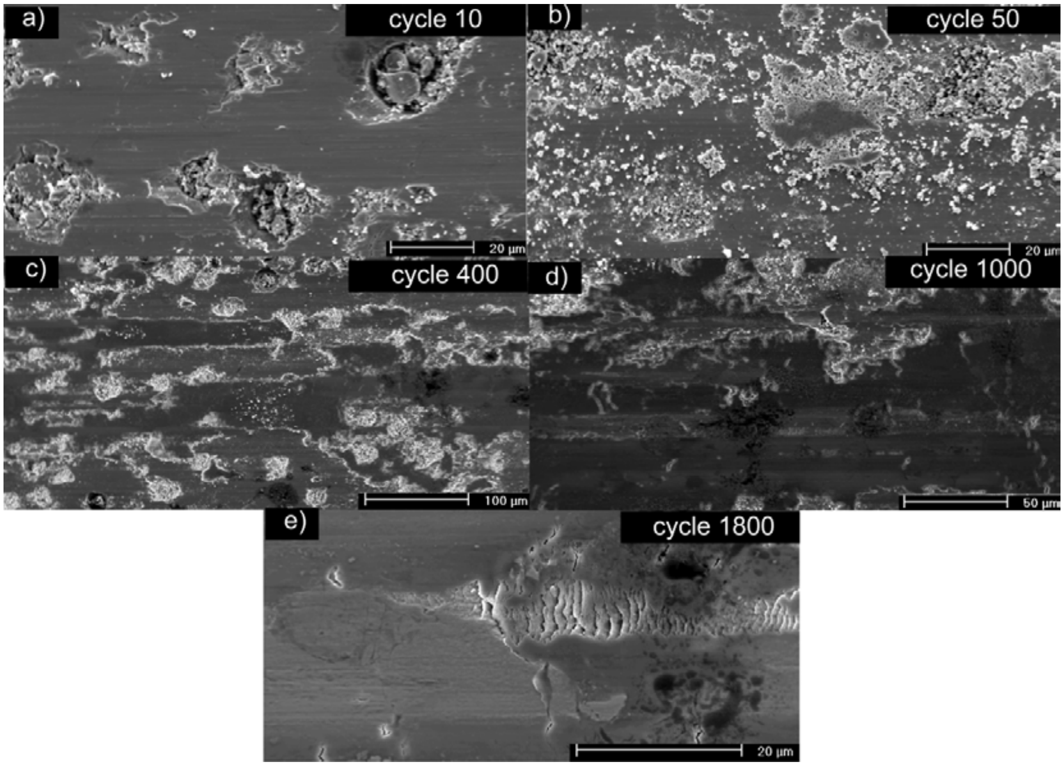

Fig. 3.12 Wear track morphologies of D-Zn–Ni

Fig. 3.13 shows the wear track images of Zn coating. Here the material was removed by shear and delamination (Fig. 3.13(a)–(b)) followed by the initiation of coating failure which resulted in contact of sapphire on steel substrate (Fig. 3.13(c)). As the test reached 400 cycles and beyond, the coating failed revealing torn patches of Zn coating being re-deposited during the progression of the wear test (Fig. 3.13(d)).

The wear track images of Cd and Cd–Ti were more similar to observations for pure Zn than for Zn–Ni. The wear track images showed initial smoothening of coating surface by extensive plastic deformation (Figs. 3.14(a) and 3.15(a)) followed by material removal by delamination (Figs. 3.14(b) and 15(b)). As the wear test progressed, both the coatings failed at 400 cycles (Figs. 3.14(c) and 15(c)) leading to the appearance of substrate steel. As the wear test progressed to further cycles, reduction in contact area of the deformed coating and widening of sapphire to steel contact was observed (Figs. 3.14(d) and 15(d)).

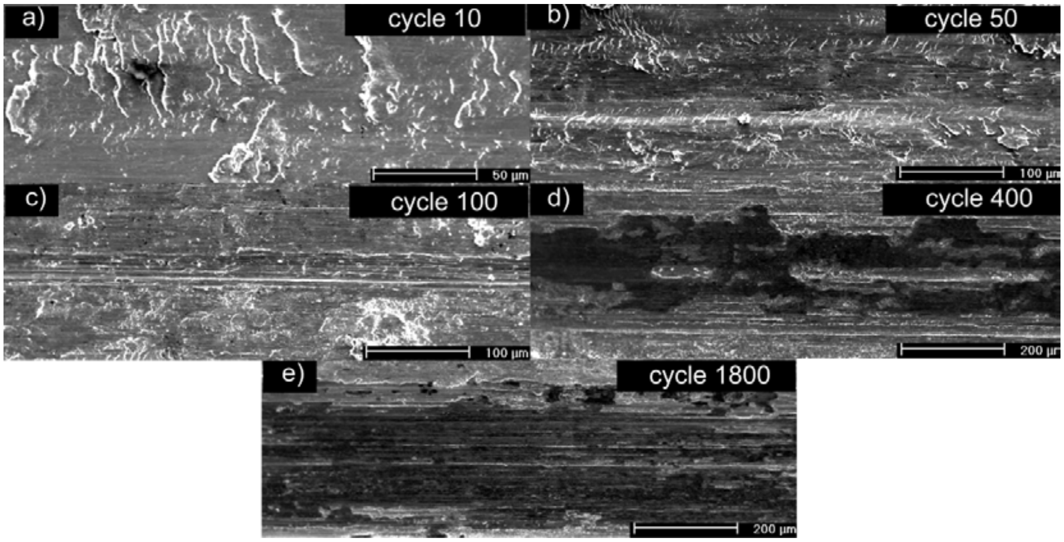

Fig. 3.13 Wear track morphologies of Zn

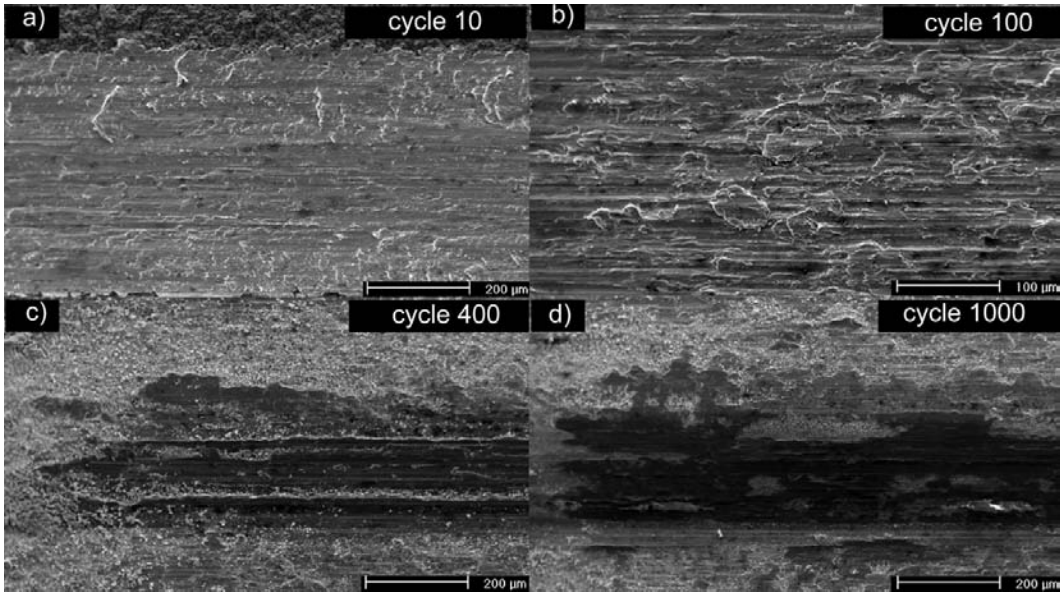

Fig. 3.14 Wear track morphologies of LHE Cd

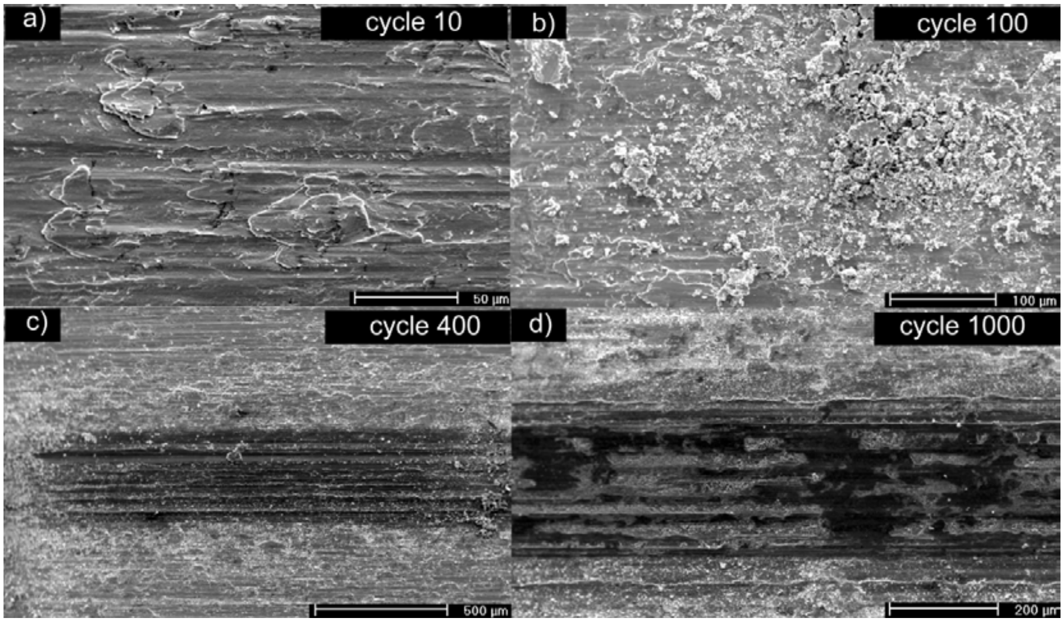

Fig. 3.15. Wear track images of Cd–Ti.

X-ray diffraction was performed on the wear tracks to investigate any phase/composition changes during wear. The results are shown in Fig. 3.16. The XRD of Zn–Ni wear tracks showed a stronger intensity of γ Zn–Ni peaks and a lower intensity of substrate Fe peak, while in the Cd coatings the intensity of Fe peaks were stronger than that of Zn–Ni which indirectly indicates more volume of coating material is lost during the wear of Cd coatings than Zn–Ni coatings. No evidence was found for phase changes or formation of crystalline oxides.

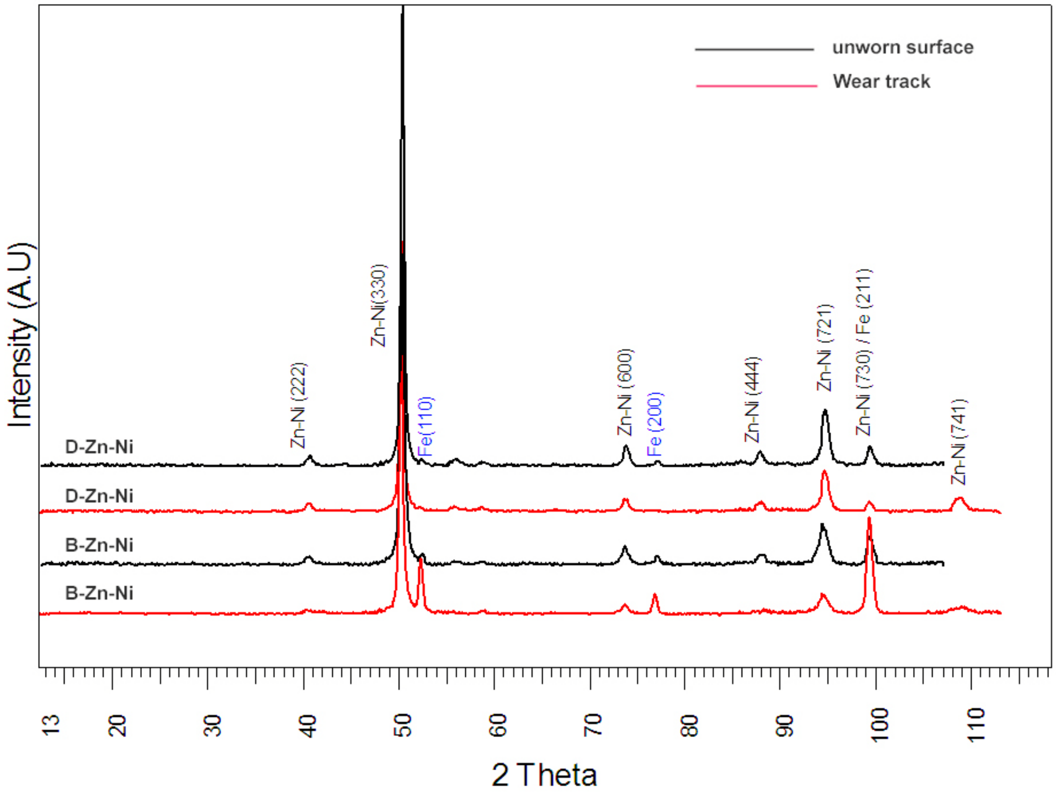
unworn surface
Wear track
Intensity (A.U)
2 Theta
D-Zn-Ni
D-Zn-Ni
B-Zn-Ni
B-Zn-Ni
Zn-Ni (222)
Zn-Ni(330)
Fe(110)
Zn-Ni (600)
Fe (200)
Zn-Ni (444)
Zn-Ni (721)
Zn-Ni (730) / Fe (211)
Zn-Ni (741)
13
20
30
40
50
60
70
80
90
100
110

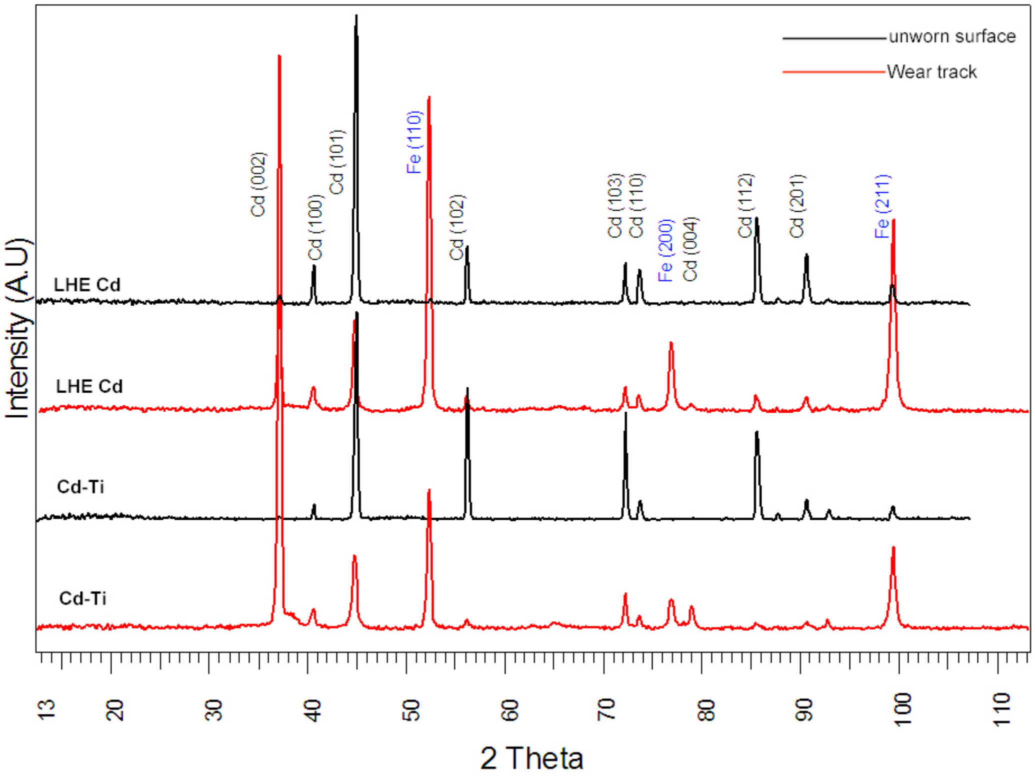

Fig. 3.16 XRD of wear tracks

Ex situ analysis of transfer film formed during wear of the coatings were performed when the transfer film was stable. Wear tests were conducted on alumina sphere for 50 sliding cycles to generate the transfer film on the counterface. The transfer film micrographs are shown in Fig. 3.17. The transfer film accumulation/removal on the alumina ball for Zn–Ni coatings are by the process of shear and delamination of the coating surface, which is evident from the continuous layer type morphology of the transfer film (Fig. 3.17(a) and (b)). The Zn transfer film was found to be composed of loose compaction of wear debris expelled from the wear track, and particle accumulation on the alumina surface (Fig. 3.17(c)). The transfer film formed during wear of Cd and Cd–Ti was found to be hard and adherent to alumina ball. The morphology of transfer film composed of flat facets, deformed layers and transverse cracks appearing due to the strain hardening (Fig.3. 17(d) and (e)).

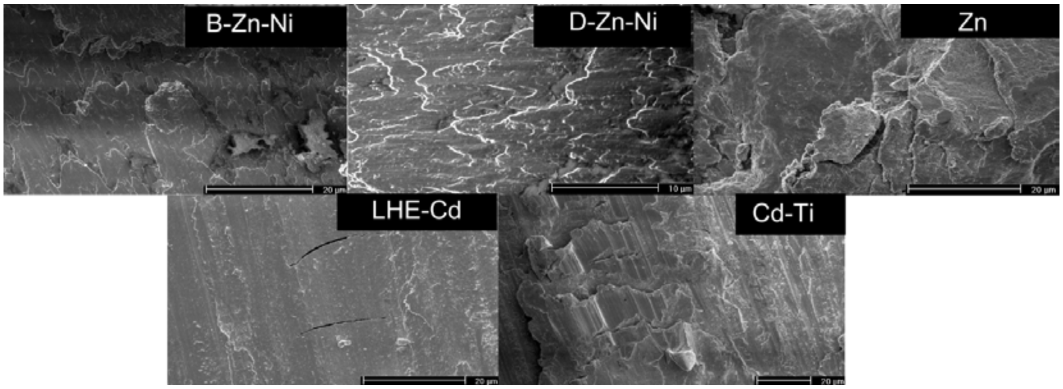

Fig. 3.17 SEM of transfer film formed on alumina sphere (a) B-Zn–Ni, (b) D-Zn–Ni, (C) Zn, (d) LHE Cd and (e) Cd–Ti.

3.3.6. Longer sliding distance wear testing of Zn–Ni coatings

From the *in situ* tests it was shown that the Zn–Ni coatings were superior to Zn and Cd coatings in terms of adhesive wear resistance. Thus, wear test on Zn–Ni coatings was performed at high speed 20 mm/s, eventually at longer sliding distance. The tests were performed for coatings with and without passivation and heat treatment. The results are shown in Fig. 3.18. The wear rates of Zn–Ni coatings after trivalent chrome passivation were slightly lower than the as-plated coatings. The reason behind the reduction in wear rates after passivation was due to the surface modification of the coatings by a very thin chromium oxide layer which resisted the material removal. Baking the coating also slightly improved the wear resistance of the coatings owing to increase in the hardness.

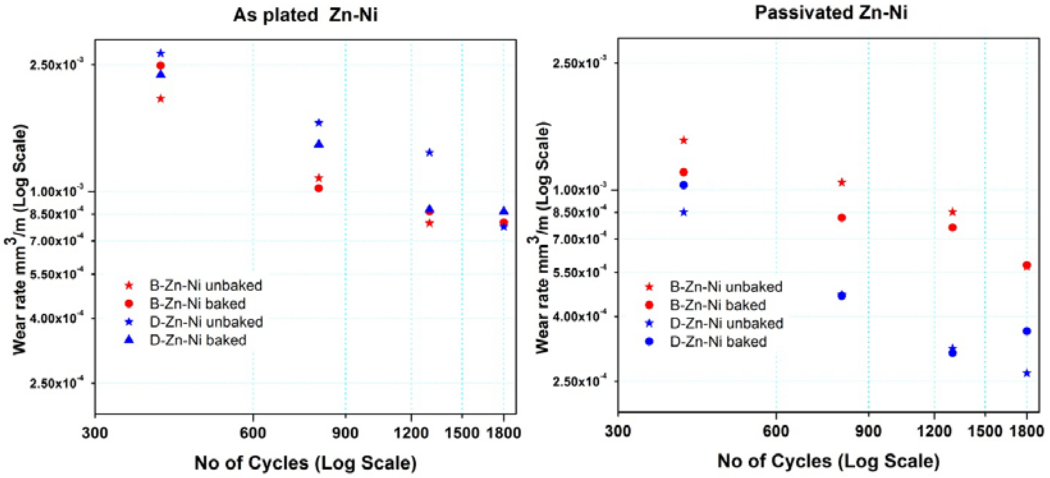

Fig. 3.18 Wear rates in mm^3/m of Zn–Ni coatings subjected to baking and passivation.

3.4. Discussion

This study is the first time that *in situ* tribometry has been used to examine the role of third bodies on metallic friction. The observations made here are remarkably consistent with the current understanding of the tribology of metals, which was entirely discovered by *ex situ* methods. In fact, a suggestion to utilize *in situ* tribology methods to understand friction and wear of contacting surfaces when there is a transfer of material from one surface to another was suggested by Blau in the early eighties [22]. The mechanism and properties of metal transfer during wear of two contacting surfaces, reported by different *ex situ* methods, did not totally account for the stability of the transfer films [39] and [40]. For all coatings studied here, there was an initial formation of a strong adherent metallic transfer film [21]. Also true for all coatings was that this transferred material was unstable in the sense that portions of the film would break away and be replenished with other third bodies, either from wear debris or materials detached directly from the coating. Eventually, the stability of the transfer film was lost entirely, which is a feature not necessarily discussed in tribology textbooks, which often portray the process of wear in metals as constantly reforming the transfer film after its stability is lost (*e.g.*[21]).

One of the utilities of using *in situ* tribology for our study of Cd and Cd-replacement coatings is that the technique provides us with precise knowledge for when the transfer films are worn away. Thus, it was determined when metal *vs.* metal friction and sapphire *vs.* metal friction was measured (see Table 3.1). This is important as the intention of a Cd coating on, for example a fastener, is that the coating will provide the initial lubricity to torque the component without being entirely worn away. For this application, the metal *vs.* metal friction and the wear resistance during this stage of the sliding process is most important. Table 3.1 lists the comparative evaluation of Zn–Ni, Zn and Cd coatings during the wear regime when the transfer film is intact.

Table 3.1. Summary of *in situ* tribology test during the stage when transfer film is in contact with the coating.

	B-Zn-Ni	**D-Zn-Ni**	**Zn**	**Cd**	**Cd-Ti**
Transfer film Stability (Cycles)	600	200	250	500	250
Coating life (based on wear depth) cycles	1800	1800	~400	~250 – 300	~250 – 300
Wear rate A_{300} X 10^{-3} (mm^3/m)	2.13	2.09	9.63	17.50	17.90
COF Before TF failure	0.47 - 0.55	0.15 - 0.51	0.5 - 0.9	0.4 - 0.7	0.5 - 0.6
COF After TF failure	0.55 - 0.80	0.5 - 0.75	0.5 - 0.65	0.45 - 0.60	0.5 - 0.90
COF After Coating failure	-	-	0.5 - 0.65	0.45 - 0.60	0.5 - 0.90

After initial cycles, the transfer film was removed within 500 cycles for B-Zn–Ni and 200 cycles for D-Zn–Ni, Zn, Cd and Cd–Ti. While a discontinuous patch of transfer film was observed in Zn–Ni coatings, a strongly adhering transfer film was found in Zn, and Cd coatings which indicate severe adhesive wear mechanism to be predominant in Zn and Cd coatings. While the Zn–Ni coatings transfer film failure was observed around 600 cycles and 250 cycles, both transfer film and the coating failed in Zn and Cd coatings around 250 cycles. Thus, to evaluate the wear rates comparatively when the coatings were intact, wear rates at cycle 300 were compared for all the coatings, and it was observed that both the Zn–Ni coatings exhibited wear resistance superior to the Zn and Cd coatings. From the *in situ* tribology studies, with respect to the friction coefficients, wear rates and *ex situ* wear track images, it can be concluded that the life of Zn–Ni coatings is superior to other coatings examined in this study. In other words Zn–Ni coatings lasted the full wear cycle compared to Zn and Cd. Thus, for the replacement of Zn and Cd with Zn–Ni, it becomes imperative to compare the friction and wear behavior of Zn–Ni with the above mentioned coatings till stable transfer film or life of the coatings.

One of the important parameters commonly used to evaluate the wear characteristic of metal on metal wear is the calculation of specific wear rate, which is the volume of wear per unit force. The method for calculating specific wear rate, proposed by Archard and Hirst [20] and [41], is based on volume of wear, which is given as follows:

$$K = \frac{Q}{S * P_n}$$

K is the specific wear rate (mm^3/Nm), Q is the wear volume (mm^3), S is the sliding distance (m), and P_n is the normal load (N).

The wear law proposed by Archard [41] predicts wear volume as a function of sliding distance, material hardness and applied load. The limitation of

Archard's law is that it does not take into account the differing contact conditions and the role of third body in micro- and nanoscale tribology experiments. In order to evaluate the coatings in microscale and to account for the third body contribution in wear, a power law for wear was utilized which was proposed by Siniawski et al. [42]

$$A(n)=A_1*n^{\beta}$$

where $A(n)$ is the averaged abrasion rate over n cycles, n is the number of cycles, A_1 is the abrasion rate during the first cycle of wear and β is the time dependent constant of abrasion rate. Also

$$A(n)=\frac{V_n}{d}$$

here V_n is the averaged wear volume of n cycles and d is the sliding distance for n cycles. By fitting the averaged abrasion rate with the number of cycles A_1 and β can be determined. The parameters A_1 and β help better understanding the abrasive wear rates of different coatings. The values of the constants A_1 and β for the coatings are listed in Table 3.2.

Table 3. 2. Summary of Siniawski's model parameters and error results.

Coating	A_1 (mm^3/m)	β	% Root mean square error
B-Zn-Ni	4.4×10^{-2}	-0.43	0.769
D-Zn-Ni	3.3×10^{-3}	-0.39	7.156
Zn	1.8×10^{-1}	-0.42	6.434
Cd	4.3	-0.73	0.171
Cd-Ti	3.7	-0.72	0.365

The constant β is negative which is common for metal on metal contacts [42]. The β values are more negative for Cd based coatings as compared to Zn and Zn–Ni which is also evident that Zn–Ni coatings are more resistant to adhesive wear and loss of material due to material transfer. This implies that during the wear regime, where the transfer film is adherent to the counter-face, Zn–Ni offers maximum wear resistance due to adhesion as compared to both Zn- and Cd-based coatings.

The different contact conditions observed during *in situ* tribology studies are described in Fig. 3.19, starting with Fig. 3.19(a) showing the initial sapphire on coating contact. As the wear test progresses wear debris is generated and a contact is established between the sapphire, wear debris and the coating as shown in Fig. 3.19(b). Fig. 3.19(c) describes the transfer film formation from the wear debris and detachment from the coating. Fig. 3.19(d) describes the intimate contact of a stable transfer film on sapphire with the metal coating. As the wear test progresses, detachment of material from the transfer film takes place leading to an unstable transfer film as observed in Fig. 3.19(e). After the transfer film is totally detached or after complete failure of transfer film, the sapphire is in complete contact with the strain hardened coating as depicted in Fig. 3.19(f). For both the Zn–Ni coatings, the above-described model seemed to be valid until Fig. 3.19(f). During the progression of wear, transfer film was generated and it was the major third body contact before losing its stability. The transfer film eventually failed or detached from the sapphire, leading to intimate contact between the sapphire and the strain hardened coating, resulting in lower wear rates and increase in friction after transfer film removal.

In the case of Zn, the different stages of wear followed the trend up to Fig. 3.19(g). After formation of the transfer film, the transfer film and the coating eventually failed, which led to a mixed mode of contact, *i.e.* sapphire on steel substrate and small bits and pieces of strain hardened coating and wear debris trapped in between the sapphire and the steel substrate.

In the case of LHE Cd and Cd–Ti, the wear model is valid until Fig. 3.19(h). The transfer film and the coating failed leading to a smeared transfer film on the coating and steel substrate as described in Fig. 3.19(h). The transfer film instability and the coating failure occurred at the same time interval. The presence of smeared transfer film resulting in mixed mode contact and obscuring the view during the *in situ* testing was the reason behind higher friction coefficient during the progression of wear test.

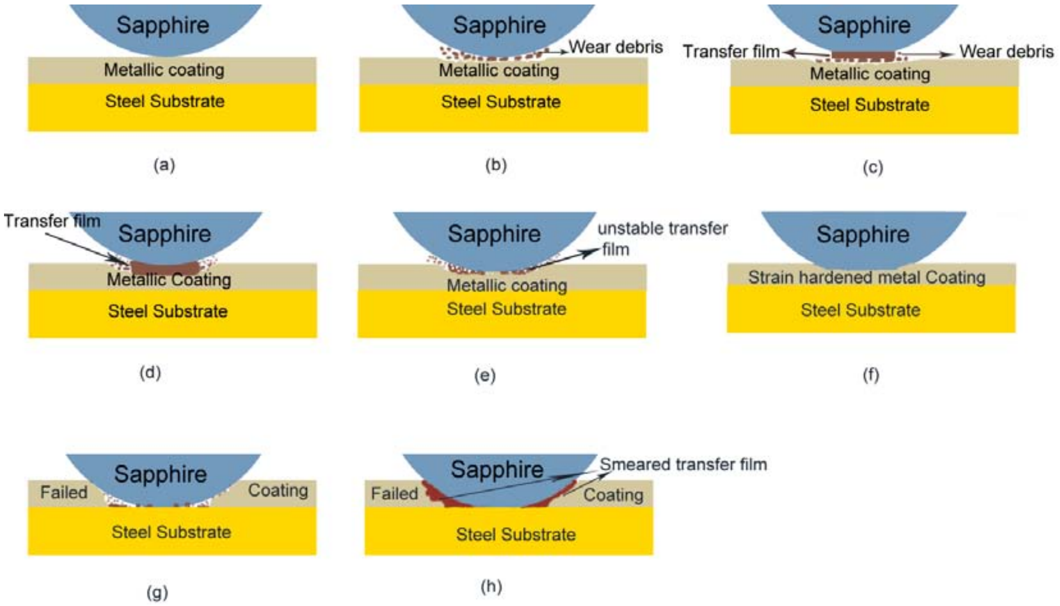

Fig. 3.19 Contact conditions encountered during *in situ* tribology testing of the investigated coatings.

3.5. Conclusions

In this chapter *in situ* tribometry was utilized to understand third body contributions in metallic friction and wear. The nature of transfer film formation and stability, wear debris generation and contact conditions was observed to be different for Zn–Ni, Zn and Cd coatings. The transfer film characteristics were found to influence the friction and wear behavior of metallic coatings. While taking into consideration the transfer of material, adhesion, and varied contact conditions which may lead to severe galling-type seizure during torquing of threaded fasteners, Zn–Ni coatings could act as a replacement for Cd and Zn coatings based on the following conclusions:

- *In situ* tests provided greater insight toward the wear mechanisms of the coatings. Mild adhesion and material removal by delamination was observed in Zn–Ni coatings, while adhesion and large material removal in form of debris was observed in Zn coatings. Rapid transfer film formation and severe adhesive nature of wear was found to be a predominant wear mechanism in Cd and Cd–Ti coatings.
- Zn–Ni coatings showed lowest wear rates when compared to Zn, Cd and Cd–Ti coatings. Wear rates of passivated Zn–Ni coatings were found to be lower than the as plated coatings, and resistance to wear improved in Zn–Ni coatings when given a post baking treatment.
- Microhardness of Zn–Ni coatings was higher than Zn, Cd and Cd–Ti coatings. A marginal increase in hardness was observed in Zn–Ni coatings as a result of baking while no significant changes were observed on other coatings.
- No phase change was observed during wear of coatings other than mild oxidation accompanying the wear process.
- Under unlubricated conditions friction coefficient of Zn–Ni coatings were found to decrease, stabilize to a constant value and then increase after the initial run-in period. Friction coefficients of Zn–Ni were comparable to Cd coatings during the initial run in

period of 500 cycles, which is beneficial when considering Zn–Ni as a replacement for Cd.

References

[1] Lambert MR, Hart RG, Townsend HE. Corrosion mechanism of Zn-Ni alloy electrodeposited coatings. Proceedings - Society of Automotive Engineers. Dearborn, MI, USA: SAE; 1983. p. 81-7.

[2] Felloni L, Fratesi R, Quadrini E, Roventi G. Electrodeposition of zinc-nickel alloys from chloride solution. Journal of Applied Electrochemistry. 1987;17:574-82.

[3] Fedrizzi L, Ciaghi L, Bonora PL, Fratesi R, Roventi G. Corrosion behaviour of electrogalvanized steel in sodium chloride and ammonium sulphate solutions; a study by E.I.S. Journal of Applied Electrochemistry. 1992;22:247-54.

[4] Wilcox GD, Gabe DR. Electrodeposited Zinc Alloy Coatings. Corrosion Science. 1993;35:1251-8.

[5] Alfantazi AM, Erb U. Corrosion properties of pulse-plated zinc-nickel alloy coatings. Corrosion. 1996;52:880-8.

[6] Fabri Miranda FJ. Corrosion behavior of zinc-nickel alloy electrodeposited coatings. Corrosion. 1999;55:732-42.

[7] Rahsepar M, Bahrololoom ME. Corrosion study of Ni/Zn compositionally modulated multilayer coatings using electrochemical impedance spectroscopy. Corrosion Science. 2009;51:2537-43.

[8] Park H, Szpunar JA. The role of texture and morphology in optimizing the corrosion resistance of zinc-based electrogalvanized coatings. Corrosion Science. 1998;40:525-45.

[9] Rajagopalan SR. Electrodeposition of nickel-zinc alloys. Metal Finishing. 1972;70:52-8.

[10] Raman V, Pushpavanam M, Jayarkrishan S, Shenio BA. A bath for the deposition of bright zinc-nickel alloy. Metal Finishing. 1983;81:85-90.

[11] Alfantazi AM, Erb U. Microhardness and thermal stability of pulse-plated Zn-Ni alloy coatings. Materials Science and Engineering A. 1996;212:123-9.

[12] Barceló G, Sarret M, Müller C, Pregonas J. Corrosion resistance and mechanical properties of zinc electrocoatings. Electrochimica Acta. 1998;43:13-20.

[13] Bories C, Bonino JP, Rousset A. Structure and thermal stability of zinc-nickel electrodeposits. Journal of Applied Electrochemistry. 1999;29:1045-51.

[14] Bruet H, Bonino JP, Rousset A, Chauveau ME. Structure of zinc-nickel alloyelectrodeposits. Journal of Materials Science. 1999;34:881-6.

[15] ASTM. 2006 F1941-00 Standard specification for electrodeposited coatings on threaded fasteners (Unified Inch Screw Threads (UN/UNR)). ASTM International, West Conshohocken, PA, 19428-2959, DOI: 10.1520/F1941-07 www.astm.org.

[16] Panagopoulos CN, Georgarakis KG, Agathocleous PE. Sliding wear behaviour of Zinc-Nickel alloy electrodeposits. Tribology International. 2003;36:619-23.

[17] Ruggeri O, Sambogna G, Balboni CP, Volpato GA. Dry lubrication with soft metals: The tribological behaviour of a thin film of cadmium rubbing on carbon steel. Wear. 1980;59:433-46.

[18] Jahanmir S, Abrahamson Ii EP, Suh NP. Sliding wear resistance of metallic coated surfaces. Wear. 1976;40:75-84.

[19] Jahanmir S, Suh NP, Abrahamson Ii EP. The delamination theory of wear and the wear of a composite surface. Wear. 1975;32:33-49.

[20] Rabinowicz E. Friction and Wear of Materials. New York: John Wiley; 1964.

[21] Stachowiak G, Batchelor AW. Engineering Tribology. 3 ed: Butterworth Heinemann; 2006.

[22] Blau PJ. Mechanisms for transitional friction and wear behavior of sliding metals. Wear. 1981;72:55-66.

[23] Dvorak SD, Wahl KJ, Singer IL. Friction Behavior of boric acid and annealed boron carbide coatings studied by *in situ* Raman tribometry. Tribology Transactions. 2002;45:354-62.

[24] Scharf TW, Singer IL. Role of Third Bodies in Friction Behavior of Diamond-like Nanocomposite Coatings Studied by *In Situ* Tribometry. Tribology Transactions. 2002;45:363 - 71.

[25] Scharf TW, Singer IL. Monitoring Transfer Films and Friction Instabilities with *In Situ* Raman Tribometry. Tribology Letters. 2003;14:3-8.

[26] Chromik RR, Baker CC, Voevodin AA, Wahl KJ. *In situ* tribometry of solid lubricant nanocomposite coatings. Wear. 2007;262:1239-52.

[27] Chromik RR, Winfrey AL, Lüning J, Nemanich RJ, Wahl KJ. Run-in behavior of nanocrystalline diamond coatings studied by *in situ* tribometry. Wear. 2008;265:477-89.

[28] Rebelo de Figueiredo M, Muratore C, Franz R, Chromik R, Wahl K, Voevodin A, et al. In Situ Studies of TiC+xNx Hard Coating Tribology. Tribology Letters. 2010;40:365-73.

[29] Strauss HW, Chromik RR, Hassani S, Klemberg-Sapieha JE. In situ tribology of nanocomposite Ti–Si–C–H coatings prepared by PE-CVD. Wear. 2011;272:133-48.

[30] Tran LM, Matthias PM, Jones JH. Low hydrogen embrittlement Zinc/Nickel plating for high strength steels. US Patent. 20120009437A1 edJanuary 12, 2012

[31] MIL-STD-870C. U.S. Military Standard (USAF) on Cadmium plating, Low embrittlement, Electrodeposition. Department of Defence Standard Practice; 27 April 2009.

[32] MIL-STD-1500C. U.S. Military Standard (USAF) on Cadmium-Titanium Plating, Low Embrittlement, Electrodeposition. Department of Defence Standard Practice; 01 March 2007.

[33] Khurshudov AG, Olsson M, Kato K. Tribology of unlubricated sliding contact of ceramic materials and amorphous carbon. Wear. 1997;205:101-11.

[34] Bruet-Hotellaz, Bonino JP, Rousset A, Marolleau, Chauveau E. Structure of zinc-nickel alloyelectrodeposits. Journal of Materials Science. 1999;34:881-6.

[35] Morón LE, Méndez A, Castañeda F, Flores JG, Ortiz-Frade L, Meas Y, et al. Electrodeposition and corrosion behavior of Zn coatings formed using as brighteners arene additives of different structure. Surface and Coatings Technology. 2011;205:4985-92.

[36] Abd El-Halim AM, Baghlaf AO, Sobahi MI. Effect of some addition agents on the electrodeposition of cadmium from acidic chloride baths. Surface Technology. 1984;22:129-42.

[37] El-Halim AMA, Sobahi MI. Effect of bath constituents and some plating variables on the electrodeposition of cadmium from acidic chloride baths. Surface Technology. 1983;19:45-57.

[38] Brooks I, Erb U. Hardness of electrodeposited microcrystalline and nanocrystalline [gamma]-phase Zn-Ni alloys. Scripta Materialia. 2001;44:853-8.

[39] Chen LH, Rigney DA. Transfer during Unlubricated Sliding Wear of Selected Metal Systems. Wear. 1985;105:47-61.

[40] Heilmann P, Don J, Sun TC, Rigney DA, Glaeser WA. Sliding Wear and Transfer. Wear. 1983;91:171-90.

[41] Archard JF, Hirst W. The Wear of Metals under Unlubricated Conditions. Proceedings of the Royal Society of London Series A Mathematical and Physical Sciences. 1956;236:397-410.

[42] Siniawski MT, Harris SJ, Wang Q. A universal wear law for abrasion. Wear. 2007;262:883-8.

4.0 Tribocorrosion behavior of Zn, Zn-Ni, Cd and Cd-Ti electrodeposited on low carbon steel substrates

Preface

In this chapter, tribocorrosion behavior of electrodeposited Zn-Ni & Cd coatings is reported. A modified pin on flat tribometer in an electrochemical cell was used to study wear enhanced corrosion of the coatings in 3.5 % NaCl solution. Wear tests were conducted at open circuit potentials, and at impressed anodic potentials to determine the corrosion resistance of coatings before, during and after the wear test. EIS was utilized to understand the polarization resistance of the coatings before and after wear tests. Ex-situ analysis of the wear tracks with XRD & SEM was performed to understand the nature of wear track under tribocorrosion and also to understand the corrosion products. Zn-Ni was found to be suitable as a Cd replacement because of its higher polarization resistance and lower mass loss due to wear enhanced corrosion. The contents of this chapter will be submitted as a manuscript to the journal Surface & Coatings Technology, Elsevier publications.

Abstract

The tribocorrosion behavior of electrodeposited Zn-Ni alloy coatings was investigated for their suitability to replace Zn and Cd based coatings. A modified pin on flat tribometer in an electrochemical cell was utilized to understand wear induced corrosion of the coatings in 3.5 % NaCl solution. Wear tests were conducted at open circuit potentials, and impressed anodic potentials of the coatings to determine the corrosion resistance of coatings before, during and after the wear test. Electrochemical impedance spectroscopy was utilized to understand the polarization resistance of the coatings before and after the wear tests. Wear tracks were analyzed with SEM and XRD to determine the nature of corrosion products and surface morphology changes during the tribocorrosion tests. Zn-Ni coatings had higher polarization resistance after wear test as compared to zinc and cadmium coatings. The mass loss due to wear enhanced corrosion was less with Zn-Ni than with Zn and Cd coatings. Zn-Ni coatings are a suitable replacement to Cd coatings when the surfaces are subjected to simultaneous wear and corrosion.

Keywords: Electrodeposited Zn-Ni, Cd, Zn coatings, tribocorrosion, EIS

4.1. Introduction

Cadmium is used as a sacrificial protective coating for various high strength steel and Ni based super alloys in the aerospace industry. The hazardous nature of cadmium has made it subject to stringent environmental regulations. Consequently, the use of Cd is restricted to small quantities; with a view to eventually eliminate cadmium from all applications. Different sacrificial coatings, namely binary and ternary alloy coatings of Zn, Fe and Co are currently being considered to replace cadmium in the aerospace applications, e.g. Zn-Co, Zn-Ni, Zn-Fe [1] and Zn-Ni-Co [2]. Among these coatings, Zn-Ni is the leading candidate. The reason for the preference of Zn-15% Ni as a cadmium replacement over other coatings is because of fewer complexities with the plating bath, higher plating efficiency, superior chemico-mechanical properties as compared to Cd and other Zn based alloy coatings [3].

One of the relevant chemico-mechanical properties for such a coating is tribocorrosion. Different types of tribocorrosion tests that are performed are: [4-7]

1. monitoring current and potential changes that result from galvanic effects between the wear scars and non damaged surface under open circuit potentials,
2. application of constant anodic over potential by a potentiostat and monitoring variation of corrosion current and time,
3. application of small amplitude a.c. signal at OCP or impressed potential and measurement of EIS to evaluate the corrosion resistance before and after wear.

In the past decade a lot of research has been undertaken in the field of surface engineering to address tribocorrosion problems of hard coatings, which are designed for engineering and wear applications while also protecting the base metal from corrosion [6, 8-12]. Zn-Ni coatings are of interest in automotive and aerospace applications because of their superior mechanical properties and corrosion behavior. Much research has been conducted in areas of corrosion behavior [3, 13-18] mechanical properties [19] and tribology of Zn-Ni alloy coatings [20, 21]. However, so far no literature is available on tribocorrosion performance of Zn-Ni alloy coatings, nor on tribocorrosion performance of Zn or Cd coatings. Thus, this work focuses on tribocorrosion behavior of electrodeposited Zn-Ni, Cd, Cd-Ti and Zn using a modified pin on flat tribometer in a three electrode electrochemical cell. The effects of heat treatment and trivalent chrome passivation on the tribocorrosion behavior of Zn-Ni coatings were also analyzed.

Three different methods are utilized for determining the tribocorrosion resistance. Measurement of corrosion characteristics with the help of OCP monitoring, EIS measurements and by current transient studies during wear, the contribution of increase in metal corrosion during wear is determined [5, 7]. This is termed as wear enhanced corrosion. The *wear enhanced corrosion* of the coatings was studied by monitoring the open circuit potential changes before during and after the wear tests. Additionally, a constant overpotential of 200 mV, with respect to standard calomel electrode (SCE) was applied to the coating surface, which was higher than the open circuit potentials of the coatings (OCP). Under the impressed electrode potential corrosion currents were monitored during wear tests. Electrochemical impedance spectroscopy with equivalent circuit modeling was utilized to determine the polarization resistance of the coatings before and after the wear tests. Mechanical characterization of the coatings was performed using indentation testing. Wear tracks and corrosion products were characterized using XRD, and SEM.

4.2. Experimental Methodology

4.2.1 Coating processes

The following five coatings were deposited on low carbon steel substrates, the plating parameters are described below. The thicknesses of all coatings were in the range of 15-20 µm.

***Boeing LHE Zn-Ni**:* Low hydrogen embrittling (LHE) Zn-Ni plating process developed by Boeing Research & Technology, USA was used [22] . An alkaline NaOH (135 g/l) based plating solution with Zn (9-11 g/l) and Ni (0.8-1.2 g/l) metal concentrations in the ratio of 10-11:1 and additives was used, and plated in an industrial pilot plating tank. The pH of the plating bath was maintained to 12-13.5 at 20-25º C and a plating current density of 48mA/cm^2 was applied to obtain a coating thickness of 15 - 20 µm in 1 hour. Substrates were aqueous degreased, abrasive grit blasted and activated in HCl before plating. Boeing LHE Zn-Ni will be referred to B-Zn-Ni henceforth in this paper.

Dipsol IZ C17+Zn-Ni: Commercially available Zn-Ni plating solution by Dipsol Inc was used. An alkaline NaOH (135 g/l) based plating solution with Zn and Ni metal concentrations in the ratio of 10-11:1, with commercial additives was used, and plated in an industrial pilot plating tank. The pH of the plating bath was maintained at 12-13.5 at 25º C and a plating current density of 28 – 30 mA/cm^2 was applied to produce a coating thickness of 15 – 20 μm in one hour. The substrates were grit blasted and acid pickled in HCl before plating. Dipsol IZ C17+ Zn-Ni will be referred to D Zn-Ni henceforth in this paper.

Zn: The plating bath was acid chloride based with $ZnCl_2$ (60g/l), KCl(250g/l), H_3BO_3 (25g/l) and HCl in smaller concentrations to maintain the pH of the bath to 4.5-4.8. The cathode efficiency was 95% and the temperature of the plating was held at 25 ºC. The electroplating was performed on a laboratory-scale plating setup. A plating current density of 5 mA/cm^2 was used to generate a coating thickness of 15 μm in 2 hours. The substrates were finished to 600 # SiC grinding paper and activated in HCl for 12 s before plating.

Low hydrogen embrittling Cd plating (LHE Cd) was plated in an industrial plating facility using an alkaline cyanide based plating solution with CdO (20-30 g/l), NaCN (90-135 g/l), Na_2CO_3 (0-60 g/l) and NaOH (11-30 g/l). A plating current density of 118 – 120 mA/cm^2 was used to generate a coating thickness of 15 μm in 5 minutes. Substrates were solvent degreased, grit blasted and acid pickled before plating. Plating temperature of 15-30ºC was used [23].

Cd-Ti: Alkaline cyanide based plating solution, with CdO (18-35 g/l), NaCN (74-200 g/l), Na_2CO_3 (0-60 g/l), and NaOH (11-30 g/l) was used, and plated in an industrial pilot plating tank. Ti was added in small concentrations (40 -100 parts per million) for grain refinement and control of surface morphology. An initial strike was applied at a plating current density of 46 – 55 mA/cm^2 for a 15 seconds to buildup a flash layer with sufficient adhesion and subsequently a plating current density of 16 -32 mA/cm^2 was applied to generate a total coating thickness of 15 μm in 15 minutes. Substrates were solvent degreased, grit blasted and acid pickled before plating. Plating temperature of 15-30 °C was used [24].

All of the sample coatings were deposited on low carbon steel (SAE 1006) substrate in the form of sheets 10 cm x 16 cm, 0.8 mm thick. The coated sheets were then mechanically sheared into 2.5 x 2.5 cm squares for wear testing and analysis. The Zn-Ni coatings were tested under four conditions: (i) as-plated, (ii) with chromate passivation (iii) as plated and baked for 24 hours at 200 °C, (iv) with chromate passivation and baked.

4.2.2 Tribocorrosion testing

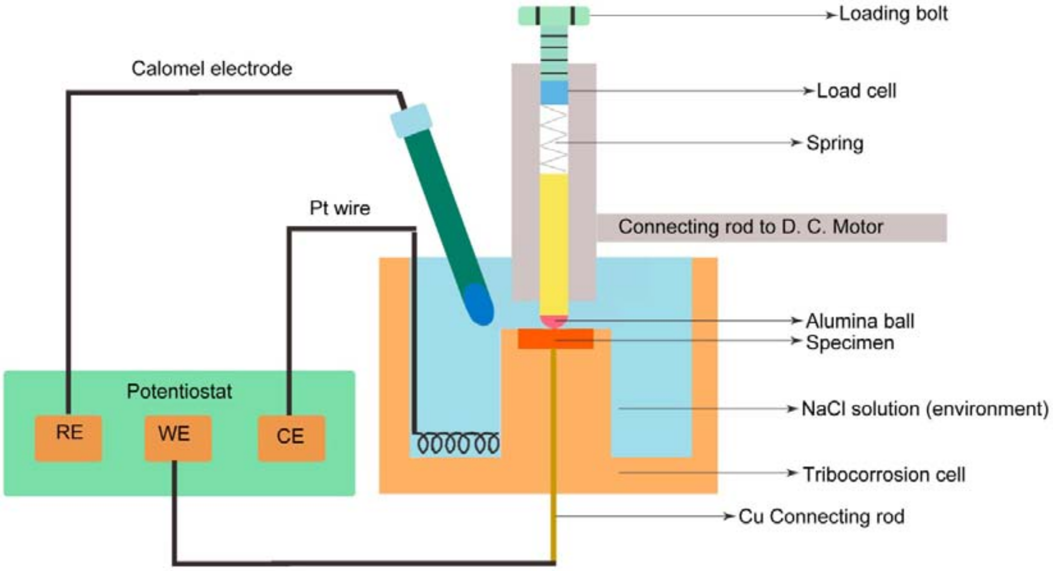

Fig. 4.1 Experimental setup used for tribocorrosion testing

The tribocorrosion studies of the coatings were performed using a reciprocating pin on flat tribometer, shown in Fig. 4.1. The test specimen is housed in an electrochemical cell capable of holding NaCl Solution. The counter face used for sliding was a pin equipped with an alumina ball of 4.8 mm diameter. Pressure was applied in the normal direction using a spring loaded bolt connected to a load cell. A three electrode configuration was used to monitor the corrosion current and the potential in the electrochemical cell. The specimen, supported by a copper backing plate and connecting rod, acted as the working electrode (WE). A platinum wire was used as counter electrode (CE) and a standard calomel electrode (SCE) was used as reference electrode. The electrodes were connected to a computer controlled potentiostat (Autolab PGSTAT302 Electrochemie). A detailed description of the equipment is given elsewhere [9, 11]. The wear tests were conducted for a track length of 12 mm at 1 Hz frequency corresponding to a sliding distance of 43.2m for 1800 cycles. All the specimens were tested under the same load of 2.5 N, leading to the initial Hertzian contact stresses of 0.59 GPa for Zn-Ni, 0.56 GPa for Zn and 0.38 GPa for Cd and Cd-Ti.

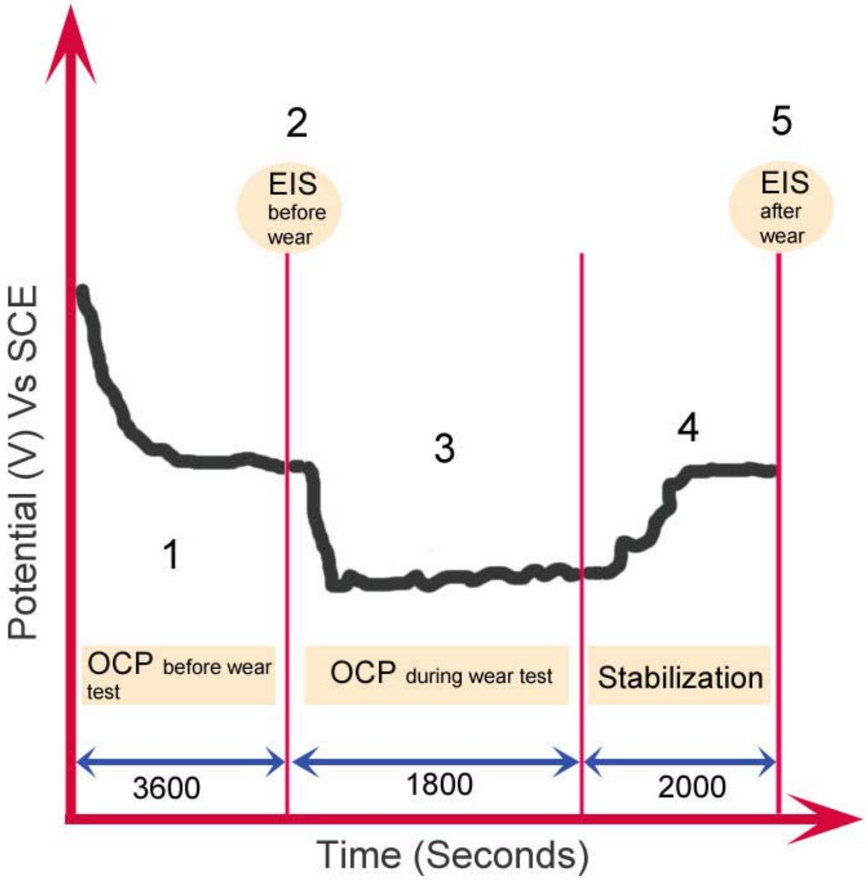

Fig. 4.2 Test schematic for tribocorrosion testing of the investigated coatings

The tribocorrosion procedure used in this test was a procedure established for a wide range of materials, e.g. Diamond like Carbon coatings by PECVD [25] , Ni-Co coatings by electrodeposition [11] on steel substrates. As shown in Fig. 4.2, the test was conducted in 5 stages: (i) The sample was mounted on the electrochemical cell and the open circuit potential (OCP) was monitored for 3,600 s; (ii) EIS spectrum was acquired for the specimen before the wear test after a stable OCP was measured for 3,600 s; (iii) wear test was conducted with the tribometer in the electrochemical cell for 1800 s at OCP; (iv) After the wear test the potential was monitored for 2,000 s until the OCP stabilized; (v) an EIS spectrum was acquired after the wear test was completed. The EIS spectra for the coatings were acquired at OCP values ranging from 10^5 Hz to 10^{-3} Hz for the coatings before and after the wear tests, with AC amplitude of 10mV. Additional tests were conducted for the coatings at a potentiostatic condition at anodic overvoltage of 200 mV to study the corrosion current during wear tests.

4.2.3 Coating characterization

All coatings considered for characterization were passivated. This was done because passivation is an established industrial process where a thin layer of oxide layer ~50nm of trivalent chromium is applied using chemical conversion methods to prolong the life of the sacrificial coating [26]. A Bruker Discover D8-2D area detector x-ray diffractometer with Cu-Kα radiation was used to characterize the coating materials. X-ray diffraction in standard θ-2θ mode was performed on the unworn coating surfaces. Grazing incidence mode with incidence angle of 2° was utilized to characterize wear tracks at different regions in the presence of loose wear debris. The wear tracks were observed and analyzed using a Philips field emission scanning electron microscope (FE-SEM) at 20 KV accelerating voltage. Compositional analysis of wear tracks was performed using Energy Dispersive Spectrometry (EDS).

4.3. Results & Discussion

4.3.1 Coating Characterization

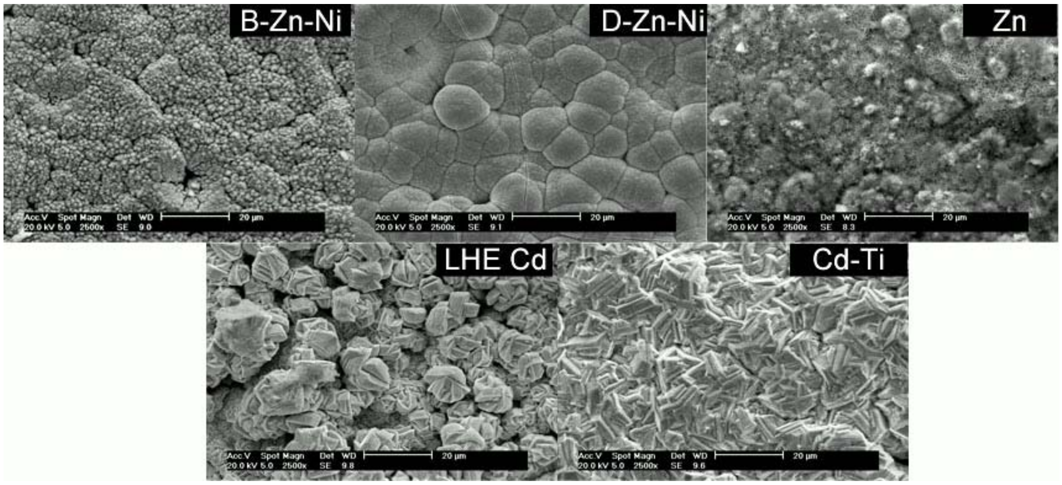

Fig. 4.3 Surface morphology of the passivated coatings

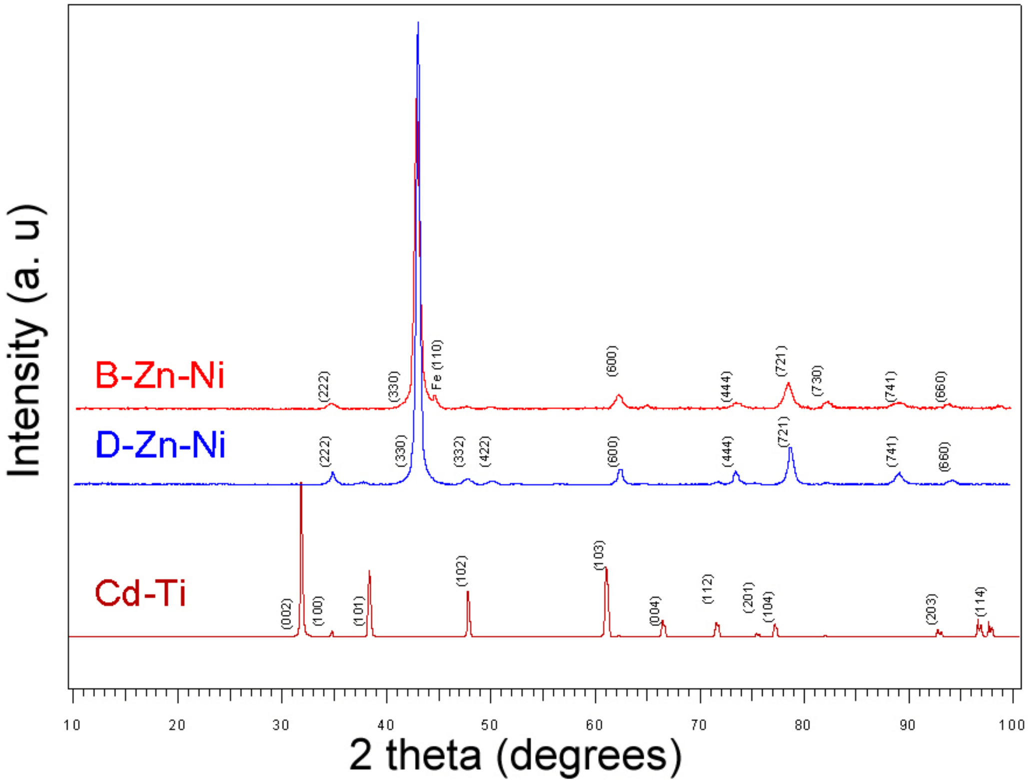

Fig. 4.4 XRD of investigated coatings (passivated)

The surface morphologies and X-ray diffraction patterns of the passivated coatings are shown in Fig. 4.3 and 4 respectively. From Fig. 4.3., it can be observed that B-Zn-Ni was composed of fine platelets [27] less than 1 µm in size while D-Zn-Ni was composed of large platelets (about 10 µm in size) with intermittent porosity and microcracks. The X-ray diffraction results in Fig. 4.4 showed that both the Zn-Ni coatings are γ Zn-Ni (Ni_2Zn_{11}) which is the typical phase observed in Zn – 15 % Ni. The differences in surface morphologies are the consequence of differences in plating parameters between the two processes. The Zn coating was composed of hemispherical clusters which are typical of most Zn coatings [27, 28]. The Cd coating was composed of spherical hexagonal platelets (Fig. 1d). More precisely, these platelets are hexagonal crystals clustered together to form a spherical structure, a common characteristic of Cd coatings [29, 30] . The Cd-Ti coating, exhibited a different morphology as compared to the Cd coating. Instead of spherical hexagonal platelet morphology, stacking of individual platelets was observed. It is believed that the addition of Ti in the plating solution resulted in the formation of Cd-Ti solid solution causing this change in morphology. The Cd-Ti coating showed typical diffraction patterns of Cd deposits as shown in Fig. 4.4. The Cd-Ti coating did not exhibit any phases apart from Cd, supporting the hypothesis that the Ti formed a solid solution with Cd [31].

The micro hardness of these coatings were reported in our previous work [32]. Both the Zn-Ni coatings exhibited higher hardness as compared to Zn, Cd and Cd-Ti coatings. It is well documented [19, 32] that Zn-Ni is harder than pure electrodeposited Zn because the Zn-Ni is almost entirely composed of intermetallic gamma phase (Ni_2Zn_{11}). The baking treatment increased the hardness of the Zn-Ni coatings slightly while it did not significantly change the hardness of other coatings. The effects of baking treatment on tribocorrosion of the Zn-Ni coatings are discussed in detail in a separate section. The difference in hardness between the two Zn-Ni coatings may be explained by the fact that the intermetallic γ Zn-Ni can exist in varying non-stoichiometric compositions (10 - 14% of Ni) [33].

4.3.2 Wear test at open circuit potentials

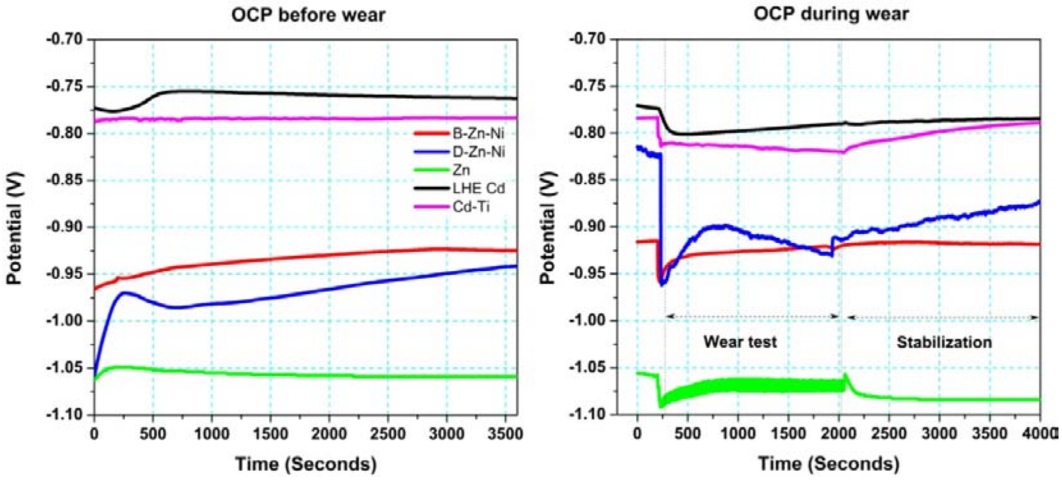

Fig. 4.5 OCP before and during wear test for the tested coatings

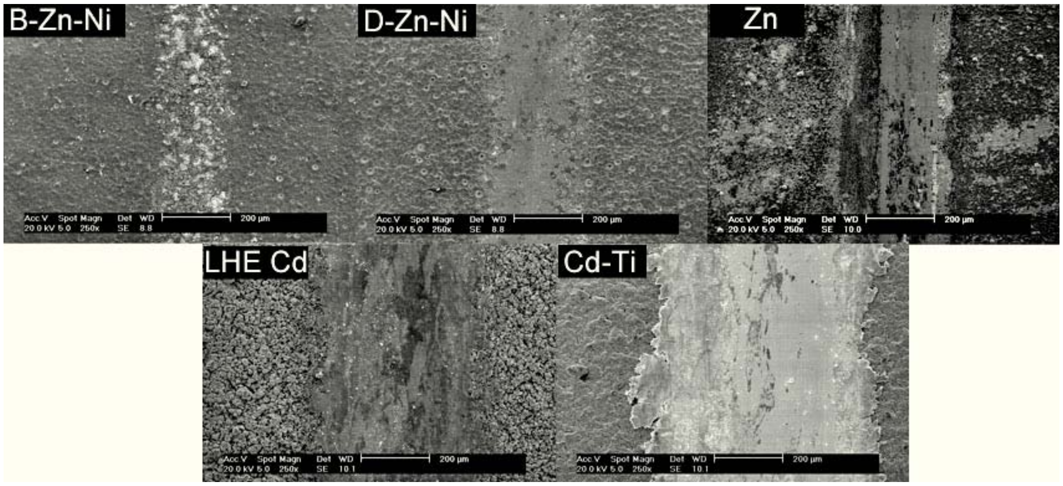

Fig. 4.6 Wear scars after OCP wear testing

Fig. 4.5 shows the open circuit potentials (OCP) of the coatings before and during wear tests. The measurement of corrosion potential during sliding or wear makes it possible to monitor the surface states of the sliding material.

From Fig. 4.5 it can be observed that the OCP of Zn-Ni is between that of Zn (less noble) and of Cd (nobler). The OCPs of Zn and Cd appear to be stable while that of Zn-Ni is quasi stable. This observation may be explained by a preferential dissolution of Zn from the Zn-Ni matrix resulting in a Ni enriched surface. From Fig. 4.5 b. it can be observed that for all the coatings there was a drop in potential during the initial cycles of wear testing followed by gradual increase and finally stabilization to a constant value almost equivalent to the potential of the coating at the start of the wear test. The drop in the open circuit potentials during wear was due to removal of the passive film on the coating surface during the initial cycles. The OCP of the D-Zn-Ni coatings is significantly higher at the start of wear because of dezincification during the 1 h time delay between step 1 and step 3 of the experiment during which EIS measurements were recorded (step 2). During wear, the OCP for the B Zn-Ni coating was in the same range as that observed in Fig. 4.5a. However, the behavior of D Zn-Ni was generally less stable. During wear, the OCP of D Zn-Ni increased above that of B Zn-Ni, up to a maximum, and then slowly decreased to a point just below the OCP of B Zn-Ni. After the wear test, the OCP of B Zn-Ni remained stable, while that of D Zn-Ni followed a constant upward trend. Tribocorrosion phenomena depend on the electrochemical reactions resulting in metal dissolution, and the parameters that affect the kinetics of these reactions. Here it can be observed that with all the coatings there was a drop in OCP at that start of wear. However, there is no measure of the kinetics of dissolution reactions which is a disadvantage of this technique [5].

Fig. 4.6 shows the wear track morphologies of the coatings after the tribocorrosion tests. Both Zn-Ni coatings survived the wear test; the wear tracks showed evidence of deformation and corrosion, but the wear process did not expose the substrate steel. The Zn, Cd and Cd-Ti did not survive the wear test; the wear tracks were considerably wider than for the Zn-Ni coatings leaving patches of exposed steel.

4.3.3 Wear test at anodic impressed potentials

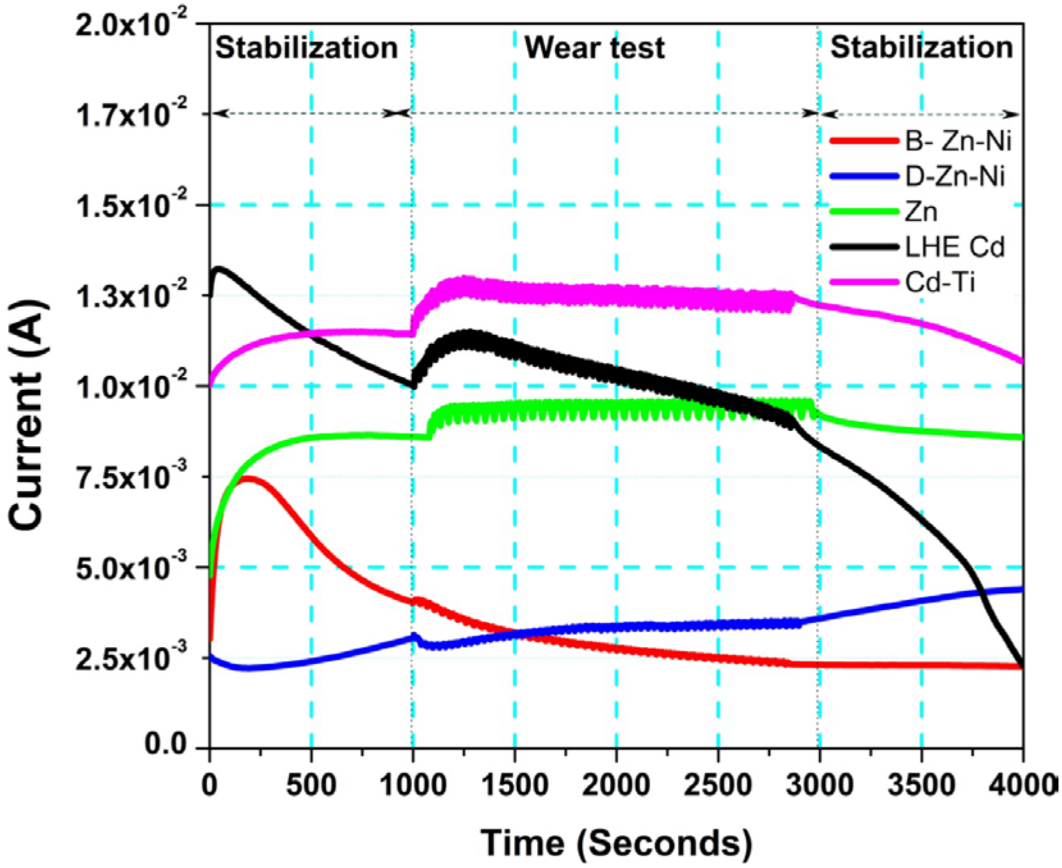

Fig. 4.7 Current transient data during anodic wear tests of the investigated coatings

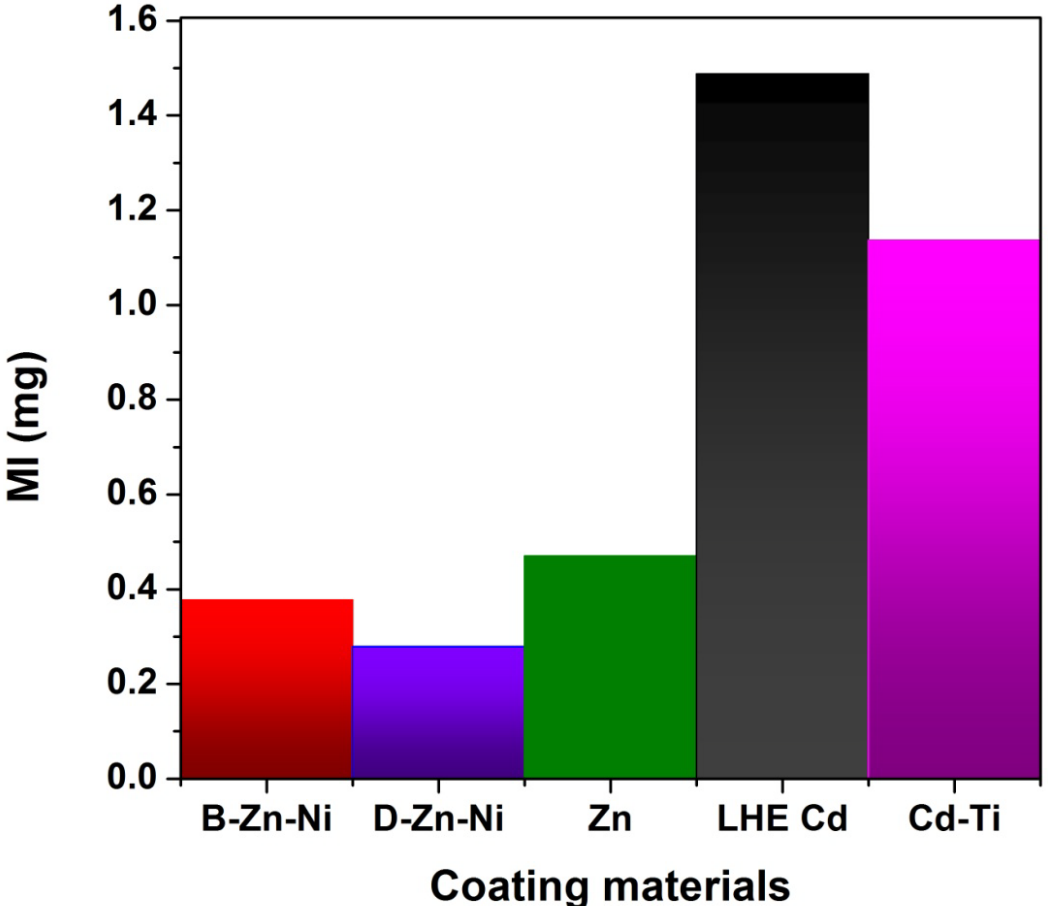

Fig. 4.8 Mass loss due to wear enhanced corrosion of the coatings

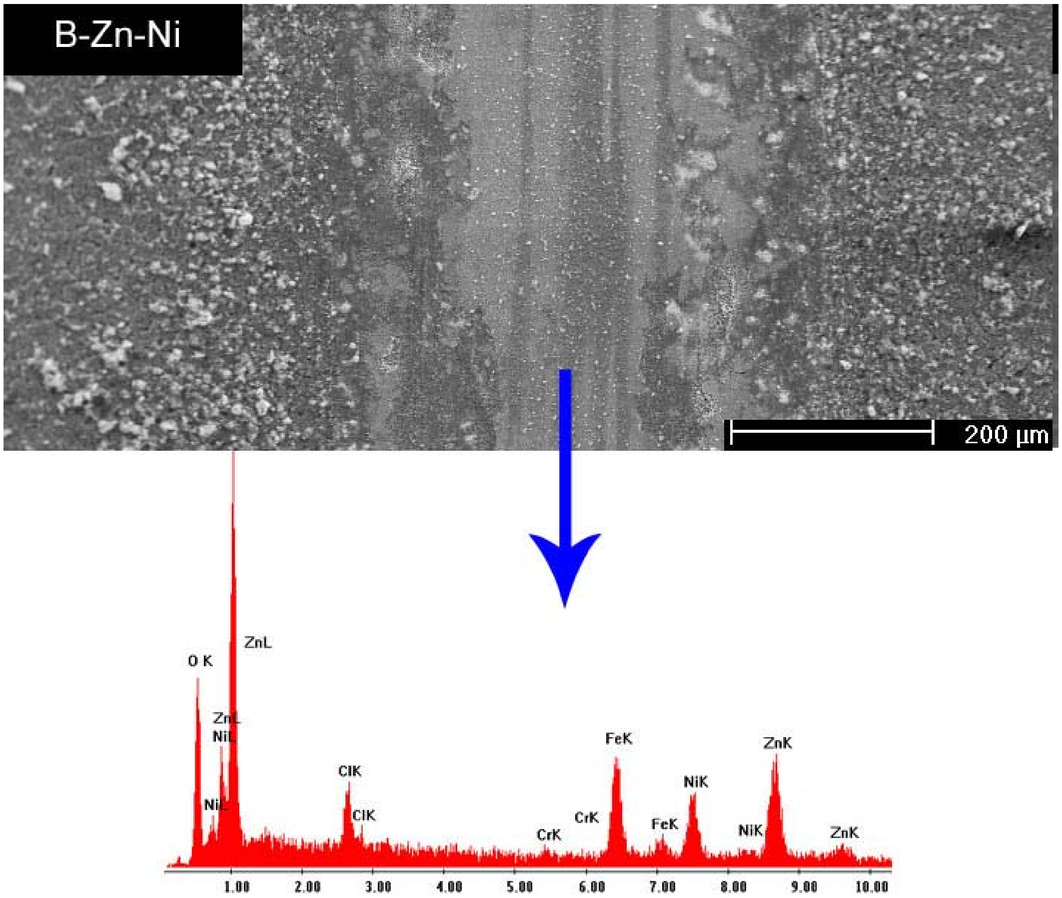
B-Zn-Ni
200 µm
O K
ZnL
ZnL
NiL
NiL
ClK
ClK
CrK
CrK
FeK
FeK
NiK
NiK
ZnK
ZnK
1.00
2.00
3.00
4.00
5.00
6.00
7.00
8.00
9.00
10.00

(a)

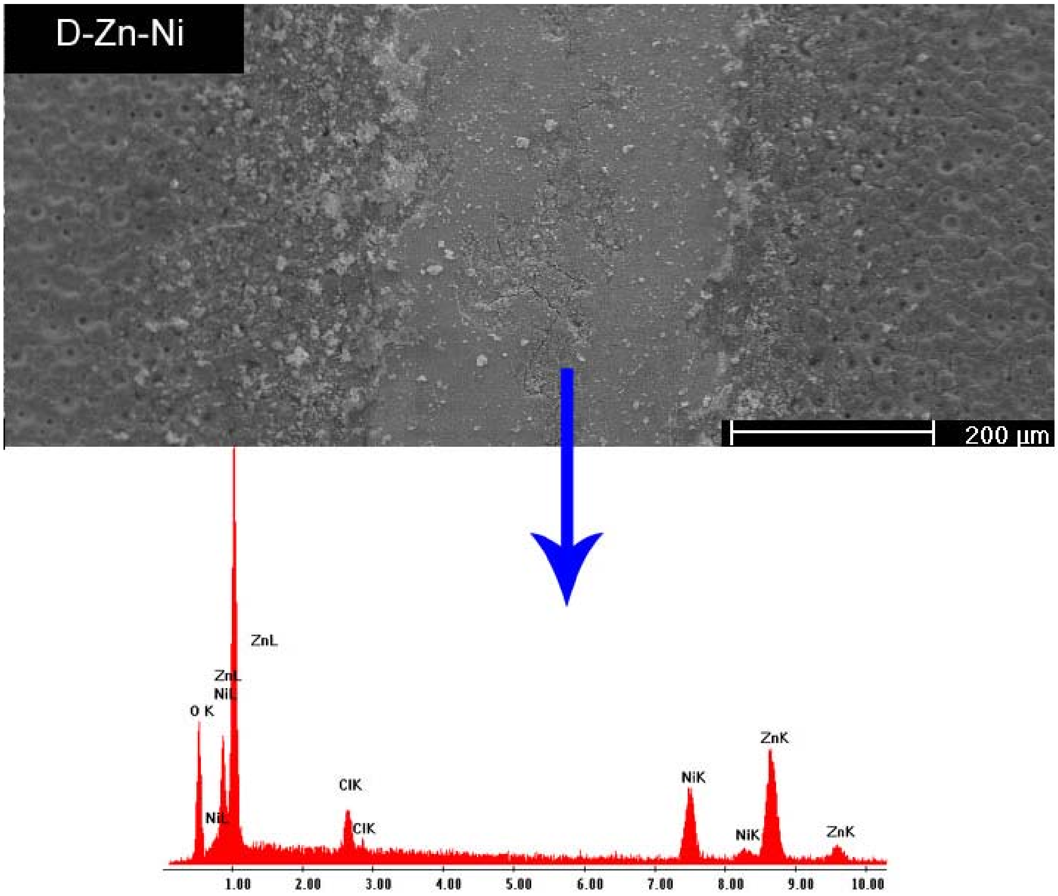
D-Zn-Ni
200 µm
ZnL
ZnL
NiL
O K
NiL
ClK
ClK
NiK
ZnK
NiK
ZnK
1.00
2.00
3.00
4.00
5.00
6.00
7.00
8.00
9.00
10.00

(b)

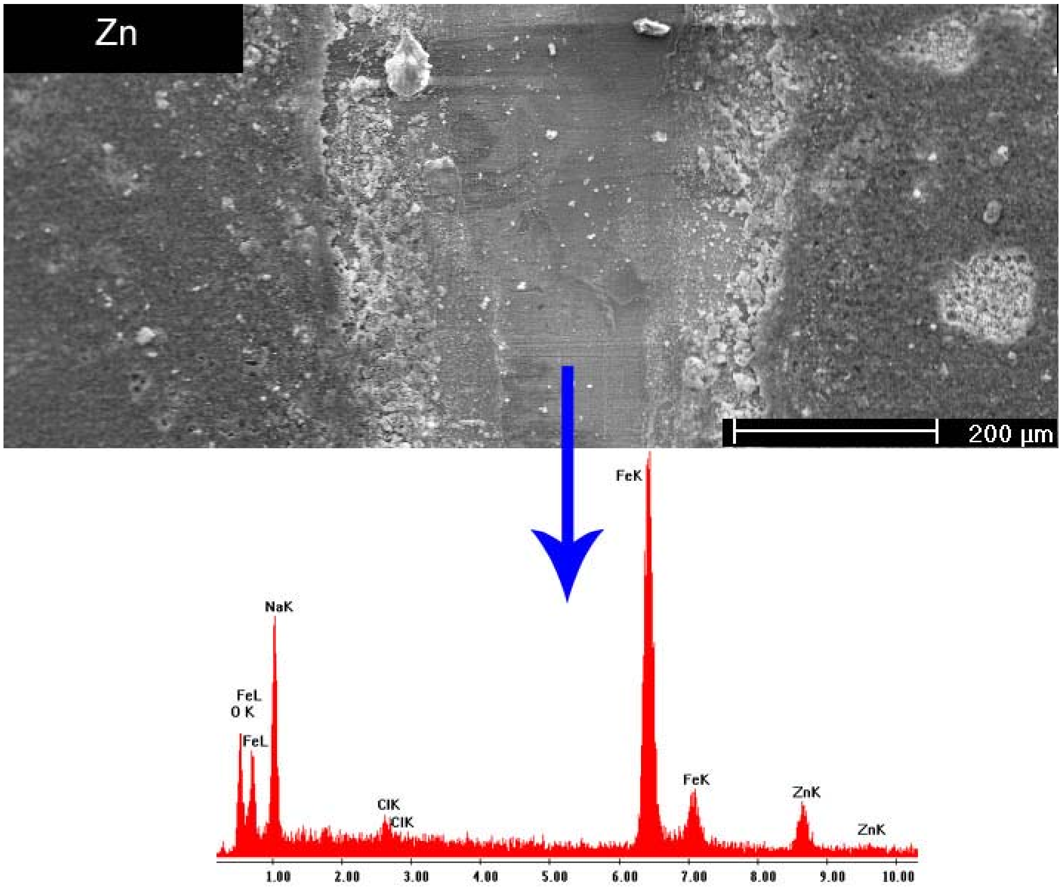
Zn
200 µm
FeK
NaK
FeL
O K
FeL
ClK
ClK
FeK
ZnK
ZnK
1.00
2.00
3.00
4.00
5.00
6.00
7.00
8.00
9.00
10.00

(c)

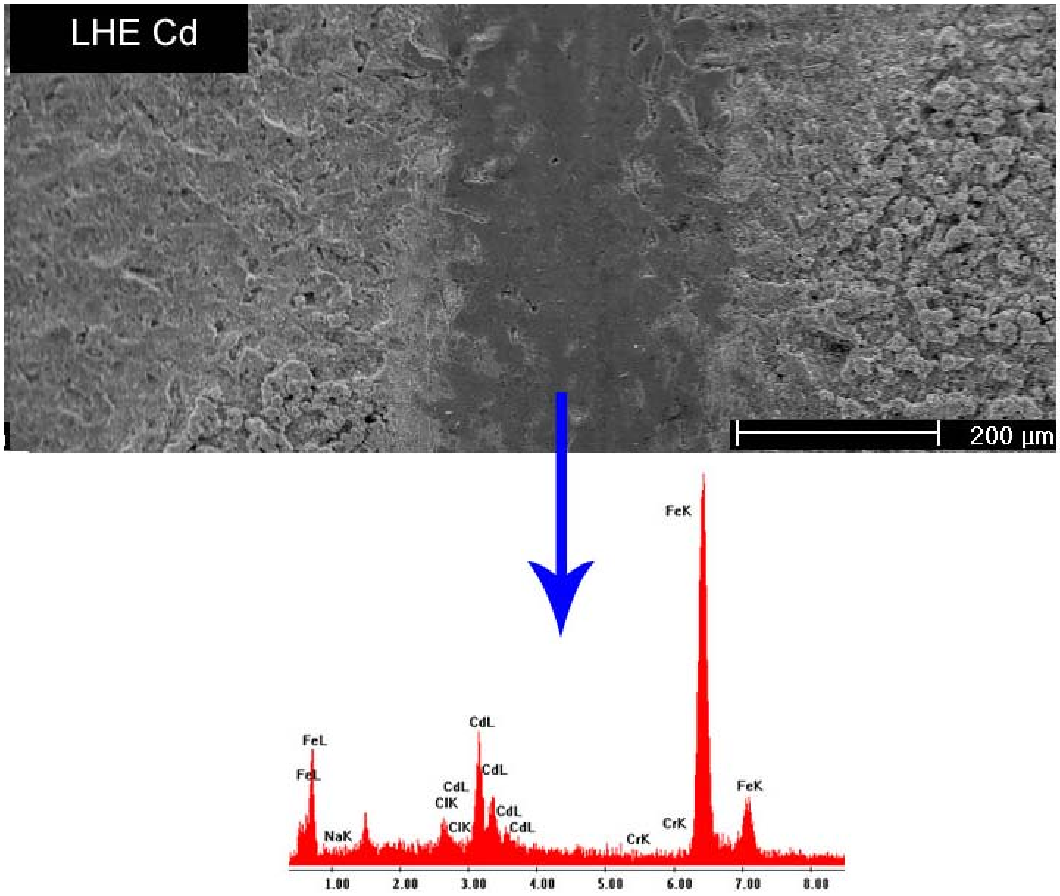
LHE Cd
200 µm
FeK
FeL
FeL
NaK
CdL
CdL
ClK
ClK
CdL
CdL
CdL
CrK
CrK
FeK
1.00
2.00
3.00
4.00
5.00
6.00
7.00
8.00

(d)

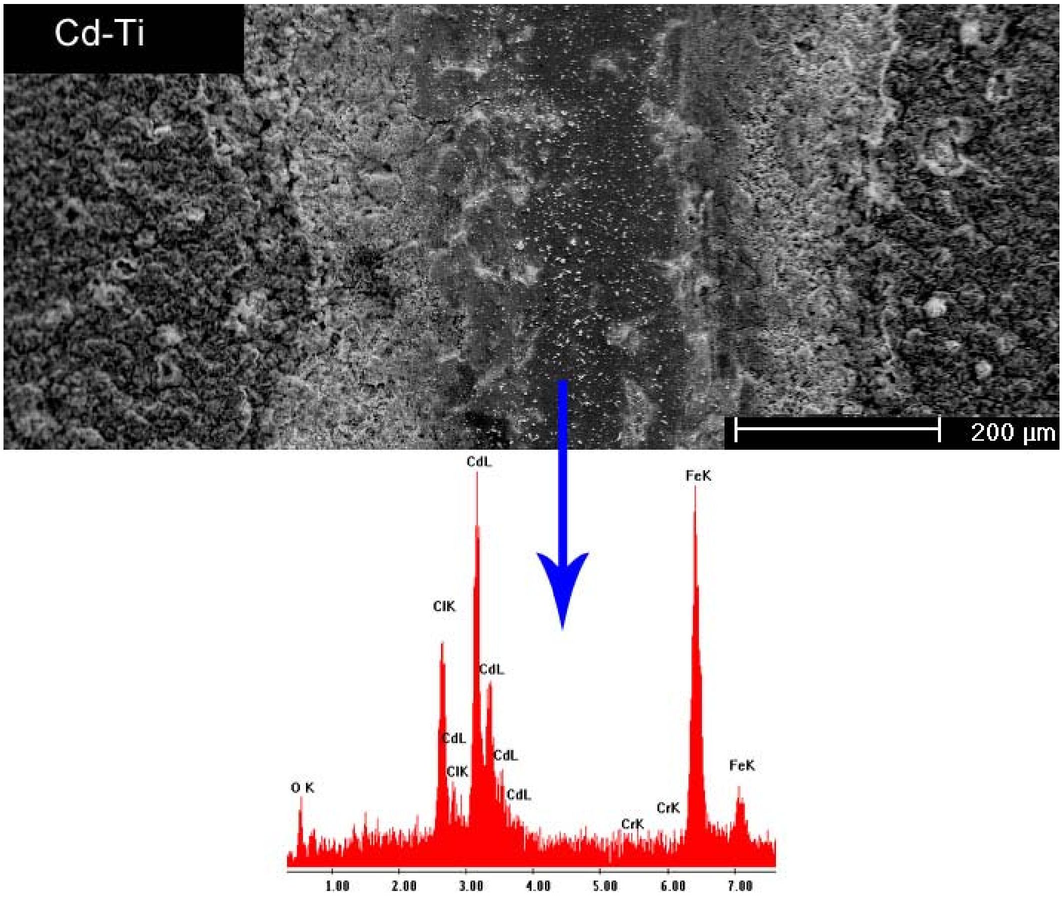

(e)

Fig. 4.9 Wear scars after anodic wear testing (a)B-Zn-Ni, (b)D-Zn-Ni (c) Zn (d) LHE Cd (e) Cd-Ti

The presence of oxidizing agents such as ferricyanide or hydrogen peroxide in the environment usually increases the corrosion rate. These oxidizing agents shift the open circuit potentials to the anodic side. To simulate this kind of severe chemical and electrochemical condition, an anodic overpotential of 200 mV (SCE) was applied during the wear test to the working electrode (the metal coating in this case). The resulting current transient recorded by the potentiostat is a measure of an *enhanced* corrosion in the wear track [5, 11].

The current transients during wear tests are shown in Fig. 4.7. From this figure it can be observed that the corrosion currents during wear of Zn-Ni coatings were lower in magnitude when compared to those of Zn and Cd coatings. This observation can be explained by Ni enrichment at the surface, a consequence of selective dissolution of Zn from the Zn-Ni matrix (i.e., dezincifiation). The total amount of metal dissolution from the wear track can be calculated by equation (1) [5, 11]

$$M_L = \frac{I*M*t}{n*F} \qquad (1)$$

Where M_L = mass of the metal oxidized in time t, M = molar mass of the sliding material t = sliding time, n = oxidation valence, F= faradays constant.

This method for calculating mass loss resulting from ***wear enhanced** corrosion* (i.e. excluding loss from wear) can be used for pure metals because the oxidation valencies for metal dissolution are known. For alloys, it is very difficult to determine oxidation valencies. For Zn-Ni coatings, because the mechanism of dissolution is dezincification, the oxidation valency corresponding to the Zn dissolution was utilized to calculate M_L. The Cd-Ti coating contained minute amounts of Ti in solid solution form. Thus for calculating M_L, the oxidation valency of Cd was utilized. The values of M_L for all the coatings are shown in Fig. 4.8. Both Zn-Ni coatings suffered lower mass loss due to wear enhanced corrosion as compared to Zn, Cd and Cd-Ti coatings. One of the accepted mechanisms for describing wear enhanced corrosion is the increase in the generation of a third body due to corrosion interacting with wear. Because the wear and corrosion resistance [14, 20] of Zn-Ni is relatively high, third body generation is much lower and therefore wear enhanced corrosion is also lower. Also the Cd complex anion could be more stable compared to the Zn anion in Zn-Ni coatings thus facilitating enhanced material removal.

Further analysis of the anodic wear scars shown in Fig. 4.9. The Zn-Ni coatings exhibited less material removal as compared to the Zn, Cd and Cd-Ti coatings for which EDS spectra show strong Fe Kα peaks inside the wear scar. Even though the wear scar width of all the coatings ranged between 200-400μ, metal dissolution during wear explains why the coating was mostly removed from the wear track for Zn, Cd and Cd-Ti.

4.3.4 Characterization of corrosion products

Fig. 4.10 shows the grazing incidence XRD of the corrosion products during OCP wear of the passivated coatings. The corrosion products of Zn-Ni coatings consisted of δ Zn-Ni (Ni_3Zn_{22}), zinc hydroxyl chloro hydride ($Zn_5(OH)8Cl_2.H_2O$) and sodium zinc hydroxide hydride ($NaZn(OH)_3.3H_2O$). Apart from the corrosion products there was strong enrichment of Ni at the surface due to dezincification. It has been reported [34] that the γ-Zn-Ni transforms to β Zn-Ni and then to α (Ni rich solid solution of Zn-Ni). While comparing XRDs in Fig. 4 and Fig. 11, the present investigation confirms the transformation of gamma Zn-Ni coatings, but to δ-Zn-Ni and Ni. The corrosion products of Zn-Ni coatings are more corrosion resistant than zinc oxide films formed in Zn coatings [35]. The corrosion products of LHE Cd and Cd-Ti coatings are cadmium chlorides [$CdCl_2 . H_2O$ / Cd (OH) Cl] .

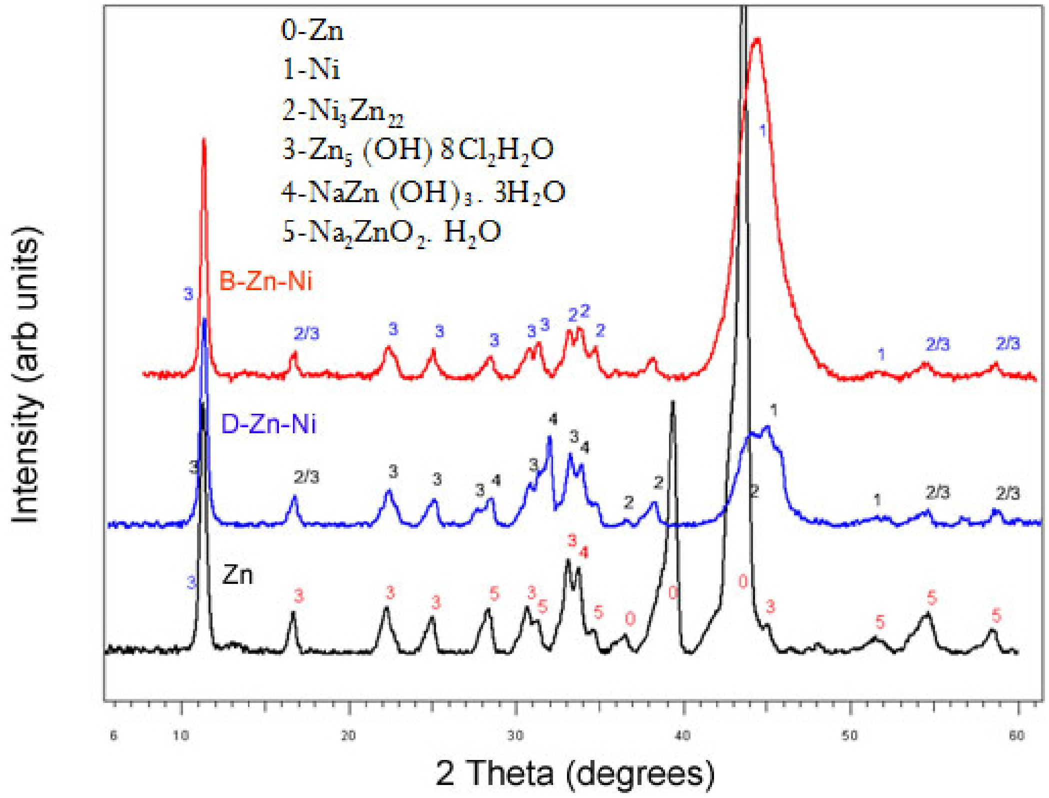

(a)

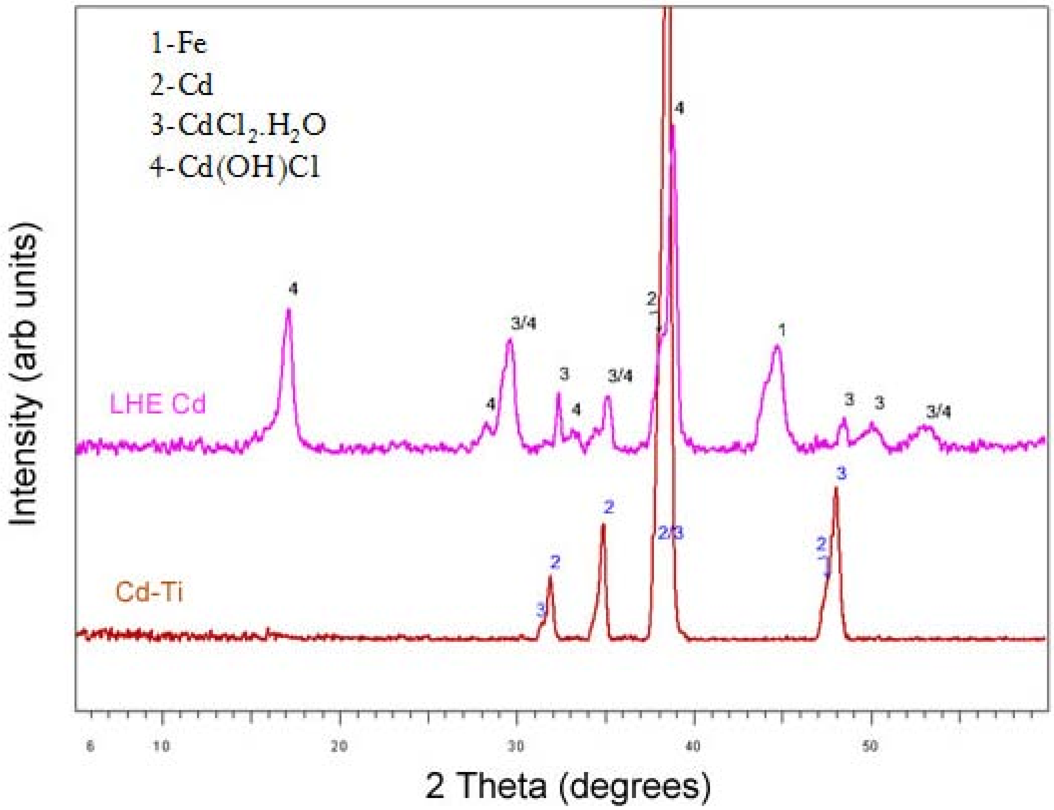

(b)

Fig. 4.10 Characterization of corrosion products on the OCP wear track of the coatings (a) Zn-Ni & Zn (b) LHE Cd & Cd-Ti using Grazing incidence XRD

4.3.5 Electrochemical impedance spectroscopy studies of the coatings

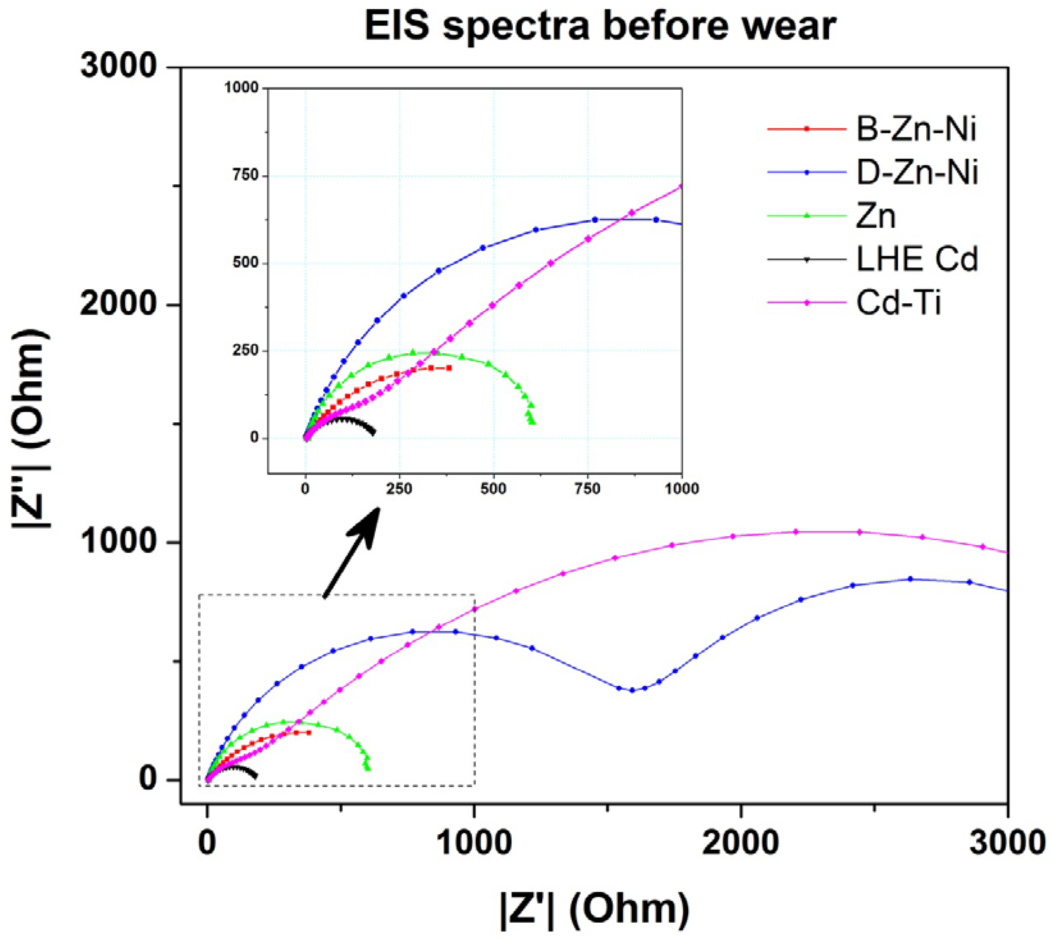

(a)

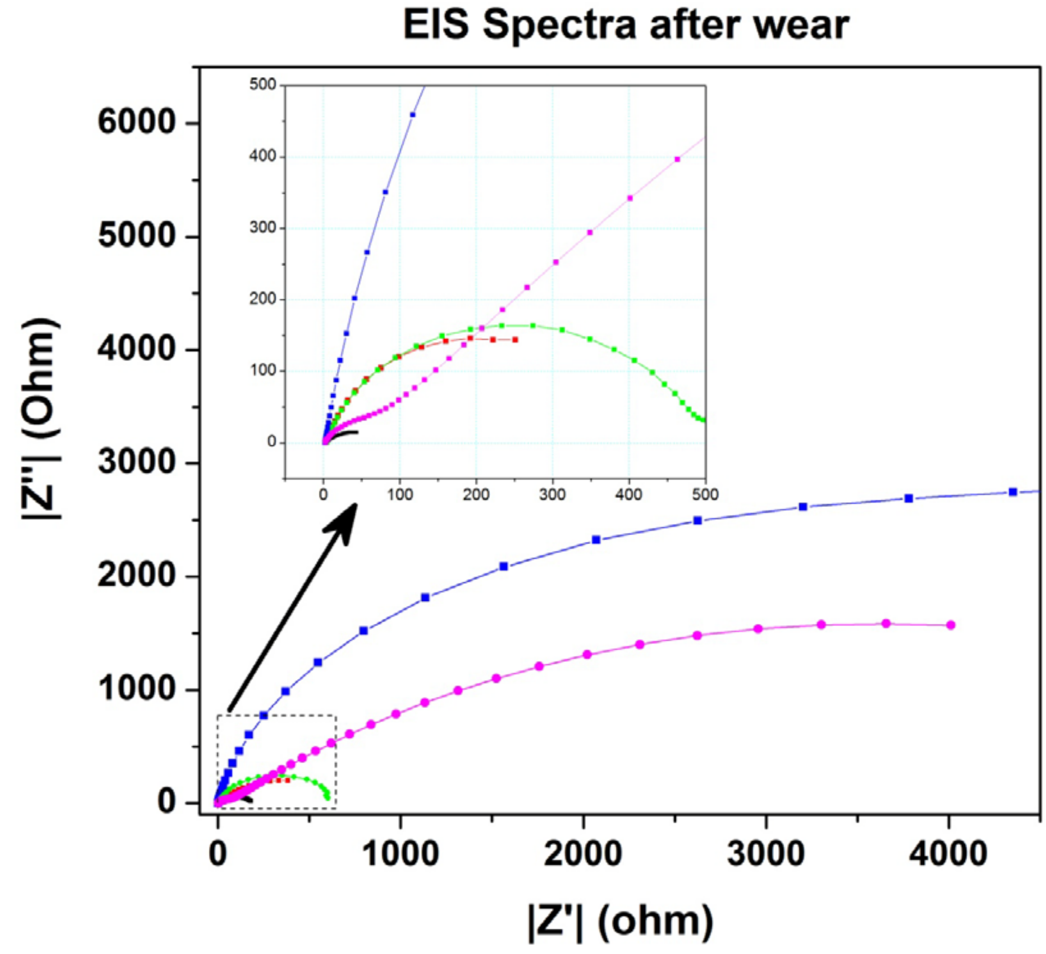

(b)

Fig. 4.11 Nyquist plots of the coatings (a) before and (b) after wear tests

EIS studies were carried out on all the passivated coatings before and after the wear tests in step 2 and step 5 as described in the experimental procedures. EIS is a versatile method to identify the corrosion mechanisms and kinetics, which are not usually observable by open circuit potential measurements during the wear tests. Fig. 4.11 show the Nyquist plots of the coatings before and after the wear tests. A Nyquist plot is a semi circular plot between the electrochemical impedance in real and imaginary axes and the experimental data can be explained by means of simple electrical circuits as shown in Fig. 12. The corrosion resistance of a coating can be explained by two different circuits i.e. a simple Randles circuit as shown in Fig. 4.12 (a) where the solution resistance (R_S) is in series with the double layer capacitance (C_{dl} or Q_{dl}), which is in turn parallel to a charge transfer resistance or polarization resistance (R_P). For a worn coating under corrosion, and for coatings exhibiting two time constant behavior, the circuit in Fig. 4.12 (b) is utilized, where an embedded parallel resistance (R_2) and a capacitance (Q_2) is in series with the main Randles circuit [9, 11, 34]. For complex electrochemical conditions where the surface is non homogeneous, the double layer capacitance is replaced by the term Q which is called the constant phase element [9, 11, 34, 35]. The impedance is then given by the equation (2) [9, 35]

$$Z_Q = \frac{1}{[Y_0 \ \ J\omega^{\,n}]} \qquad (2)$$

where Z is the impedance (Ω), Y0 is the capacitance factor (Ω^{-1} s^n), ω is the angular frequency (rad S^{-1}) , and *n* is the empirical exponent of *Q*. When Q is close to 1 the behavior can be equalized to a double layer capacitance. In a

Nyquist plot the polarization resistance approximately corresponds to the size of the semicircle [6].

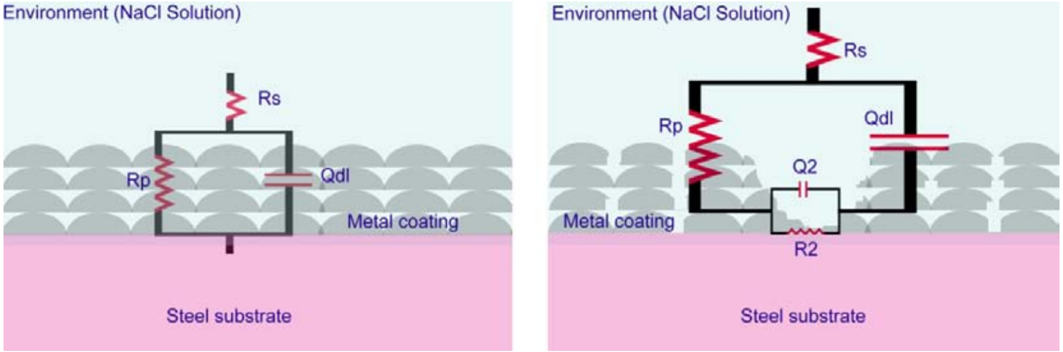

(a) (b)

Fig. 4.12 Description of Equivalent electrical circuits used to model the EIS test parameters before and after wear tests

From Fig. 4.11 (a), it can be observed that, except for D-Zn-Ni and Cd-Ti, all the coatings exhibited single time constant i.e. they exhibited single semi circle corresponding to the simple Randles circuit as shown in Fig. 4.12a. D-Zn-Ni and Cd-Ti coating exhibited a second time constant at lower frequencies, which yielded an equivalent circuit corresponding to Fig. 4.12b, where the embedded resistance corresponded to the pore infiltration resistance. Thus by utilizing the equivalent circuits and modeling the experimental parameters, the results obtained for various circuit components are shown in Table 4.1 and Table 4.2.

Polarization resistances of the coatings before and after wear are shown in Fig. 4.13. When comparing the polarization resistance of all the coatings (R_p)

before wear, D- Zn-Ni coating exhibited higher corrosion resistance as compared to Zn and Cd coatings. The polarization resistances of both the Cd coatings were similar before the wear tests. The polarization resistance of B-Zn-Ni is marginally higher or in other words almost equivalent to the Zn coating and higher than Cd and Cd-Ti coatings. It can be observed from Fig. 4.3, there is a difference in the morphology of B-Zn-Ni and D-Zn-Ni. The amount of porosity and microcracks observed in these coatings differ. Presence of cracks and defects in the Zn-Ni coatings may result in increase in rate of dezincification of the coatings resulting in formation of a nickel rich surface [18]. This may have resulted in the higher polarization resistance of D-Zn-Ni coating compared to the B-Zn-Ni coating. Even though, this difference in the rate of dezincification in B Zn-Ni results in lower polarization resistance but it may in turn increase the service life of the coating.

The embedded parallel resistance R_2 derived in the EIS model for D-Zn-Ni and Cd-Ti can be referred to as a measure of their pore infiltration resistance. As shown in Fig. 4.3, intermittent porosity observed on the surface of D Zn-Ni was greater than for the Cd-Ti coating, may explain the lower R_2 value before wear obtained for D Zn-Ni.

From Fig. 4.11 (b), illustrating the EIS spectra after the wear tests, it can be observed in the coatings that B-Zn-Ni, Zn, and the Cd coatings exhibited single time constants, which was not the case for D-Zn-Ni and Cd-Ti. The polarization resistances of both the Cd coatings were almost equal, and they were observed to be lower than the Zn-Ni coatings after the wear tests. The polarization resistance of all the coatings decreased after the wear tests in all cases except for D-Zn-Ni. The polarization resistance of D-Zn-Ni was much higher in magnitude as compared to B-Zn-Ni. As explained above the increase in polarization resistance, could be attributed to the difference in the coating morphology, the rate of dezincification of the coating and the extent of surface Ni enrichment. From Fig. 4.13, while comparing the R_P of all coatings after wear, D-Zn-Ni exhibited higher corrosion resistance than the Zn and Cd coatings. The equivalence in corrosion resistance of B- Zn-Ni and Zn after wear may be attributed to the slower rate of dezincification as mentioned above.

After wear, the R_2 values for D-Zn-Ni and Cd-Ti cannot be categorically distinguished as either pore infiltration resistance or the resistance offered by the subsurface layers (i.e., deformed wear track of the coating). Variables include the nature of wear scar, strain hardening of the coating surface subjected to wear, the nature of corrosion products, phase transformation during corrosion, and the area ratio of worn to un-worn area. Of the corrosion products in Zn-Ni, the hydroxide films are more stable and protect further infiltration than the chloride films formed in Cd [34, 35] . Thus the resultant impedance is attributed to all these factors and it could not be definitely concluded what caused such high impedance at lower frequencies. This analysis is further complicated for Zn-Ni coatings because of the phenomena of Ni enrichment on the surface accompanied by phase transformation of the coating during dezincification.

These findings require further analysis with surface analytical techniques and composition analysis of tribo layers under corrosion.

Table 4.1 EIS model fit parameters before wear test

Coating	R_{sol}	R_p	Q_1		R_2	Q_2	
			Y_0	n		Y_0	n
	Ω	Ω	µF			µF	
B-Zn-Ni	2.03	718	142.8	0.65			
D-Zn-Ni	2.28	1662	25.17	0.82	2139	1469	0.82
Zn	4.74	626	45.92	0.85			
LHE Cd	2.92	187.4	1527	0.69			
Cd-Ti	2.51	218.6	69.81	0.67	4250	483	0.56

Table 4.2 EIS model fit parameters after wear test

Coating	R_{sol}	R_p	Q_1		R_2	Q_2	
			Y_0	n		Y_0	n
	Ω	Ω	µF			µF	
B-Zn-Ni	2.50	432	972.4	0.77			
D-Zn-Ni	2.32	4540	41.95	0.91	9750	290.0	0.57
Zn	4.28	487	73.61	0.79			
LHE Cd	2.60	75.3	45790	0.47			
Cd-Ti	2.22	79.8	102.1	0.71	7120	1405	0.53

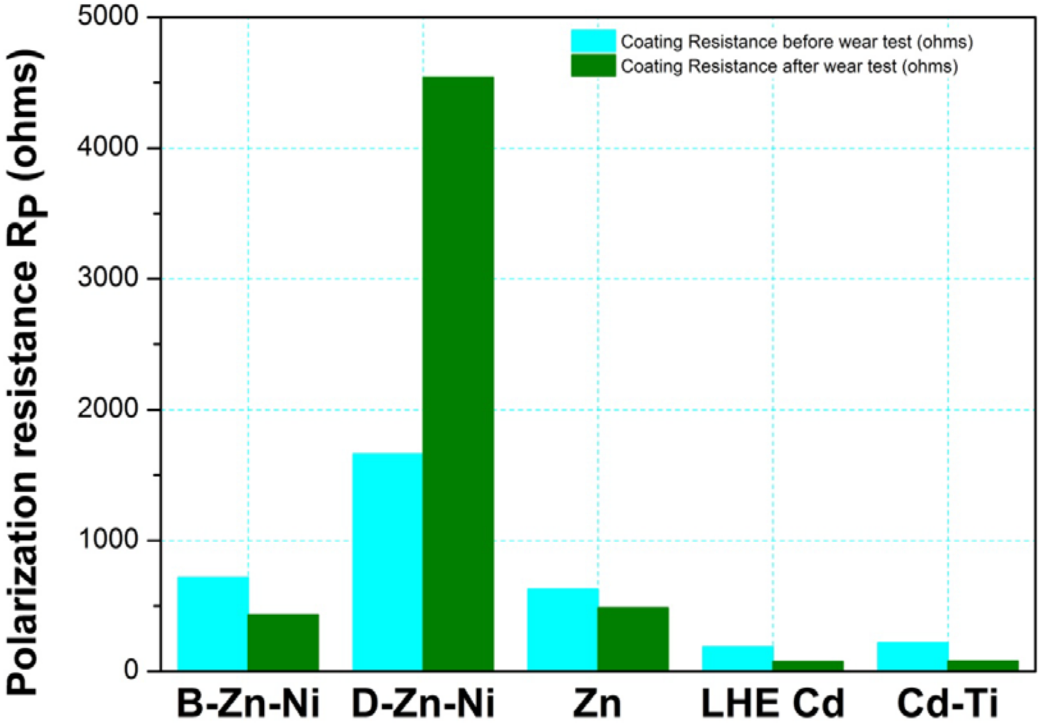

Fig. 4.13 Polarization resistances of the coatings before and after wear tests

4.3.6 Effect of passivation and heat treatment on tribocorrosion of Zn-Ni

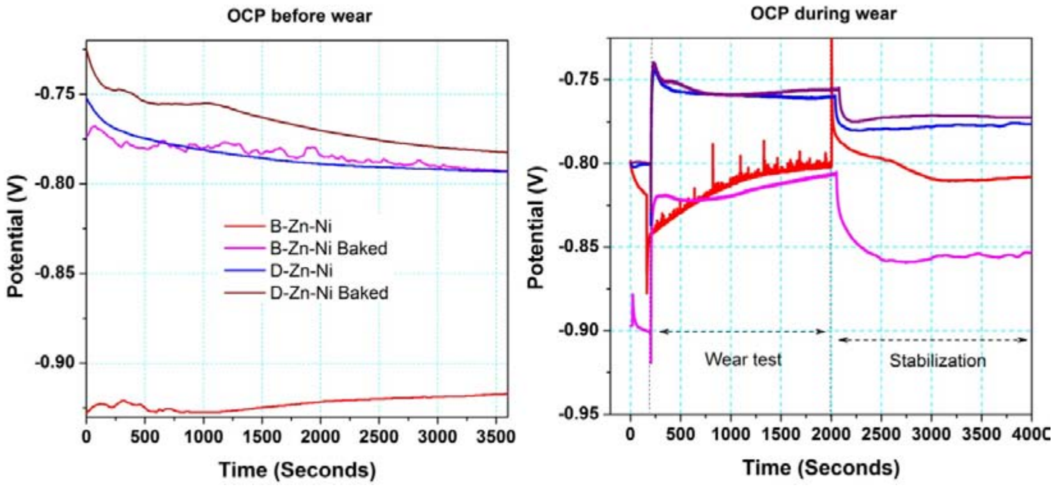

Fig. 4.14 OCP of as plated Zn-Ni coatings before wear

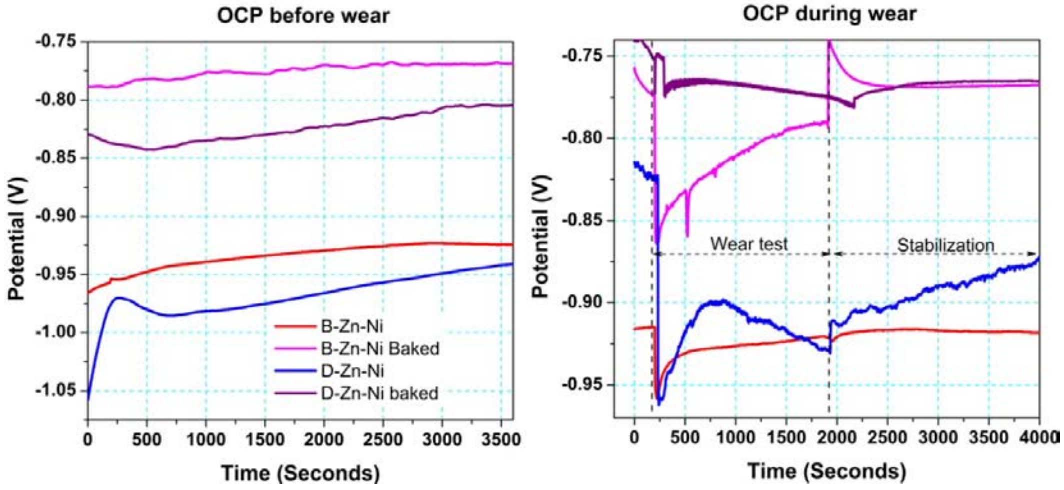

Fig. 4.15 OCP of passivated Zn-Ni coatings after wear

By the above methods, it can be established that the tribocorrosion behavior of Zn-Ni coatings were superior to Zn and Cd coatings. An additional component in these coating systems is the application of a chromate passivation treatment that is designed to protect the coating itself and prolong the overall life of the coating. Also, a post plating hydrogen relief heat treatment (baking) of coated high strength steel components is performed at 200°C [26]. The effects of chromate passivation and baking heat treatment on tribocorrosion behavior of Zn-Ni coatings were investigated. Fig. 4.14 shows the OCP of as plated Zn-Ni coatings, baked and unbaked, before and after the wear tests. The OCP values are given in Table 4.3. It can be observed that the OCP of B-Zn-Ni increased (became more noble) after baking. This may be explained by a non uniform thermal expansion of the coating during baking, causing microcracks and thereby distributing the anodic reactions throughout the surface of the coating [18]. On the other hand, a relatively small increase in OCP was observed in D-Zn-Ni after baking. This may be attributed to the presence of distributed porosity and microcracks even before baking as shown in Fig. 4.3. During the wear tests the OCP of both the Zn-Ni coatings increased because of dezincification and surface Ni enrichment and also because of corrosion products and third bodies generated due to wear. After the wear tests the OCP stabilized at a higher value than the initial ones due to Ni enrichment.

Fig. 4.15 shows the OCP of the passivated Zn-Ni coatings. Here, baking increased the OCP of both Zn-Ni coatings before wear. Once again, potentials increased during wear due to dezincification of the surface; they reached higher values at the end of the wear test. The effect of passivation treatment was not clearly visible through open circuit potential measurements refer Table 4.3.

Table 4.3 OCPs of Zn-Ni coatings in as plated and passivated conditions before and after wear test

OCPs of As plated Zn-Ni				
Coating	As plated		As plated & baked	
	Before wear	After wear	Before wear	After wear
B-Zn-Ni	-0.92	-0.81	-0.79	-0.85
D-Zn-Ni	-0.79	-0.78	-0.78	-0.77
OCPs of Passivated Zn-Ni				
Coating	Passivated		Passivated & Baked	
	Before wear	After wear	Before wear	After wear
B-Zn-Ni	-0.92	-0.92	-0.77	-0.77
D-Zn-Ni	-0.94	-0.87	-0.80	-0.77

The passivation treatment applied to the coatings lead to improved corrosion resistance, which means an increase in the OCP. This trend was not observed in Zn-Ni coating, owing to the fact that the Ni enrichment and dezincification supersedes the protection effect offered by the passive film, which are a few nanometers thick. In the case of D Zn-Ni, this is validated by the fact that the potentials were unstable in both as plated and passivated conditions.

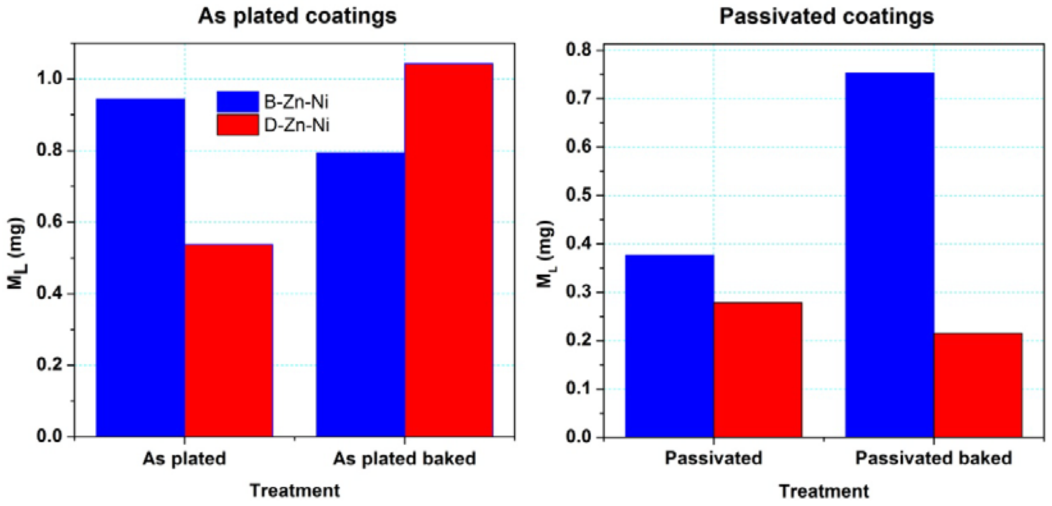

Fig. 4.16 calculated mass loss due to wear enhanced corrosion of Zn-Ni coatings due to heat treatment on (a) as plated coatings (b) passivated coatings

An anodic impressed potential wear test was performed for Zn-Ni coatings to distinguish the effect of passivation and heat treatment; the results are shown in Fig. 4.16. The mass loss due to wear enhanced corrosion was lower for both Zn-Ni coatings with passivation. At impressed anodic potentials higher than the OCP the passive film offered additional corrosion protection. The effect of baking treatment on the mass loss of the coating could not be isolated from the rate of dezincification of the coating.

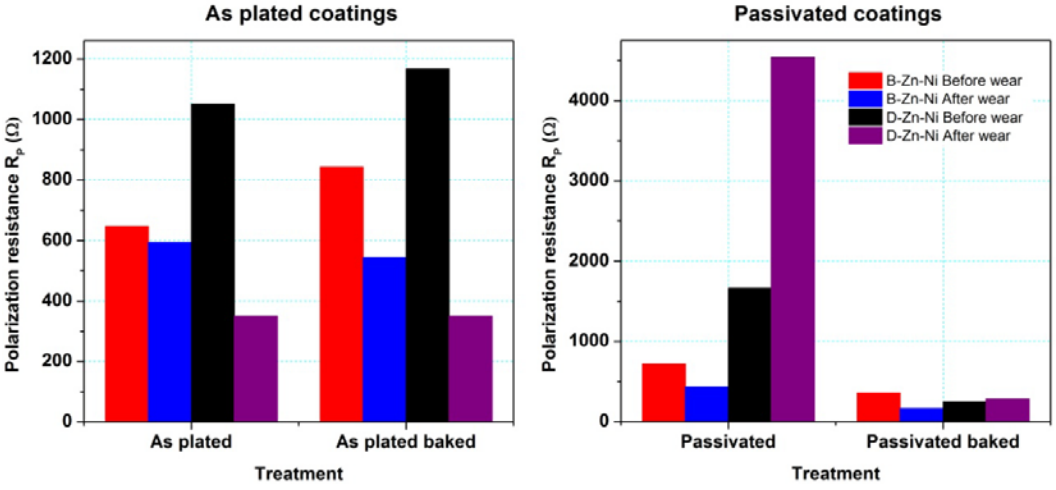

Fig. 4.17 Effect of heat treatment on Polarization resistance of Zn-Ni coatings (a) as plated coatings (b) passivated coatings

Polarization measurements of the coatings with heat treatment and passivation are shown in Fig. 4.17. Polarization resistance of the coatings decreased when the baking treatment was applied after passivation. The lower R_p may be explained by the fact that baking is known to damage in the passive film resulting in the lower corrosion protection. With the as plated coatings R_P was not significantly affected by baking. The same observation is true after the wear test. Given that the passive film thickness is negligible compared to the coating itself, the dominant factor affecting corrosion resistance is the protection offered by the coating and its corrosion products. Therefore the damage caused by baking to the passive layer is negated. Overall the passivation treatment increases the polarization resistance provided it is applied after baking treatment. In the as plated alloys, the baking treatment had minimal effect on the polarization resistance before and after the wear tests.

4.4 Conclusions

Three different methods were utilized to determine the tribocorrosion resistance of the coatings. From the open circuit potential measurements during the wear tests, it was observed that the OCP of Zn-Ni coatings increased (became nobler) because of preferential dezincification from the matrix. For all other coatings the change in corrosion potential was not appreciable. Zn-Ni coatings exhibited OCP values between Zn and Cd coatings.

The impressed potential studies showed the corrosion current during wear tests were lowest for the Zn-Ni coatings as compared to the Cd and Zn coatings. The same was true for mass loss during corrosion. The EIS studies before and after wear tests revealed that the polarization resistance of Zn-Ni coatings was higher than for Zn and Cd coatings. Yet the resistance exhibited by the wear track and the pore infiltration resistance of the coatings could not be distinguished.

The XRD and EDS analyses after the tribocorrosion studies showed that Zn-Ni coatings survived the entire wear cycle as compared to the Zn and Cd coatings. Also phase transformation and surface Ni enrichment was observed in Zn-Ni coatings. Even though the Zn-Ni coatings were slowly being depleted of Zn during tribocorrosion, the corrosion products and the Ni rich surface exhibited better corrosion resistance during wear as compared to the Zn and Cd coatings.

The passivation treatment was beneficial to Zn-Ni coatings by improving corrosion resistance. The effect of baking heat treatment could not be distinguished from the basic corrosion mechanism of Zn-Ni. Consequently, it appears that the effect of baking heat treatment on tribo corrosion resistance is negligible.

References

[1] Winand R. Electrodeposition of Zinc and Zinc Alloys. Modern Electroplating: John Wiley & Sons, Inc.; 2010. p. 285-307.

[2] Eliaz N, Venkatakrishna K, Hegde AC. Electroplating and characterization of Zn–Ni, Zn–Co and Zn–Ni–Co alloys. Surface and Coatings Technology. 2010;205:1969-78.

[3] Wilcox GD, Gabe DR. Electrodeposited Zinc Alloy Coatings. Corrosion Science. 1993;35:1251-8.

[4] Landolt D, Mischler S, Stemp M. Electrochemical methods in tribocorrosion: a critical appraisal. Electrochimica Acta. 2001;46:3913-29.

[5] Mischler S. Triboelectrochemical techniques and interpretation methods in tribocorrosion: A comparative evaluation. Tribology International. 2008;41:573-83.

[6] Ponthiaux P, Wenger F, Drees D, Celis JP. Electrochemical techniques for studying tribocorrosion processes. Wear. 2004;256:459-68.

[7] Wood RJK. Tribo-corrosion of coatings: a review. Journal of Physics D-Applied Physics. 2007;40:5502-21.

[8] Azzi M, Benkahoul M, Szpunar JA, Klemberg-Sapieha JE, Martinu L. Tribological properties of CrSiN-coated 301 stainless steel under wet and dry conditions. Wear. 2009;267:882-9.

[9] Azzi M, Paquette M, Szpunar JA, Klemberg-Sapieha JE, Martinu L. Tribocorrosion behaviour of DLC-coated 316L stainless steel. Wear. 2009;267:860-6.

[10] Guruvenket S, Azzi M, Li D, Szpunar JA, Martinu L, Klemberg-Sapieha JE. Structural, mechanical, tribological, and corrosion properties of a-SiC:H coatings prepared by PECVD. Surface and Coatings Technology. 2010;204:3358-65.

[11] Hassani S, Raeissi K, Azzi M, Li D, Golozar MA, Szpunar JA. Improving the corrosion and tribocorrosion resistance of Ni–Co nanocrystalline coatings in NaOH solution. Corrosion Science. 2009;51:2371-9.

[12] Li D, Guruvenket S, Azzi M, Szpunar JA, Klemberg-Sapieha JE, Martinu L. Corrosion and tribo-corrosion behavior of a-SiCx:H, a-SiNx:H and a-SiCxNy:H coatings on SS301 substrate. Surface and Coatings Technology. 2010;204:1616-22.

[13] Alfantazi AM, Erb U. Corrosion properties of pulse-plated zinc-nickel alloy coatings. Corrosion. 1996;52:880-8.

[14] Fabri Miranda FJ. Corrosion behavior of zinc-nickel alloy electrodeposited coatings. Corrosion. 1999;55:732-42.

[15] Fedrizzi L, Ciaghi L, Bonora PL, Fratesi R, Roventi G. Corrosion behaviour of electrogalvanized steel in sodium chloride and ammonium sulphate solutions; a study by E.I.S. J Appl Electrochem. 1992;22:247-54.

[16] Park H, Szpunar JA. The role of texture and morphology in optimizing the corrosion resistance of zinc-based electrogalvanized coatings. Corrosion Science. 1998;40:525-45.

[17] Rahsepar M, Bahrololoom ME. Corrosion study of Ni/Zn compositionally modulated multilayer coatings using electrochemical impedance spectroscopy. Corrosion Science. 2009;51:2537-43.

[18] Siitari DW, Sagiyama M, Hara T. Corrosion of Ni-Zn Electrodeposited Alloy. Transactions of the Iron and Steel Institute of Japan. 1983;23:959-66.

[19] Rajagopalan SR. Electrodeposition of nickel-zinc alloys. Metal Finishing. 1972;70:52-8.

[20] Panagopoulos CN, Georgarakis KG, Agathocleous PE. Sliding wear behaviour of Zinc-Nickel alloy electrodeposits. Tribology International. 2003;36:619-23.

[21] Sriraman KR, Strauss HW, Brahimi S, Chromik RR, Szpunar JA, Osborne JH, et al. Tribological behavior of electrodeposited Zn, Zn-Ni, Cd and Cd-Ti coatings on low carbon steel substrates. Tribology International. 2011;Article under review.

[22] Tran LM, Matthias PM, Jones JH. Low hydrogen embrittlement Zinc/Nickel plating for high strength steels. US Patent 8048285. 8048285 edNovember 1, 2011

[23] MIL-STD-870C. U.S. Military Standard (USAF) on Cadmium plating, Low embrittlement, Electrodeposition. Department of Defence Standard Practice; 27 April 2009.

[24] MIL-STD-1500C. U.S. Military Standard (USAF) on Cadmium-Titanium Plating, Low Embrittlement, Electrodeposition. Department of Defence Standard Practice; 01 March 2007.

[25] Guruvenket S, Azzi M, Li D, Szpunar JA, Martinu L, Klemberg-Sapieha JE. Structural, mechanical, tribological, and corrosion properties of a-SiC:H coatings prepared by PECVD. Surface & Coatings Technology. 2010;204:3358-65.

[26] ASTM. 2006 F1941-00 Standard specification for electrodeposited coatings on threaded fasteners (Unified Inch Screw Threads (UN/UNR)). ASTM International, West Conshohocken, PA, 19428-2959, DOI: 10.1520/F1941-07 www.astm.org.

[27] Thomas BK, Fray DJ. The Effect of Additives on the Morphology of Zinc Electrodeposited from a Zinc-Chloride Electrolyte at High-Current Densities. J Appl Electrochem. 1981;11:677-83.

[28] Morón LE, Méndez A, Castañeda F, Flores JG, Ortiz-Frade L, Meas Y, et al. Electrodeposition and corrosion behavior of Zn coatings formed using as brighteners arene additives of different structure. Surface and Coatings Technology. 2011;205:4985-92.

[29] Abdelhalim AM, Baghlaf AO, Sobahi MI. Effect of Some Addition Agents on the Electrodeposition of Cadmium from Acidic Chloride Baths. Surf Technol. 1984;22:129-42.

[30] Elhalim AMA, Sobahi MI. Effect of Bath Constituents and Some Plating Variables on the Electrodeposition of Cadmium from Acidic Chloride Baths. Surf Technol. 1983;19:45-57.

[31] Murray J. The Cd-Ti (Cadmium -Titanium) system. Journal of Phase Equilibria. 1983;4:399-401.

[32] Sriraman KR, Strauss HW, Brahimi S, Chromik RR, Szpunar JA, Osborne JH, et al. Tribological behavior of electrodeposited Zn, Zn–Ni, Cd and Cd–Ti coatings on low carbon steel substrates. Tribology International. 2012;http://dx.doi.org/10.1016/j.triboint.2012.06.008.

[33] Bruet H, Bonino JP, Rousset A, Chauveau ME. Structure of zinc-nickel alloyelectrodeposits. Journal of Materials Science. 1999;34:881-6.

[34] Gavrila M, Millet JP, Mazille H, Marchandise D, Cuntz JM. Corrosion behaviour of zinc–nickel coatings, electrodeposited on steel. Surface and Coatings Technology. 2000;123:164-72.

[35] Tian W, Xie FQ, Wu XQ, Yang ZZ. Study on corrosion resistance of electroplating zinc-nickel alloy coatings. Surface and Interface Analysis. 2009;41:251-4.

5.0 Corrosion behavior of Zn, Zn-Ni, Cd and Cd-Ti electrodeposited on low carbon steel substrates

Preface

In this chapter the corrosion behavior of Zn-Ni, Zn, Cd and Cd-Ti coatings was evaluated with the view of replacing Cd and Zn coatings with Zn-Ni coatings. The corrosion resistances of the coatings were studied with potentiodynamic polarization curves and the EIS. The EIS of the coatings were performed over intermittent time intervals to understand the extent of dezincification in Zn-Ni alloys. The effect of heat treatment and passivation on the Zn-Ni coating corrosion was also reported. The corrosion resistance of the coatings was correlated with the microstructure of the coatings and the composition of corrosion products. On the basis of corrosion Zn-Ni coatings were found to be suitable replacements for Zn and Cd coatings. This chapter is to be submitted as an article in the Journal *Coatings Research & Technology,* Springer publications.

Abstract

The corrosion behavior of electrodeposited Zn-Ni alloy coatings was studied with a view to replace Zn and Cd coatings. A three electrode electrochemical cell was utilized to understand corrosion of the coatings in 3.5 % NaCl solution by measuring the open circuit potentials (OCP), polarization curves and electrochemical impedance spectroscopy (EIS). EIS was performed at intermittent time intervals to understand the extent of dezincification in Zn-Ni alloys and to determine the polarization resistance change with respect to time. Coatings were examined with SEM and XRD to correlate the corrosion behavior with the surface / interface morphology and residual stresses and to understand the nature of corrosion products. The effect of heat treatment and trivalent chrome passivation on the corrosion behavior of Zn-Ni coatings is also reported. Zn-Ni coatings studied here have higher polarization resistance, lower corrosion currents and the corrosion products offer additional protection in increasing the life of the coatings compared with Zn and Cd coatings. Based on these results Zn-Ni coatings are an attractive alternative to Cd and Zn coatings.

Keywords: Electrodeposited Zn-Ni, Cd, Zn coatings, EIS, Polarization

5.1. Introduction

The use of Zn for anodic protection of steel has been well documented in the past [1]. In the aerospace industry, cadmium is used because of its superior sacrificial surface protection (i.e. Cd coatings last longer than pure Zn) and reduced environmentally induced embrittlement of high strength steel alloys. However, the use of Cd has been very restricted due to stringent environmental regulations. Moreover, the automotive industry is also looking for a better material to impart superior corrosion resistance than pure Zn, which has proven to be insufficient and also to find a better product than Zn-Al flake coatings. These factors have led to the development of Zn alloy coatings. At present various binary and ternary alloy coatings of Zn with Fe group metals are under consideration to replace Zn in automotive and Cd in aerospace industries. To name a few, Zn-Ni, Zn-Fe, Zn-Co [2], Zn-Ni-Co [3] and Zn-Ni-Fe [4] have been considered as potential candidates. Zn-Ni coatings have been shown to have superior corrosion resistance compared to Zn, owing to the formation of complex corrosion products that act as a barrier against diffusion of the corrosive environment, thereby preventing corrosion of the underlying coating layer [5]. The fine cracked structure of Zn-Ni coating also spreads out the anodic reactions throughout the coating layer thereby avoiding localized corrosion of the coating [6]. Various modifications in plating processes, such as pulse plating procedure [7] and alternatives to electrodeposition, such as physical vapor deposition (PVD), [8] have also been attempted. Modifications of the Ni content in Ni/Zn compositionally modified coating layers have also been investigated [9]. Corrosion mechanisms involving dealloying [10] and dezincification of Zn from the Zn-Ni matrix have also been studied [11] . The effect of surface modification with chromium conversion coatings and also the effect of heat treatment after surface modification of Zn-Ni coatings on corrosion resistance of Zn-Ni coatings were reported by Muller et al [12, 13]. The effect of composition, microstructure and plating parameters on corrosion resistance of Zn-Ni has also been investigated in the past [14-16]. Of all these studies, very few have attempted [17] to compare the corrosion resistance of Zn-Ni and Cd under similar testing conditions. Corrosion characterization of the coatings include various techniques such as the salt spray chamber, prolonged long term exposure, potentiodynamic polarization curves and determination of corrosion currents and potentials, and the latest method, electrochemical impedance spectroscopy (EIS) [18]. The focus of the present investigation was on determination of corrosion resistance of the coatings using polarization and EIS techniques. Two Zn-Ni coatings are compared with Zn, LHE Cd, and Cd-Ti coatings. All coatings were deposited on low carbon steel substrates using industrial plating processes. The microstructure, phases, composition and nature of corrosion products were correlated to the corrosion resistances of the coatings. The effect of trivalent chromium passivation and post plating heat treatment of the coated layer on the corrosion resistance of Zn-Ni coatings are also reported.

5.2. Experimental Methodology

5.2.1 Coating processes

The following five coatings were deposited on low carbon steel substrates, using plating parameters described below. The thickness of all coatings was maintained in the range of 15 – 20 µm.

Boeing LHE Zn-Ni*:* Low hydrogen embrittling (LHE) Zn-Ni plating process developed by Boeing Research & Technology, USA was used [19] . An alkaline NaOH (135 g/l) based plating solution with Zn (9-11 g/l) and Ni (0.8-1.2 g/l) metal concentrations in the ratio of 10-11:1 and additives was used, and plated in an industrial pilot plating tank. The pH of the plating bath was maintained to 12-13.5 at 20-25° C and a plating current density of 48mA/cm^2 was applied to obtain a coating thickness of 15 - 20 µm in 1 hour. Substrates were aqueous degreased, abrasive grit blasted and activated in HCl before plating. Boeing LHE Zn-Ni will be referred to B-Zn-Ni henceforth in this paper.

Dipsol IZ C17+Zn-Ni: Commercially available Zn-Ni plating solution by Dipsol Inc was used. An alkaline NaOH (135 g/l) based plating solution with Zn and Ni metal concentrations in the ratio of 10-11:1, with commercial additives was used, and plated in an industrial pilot plating tank. The pH of the plating bath was maintained at 12-13.5 at 25° C and a plating current density of 28 – 30 mA/cm^2 was applied to produce a coating thickness of 15 – 20 µm in one hour. The substrates were grit blasted and acid pickled in HCl before plating. Dipsol IZ C17+ Zn-Ni will be referred to D Zn-Ni henceforth in this paper.

Zn: The plating bath was acid chloride based with $ZnCl_2$ (60 g/l), KCl (250 g/l), H_3BO_3 (25 g/l) and HCl in smaller concentrations to maintain the pH of the bath to 4.5-4.8. The cathode efficiency was 95% and the temperature of the plating was held at 25 °C. The electroplating was performed on a laboratory-scale plating setup. A plating current density of 5 mA/cm^2 was used to generate a coating thickness of 15 μm in 2 hours. The substrates were finished with 600 # SiC grinding paper and activated in HCl before plating.

Low hydrogen embrittling Cd plating (LHE Cd) was performed in an industrial plating facility using an alkaline cyanide based plating solution with CdO (20-30 g/l), NaCN (90-135 g/l), Na_2CO_3 (0-60 g/l) and NaOH (11-30 g/l) [20]. A plating current density of 118 – 120 mA/cm^2 was used to generate a coating thickness of 15 μm in 5 minutes. Substrates were solvent degreased, grit blasted and acid pickled before plating. Plating temperature of 15-30ºC was used.

Cd-Ti: Alkaline cyanide based plating solution, with CdO (18-35 g/l), NaCN (74-200 g/l), Na_2CO_3 (0-60 g/l), and NaOH (11-30 g/l) was used, and plated in an industrial production plating tank [21]. Ti was added in small concentrations (40 -100 parts per million) for grain refinement and control of surface morphology. An initial strike was applied at a plating current density of 46 – 55 mA/cm^2 for a 15 seconds to buildup a flash layer with sufficient adhesion and subsequently a plating current density of 16 -32 mA/cm^2 was applied to generate a total coating thickness of 15 μm in 15 minutes. Substrates were solvent degreased, grit blasted and acid pickled before plating. Plating temperature of 15-30ºC was used.

All of the sample coatings were deposited on a low carbon steel (SAE 1006) substrate in the form of sheets 10 cm x 16 cm, 0.8 mm thick. The coated sheets were then mechanically sheared into 2.5 x 2.5 cm squares for corrosion testing and analysis. All the coatings investigated for characterization and corrosion testing were tested after passivation treatment. The Zn-Ni coatings alone were tested under four conditions: (i) as-plated, (ii) with chromate passivation (iii) as plated and baked for 24 hours at 200 °C, (iv) with chromate passivation and baked.

5.2.2 Coating characterization

A Bruker Discover D8-2D area detector x-ray diffractometer with Cu-Kα radiation was used to characterize the coatings. X-ray diffraction in standard θ-2θ mode was performed on the coating surfaces. Grazing incidence mode with incidence angle of 2° was utilized to characterize the corrosion products. Residual stress analysis on the Zn-Ni coatings was done with a Bruker Discover D8-2D area detector with Co- Kα radiation. Bruker GAADS software was utilized to calculate the biaxial stress along the lateral and longitudinal directions with 2D area detector using a standard 2θ $\sin^2\psi$ method [22]. The room temperature Young's modulus (E) of 118 GPa and poisons ratio (ν) of 0.22 was used [23, 24]. High angle reflection peak corresponding to (721) miller index was chosen for measuring the residual stress. The coating surface and cross sections were observed and analyzed using a Philips field emission scanning electron microscope (FE-SEM) at 20 KV accelerating voltage. The coating cross sections were made by sectioning with a diamond saw, fine mechanical polishing up to 1200 grit SiC papers and final polished with 0.05μ Colloidal Silica / Alumina suspension in iso- propyl alcohol. Compositional analysis of Zn-Ni coatings was performed using Energy Dispersive Spectrometry (EDS).

5.2.3 Corrosion testing

Characterization of corrosion behavior of the coatings were done by three different techniques namely

1. Measurement of the open circuit potentials
2. Potentiodynamic polarization method – Measurement of corrosion potential (E_{corr}) and corrosion current (I_{Corr})
3. Determination of polarization resistance of the coatings with electrochemical impedance spectroscopy (EIS)

The open circuit potentials (OCP) of the coatings were measured using a VERSASTAT 4 potentiostat in a three electrode electrochemical cell, where the coating of interest acts as a working electrode, a platinum wire as a counter electrode and a standard saturated calomel electrode as a reference. The OCPs were monitored for 24 hours and subsequently the electrodes were polarized potentiodynamically in a continuous sweep. The rate of potential sweep was 1.66 mV/sec and the scanning potential range varied from -250 to 250 mV with respect to the OCP. The E_{Corr} and I_{Corr} were determined from the intercepts by Tafel's extrapolation method. EIS was also performed in a three electrode electrochemical cell as mentioned above in a computer controlled potentiostat (Autolab PGSTAT302 Electrochemie). The EIS spectra for the coatings were acquired at OCP with AC frequencies ranging from 10^5 Hz to 10^{-3} Hz and amplitude of 10mV. The impedance spectrum was acquired at a time interval of every four hours resulting in data acquisition at the end of 4, 8, 12, 16, 20 and 24 hours. For all the electrochemical characterization the medium used was 3.5 % NaCl solution which simulates the marine environment.

5.3. Results & Discussion

5.3.1 Coating Characterization

The surface morphologies of passivated coatings are shown in Fig. 5.1. From Fig. 5.1e it can be observed that B-Zn-Ni was composed of fine *platelets* [25] less than 1 µm in size while D-Zn-Ni was composed of large platelets (about 10 µm in size) (Fig. 5.1b) with intermittent porosity and microcracks. The X-ray diffraction results (Fig. 5.3) showed that both the Zn-Ni coatings are γ Zn-Ni (Ni_2Zn_{11}) which is the typical phase observed in Zn – 15 % Ni. The differences in surface morphologies are the consequence of differences in plating parameters between the two processes. The cross sectional SEM of the Zn-Ni coatings are shown in Fig. 5.2.

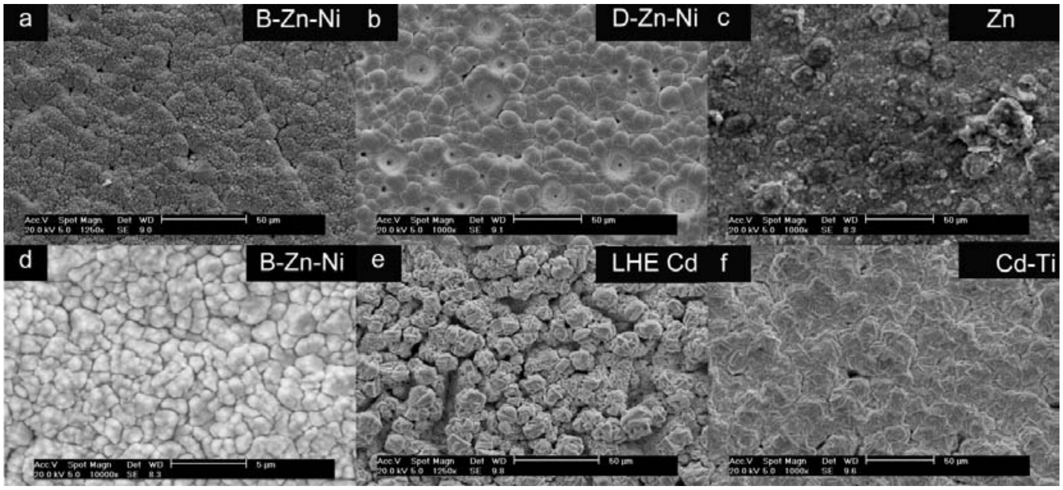

Fig. 5.1 Surface morphology of the passivated coatings

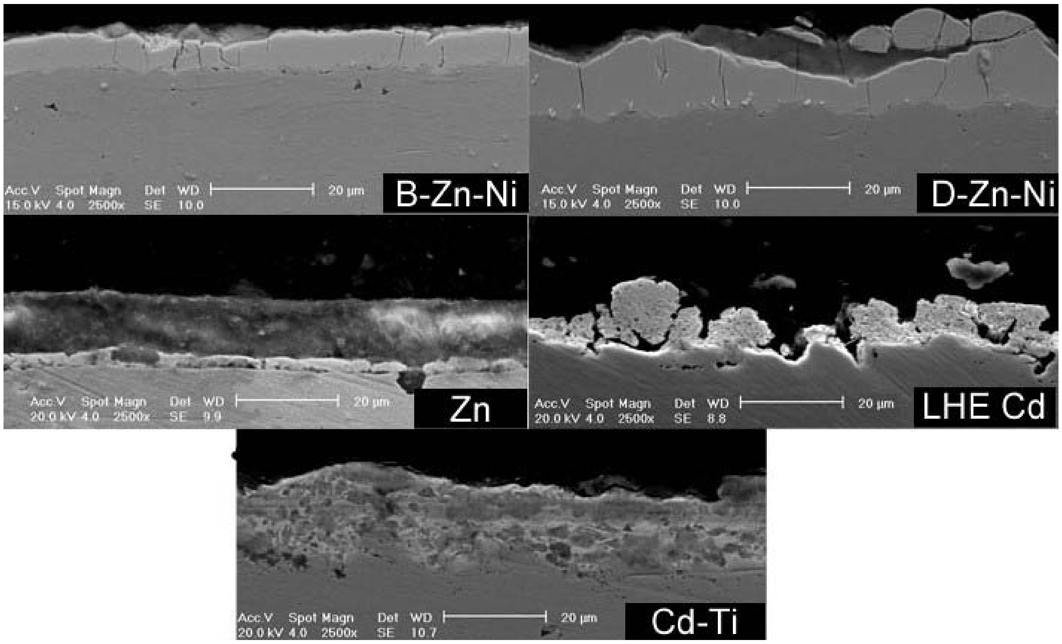

Fig. 5.2 Interface morphology of passivated coatings

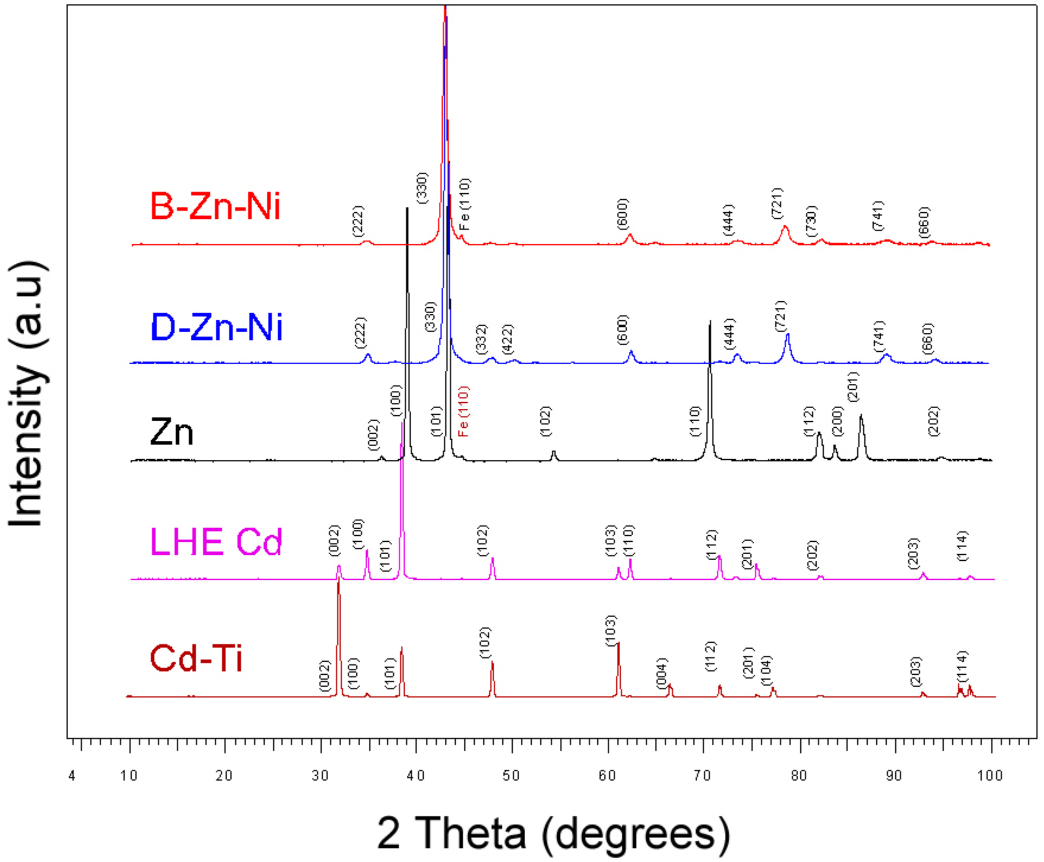

Fig. 5.3 XRD of investigated coatings

Both the Zn-Ni coatings consisted of through thickness microcracks which are a typical of intermetallic gamma Zn-Ni. The Zn coating was composed of hemispherical clusters with a uniform cross section shown in Fig. 5.2 which are typical of most Zn coatings [25, 26]. The LHE Cd coating was composed of hexagonal crystals clustered together to form a spherical structure, a common characteristic of Cd coatings [27, 28] . The cross section of LHE Cd coating shown comprises columns made up of spheres with intermittent discontinuities. The Cd-Ti coating, exhibited a different morphology as compared to the Cd coating. Instead of spherical hexagonal platelet morphology, stacking of individual platelets was observed. The cross section of

Cd-Ti (Fig. 5.2) was also different from LHE Cd. The platelets were more densely packed without discontinuities. It is believed that the addition of Ti in the plating solution resulted in the formation of a Cd-Ti solid solution causing this change in morphology. Both Cd and Cd-Ti coatings showed typical diffraction patterns of Cd deposits as shown in Fig. 5.3. The Cd-Ti coating did not exhibit any phases apart from Cd, supporting the phase diagram prediction by Murray [29] that the Ti formed a solid solution with Cd.

5.3.2. Effect of heat treatment on cross sectional morphology of Zn-Ni coatings

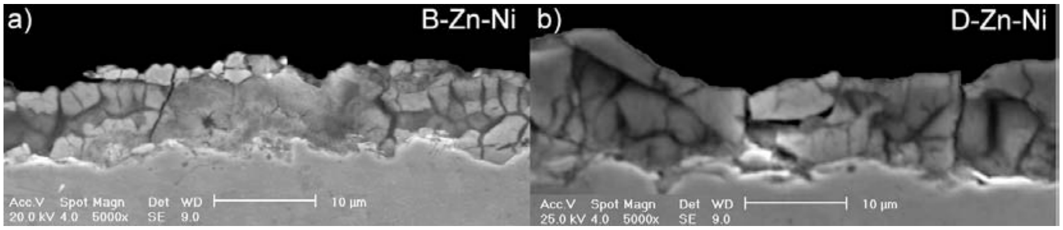

Fig. 5.4 Effect of baking treatment on interface morphology of Zn-Ni coatings

Table 5.1 Residual stress analysis by XRD of Zn-Ni coatings with and without heat treatment

Coating	**Condition**	**σ_{XX} (MPa)**	**σ_{YY} (MPa)**
B-Zn-Ni	Passivated	-14.87±17.15	5.70 ±17.03
B-Zn-Ni	Baked	17.24±10.15	19.59±10.18
D-Zn-Ni	Passivated	50.13±15.13	61.80±15.03
D-Zn-Ni	Baked	131.05±15.48	100.63±15.58

Both the Zn-Ni coatings, as shown in Fig. 5.2, had through thickness cracks. After the post plating heat treatment the number of cracks increased in both the Zn-Ni coatings, as shown in Fig. 5.4. Residual stress analysis results of the coatings with and without heat treatment by XRD are shown in Table 1. The residual stresses in both the coatings were observed to be tensile in nature. The magnitude of residual stress increased after the heat treatment. The observations in this work appear to be supported by the work of Lin et al and Saski et al [23, 24] , who noted that the residual stress distribution in Zn-Ni coatings was compressive towards the substrate and transformed to tensile towards the surface [23, 24]. They also reported that tensile residual stresses are accompanied by cracking of the coatings [23, 24]. Zn-Ni coatings were found to be susceptible to cracking when exposed to acid solutions even for a small time interval of 10 sec [23]. In the present work, during passivation, all coatings were exposed to a trivalent chrome passivation solution, which is an acidic medium, for 10 -15 sec. During the passivation process, a small amount of Zn is dissolved from the surface of the coating, resulting in a Ni rich surface. This leads to a decrease in unit cell volume and the change in residual stresses, which possibly results in the observed surface microcracks. The lattice mismatch (a = 0.892 nm for Zn-Ni and *a*= 0.286 nm for the steel) between the Zn-Ni coating and the substrate could also contribute to surface cracks.

All electroplated components for aerospace industries are subjected to plating heat treatment at 200ºC to reduce the risk of hydrogen embrittlement. There is a mismatch of coefficients of thermal expansion between the Zn-Ni coating and the steel substrate. Thus, after baking, the tensile residual stresses increases in both the lateral and longitudinal directions in the coatings, resulting in extensive cracking across the interface. This is also corroborated with the increase in residual stresses. The increase in tensile residual stress in D-Zn-Ni was more pronounced than the B-Zn-Ni. This could be attributed to the difference in coating morphology and the coating process such as current density and plating conditions.

5.3.3. Corrosion tests

5.3.3.1 Measurement of open circuit potentials (OCP) and Potentiodynamic polarization

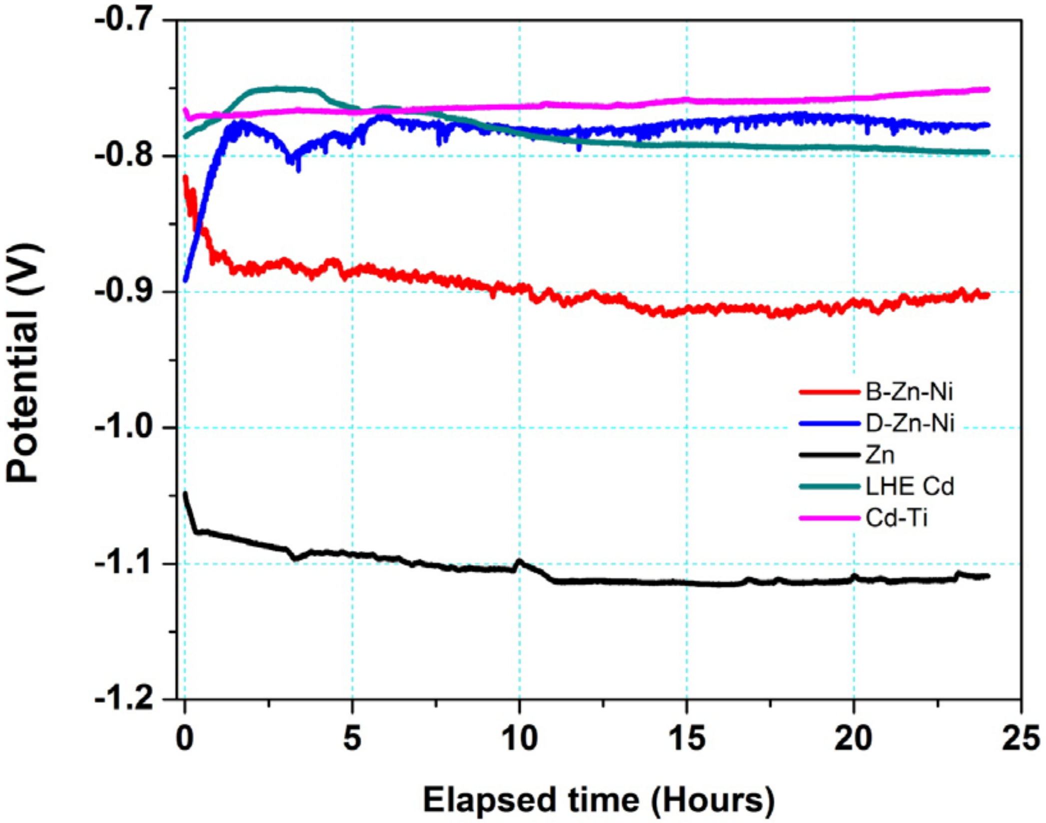

Fig. 5.5 Open circuit potentials of the passivated coatings for 24 hrs

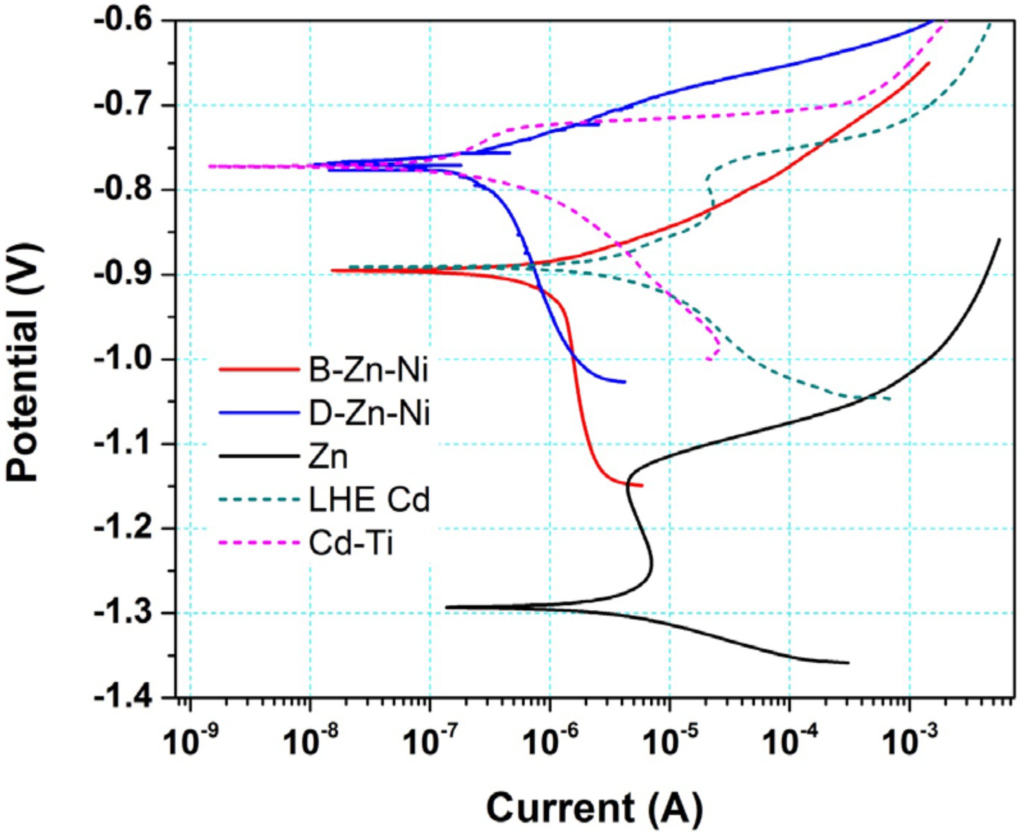

Fig. 5.6 Potentiodynamic polarization curves for the passivated coatings

The open circuit potential measurements of the passivated coatings for 24 hours are shown in Fig. 5.5. The OCPs of the Zn and Cd coatings are stable throughout the test. The OCPs of Zn-Ni coatings showed a transition range in the initial 2 to 5 hours of the test. The OCP of D-Zn-Ni started to increase and then stabilize close to 5 hours to a stable value of -0.79 V (SCE) owing to dezincification[11]. The D-Zn-Ni coating exhibited higher OCP compared to B-Zn-Ni with the OCP much closer to that of the Cd. The OCP of B-Zn-Ni (-

0.9V SCE) coatings was in between the Zn (-1.1V SCE) and Cd (-0.77V SCE) coating. Even though both the Zn-Ni coatings were of similar composition the change in the nature of the OCP shift was due to the fact that D-Zn-Ni was losing Zn at a faster rate than the B-Zn-Ni. The reason could be attributed to the change in surface morphologies, microcracks distribution, the passivation layers and the plating parameters. However, the OCP measurements are qualitative measurements do not quantify the corrosion rates.

After stabilization of the OCPs the potentiodynamic polarization tests were carried out for the coatings. The results are shown in Fig. 5.6. All the coatings showed active dissolution characteristics without passivation behavior i.e. all the coatings will sacrificially protect the steel. From the polarization curves it could be observed that both the Zn-Ni coatings are equivalent, to the Cd coatings in the sense that these will act as sacrificial coatings on steel. Based on the Tafel extrapolation method, the corrosion current (I_{corr}) and the corrosion potential (E_{corr}) was determined and the results are tabulated in Table 5.2. The E_{corr} of B-Zn-Ni and D-Zn-Ni are the same as those of the LHE Cd and Cd-Ti, respectively. From the I_{corr} values, both the Zn-Ni coatings were superior to the Zn coating in terms of corrosion resistance. The corrosion resistance of LHE Cd was found to be inferior compared to Cd-Ti possibly owing to the morphology of the coating. The discontinuities observed in the interface of the LHE Cd could have led to the diffusion of the corrosive environment leading to more active corrosion which resulted in a higher I_{corr} compared to Cd-Ti. The I_{corr} of B-Zn-Ni was observed to be higher than D-Zn-Ni, possibly owing to differences in the rate of dezincification and distribution of corrosion products on the surface of the coatings.

Table 5.2 Corrosion current and potentials of passivated coatings from Tafel's extrapolation

Coating	Corrosion potential E_{Corr} (V)	Corrosion current I_{Corr} (μA)
B-Zn-Ni	-0.89	1.638
D-Zn-Ni	-0.77	0.768
Zn	-1.29	4.479
LHE Cd	-0.89	6.21
Cd-Ti	-0.77	1.058

Corrosion products on the surface of the coatings after the potentiodynamic polarization experiments, determined by grazing incidence XRD, are shown in Fig. 5.7. In the Zn-Ni coatings it was observed that dezincification transforms γ-Zn-Ni into δ-Zn-Ni with $Zn_5(OH)8Cl2.H2O$ being formed as the primary corrosion product. These corrosion products offered additional protection to the underlying coating compared to the corrosion products formed on the Zn ($Na_2ZnO_2.H_2O$) and Cd ($CdCl_2.H_2O$). Thus from the E_{corr} and I_{corr} measurements it could be observed that Zn-Ni coatings have superior corrosion resistance than the Zn, Cd and Cd-Ti coatings.

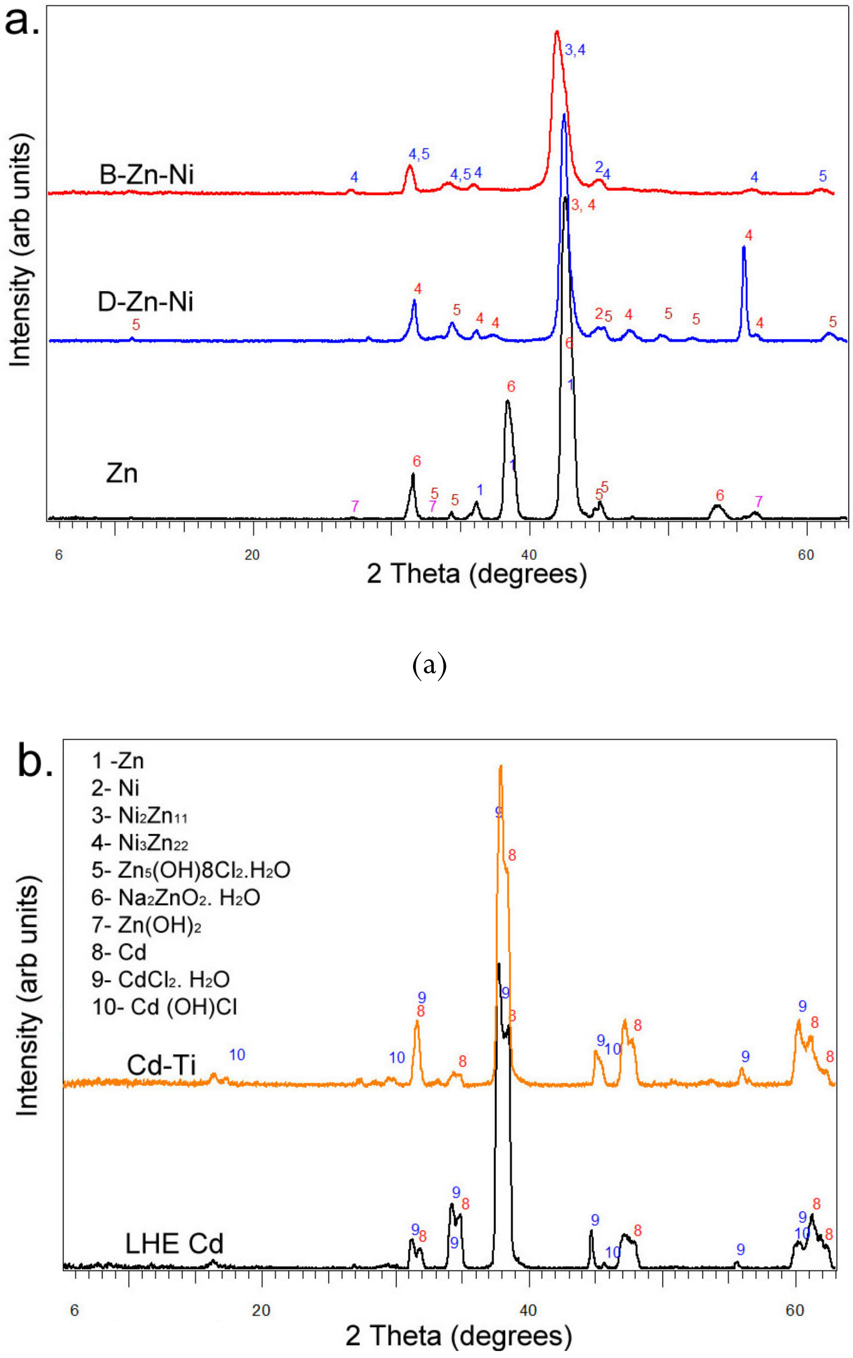

(a)

(b)

Fig. 5.7 Characterization of Corrosion products with grazing incidence XRD

(a) Zn & Zn-Ni coatings (b) LHE Cd & Cd-Ti coatings

5.3.3.2 Electrochemical impedance spectroscopy

EIS studies were carried out on all the passivated coatings. EIS is a versatile method to identify the corrosion mechanisms and kinetics, which are not usually observable by open circuit potential measurements and the potentiodynamic studies. A Nyquist plot is a semi circular plot between the electrochemical impedance in real and imaginary axes and the experimental data can be explained by means of simple electrical circuits as shown in Fig. 5.8. The corrosion resistance of a coating can be explained by two different circuits i.e. a simple Randles circuit as shown in Fig. 5.8 (a) where the solution resistance (R_S) is in series with the double layer capacitance (C_{dl} or Q_{dl}), which is in turn parallel to a charge transfer resistance or polarization resistance (R_P). For coatings exhibiting two time constant behavior, the circuit in Fig. 5.8 (b) is utilized. Here an embedded parallel resistance (R_2) and a capacitance (Q_2) are in series with the main Randles circuit [3, 4, 30]. For complex electrochemical conditions where the surface is non homogeneous, the double layer capacitance is replaced by the term Q which is called the constant phase element [30-32]. The impedance is then given by the equation (2)

$$Z_Q = \frac{1}{[Y_0 \quad J\omega^{\,n}]} \qquad (2)$$

where Z is the impedance (Ω), Y_0 is the capacitance factor (Ω^{-1} s^n), ω is the angular frequency (rad S^{-1}) , and *n* is the empirical exponent of *Q*. When Q is close to 1 the behavior can be equalized to a double layer capacitance. In a Nyquist plot the polarization resistance approximately corresponds to the size of the semicircle [30].

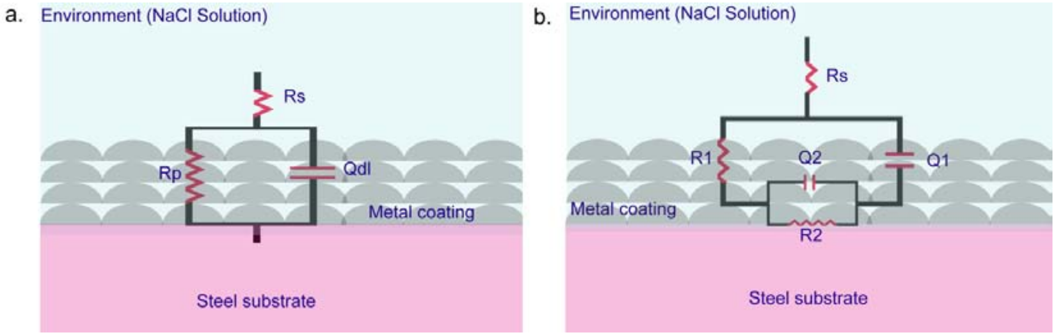

Fig. 5.8 Equivalent circuit models used for fitting the Nyquist data

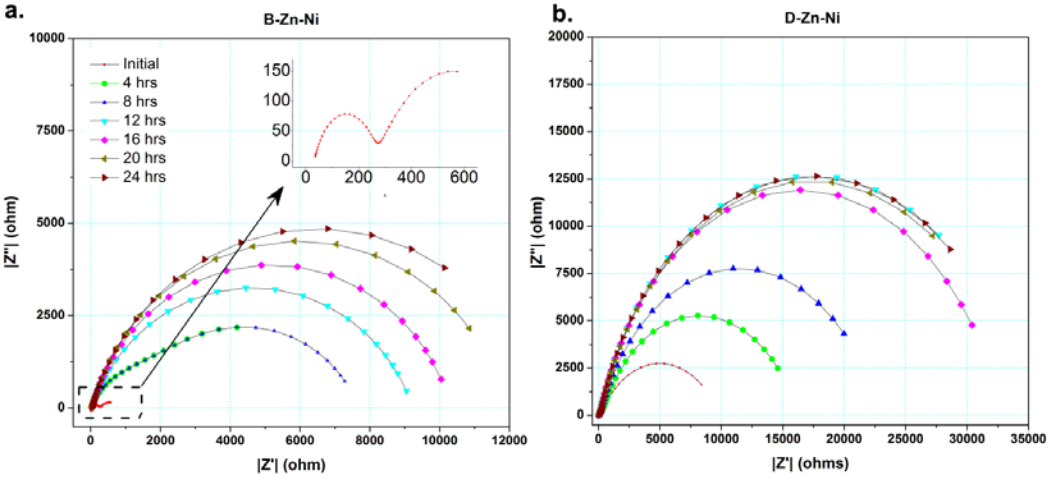

Fig. 5.9 Nyquist plot of (a) B-Zn-Ni and (b) D-Zn-Ni coatings

Table 5.3 Equivalent circuit parameters of Zn-Ni coatings from the Nyquist plot

Elapsed time (Hrs)	Rs (KΩ)	R1 (KΩ)	Q1		R2 (KΩ)	Q2	
			Y0	n		Y0	n
	B-Zn-Ni						
0	0.032	0.2393	5.96E-06	0.74	0.578	2.02E-03	0.61
4	0.034	2.619	6.19E-05	0.80	5.02	2.55E-04	0.75
8	0.034	9.21	1.22E-04	0.78			
12	0.0337	10.85	1.63E-04	0.81			
16	0.0335	10.3	1.85E-04	0.82			
20	0.0335	11.91	2.00E-04	0.83			
24	0.0336	12.95	2.16E-04	0.82			

Elapsed time (Hrs)	Rs (KΩ)	R1 (KΩ)	Q1		R2 (KΩ)	Q2	
			Y0	n		Y0	N
	D-Zn-Ni						
0	0.0296	0.387	1.51E-06	0.83	9.46	1.48E-05	0.63
4	0.0297	0.936	1.99E-05	0.69	15.31	1.49E-05	0.81
8	0.0313	0.367	1.72E-05	0.74	22.45	1.38E-05	0.80
12	0.0321	0.1621	1.46E-05	0.78	34.6	1.94E-05	0.82
16	0.0323	0.1709	2.04E-05	0.78	32.6	2.14E-05	0.83
20	0.0323	0.214	2.09E-05	0.75	34.4	2.38E-05	0.83
24	0.0322	0.21	2.09E-05	0.75	34.6	2.87E-05	0.84

The EIS spectrum of B-Zn-Ni and D-Zn-Ni are shown in Fig. 5.9 (a) and (b) respectively. The Nyquist plot of B-Zn-Ni exhibits two time constants, which is characterized by the appearance of two semi circles. This behavior exists until 4 hrs and then the character changes to single time constant. The initial two time constant behavior is due to the passive film and the coating underneath. As the exposure time increases the corrosion resistance of the coating increases progressively due to Ni enrichment of the surface. Unlike B-Zn-Ni, D-Zn-Ni shows two time constant behavior until 24 hour exposure cycle. The two resistances R_1 and R_2 in Zn-Ni coatings could be characterized as the polarization resistance of the corrosion product and the coating respectively. Thus the total polarization resistance of the coating R_P could be assumed to be the sum of two resistances if the empirical exponent (n) of the constant phase element (Q) is close to unity. The EIS parameters determined from the equivalent circuit models are shown in Table 3 for both the Zn-Ni coatings.

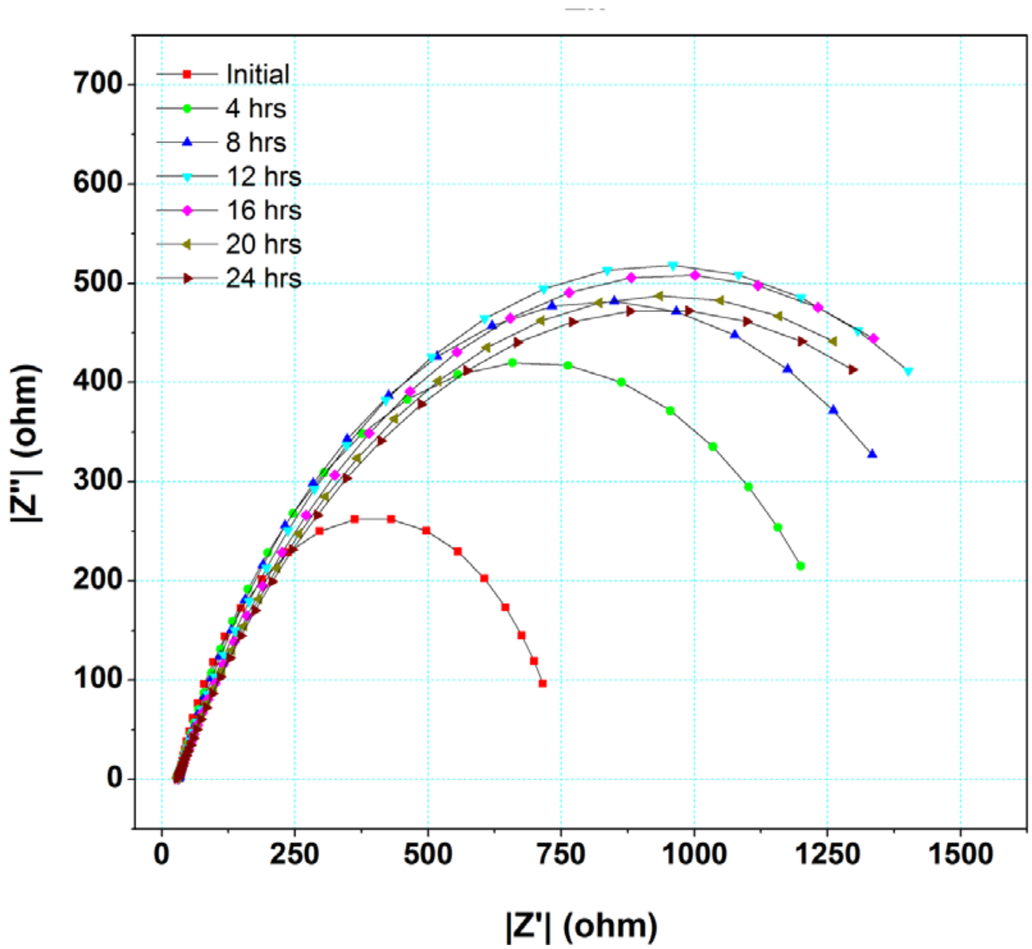

Fig. 5.10 Nyquist plot of Zn coating

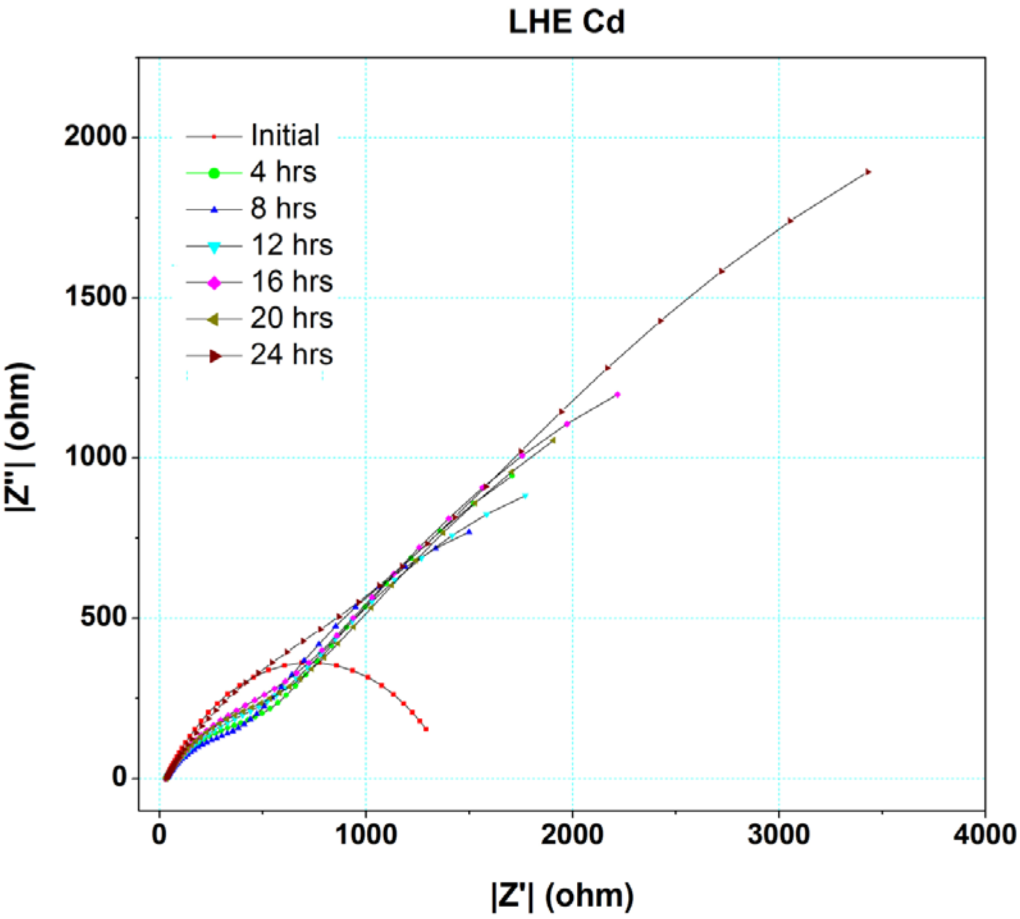
LHE Cd
Initial
4 hrs
8 hrs
12 hrs
16 hrs
20 hrs
24 hrs
|Z''| (ohm)
0
500
1000
1500
2000
|Z'| (ohm)
0
1000
2000
3000
4000

(a)

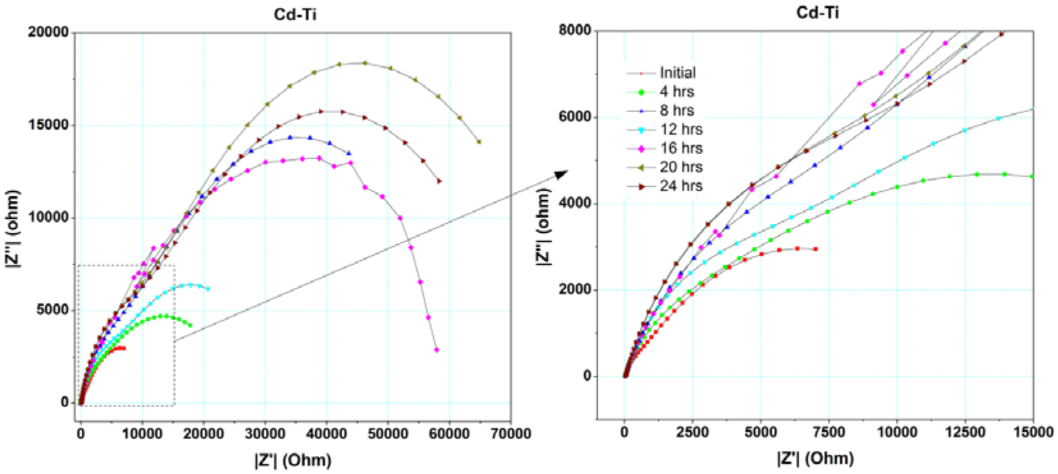

(b)

Fig. 5.11 Nyquist plot of (a) LHE Cd and (b) Cd-Ti coating

Table 5.4 Equivalent circuit parameters of Zn, LHE Cd and Cd-Ti coatings from the Nyquist plot

Elapsed time (Hrs)	Rs (KΩ)	R1 (KΩ)	Q1	
			Y0	n
	Zn			
0	0.032	0.732	2.43E-05	0.79
4	0.031	1.32	9.00E-05	0.72
8	0.031	1.596	1.40E-04	0.69
12	0.03	1.82	2.00E-03	0.66
16	0.029	1.869	2.39E-04	0.63
20	0.029	1.835	2.67E-04	0.62
24	0.028	1.816	2.96E-04	0.61

Elapsed time (Hrs)	Rs (KΩ)	R1 (KΩ)	Q1		R2 (KΩ)	Q2	
			Y0	n		Y0	n
	LHE Cd						
0	0.0306	1.401	4.63E-04	0.61			
4	0.0311	0.65	1.10E-03	0.52	4.85	8.39E-03	0.58
8	0.0311	0.535	1.37E-03	0.50	3.24	9.43E-03	0.61
12	0.0313	0.785	1.43E-03	0.52	3.57	8.49E-03	0.61
16	0.0314	0.89	1.21E-03	0.54	5.37	5.99E-03	0.59
20	0.0312	0.807	1.21E-03	0.54	5.72	7.22E-03	0.57
24	0.0311	1.517	9.73E-04	0.56	9.15	3.40E-03	0.56

Elapsed time (Hrs)	Rs (KΩ)	R1 (KΩ)	Q1		R2 (KΩ)	Q2	
			Y0	n		Y0	n
	Cd-Ti						
0	0.0318	0.79	1.09E-06	0.86	11.95	2.26E-05	0.55
4	0.0269	4.07	7.33E-06	0.71	21.84	5.43E-05	0.45
8	0.0259	10.4	8.35E-06	0.70	54.6	4.62E-05	0.56
12	0.0279	7.15	7.15E-06	0.74	24.57	6.13E-05	0.54
16	0.0285	11.16	6.96E-06	0.74	52.1	5.33E-05	0.56
20	0.0284	12.06	6.88E-06	0.74	70.6	4.73E-05	0.57
24	0.0286	12.08	6.78E-06	0.75	61.7	5.15E-05	0.56

Fig. 5.10 shows the Nyquist plot of the Zn coating. Single time constant behavior was observed during the complete exposure cycle, thus a simple Randles circuit was utilized to model the polarization resistance. The results are shown in Table 5.4.

The Nyquist plots of LHE Cd and Cd-Ti coatings are shown in Fig. 5.11 (a) and Fig. 5.11(b). It can be observed that both the Cd coatings exhibit two time constants. The low frequency resistances R_2 were observed to be much higher in magnitude than the R_1 values. Thus R_2 can be classified as the infiltration resistance or the resistance at the interface. R_2 was observed to be very high in magnitude in Cd-Ti coating compared to the LHE Cd coating due to the difference in morphology in both the coatings. The LHE Cd coating had a discontinuous interface, which exposes the interface to some extent. This resulted in increased corrosion of the LHE Cd coating to protect the substrate, resulting in a lower R2 compared to Cd-Ti. Since the R_2 values of the Cd coatings were much higher in magnitude compared to R_1, which reflects the corrosion resistances offered by the steel substrates and also the exponents (n) of Q_2 were not close to unity, the polarization resistance of the coating was assumed to be R_1 alone for Cd coatings.

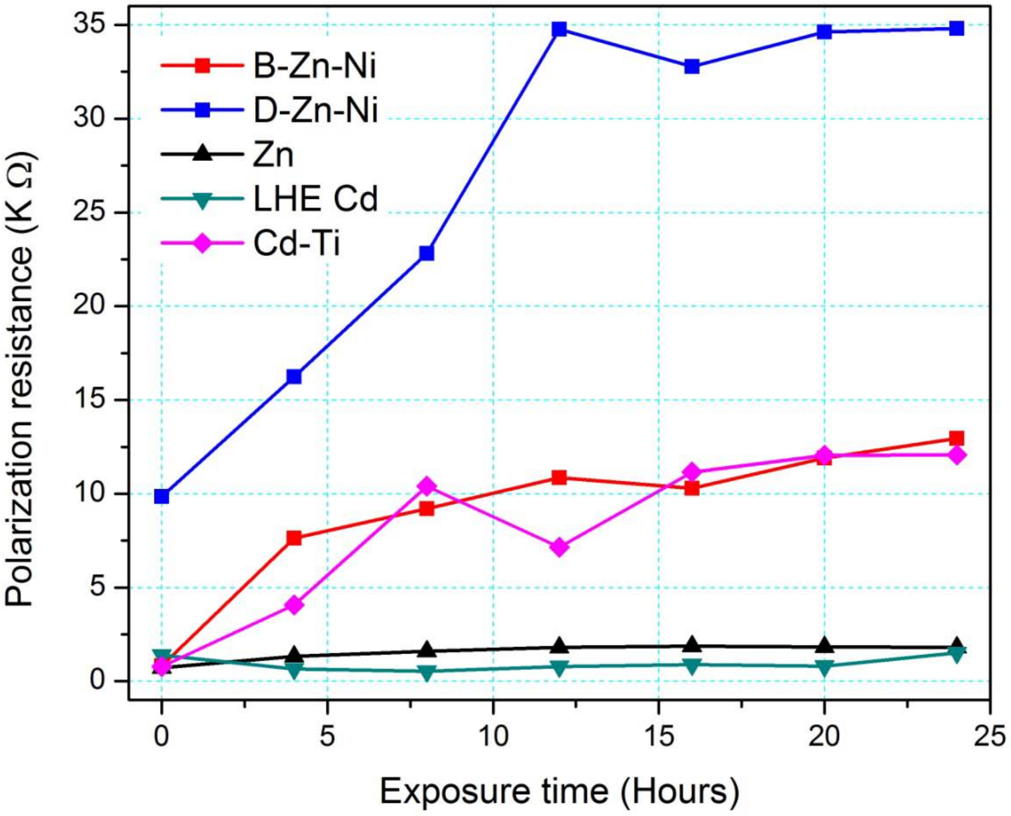

Fig. 5.12 Polarization resistances of the passivated coatings

The variation of polarization resistances of the coatings with respect to time is shown in Fig. 5.12. LHE Cd and the Zn coating exhibited the lowest polarization resistances compared to the Zn-Ni and Cd-Ti coatings. The γ Zn-Ni phase in the Zn-Ni coatings resulted in better corrosion protection compared to the pure Zn coating. The Ni rich surface formed on Zn-Ni coatings offered additional cathodic protection of the coating surface, resulting in better corrosion resistance than the Zn and Cd coatings. The addition of Ti in the plating bath changed the morphology of Cd-Ti coating compared to the LHE Cd which resulted in a uniform interface of the coating. This in turn resulted in better surface coverage and more uniform corrosion of the coating. The D-Zn-Ni coating showed higher polarization resistance compared to B-Zn-Ni. This can be attributed to the difference in the dezincification rates in both the coatings, which in turn can be attributed to the difference in the surface morphology arising due to the plating conditions. The Ni rich surface formed on the D-Zn-Ni is formed at much quicker rate than the B-Zn-Ni. Even though the polarization resistances of B-Zn-Ni is lower than D-Zn-Ni, the life of the coating could eventually be increased by the slower dezincification process.

5.3.3.3 Effect of heat treatment and passivation on corrosion resistance of Zn-Ni coatings

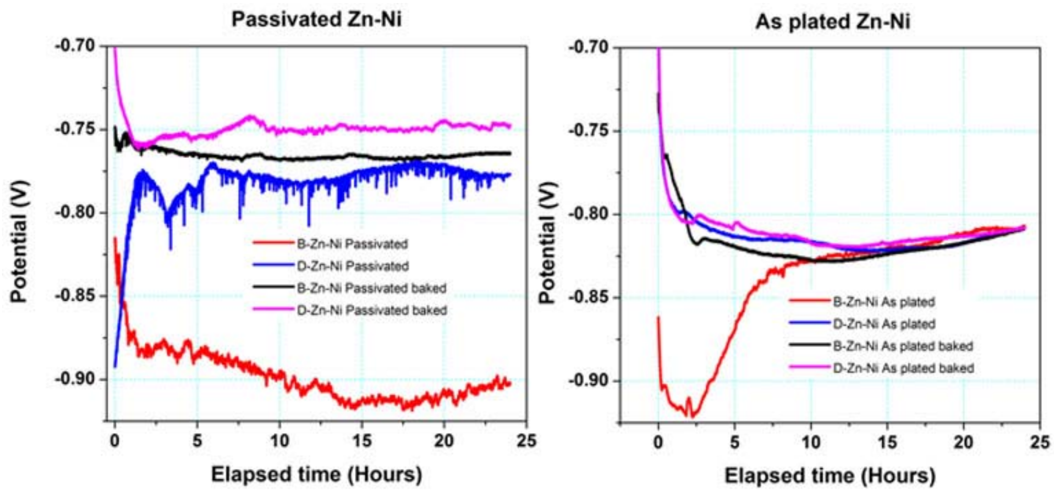

(a) (b)

Fig. 5.13 Effect of heat treatment on open circuit potentials in (a) as plated Zn-Ni (b) passivated Zn-Ni coatings

Components used in aerospace industries typically require a 24 hour heat treatment cycle at 200°C on electroplated parts to reduce the risk of hydrogen embrittlement. Thus the effect of post plating heat treatment on corrosion resistance of the coatings were determined in as plated condition and with chrome passivation treatment.

The open circuit potentials of the coatings were determined before potentiodynamic polarization. The OCPs of passivated coatings are shown in Fig. 5.13 (a) and the as plated coatings are shown in Fig. 5.13 (b). The OCP of as plated B-Zn-Ni was lower than D-Zn-Ni. The trends observed in the passivated Zn-Ni coatings were discussed in the previous sections, which was owing to difference in the rate of loss of Zn from the matrix. After heat treatment the OCP for both Zn-Ni coatings shifted towards cathodic regime, i.e. the coatings became nobler after the heat treatment. The difference in the shift of OCP was higher for B-Zn-Ni than D-Zn-Ni. The reason for the shift in potentials can be attributed to the crack network in the coating, which expanded due to heat treatment as was explained earlier with the help of interface morphology and residual stress measurements. The heat treatment could also result in damage of the passivation layer, thus resulting in formation of the Ni rich layer at a much quicker rate resulting in the shift.

The OCPs of D-Zn-Ni were higher than the B-Zn-Ni even before the heat treatment owing to the presence of intermittent porosity in the D-Zn-Ni coating. Thus the shift in potential was less after the heat treatment due to the presence of pre existing defects in D-Zn-Ni than the B-Zn-Ni. The OCPs of the as plated coatings are shown in Fig. 5.13 (b). The rate of dezincification was observed to be different for both the Zn-Ni coatings before heat treatment until

10 hours of exposure time. After that the OCPs stabilized to similar values. There was no visible difference in the OCPs of the as plated coatings with or without heat treatment once the Ni enrichment of the surface has been completed. The same trend is reflected in the potentiodynamic polarization measurements.

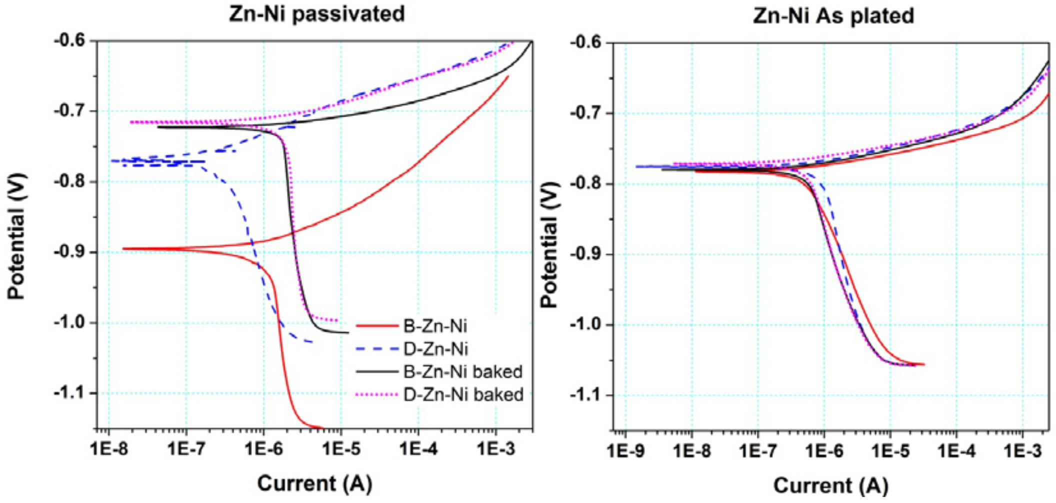

Fig. 5.14 Effect of heat treatment polarization behavior in (a) as plated Zn-Ni (b) passivated Zn-Ni coatings

Table 5.5 Corrosion current and potentials of Zn-Ni coatings with all treatments from Tafel's extrapolation

Coating	**Treatment**	Corrosion potential	Corrosion current
		E_{Corr} (V)	I_{Corr} (μA)
B-Zn-Ni	As plated	-0.78	0.627
D-Zn-Ni	As plated	-0.77	0.997
B-Zn-Ni	As plated & baked	-0.78	0.554
D-Zn-Ni	As plated & baked	-0.77	0.512

Coating	**Treatment**	Corrosion potential	Corrosion current
		E_{Corr} (V)	I_{Corr} (μA)
B-Zn-Ni	Passivated	-0.89	1.638
D-Zn-Ni	Passivated	-0.77	0.768
B-Zn-Ni	Passivated & baked	-0.72	1.9
D-Zn-Ni	Passivated & baked	-0.72	2.096

Fig. 5.14 (a) shows the polarization curves of passivated coatings. After heat treatment the polarization curves are shifted to nobler potentials which are indicated by the shift in E_{corr} shown in Table 5. The corrosion potential shifted to nobler values (from -0.89 to -0.72 for B-Zn-Ni and from -0.77 to -0.72 for D-Zn-Ni) but the corrosion currents were higher. The reason could be attributed to the damage in the passivation layer after heat treatment. The polarization curves of as plated coatings are shown in Fig. 5.14 (b). No significant difference in polarization behavior of the coatings can be observed here before and after the heat treatment. After the Tafel's extrapolation the corrosion potentials of B-Zn-Ni and D-Zn-Ni coatings were the same but corrosion currents differed slightly. The effect of heat treatment was negligible in the as plated coatings once a stable corrosion product was formed.

EIS was utilized to understand the corrosion mechanism and the effect of heat treatment on Zn-Ni coatings. The polarization resistances of passivated coatings are shown in Fig. 5.15 (a). The rate of dezincification in D-Zn-Ni was observed to be much higher than B-Zn-Ni which is shown by a sharp increase in the polarization resistance of D-Zn-Ni and more stable corrosion product. The heat treatment of passivated coatings reduced the polarization resistances. This observation can be attributed to damage of the passive film after heat treatment. The difference in polarization resistance after heat treatment was less in B-Zn-Ni compared to D-Zn-Ni which can also attributed to the difference in dezincification rates.

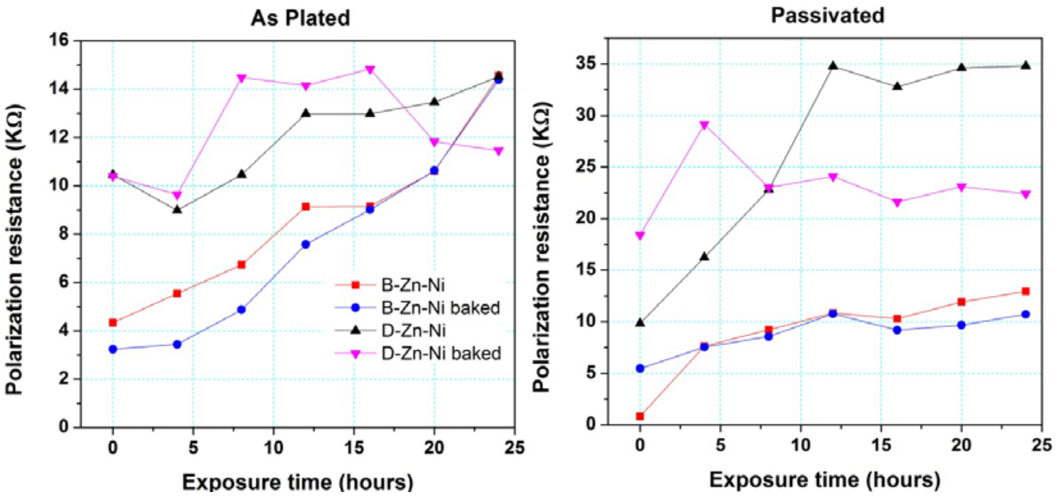

Fig. 5.15 Effect of heat treatment polarization resistances in (a) passivated Zn-Ni coatings (b) as plated Zn-Ni

The polarization resistances of as plated coatings are shown in Fig. 5.15 (b). Both the Zn-Ni coatings show dezincification of the coating with respect to time. The rate of dezincification for B-Zn-Ni was slower than D-Zn-Ni. But after the end of the test cycle and eventually after uniform corrosion products were formed on the surface the polarization resistances were found to be the same. The heat treatment in B-Zn-Ni did not change the polarization resistance once a stable corrosion product was formed on the surface but it lowered the dezincification rate below 15 hours of exposure time. The reason can be attributed to the difference in diffusion mechanism and the stability of the corrosion products which prevent diffusion.

5.4. Conclusions

Corrosion resistance of Zn, Zn-Ni, LHE Cd and Cd-Ti coatings were measured using three different techniques. The corrosion resistances of the coatings were correlated to the microstructure, phase and composition of the coatings and the nature of corrosion products. From the present investigation following conclusions can be made:

- Zn-Ni coatings had microcracks across the thickness of the coating; these cracks widened and formed a network when the coatings were heat treated.
- OCP measurements on Zn-Ni coatings showed progressive enrichment of the surface of the coating with Ni owing to dezincification.
- Potentiodynamic polarization experiments showed lower corrosion currents in Zn-Ni coatings than Zn and Cd coatings.
- EIS studies on the coatings revealed a higher infiltration resistance for Cd coatings than Zn-Ni, however the polarization resistances of the Zn-Ni coatings were higher than Cd and Cd-Ti coatings owing to the phase transformation and Ni enrichment of the surface of the coating.
- D-Zn-Ni coating showed higher polarization resistance and lower corrosion current than the B-Zn-Ni due to the difference in coating morphology and the rate of dezincification. The presence of micro-pores in D-Zn-Ni resulted in higher diffusion of corrosive environment resulting in distribution of anodic reaction throughout the coating resulting in higher rate of dezincification compared to the compact microstructure of B-Zn-Ni.

- Heat treatment effects were negligible in as plated Zn-Ni coatings. Heat treatment after passivation of the coatings resulted in lower polarization resistance and higher corrosion currents due to localized damage of the passive film due to heat treatment.
- Summarizing all aspects of the present investigation, it can be concluded that Zn-Ni coatings offer better sacrificial corrosion protection compared to Zn and Cd coatings.

References

[1] Wilcox GD, Gabe DR. Electrodeposited Zinc Alloy Coatings. Corrosion Science. 1993;35:1251-8.

[2] Winand R. Electrodeposition of Zinc and Zinc Alloys. Modern Electroplating: John Wiley & Sons, Inc.; 2010. p. 285-307.

[3] Eliaz N, Venkatakrishna K, Hegde AC. Electroplating and characterization of Zn–Ni, Zn–Co and Zn–Ni–Co alloys. Surface and Coatings Technology. 2010;205:1969-78.

[4] Hegde AC, Venkatakrishna K, Eliaz N. Electrodeposition of Zn–Ni, Zn–Fe and Zn–Ni–Fe alloys. Surface and Coatings Technology. 2010;205:2031-41.

[5] Tian W, Xie FQ, Wu XQ, Yang ZZ. Study on corrosion resistance of electroplating zinc-nickel alloy coatings. Surface and Interface Analysis. 2009;41:251-4.

[6] Siitari DW, Sagiyama M, Hara T. Corrosion of Ni-Zn Electrodeposited Alloy. Transactions of the Iron and Steel Institute of Japan. 1983;23:959-66.

[7] Alfantazi AM, Erb U. Corrosion properties of pulse-plated zinc-nickel alloy coatings. Corrosion. 1996;52:880-8.

[8] Bowden C, Matthews A. A study of the corrosion properties of PVD Zn-Ni coatings. Surf Coat Tech. 1995;76-77:508-15.

[9] Rahsepar M, Bahrololoom ME. Corrosion study of Ni/Zn compositionally modulated multilayer coatings using electrochemical impedance spectroscopy. Corrosion Science. 2009;51:2537-43.

[10] Stein M, Owens SP, Pickering HW, Weil KG. Dealloying studies with electrodeposited zinc-nickel alloy films. Electrochim Acta. 1998;43:223-6.

[11] Giridhar J, van Ooij WJ. Study of Zn-Ni and Zn-Co alloy coatings electrodeposited on steel strips II: Corrosion, dezincification and sulfidation of the alloy coatings. Surface and Coatings Technology. 1992;53:35-47.

[12] Muller C, Sarret M, Garcia E. Heat-treatment on black-passivated ZnNi alloys. Journal of The Electrochemical Society. 2003;150:C212-C8.

[13] Müller C, Sarret M, Garc´a E. Heat treatment effect on the corrosion behaviour of black passivated ZnNi alloys. Corrosion Science. 2005;47:307-21.

[14] Fedrizzi L, Ciaghi L, Bonora PL, Fratesi R, Roventi G. Corrosion behaviour of electrogalvanized steel in sodium chloride and ammonium sulphate solutions; a study by E.I.S. Journal of Applied Electrochemistry. 1992;22:247-54.

[15] Girčienė O, Gudavičiūtė L, Juškėnas R, Ramanauskas R. Corrosion resistance of phosphated Zn–Ni alloy electrodeposits. Surface and Coatings Technology. 2009;203:3072-7.

[16] Ramanauskas R, Juskenas R, Kalinicenko A, Garfias-Mesias LF. Microstructure and corrosion resistance of electrodeposited zinc alloy coatings. Journal of Solid State Electrochemistry. 2004;8:416-21.

[17] Gavrila M, Millet JP, Mazille H, Marchandise D, Cuntz JM. Corrosion behaviour of zinc–nickel coatings, electrodeposited on steel. Surface and Coatings Technology. 2000;123:164-72.

[18] Fabri Miranda FJ. Corrosion behavior of zinc-nickel alloy electrodeposited coatings. Corrosion. 1999;55:732-42.

[19] Tran LM, Matthias PM, Jones JH. Low hydrogen embrittlement Zinc/Nickel plating for high strength steels. US Patent 8048285. 8048285 edNovember 1, 2011

[20] MIL-STD-870C. U.S. Military Standard (USAF) on Cadmium plating, Low embrittlement, Electrodeposition. Department of Defence Standard Practice; 27 April 2009.

[21] MIL-STD-1500C. U.S. Military Standard (USAF) on Cadmium-Titanium Plating, Low Embrittlement, Electrodeposition. Department of Defence Standard Practice; 01 March 2007.

[22] He BB. Stress Measurement. Two-Dimensional X-Ray Diffraction: John Wiley & Sons, Inc.; 2009. p. 249-328.

[23] Lin C, Lee H, Hsieh S. Microcracking of flash coatings and its effect on the Zn-Ni coating adhesion of electrodeposited sheet steel. Metallurgical and Materials Transactions A. 1999;30:437-48.

[24] Sasaki T, Hirose Y. Residual stress distribution in electroplated Zn□Ni alloy layer determined by X-ray diffraction. Thin Solid Films. 1994;253:356-61.

[25] Thomas BK, Fray DJ. The Effect of Additives on the Morphology of Zinc Electrodeposited from a Zinc-Chloride Electrolyte at High-Current Densities. Journal of Applied Electrochemistry. 1981;11:677-83.

[26] Morón LE, Méndez A, Castañeda F, Flores JG, Ortiz-Frade L, Meas Y, et al. Electrodeposition and corrosion behavior of Zn coatings formed using as brighteners arene additives of different structure. Surface and Coatings Technology. 2011;205:4985-92.

[27] Abdelhalim AM, Baghlaf AO, Sobahi MI. Effect of Some Addition Agents on the Electrodeposition of Cadmium from Acidic Chloride Baths. Surf Technol. 1984;22:129-42.

[28] Elhalim AMA, Sobahi MI. Effect of Bath Constituents and Some Plating Variables on the Electrodeposition of Cadmium from Acidic Chloride Baths. Surf Technol. 1983;19:45-57.

[29] Murray J. The Cd-Ti (Cadmium -Titanium) system. Journal of Phase Equilibria. 1983;4:399-401.

[30] Mansfeld F, Shih H, Greene H, Tsai CHR. Analysis of Eis Data for Common Corrosion Processes. Am Soc Test Mater. 1993;1188:37-53.

[31] Azzi M, Paquette M, Szpunar JA, Klemberg-Sapieha JE, Martinu L. Tribocorrosion behaviour of DLC-coated 316L stainless steel. Wear. 2009;267:860-6.

[32] Hassani S, Raeissi K, Azzi M, Li D, Golozar MA, Szpunar JA. Improving the corrosion and tribocorrosion resistance of Ni–Co nanocrystalline coatings in NaOH solution. Corrosion Science. 2009;51:2371-9.

Chapter 6 Hydrogen embrittlement in coated steel

6.0 Hydrogen embrittlement of Zn, Zn-Ni and Cd coated high strength steel

Preface

In this chapter the effect of Zn, Zn-Ni and Cd coatings on hydrogen embrittlement susceptibility of high strength steel is discussed. Two principle variables which are responsible for hydrogen embrittlement of the coated steel specimen were identified. (1) The hydrogen generated during the plating process (2) hydrogen permeability of the coating. The presence of microcracks and defects in the coatings played a huge part in determining the permeability of the coating, which directly relates to how easily hydrogen could be baked out of the system. A uniform Zn-Ni coatings free of defects was observed to lower the hydrogen diffusion coefficient. During the initial stages of the plating process this uniform monolayer prevented further ingress of hydrogen during the plating process. As successive layers of coatings are built up, crack networks in the coatings facilitated hydrogen removal thereby reducing the hydrogen embrittlement susceptibility. Among Zn, Zn-Ni and Cd plating processes Zn-Ni process was identified as the process with least hydrogen embrittlement susceptibility. This chapter is to be submitted as a manuscript to the journal Material Science & Engineering A, Elsevier publications.

Chapter 6 Hydrogen embrittlement in coated steel

Abstract

Sacrificial coatings, such as Zn and Cd are used to protect steel against corrosion. During the electrodeposition of metals, hydrogen is evolved due to electrolysis. The evolved hydrogen may diffuse outward and become trapped in the substrate/coating interface or migrate inward into the steel lattice causing delayed embrittlement when the component is subjected to stress. This study reports two principal variables for Zn, Zn-Ni, and Cd coatings: (i) quantity of hydrogen absorbed by the coating and substrate, by vacuum thermal desorption (ii) permeability of the coating material to hydrogen, by electrochemical permeation. The findings were analyzed in correlation with microstructural characteristics of both the coating material and the coating/substrate interface. With Zn-Ni, both coating process and coating material combined to significantly reduce the risk of internal hydrogen embrittlement by: (i) introducing the least amount hydrogen during the electrodeposition process, and (ii) by the ease with which hydrogen can be extracted by baking due to the presence of cracks in the coating.

Keywords: Electrodeposited Zn-Ni, Cd, Zn coatings, thermal desorption, H_2 permeability.

Chapter 6 Hydrogen embrittlement in coated steel

6.1 Introduction

Hydrogen embrittlement is an infrequent yet insidious problem that can lead to sudden catastrophic failure of high strength steel components. Hydrogen is practically insoluble in steel at room temperature. It can either remain trapped in microstructural features such as defects and inclusions, or it can become mobile within the steel matrix. Broadly speaking, hydrogen embrittlement is caused by mobile (diffusible) hydrogen. Two primary ingredients present in sufficient quantities will cause hydrogen embrittlement failure of a high strength steel component. These are: (i) a critical level of diffusible hydrogen in the microstructure, (ii) a threshold stress that is exceeded by applied stress, residual stress, or a combination of both. Threshold stress is a function of susceptibility of the steel, which is primarily increased with increasing strength, but can also be affected by microstructure. The source of hydrogen can either be external, such as with service corrosion, classified under environmental hydrogen embrittlement (EHE), or as a result of processing such as steel making, electrodeposition of coatings, or pickling, classified under internal hydrogen embrittlement (IHE) [1, 2]. Hydrogen embrittlement in steel is typically characterized mechanically by various types of slow strain rate tests that quantify the loss of strength and ductility resulting from the migration of diffusible hydrogen to the point of maximum stress concentration. Quantification of hydrogen, notably hydrogen present in bulk metal, is an additional tool for understanding the mechanisms affecting embrittlement of coated high strength steel.

Zn-14% Ni coatings applied over high strength steel are of interest because they have been shown to have a low propensity for internal hydrogen embrittlement, and also more responsive to baking for hydrogen removal [3]. Zn-14% Ni coatings also provide excellent corrosion resistance, comparable to that of pure electrodeposited Cd.

However, the microstructure of Zn-Ni coatings poses a number of contradictory challenges. Coleman et al. [4] investigated the hydrogen permeability of electrodeposited Zn-Ni, Zn and Ni membranes, and found that the permeability of Zn-Ni alloy was comparable to the permeability of both Zn and Ni, which is roughly 80 % lower than that of bare iron. In other words, Zn-Ni is relatively impermeable to hydrogen diffusion. However, other Zn-Ni coatings typically exhibit defects, such as intergranular cracks and through thickness pores, which are formed in the coating by residual stresses in the coating/substrate interface [5]. It has been postulated that these defects may make Zn-Ni coatings susceptible to environmental hydrogen embrittlement as they provide pathways for hydrogen diffusion inward from the surface of the coating to the steel substrate [5]. On the other hand, it can also be argued that such defects can facilitate hydrogen diffusion outward, from the substrate to the environment.

Other studies performed with Zn-10%Ni and Zn-1%Co attributed the lower propensity to IHE than with the pure Zn to the formation of nickel or cobalt rich layers in the initial stages of deposition. These layers exhibited even lower hydrogen diffusivity in comparison to Zn, thus acting as barriers to hydrogen absorption during electroplating [6]. An attempt was made to measure the rate of hydrogen absorbed during different plating processes (Zn, Zn-Ni and Zn-Co) by means of the electrochemical permeation method. The investigators reported that the Zn-Ni plating process exhibited the lowest hydrogen absorption [7].

Another consideration in the elimination of the risk of IHE in high strength steels is the effect a post electroplating heat treatment (baking) for eliminating hydrogen. Baking is a standard practice where electroplating of high strength steel is performed. Most notably, the fastener and the aerospace industry standards require electroplated parts to be baked between 4 hours and 24 hours, typically at temperatures not exceeding 200º C [8]. Hiller and Robinson reported full recovery of mechanical strength and ductility of electrodeposited Zn, Zn-Ni, Zn-Co and Cd plated high strength steel specimens [6] after the baking cycle. More specifically, they reported 89% recovery for Zn and Zn-Co, and 100% recovery for cadmium and Zn-Ni electroplated specimens, after 24 hours of baking at 200º C. This study did not quantify the amount of diffusible hydrogen eliminated during the baking cycles. Additionally, apart from mechanical strength, other aspects such as microstructure, coating permeability and process generated hydrogen were not addressed.

This paper reports two principle parameters: (i) the amount of hydrogen generated due to the plating process of Zn, Zn-Ni and Cd coatings, and (ii) the hydrogen permeability of the coated steel. These parameters are then correlated with the microstructure of the coating /substrate interface of the coated steel.

6.2 Experimental Methodology

6.2.1 Substrate materials

Two different types of substrates were utilized in this study: (i) shim stock, 100 µm thick, made of low carbon SAE 1006 steel for coatings that were used for permeation measurements (ii) ASTM F519 Type 1e specimens, which were coated for vacuum thermal desorption experiments [9]. The specimens were notched square bars made of SAE 4340 steel, heat treated to 51-53 Rockwell C. The dimensions of the notch bars are 55.9 mm length, 10 mm width and 10 mm height.

6.2.2 Coating processes

The sample substrates (notch bars and shim stock) were coated by electrodeposition of Zn, Zn-Ni and Cd using industrial electroplating processes. The basic parameters for the coating processes are listed below. The thicknesses of all the coatings were maintained in the range of 15-25 µm.

Zn-Ni: Commercially available Zn-Ni plating solution IZ C17+ provided by Dipsol Inc. was used. An alkaline plating solution with Zn and Ni metal concentrations in the ratio of 10-11:1 was used. The individual bath constituents were: Zn concentrate (9-11 g/l) Ni concentrate (08-1.2 g/l), Na_2CO_3 (59 g/l) and Noah (135 g/l). The substrates were subjected to various pretreatments like aqueous degreasing, water rinsing, abrasive grit blasting and acid activation and plated in an industrial pilot plating tank. The pH of the plating bath was maintained at 12-13.5 at 25° C and a plating current density of 28 – 30 mA/cm^2 was applied to produce a coating thickness of 15 – 20 µm in one hour.

Zn: The plating bath was acid chloride based with $ZnCl_2$ (60 g/l), KCl (250 g/l), H_3BO_3 (25 g/l) and HCl in smaller concentrations to maintain the pH of the bath to 4.5-4.8. The cathode efficiency was 95% and the temperature of the plating was held at 25 ºC. The electroplating was performed on a laboratory-scale plating setup. A plating current density of 5 mA/cm^2 was used to generate a coating thickness of 15 μm in 2 hours. The substrates were mechanically finished with 600 grit SiC grinding paper and activated in HCl for 10-12 s before plating.

Low hydrogen embrittling Cd plating (LHE Cd) was plated in an industrial plating facility using an alkaline cyanide based plating solution with CdO (20-30 g/l), NaCN (90-135 g/l), Na_2CO_3 (0-60 g/l) and NaOH (11-30 g/l). A plating current density of 118 – 120 mA/cm^2 was used to generate a coating thickness of 15 μm in 5 minutes. Substrates were solvent degreased, grit blasted and acid pickled before plating. Plating temperature was 15-30 ºC [10].

6.2.3 Characterization of coatings

The coatings were characterized based on surface and interface morphology, thickness determination and defect distribution with a Philips Field Emission Gun scanning electron microscope (FEG-XL30). The phase distribution, crystal structure and of coatings were determined using a Bruker Discover D8 – 2D VANTEC 2000 X-ray diffractometer (XRD) with Cu Kα source.

6.2.4 Vacuum thermal desorption spectroscopy

Thermal desorption spectroscopy (TDS) is a versatile method to quantify hydrogen in bulk metals. The method is based on the fact that hydrogen, either in a metal lattice, or trapped in various trap sites like dislocations, grain boundaries, diffuses upon heating [11]. Given enough time and energy, hydrogen diffuses outward from the bulk material (desorption) into the atmosphere, and can be detected within a closed vacuum system by an analytical instrument, namely, a pressure gauge, a gas chromatograph, or a mass spectrometer [12]. The thermal desorption method has been used in previous investigations to determine the amount of hydrogen desorbed from electroplated Zn and Cr based coatings [12]. In this investigation a mass spectrometer was used to measure the quantity of hydrogen being desorbed over time. The TDS schematic is shown in Fig. 6.1. The specimen chamber is made from ultrahigh vacuum (UHV) grade 304 stainless steel. The chamber is evacuated by means of two turbo molecular pumps backed by two rotary vane pumps. The specimen chamber was used to house the notch bars (bare and coated). The chamber was sealed then pumped down to a vacuum of less than 5 X 10 $^{-6}$ torr. After achieving the required vacuum, the mass spectrometer was turned on to measure the hydrogen ion intensity. The chamber was heated with resistive heating tape, and temperature was controlled by means of a temperature controller connected to a thermocouple that was placed directly on the specimen surface. This mechanism provided direct control and monitoring of the specimen temperature. After the background subtraction, the net hydrogen ion intensity measured by the quadruple mass spectrometer represented hydrogen being desorbed from the specimen.

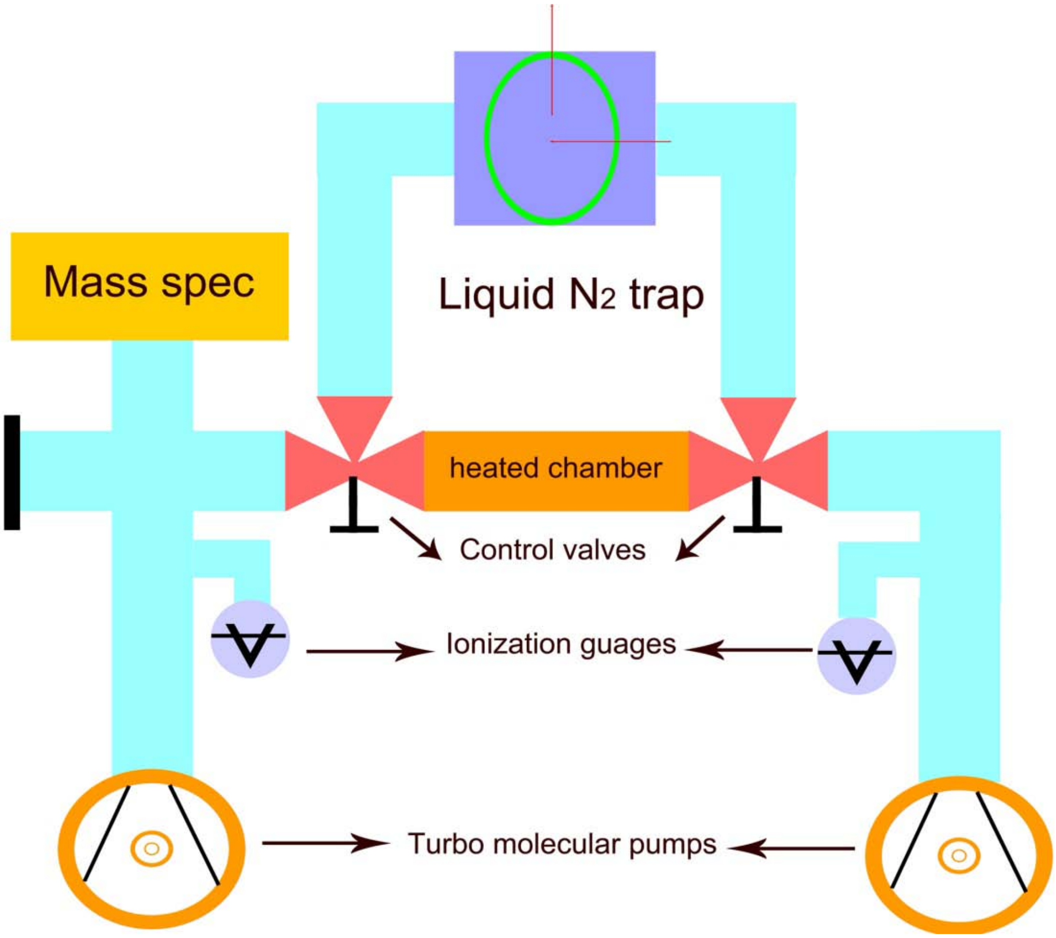

Fig. 6.1 Vacuum thermal desorption experimental setup

6.2.5 Electrochemical permeation studies on the coated steel

The electrochemical permeation cell schematic is shown in Fig. 6.2. Bare and coated shim steel sheets were cut to 40 mm X 40 mm dimensions and finished to 600 grit finish. The twin compartment permeation cell was made of Teflon, with specimen exposure area of 0.720 cm^2. The cell was placed inside a Faraday cage to minimize external noise or disturbance. A 6 V battery with variable rheostat was used as the charging source. Palladium was sputtered on the steel using a plasma sputtering apparatus. The specimen arrangement was such that the Zn/Cd coating was used as the charging side and the palladium sputtered steel surface was used as the discharge side. The specimen acts as the working electrode for both cells. Platinum wire was used as a counter electrode in both cells. The electrolyte used in the charging side was a mixture of 0.5M H_3BO_3 and 0.5M Na_2SO_4; As_2O_3 (200 ppm) was added on the charging side as atomic hydrogen recombination poison. A constant current of 0.1 mA was applied to the charging side. The electrolyte used in the discharge side was 0.1M NaOH. The exit side of the permeation cell was maintained at constant potential of -300 mV with respect to a standard calomel electrode [13, 14]. After a sufficient time interval, the oxidation current in the anodic side reached less than 50 nA, and the hydrogen charging in the cathodic cell was commenced. Hydrogen oxidation current was monitored on the exit side (anodic side) of the permeation cell. This oxidation current was monitored with respect to time and the output was recorded for calculation of diffusion coefficient and the permeation flux. A detailed description of the experimental methodology is given in the literature [13, 14].

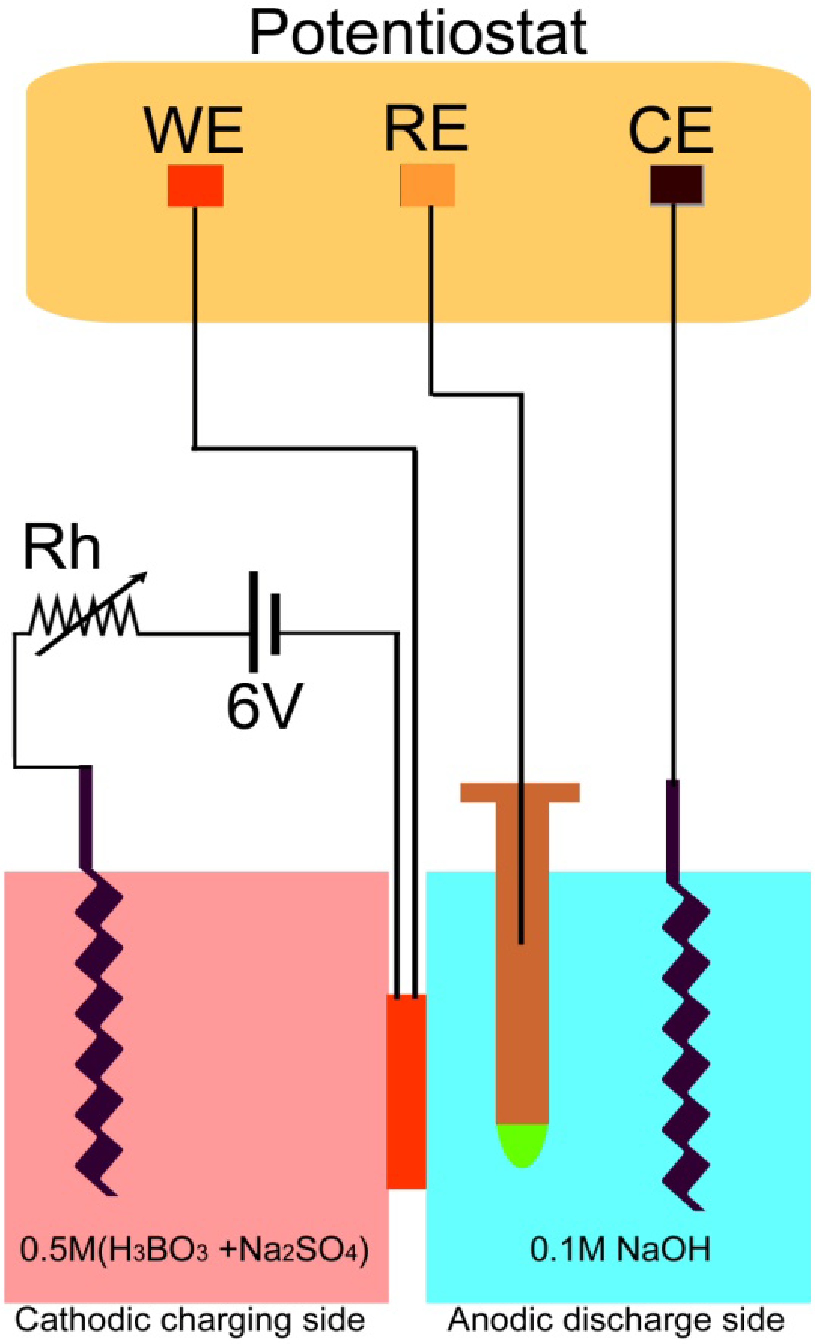

Fig. 6.2 Electrochemical permeation cell schematic

6.3 Results

6.3.1 Coating Characterization

The X-ray diffraction patterns and surface morphologies of the investigated coatings are shown in Figs. 6.3 and 4 respectively. From Fig. 6.4, it can be observed that Zn-Ni was composed of large platelets [15] (about 10 µm in size) with intermittent porosity and microcracks. The X-ray diffraction results showed that the Zn-Ni coating comprised of uniform γ Zn-Ni (Ni_2Zn_{11}) which is the typical phase observed in Zn – 15 % Ni [16-18]. The Zn coating was composed of hemispherical clusters which are typical of most Zn coatings [15, 19]. The Cd coating was composed of spherical hexagonal platelets (Fig. 6.4c). More precisely, these platelets are hexagonal crystals clustered together to form a spherical structure, a common characteristic of Cd coatings [20, 21] . The XRD patterns of Zn and Cd reflected pure metal without any detectable contaminants. The cross sectional morphologies of the coatings plated on the notch bar are shown in Fig. 6.5. The Zn-Ni coating consisted of through thickness microcracks which expanded during the heat treatment as shown in Fig. 6.5. The reason behind the cracks is due to the inherent lattice strain associated with the formation of γ-Zn-Ni (Ni_2Zn_{11}). These cracks expanded due to the mismatch in the coefficient of thermal expansion between the substrate and the coating material, accompanied by an increase in the magnitude of residual stress distribution across the coating thickness [22, 23]. The Zn coating had a uniform interface while the LHE Cd coating had intermittent discontinuities designed to facilitate removal of co-evolved hydrogen [10].

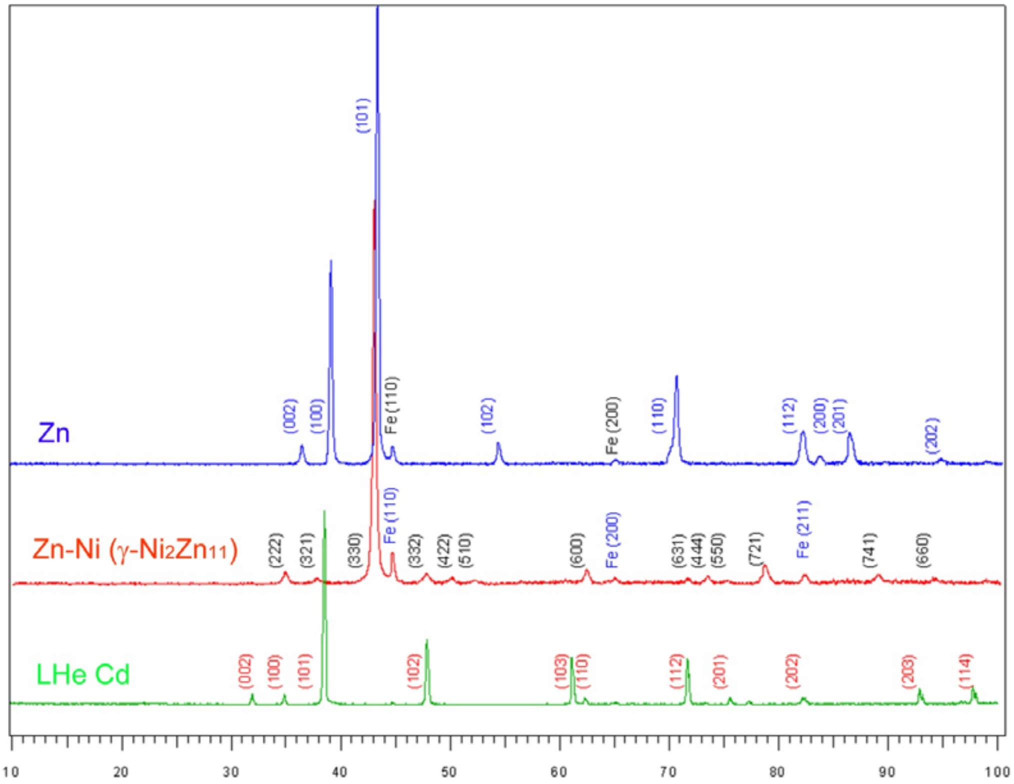

Fig. 6.3 XRD of the investigated coatings

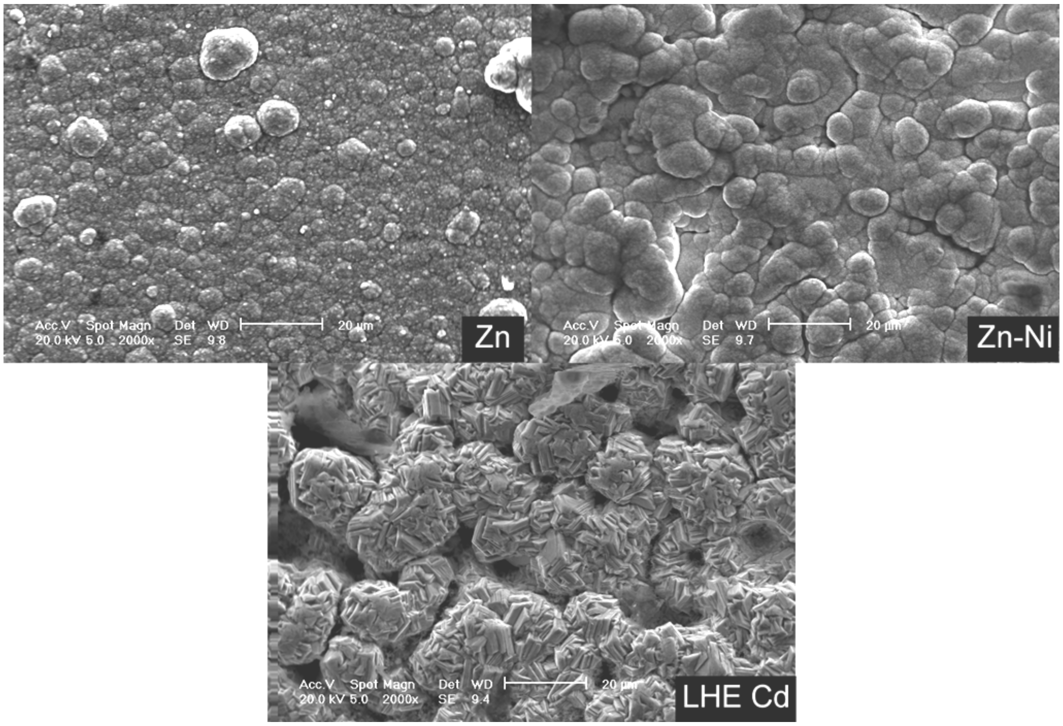

Fig. 6.4 SEM images of the coating surfaces

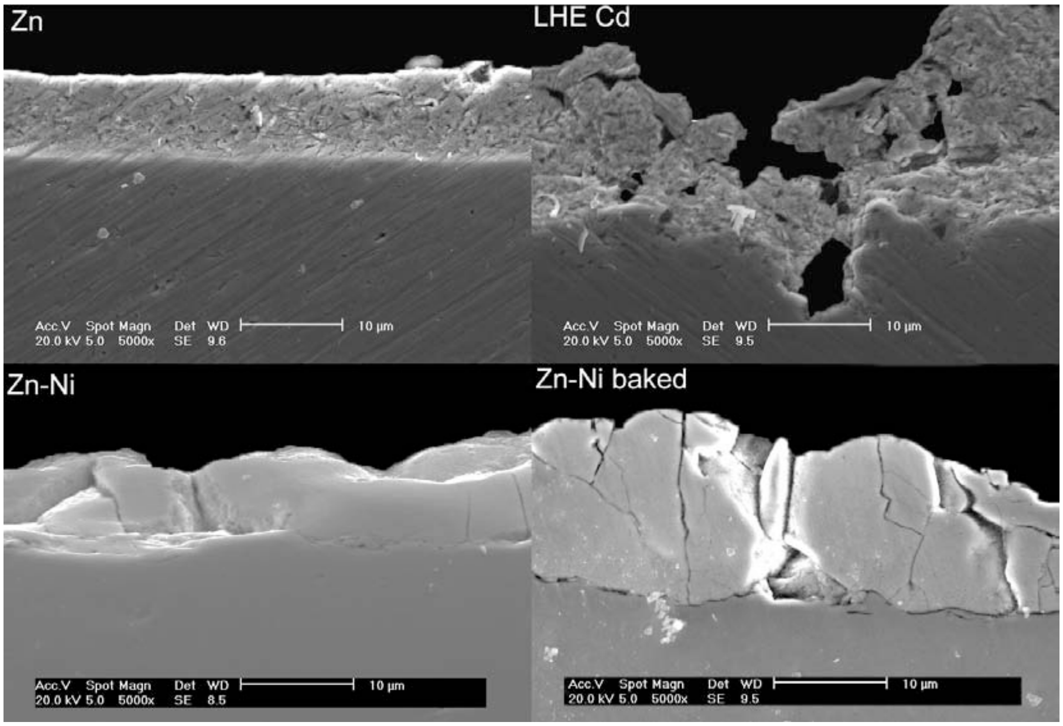

Fig. 6.5 Cross sectional SEM images of the investigated coatings on the notch bar specimen

6.3.2 Vacuum thermal desorption spectroscopy

The hydrogen discharge distribution of the bare and coated notch bar specimens is shown in Fig. 6.6. The quadruple mass spectrometer has two types of detectors namely a Faraday cup and a secondary electron multiplier. In our present investigation the Faraday cup detector was used. The experimental output of the Faraday cup was hydrogen ion intensity vs. time. The number of hydrogen ions discharged was calculated by using Faradays law:

$$N = \frac{It}{e}$$

N = Number of hydrogen ions I = Ion current in Amperes t = time in seconds e = charge of an electron 1.602 X 10^{-19} C. The ion count was subsequently converted into parts per million by mass ratio calculations.

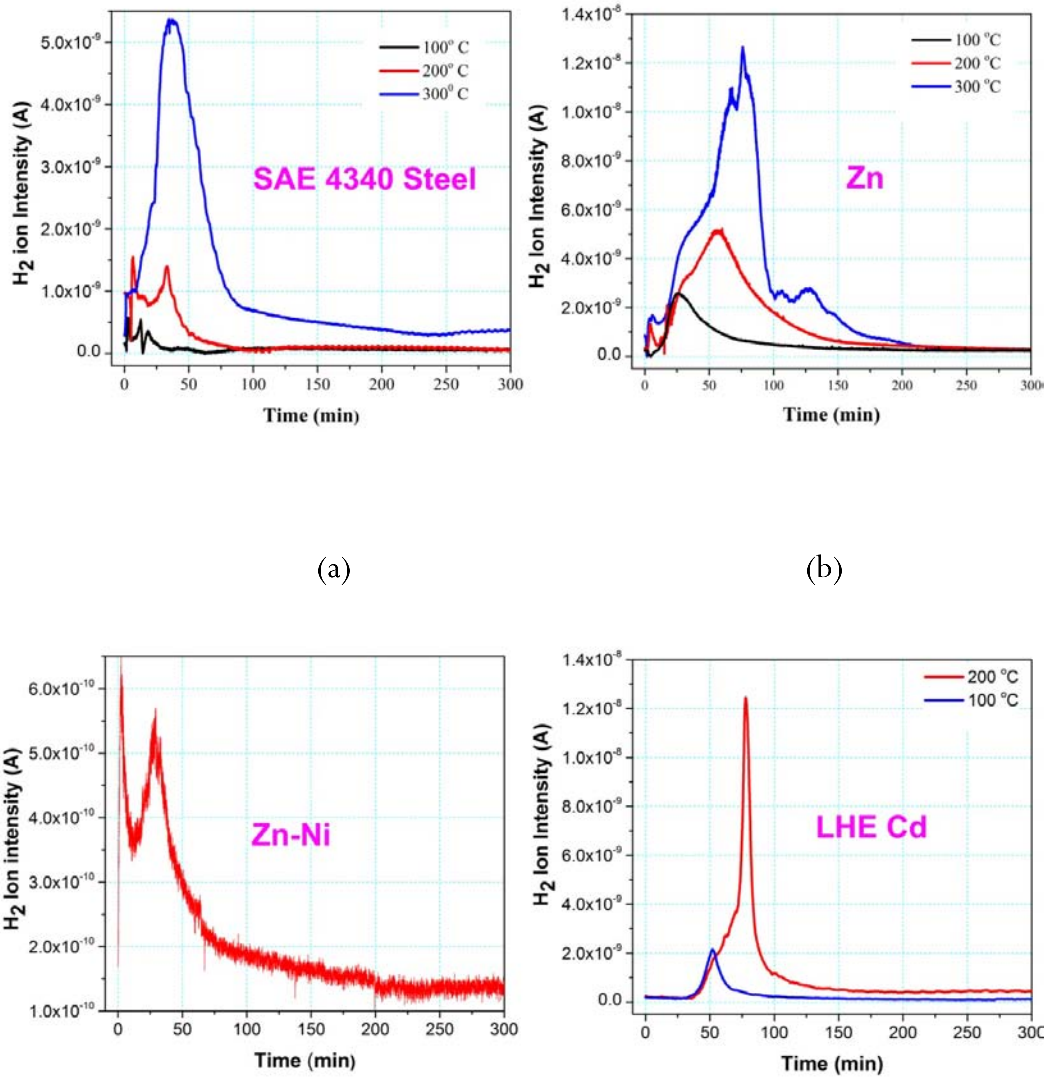

(a) (b)

(c) (d)

Fig. 6.6 TDS ion intensity spectrum for (a) substrate steel (b) Zn (c) Zn-Ni (d) LHE Cd from the mass spectrometer

From Fig. 6.6a, in the steel specimen, as baking temperature was varied from 100 to 300º C, higher baking temperature resulted in higher hydrogen discharge. Zn coatings (Fig. 6.6b) discharged the greatest amount of hydrogen when baked at 300º C. However, the extreme vacuum also caused the Zn to volatilize at 300º C. A similar trend was observed for Cd coatings (Fig. 6.6d) where at 200º C, Cd was also volatilized. These results indicate that maximum baking temperatures in this experimental setup were constrained to 200º C for Zn and 100º C for Cd for studying the amount of hydrogen discharged from coated specimens.

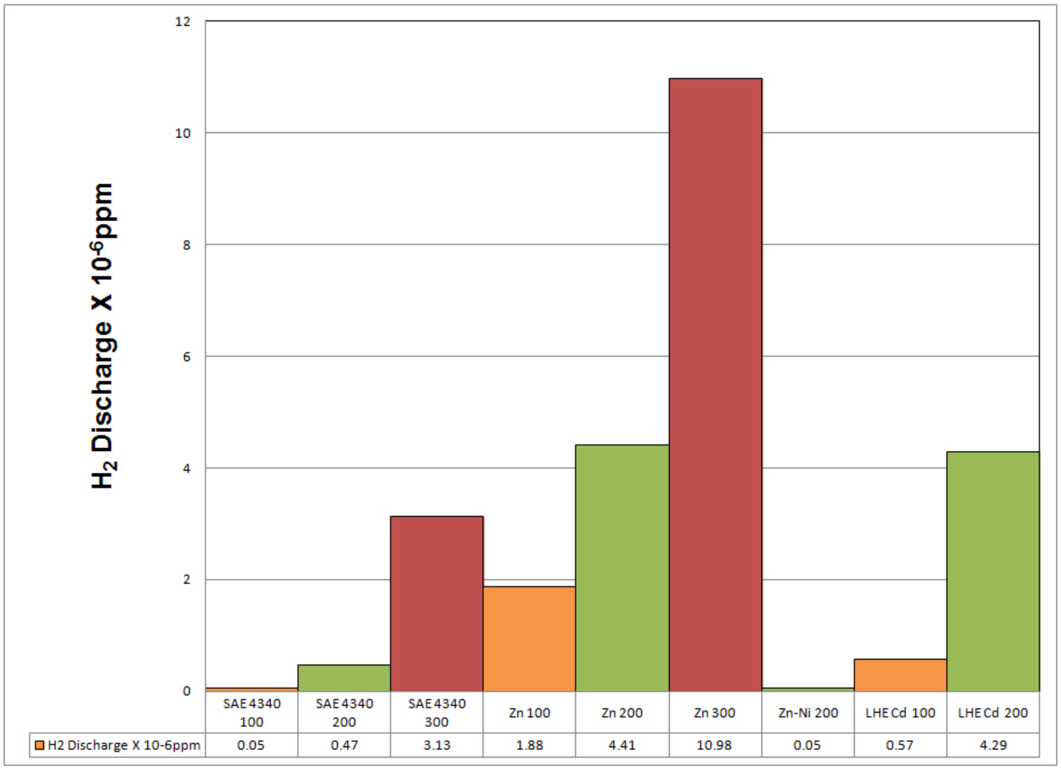

Fig. 6.7 Summary of TDS data of the substrate and coatings at different temperature

The results of the TDS studies are summarized in Fig. 6.7. At 200º C baking temperature, hydrogen discharge was lowest for Zn-Ni (0.05E-6 ppm) as compared to Zn (4.41E-06 ppm) and Cd (0.57E-06 ppm). The hydrogen discharged by the coated specimens is attributed to the amount of hydrogen absorbed during the plating process and the permeability of the coating. More precisely, the amount of hydrogen absorbed during the plating process is a function of processing parameters, such as current density, plating time, batch efficiency, etc., and the permeability of the coating, which is a function of its microstructure and general morphology. If the coating happens to be extremely permeable to hydrogen, as is the case with phosphate coatings [3], it does not act as a barrier to hydrogen diffusion, and given sufficient time hydrogen will escape at room temperature.

Defects in the coatings also contribute to hydrogen escape from the matrix. In case of the Zn coating shown in Fig. 6.5 (a) the cross section is uniform without any defects, which led to the trapping of hydrogen in the interface, which was then released during the baking process. In the case of the Cd coating, as shown in Fig. 6.5 (b) the more discontinuous interface led to the escape of hydrogen from the interface within short duration of the plating, which was indicated by lower amount of hydrogen present in the coating. Zn-Ni coatings had inherent microcracks across the interface Fig. 6.5(c) which expanded during the heat treatment Fig. 6.5(d) acting as hydrogen escape pathways. The results appear to indicate that the Zn-Ni process introduced the least amount of hydrogen into the specimens, as compared to Zn and Cd processes.

6.3.4 Electrochemical hydrogen permeability of coated steel

Permeability of the steel and coated steel specimens to hydrogen was determined by the twin cell method. A relatively permeable low carbon steel substrate was chosen for the experiments. From the coating cross sectional morphologies on the notch bar (Fig. 6.5) it was evident that the Zn coating had a uniform defect free cross section, the Zn-Ni coatings had microcracks, and the Cd coating had intermittent discontinuities. Since the substrate geometry was changed, the microcracks distribution in the Zn-Ni coatings also changed.

The microcracks were randomly distributed with some areas having uniform cross section as shown in Fig. 6.8 (a), and discontinuous cracked microstructure shown in Fig. 6.8 (b). When the low carbon steel shims were subjected to heat treatment at 200º C the crack network increased to form a morphology shown in Fig. 6.8 (c). Similar observations were recorded for the Cd coatings with some areas of the coated shim having a uniform interface as shown in Fig. 6.9 (a) and with intermittent discontinuities in Fig. 6.9 (b). The permeation tests were performed both uniform and non uniform coating interfaces. The output of the experiments is permeation current density vs. time as shown in Fig. 6.10. Fig. 6.10 (a) shows the current transient characteristics of the bare SAE 1006 steel and Fig. 6.10(b) shows the transient behaviors of uniform defect free Zn, Zn-Ni and Cd coatings on steel substrate. From the current transient graphs the diffusion coefficient, subsurface hydrogen concentration and the steady state permeation flux were determined by using the following equations [24-26]:

$$D_{eff} = \frac{L^2}{2*t_{lag}} \qquad D_{eff} = \frac{L^2}{12.98*t_b} \qquad J_{SS} = \frac{I_{SS}}{A*F} \qquad C_0 = \frac{J_{SS}}{L*D_{eff}}$$

D_{eff} = Effective diffusion coefficient (cm^2s^{-1}); Jss = Steady state permeation flux (mol s^{-1} cm^{-2}); C_0 = Subsurface hydrogen ion concentration (mol cm^3);I_{ss} = Steady state permeation current (A); T_b= Break through time (s); t_{lag} = Time lag – $0.63t_{ss}$ t_{ss} = steady state time (s) ; L = Membrane thickness; A = exposed area (cm^2)

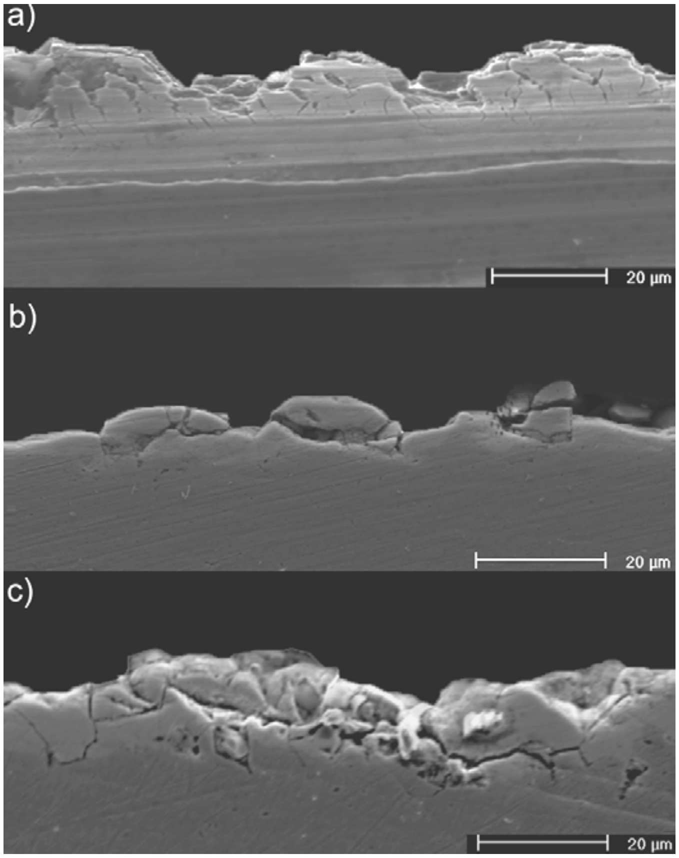

Fig. 6.8 Cross sectional SEM images of Zn-Ni coatings on low carbon steel shims (a) uniform defect free cross section (b) as plated Zn-Ni coatings with discontinuities and microcracks (c) Zn-Ni cross section after post baking heat treatment with microcracks and discontinuities

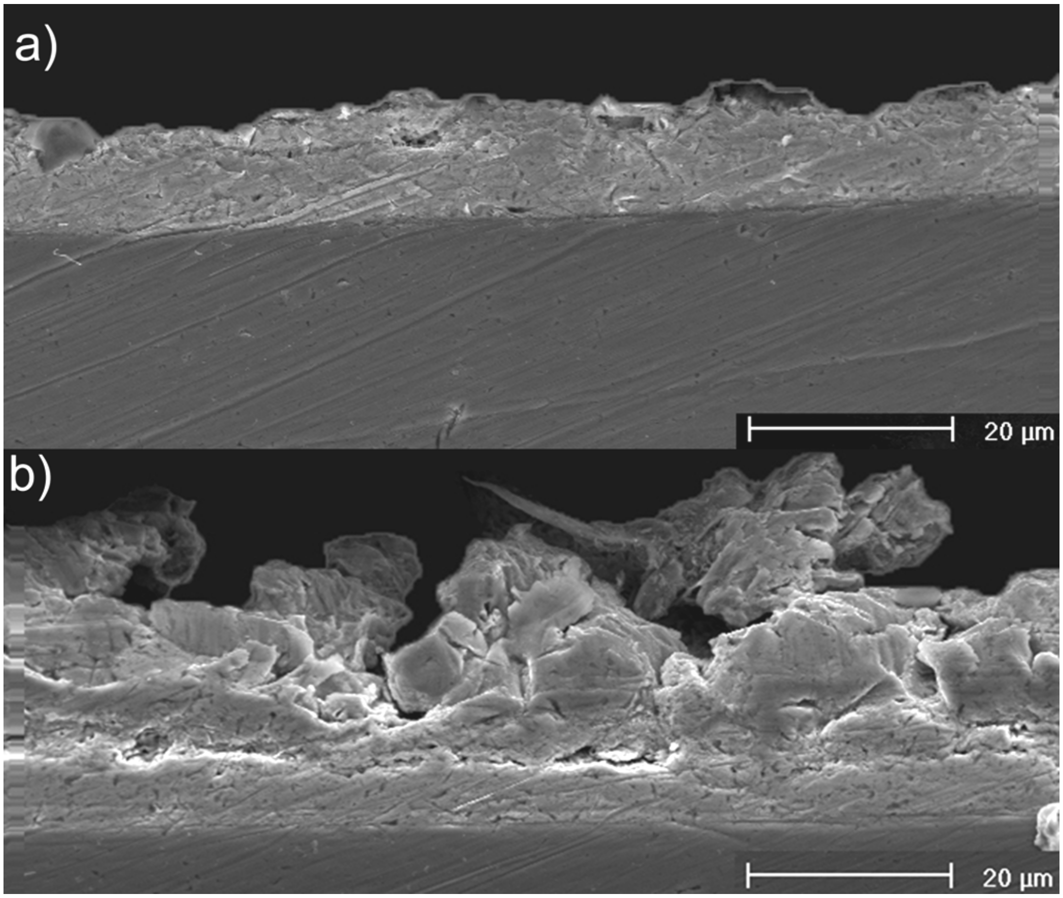

Fig. 6.9 Cross sectional SEM images of LHE Cd coatings on low carbon steel shims (a) uniform cross section (b) cross section with discontinuities

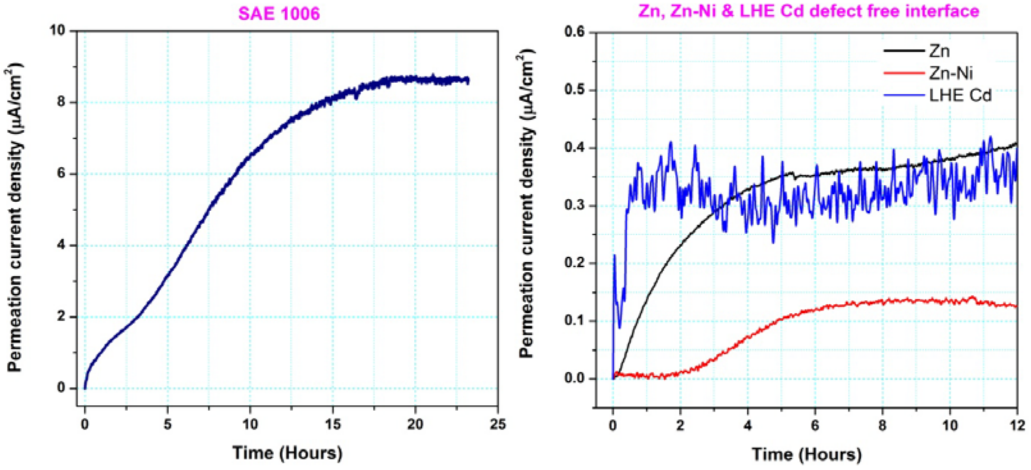

Fig. 6.10 Hydrogen permeation current density distribution with respect to time for (a) SAE 1006 steel substrate (b) Zn, Zn-Ni and LHE Cd coating with defect free interface

From Fig. 6.10(a) it can be observed that SAE 1006 steel was easily permeable to atomic hydrogen, which was evident from very short break through time (10s) and a very high permeation current density (8.52 μA/cm^2). Fig. 6.10(b) shows the permeation characteristic of Zn, Zn-Ni and Cd coated steel surfaces. From Fig. 6.10 (b) it is evident that all the three coatings, Zn, Zn-Ni and Cd acted as a barrier for hydrogen diffusion in steel. This is evident by the fact that the permeation current density was drastically reduced and the break through time was increased significantly, 720 s for Zn, 6400 s for Zn-Ni and 365 s for Cd as compared to the 10 s for steel substrate alone. Using the equations (1) mentioned above, the diffusion coefficients were calculated for the coated steels, which are listed in Table 6.1. The effective diffusion coefficients and the steady state hydrogen permeation flux of Zn-Ni coatings were one order of magnitude lower compared to the Zn and Cd coated steel, which indicated that Zn-Ni coatings offer much better barriers to hydrogen diffusion than Zn and Cd coatings.

Table 6.1 Diffusion coefficients and hydrogen permeability constants for Steel, Zn and Zn-Ni

Material	**Diffusion Coefficient D X 10^{-08} (cm^2s^{-1})**	**Subsurface hydrogen conc. C_0 X 10^{-06} (Mol cm^{-3})**	**Permeation flux J_{ss} X 10^{-11} (mol $s^{-1}cm^{-2}$)**
Bare steel	38.600	2.285	8.821
Zn	1.009	4.380	0.395
Zn-Ni	0.391	2.711	0.087
Cd	4.543	1.041	0.378

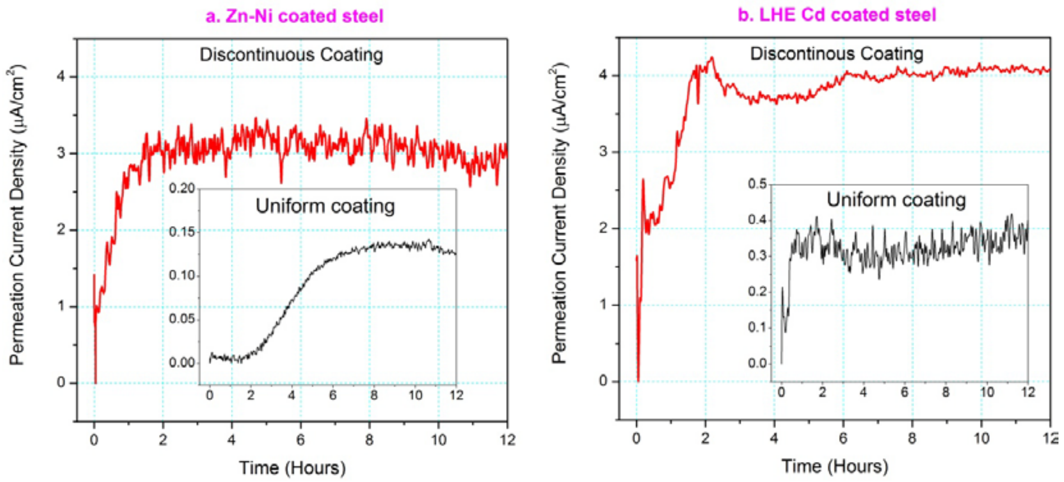

Fig. 6.11 Permeation current densities of (a) uniform and discontinuous Zn-Ni coated steel (b) uniform and discontinuous LHE Cd coated steel

Fig. 6.11 (a) shows the H_2 permeation transient of Zn-Ni coated steel with microcracks and Fig. 6.11 (b) shows the transient of Cd coated steel with discontinuities. It can be observed that the breakthrough time was a lot shorter, 140 s as opposed to 6400 s in case of Zn-Ni and 25 s as opposed to 350 s in case of Cd coatings. Steady state permeation flux was higher in both the cases than the steel with uniform coating interface.

The hydrogen permeation constants for the defective coatings are compared with defect free uniform coatings as shown in Table 2. It can be observed that the uniform Zn-Ni coating provided much better permeation resistance as compared to the coating interface with cracks and discontinuities. The microcracks are a common feature in Zn-Ni coatings, and their distribution could be due to different factors such as residual stress and also specimen geometry. The residual stresses present in the surface of the Zn-Ni coating are tensile in nature. Since the thickness of the steel substrate was 100 μm, the resistance offered by the steel substrate against bending and warping of the specimen was lower, which again resulted in non uniform distribution of microcracks across the coating interface.

Hydrogen permeation tests were also performed on Zn-Ni coated steels that were subjected to post plating heat treatment. From the result is shown in Fig. 6.12, it can be observed that the breakthrough time was instantaneous and the permeation current showed increasing trend after an initial reduction. This reduction in the permeation current following a sudden surge can be explained by the uniform monolayer close to the interface impeding further flow, which in turn resulted in an accumulation of hydrogen within the crack networks, distributed randomly across the coating thickness. Once the break through happened again the flux started increasing. Because a steady state condition was not obtained and the cracked coating did not provide uniform diffusion transient, the diffusion coefficients could not be calculated. Nevertheless, it can be observed that the permeation current was close to that of the bare steel substrate. This observation indicated that the crack network allowed the hydrogen diffuse out when subjected to post plating heat treatment.

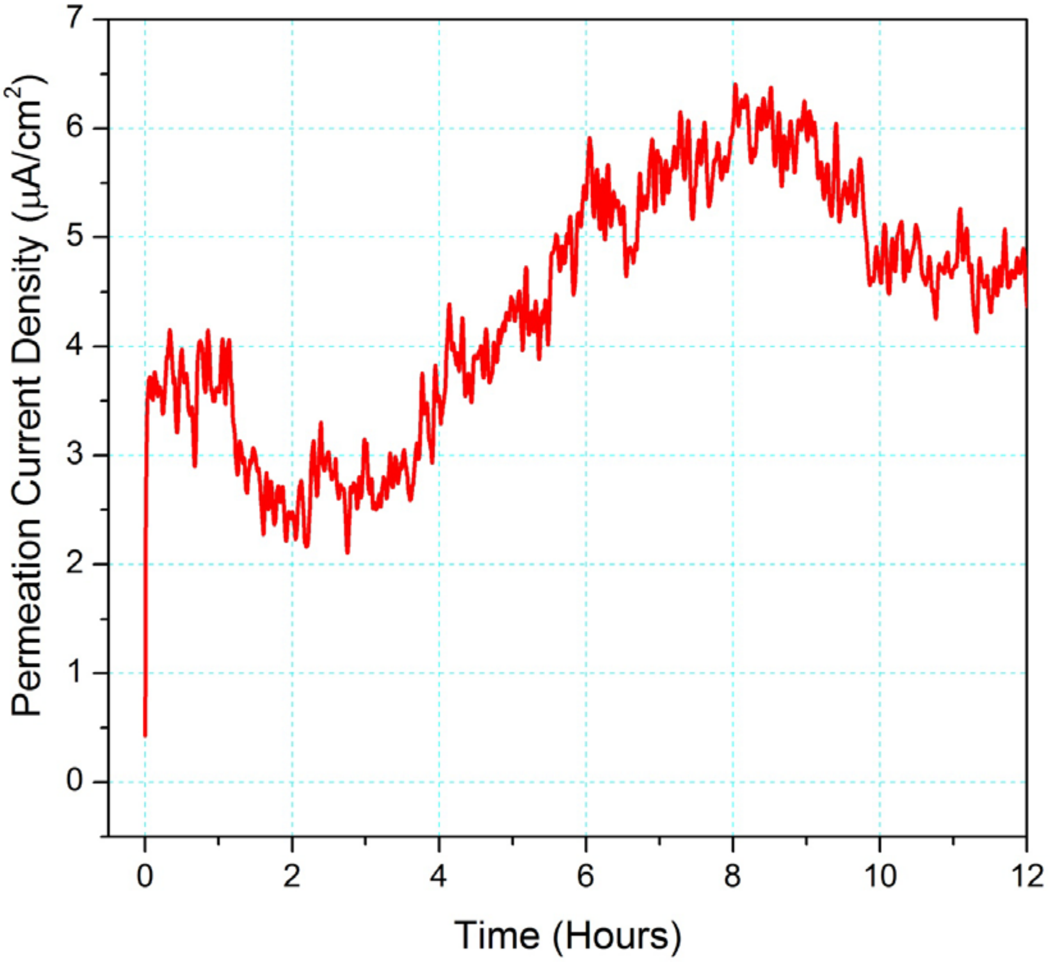

Fig. 6.12 Permeation current density of Zn-Ni coated steel subjected to post plating heat treatment at 200° C

The Cd coating with intermittent discontinuities also exhibited a higher permeation transients as shown in Fig. 6.11 (b) compared to the uniform coating. The discontinuities can become preferred sites for hydrogen adsorption, from where hydrogen accumulates and then permeation into the steel. A uniform coating surface would have acted as a barrier to further diffusion. This hypothesis is supported by higher subsurface hydrogen concentrations in both coatings that contained microcracks and discontinuities.

Table 6.2 Comparison of hydrogen permeability constants for uniform and defect free coatings and coatings with discontinuities and microcracks

Material	**Diffusion Coefficient $D \times 10^{-08}$ (cm^2s^{-1})**	**Subsurface hydrogen conc. $C_0 \times 10^{-06}$ (Mol cm^{-3})**	**Permeation flux $J_{ss} \times 10^{-11}$ (mol $s^{-1}cm^{-2}$)**
Zn-Ni	0.391	2.711	0.087
Zn-Ni with microcracks	5.778	6.707	3.177
Cd	4.543	1.041	0.378
Cd with discontinuities	25.135	2.080	4.183

6.4 Discussion

From the thermal desorption studies it was observed that a uniform, defect free, Zn coating had the highest amount of hydrogen trapped in the interface. It was followed by the Cd coating with discontinuities in the matrix, which facilitated the escape of absorbed hydrogen. The Zn-Ni coating process appears to have introduced the least amount of adsorbed hydrogen during the plating process.

However, upon comparing the microstructures of the three coatings, it can be seen from Fig. 6.5 (a) that Zn has a smooth uniform surface without any apparent defects or porosity. On the other hand, the Zn-Ni interface shown in Fig. 6.5(c) has microcracks which originate during plating process. These microcracks tend to increase in size it the coated part is baked, as shown in Fig. 6.5(d).

The presence of microcracks in the coating facilitates hydrogen escape, possibly reducing the hydrogen concentration in the specimen. During the baking process, as a result of development of network of microcracks, the hydrogen diffusion was increased to a larger scale, which was evident from the permeation current observed in Fig. 6.12. However, the permeability studies showed that in the absence of microcracks, the Zn-Ni coating acted as a superior barrier against hydrogen diffusion (Fig. 6.11 (a)). Conversely, in the presence of discontinuities and microcracks, hydrogen diffusion was much higher than for the uniform defect free coating. Therefore, it is likely that the process introduced less hydrogen because the Zn-Ni coating acted as a barrier to further H absorption during the initial stages of deposition. Later during baking, microcracks which originated due to lattice strain and mismatch facilitated escape of any absorbed hydrogen. Combined, these phenomena led to the low quantity of hydrogen measured during the desorption test.

6.5 Conclusions

The Zn-Ni plating process was found to be less susceptible to internal hydrogen embrittlement as compared to the Zn and Cd plating processes. The Zn-Ni plating process induced microcracks and defects in the coating microstructure.

These defects expanded during the baking treatment, and acted as hydrogen escape pathways. From the permeability experiments it was observed that the defect free Zn-Ni coating had superior resistance to hydrogen diffusion. In the presence of microcracks, the permeability of hydrogen can be improved to a large extent, which would facilitate the escape of hydrogen during post plating heat treatment. Hence, from this investigation, it is concluded that, during the initial stages of plating, the defect free Zn-Ni layer acts as a barrier to hydrogen absorption. During the baking process, the defects present in the coating acted as a pathways for any absorbed hydrogen to diffuse out of the coated steel, thereby further minimizing the risk of embrittlement due to plating process.

References

[1] Oriani RA. Hydrogen Embrittlement of Steels. Annual Review of Materials Science. 1978;8:327-57.

[2] Oriani RA, Hirth, John P.; Smialowski, Michael Hydrogen Degradation of Ferrous Alloys: William Andrew Publishing/Noyes.; 1985.

[3] Brahimi S, and S. Yue, . Effect of surface processing variables and coating characteristics on hydrogen embrittlement of steel fasteners Part 2 : Electroplating and non electrolytic processes. SUR/FIN 2009. Louisville KY: NASF; 2009.

[4] Coleman DH, Popov BN, White RE. Hydrogen permeation inhibition by thin layer Zn–Ni alloy electrodeposition. J Appl Electrochem. 1998;28:889-94.

[5] Figueroa D, Robinson MJ. The effects of sacrificial coatings on hydrogen embrittlement and re-embrittlement of ultra high strength steels. Corrosion Science. 2008;50:1066-79.

[6] Hillier EMK, Robinson MJ. Hydrogen embrittlement of high strength steel electroplated with zinc-cobalt alloys. Corrosion Science. 2004;46:715-27.

[7] Hillier EMK, Robinson MJ. Permeation measurements to study hydrogen uptake by steel electroplated with zinc-cobalt alloys. Corrosion Science. 2006;48:1019-35.

[8] ASTM. F1941-00 Standard specification for electrodeposited coatings on threaded fasteners (Unified Inch Screw Threads (UN/UNR)). ASTM International, West Conshohocken, PA, 19428-2959, DOI: 10.1520/F1941-07 www.astm.org2006

[9] ASTM. F519-10, Standard Test Method for Mechanical Hydrogen Embrittlement Evaluation of Plating/Coating Processes and Service Environments. ASTM International, West Conshohocken, PA, DOI :10.1520/F0519-10, www.astm.org.; 2010

[10] MIL-STD-870C. U.S. Military Standard (USAF) on Cadmium plating, Low embrittlement, Electrodeposition. Department of Defence Standard Practice; 27 April 2009.

[11] Turnbull A, Hutchings RB, Ferriss DH. Modelling of thermal desorption of hydrogen from metals. Materials Science and Engineering A. 1997;238:317-28.

[12] Addach H, Bercot P, Wery M, Rezrazi M. Quantitative determination of hydrogen in solids by gas chromatography. Journal of Chromatography A. 2004;1057:219-23.

[13] ASTM. G148-97 Standard Practice for Evaluation of Hydrogen Uptake, Permeation, and Transport in Metals by an Electrochemical Technique ASTM International, West Conshohocken, PA, DOI :10.1520/G0148-97R11, www.astm.org2011.

[14] Devanathan MAV, Stachurski Z. The Adsorption and Diffusion of Electrolytic Hydrogen in Palladium. Proceedings of the Royal Society of London Series A, Mathematical and Physical Sciences. 1962;270:90-102.

[15] Thomas BK, Fray DJ. The Effect of Additives on the Morphology of Zinc Electrodeposited from a Zinc-Chloride Electrolyte at High-Current Densities. J Appl Electrochem. 1981;11:677-83.

[16] Bories C, Bonino JP, Rousset A. Structure and thermal stability of zinc-nickel electrodeposits. J Appl Electrochem. 1999;29:1045-51.

[17] Brooks I, Erb U. Hardness of electrodeposited microcrystalline and nanocrystalline gamma-phase Zn-Ni alloys. Scripta Mater. 2001;44:853-8.

[18] Bruet-Hotellaz, Bonino JP, Rousset A, Marolleau, Chauveau E. Structure of zinc-nickel alloyelectrodeposits. Journal of Materials Science. 1999;34:881-6.

[19] Morón LE, Méndez A, Castañeda F, Flores JG, Ortiz-Frade L, Meas Y, et al. Electrodeposition and corrosion behavior of Zn coatings formed using as brighteners arene additives of different structure. Surface and Coatings Technology. 2011;205:4985-92.

[20] Abdelhalim AM, Baghlaf AO, Sobahi MI. Effect of Some Addition Agents on the Electrodeposition of Cadmium from Acidic Chloride Baths. Surf Technol. 1984;22:129-42.

[21] Elhalim AMA, Sobahi MI. Effect of Bath Constituents and Some Plating Variables on the Electrodeposition of Cadmium from Acidic Chloride Baths. Surf Technol. 1983;19:45-57.

[22] Lin C, Lee H, Hsieh S. Microcracking of flash coatings and its effect on the Zn-Ni coating adhesion of electrodeposited sheet steel. Metallurgical and Materials Transactions A. 1999;30:437-48.

[23] Sasaki T, Hirose Y. Residual stress distribution in electroplated Zn□Ni alloy layer determined by X-ray diffraction. Thin Solid Films. 1994;253:356-61.

[24] Boes N, Züchner H. Electrochemical methods for studying diffusion, permeation and solubility of hydrogen in metals. Journal of the Less Common Metals. 1976;49:223-40.

[25] Cao Y. Influence of structure of palladium and nickel based membranes on hydrogen permeation [Thesis (Ph D)]. Montreal, Quebec, Canada: McGill University; 2002.

[26] Early JG. Hydrogen diffusion in palladium by galvanostatic charging. Acta Metallurgica. 1978;26:1215-23.

7.1 Tribological behavior of electrodeposited Zn, Zn-Ni, Cd and Cd-Ti coatings on low carbon steel substrates

In this study *in situ* tribometry was utilized to understand third body contributions in metallic friction and wear. The nature of transfer film formation and stability, wear debris generation and contact conditions was observed to be different for Zn–Ni, Zn and Cd coatings. The transfer film characteristics were found to influence the friction and wear behavior of metallic coatings. While taking into consideration the transfer of material, adhesion, and varied contact conditions which may lead to severe galling-type seizure during torquing of threaded fasteners, Zn–Ni coatings could act as a replacement for Cd and Zn coatings based on the following conclusions:

1. *In situ* tests provided greater insight toward the wear mechanisms of the coatings. Mild adhesion and material removal by delamination was observed in Zn–Ni coatings, while adhesion and large material removal in form of debris was observed in Zn coatings. Rapid transfer film formation and severe adhesive nature of wear was found to be a predominant wear mechanism in Cd and Cd–Ti coatings.
2. Zn–Ni coatings showed lowest wear rates when compared to Zn, Cd and Cd–Ti coatings. Wear rates of passivated Zn–Ni coatings were found to be lower than the as plated coatings, and resistance to wear improved in Zn–Ni coatings when given a post baking treatment.

3. Microhardness of Zn–Ni coatings was higher than Zn, Cd and Cd–Ti coatings. A marginal increase in hardness was observed in Zn–Ni coatings as a result of baking, while no significant changes were observed on other coatings.
4. No phase change was observed during wear of coatings other than mild oxidation accompanying the wear process.
5. Under unlubricated conditions, the friction coefficient of Zn–Ni coatings were found to decrease, stabilize to a constant value and then increase after the initial run-in period. Friction coefficients of Zn–Ni were comparable to Cd coatings during the initial run in period of 500 cycles, which is beneficial when considering Zn–Ni as a replacement for Cd.

7.2 Tribocorrosion behavior of Zn, Zn-Ni, Cd and Cd-Ti electrodeposited on low carbon steel substrates

In this study the simultaneous action of wear and corrosion on the above mentioned coatings were investigated. Open circuit potentials during the wear tests determined whether the coatings were still protecting the steel anodically during the wear tests, and also gave the shift in potentials. The synergy between wear and corrosion was determined by the impressed potential wear tests. Electrochemical impedance spectroscopy before and after the wear tests helped to determine the effect of material removal by wear on the polarization resistance of the coating before and after the wear tests. From the experimental investigation the following conclusions were made

1. During the wear tests, it was observed that the OCP of Zn-Ni coatings increased (became nobler) because of preferential dezincification from the matrix. For all other coatings, the change in corrosion potential was not appreciable. Zn-Ni coatings exhibited OCP values between Zn and Cd coatings.
2. The impressed potential studies showed the corrosion current during wear tests were lowest for the Zn-Ni coatings as compared to the Cd and Zn coatings. The same was true for mass loss during corrosion. The EIS studies before and after wear tests revealed that the polarization resistance of Zn-Ni coatings was higher than for Zn and Cd coatings. However, the resistance exhibited by the wear track and the pore infiltration resistance of the coatings could not be distinguished.
3. The XRD and EDS analyses after the tribocorrosion studies showed that Zn-Ni coatings survived the entire wear cycle, in contrast to the Zn and Cd coatings. Also phase transformation and surface Ni enrichment was observed in Zn-Ni coatings. Since the Zn-Ni coatings were slowly being depleted of Zn during tribocorrosion, the corrosion products and the Ni rich surface exhibited better corrosion resistance during wear as compared to the Zn and Cd coatings.
4. The passivation treatment was beneficial to Zn-Ni coatings by improving corrosion resistance.
5. The effect of baking heat treatment on tribo corrosion resistance is negligible.

6. Zn-Ni were found to be an ideal replacement for Zn and Cd coatings because of its higher polarization resistance after the wear tests, lower mass loss due to wear enhanced corrosion and also the corrosion products of the Zn-Ni coatings protect the underlying coating from further corrosion thereby increasing the life of the coating.

7.3 Corrosion behavior of Zn, Zn-Ni, Cd and Cd-Ti electrodeposited on low carbon steel substrates

In this study corrosion resistance of Zn, Zn-Ni, LHE Cd and Cd-Ti coatings were measured using three different techniques. Corrosion resistance of the coatings was determined using potentiodynamic polarization curves, open circuit potential measurements and the EIS. The EIS was performed over intermittent time intervals to understand the extent of dezincification in Zn-Ni coatings. The corrosion resistances of the coatings were correlated to the microstructure, phase and composition of the coatings and the nature of corrosion products. From this investigation the following conclusions were made:

1. OCP measurements on Zn-Ni coatings showed progressive enrichment of the surface of the coating with Ni owing to dezincification.
2. Potentiodynamic polarization experiments showed lower corrosion currents in Zn-Ni coatings than Zn and Cd coatings.
3. EIS studies on the coatings revealed a higher infiltration resistance for Cd coatings than Zn-Ni, however the polarization resistances of the Zn-Ni

coatings were higher than Cd and Cd-Ti coatings owing to the phase transformation and Ni enrichment of the surface of the coating.

4. D-Zn-Ni coating showed higher polarization resistance and lower corrosion current than the B-Zn-Ni due to the difference in coating morphology and the rate of dezincification. The presence of micro-pores in D-Zn-Ni resulted in higher diffusion of corrosive environment resulting in distribution of anodic reaction throughout the coating resulting in higher rate of dezincification compared to the compact microstructure of B-Zn-Ni.
5. In as plated Zn-Ni coatings, heat treatment effects were negligible. In passivated coatings, heat treatment resulted in lower polarization resistance and higher corrosion currents due to localized damage of the passive film due to heat treatment.

7.4 Hydrogen embrittlement of Zn, Zn-Ni and Cd coated high strength steel

Hydrogen embrittlement susceptibility due to Zn, Zn-Ni and Cd electrodeposition was investigated by means of electrochemical permeation method and the vacuum thermal desorption method. The hydrogen permeability was correlated to the defects of coatings. Based on the experimental investigations following conclusions were made:

1. Zn-Ni plating process generated least amount of hydrogen compared to the Zn and Cd plating process which was determined by the vacuum thermal desorption method.
2. The Zn-Ni plating process induced microcracks and defects in the coating microstructure. These defects expanded during the baking treatment, and acted as hydrogen escape pathways.
3. From the permeability experiments it was observed that the defect free Zn-Ni coating had superior resistance to hydrogen diffusion. In the presence of microcracks, the permeability of hydrogen can be increased to a large extent, which would facilitate the escape of hydrogen during post plating heat treatment.
4. From this investigation, it is concluded that, during the initial stages of plating, the defect free Zn-Ni layer acts as a barrier to hydrogen absorption. During the baking process, the defects present in the coating acted as a pathways for any absorbed hydrogen to diffuse out of the coated steel, thereby further minimizing the risk of embrittlement due to plating process.

7.5 Summary

From experimental investigations on Zn-Ni and Cd coatings detailed in individual chapters namely the wear resistance, corrosion resistance, tribocorrosion resistance and the hydrogen embrittlement susceptibility of the coating process, it is evident that the Zn-Ni coatings possess higher hardness, superior resistance to adhesive wear and comparable friction coefficient. The friction coefficient of Zn-Ni coatings can be minimized by use of lubrication to increase the performance of the coatings

Under simultaneous action of wear and corrosion the Zn-Ni coatings performed much better than the Zn and Cd coatings, owing to its superior mechanical properties, minimal third body formation and better corrosion product coverage on the surface, which prevented further corrosion of the coating layer during wear. The Zn-Ni coatings also had better corrosion resistance in neutral NaCl solution due to polarization resistance and lower corrosion currents. The heat treatment of Zn-Ni alloys resulted in a distributed crack network, hence preventing localized corrosion attack. Passivation of the Zn-Ni coatings should be performed followed by the heat treatment in order to prolong the life of the coatings.

The Zn-Ni plating process was least susceptible to hydrogen induced damage of the substrate steel due to least amount of hydrogen being generated by this process. The Zn-Ni coating had lowest permeability to hydrogen compared to Zn and Cd coatings. During the initial stages of the plating process, the monolayer of the Zn-Ni coating prevented further hydrogen ingress and, as subsequent layers of coating were deposited the microcracks present in the coating facilitates the easy escape of hydrogen. These cracks further expand during the post plating heat treatment process, further facilitating hydrogen removal. The passivation and sealing treatment could be performed after the heat treatment so that the surface cracks are sealed in the Zn-Ni coatings, which helps in enhancing the service life of the coating as well as sealing the avenues for hydrogen ingress during sacrificial corrosion of the coating.

From this dissertation it was concluded that the Zn-Ni is a very good replacement for Cd due to the superior wear, corrosion and tribocorrosion resistance, minimal hydrogen generation during plating process and lower hydrogen permeability. However, the electrical conductivity of the coating, for electrical connector applications in aerospace industries and the fatigue life of the plated components have to be addressed and investigated before replacing Cd coatings which are currently used for the above mentioned applications.

Chapter 8 Contributions to original knowledge

8.1 Tribological behavior of electrodeposited Zn, Zn-Ni, Cd and Cd-Ti coatings

In situ tribology has been utilized to understand the friction and wear behavior of metallic materials for the first time. The role of third bodies, in the friction and wear behavior, various contact conditions encountered when the transfer film is generated during metallic wear has been experimentally investigated for the first time in metallic wear. Sliding micro contact conditions encountered in Zn-Ni, Zn and Cd coatings have been evaluated for the first time under dry sliding conditions. These characteristics were correlated with the material and mechanical properties for the first time.

8.2 Tribocorrosion behavior of electrodeposited Zn, Zn-Ni, Cd and Cd-Ti coatings

The synergy between wear and corrosion for sacrificial type coatings has been evaluated in neutral 3.5 % NaCl solution. Wear enhanced corrosion, and the corrosion resistance of the strain hardened sacrificial Zn, Zn-Ni and Cd coatings after the wear tests were evaluated with the help of EIS for the first time. The nature of corrosion products in tribocorrosion resistance of Zn-Ni, Zn and Cd coatings were also reported.

8.3 Corrosion resistance of electrodeposited Zn, Zn-Ni, Cd and Cd-Ti coatings

For the first time, electrodeposited Zn-Ni, Zn and Cd and Cd-Ti coatings prepared from industrial processes were evaluated for corrosion resistance under identical experimental conditions and coating thicknesses. For the first time, the extent of dezincification of Zn-Ni alloys and its role in polarization resistance of the coating was evaluated by EIS technique.

8.4 Hydrogen embrittlement of Zn, Zn-Ni and Cd coated high strength steel

For the first time electrochemical permeation technique was utilized to understand the role of coating defects in Zn-Ni coating, in particular discontinuities and microcracks in hydrogen diffusion and transport.

For the first time, the vacuum thermal desorption technique was utilized to analyze the amount of diffusible hydrogen responsible for embrittling the substrate steel by Zn-Ni and Cd coating process.